The role of zinc nanoparticles in the initial events of olfaction, their characterization, preservation, and microenvironmental influence

by

Melissa A. Singletary

A dissertation submitted to the Graduate Faculty of
Auburn University
in partial fulfillment of the
requirements for the Degree of
Doctor of Philosophy

Auburn, Alabama
May 5, 2018

Key words: olfaction, electroolfactogram, odorant receptors, zinc nanoparticles, polyethylene glycol, microbiota

Approved by

Vitaly J. Vodyanoy, Chair, Alumni Professor of Anatomy, Physiology & Pharmacology
Edward E. Morrison, Department Head, Professor of Anatomy, Physiology & Pharmacology
Iryna B. Sorokulova, Professor of Anatomy, Physiology & Pharmacology
Robert L. Judd, Professor of Anatomy, Physiology & Pharmacology

Abstract

Olfactory responses are intensely enhanced with the addition of endogenous and engineered primarily-elemental small zinc nanoparticles (ZnNPs). The endogenous ZnNPs have been found as proteon nucleating centers (PNCs) present in human and animal blood along with other PNCs such as gold and copper nanoparticles. Engineered ZnNPs, mimicking the endogenous subset, which range in size from 1 to 2 nm, have been studied in their influence on olfaction. At low concentrations, ZnNPs can enhance electroolfactogram (EOG) or whole cell patch-clamp responses to odorants by about 3-fold, not seen with the other PNC identified metal nanoparticles or with zinc ions (Zn^{2+}).

To evaluate the role of ZnNPS in the initial events of olfaction, physiochemical characterization of the ZnNPs was performed. Particle size was determined by atomic force microscopy (AFM), crystallinity by transmission electron microscopy (TEM), oxidation by X-ray photoelectron spectroscopy (XPS), and zeta potential by laser Doppler velocimetry (LDV). Characterization by AFM revealed the zinc metal nanoparticles were in the size of 1-2 nm range of PNC's at an average diameter of 1.2±0.3 nm. XPS demonstrated 94% of atoms in the zinc nanoparticle were non-oxidized with the shell atoms constituting 80% of the total atom number. Crystalline lattice fringes corresponding to elemental zinc were demonstrated on TEM. The zeta potential with LDV was found of -42.4±4.8 (SE) mV. The characteristics of the small Zn nanoparticles implied high stability and high potential chemical reactivity. Evaluation of

the effects oxidation has on zinc nanoparticle function in olfaction was evaluated by EOG. ZnNPs were subjected to oxygen percolation and characterized in relation to bare ZnNPs. The oxidation levels of 12% was determined by the XPS spectra. This oxidation of bare ZnNPs resulted in halting the olfaction enhancement as measured by EOG.

With aging throughout storage and at elevated temperatures, ZnNPs are also oxidized and no longer manifest the same degree of olfactory enhancement. The design of a polyethylene glycol coating to meet storage requirements of engineered zinc nanoparticles was evaluated in an effort to achieve maximal olfactory benefit. The zinc nanoparticles were covered with 1000 g/mol or 400 g/mol molecular weight polyethylene glycol (PEG). Non-PEGylated and PEGylated zinc nanoparticles were tested by EOG with isolated rat olfactory epithelium and odorant responses evoked by the mixture of eugenol, ethyl butyrate and (±) carvone after storage at 278 K (5 ^{o}C), 303 K (30 ^{o}C), and 323 K (50 ^{o}C). The particles were analyzed by AFM, TEM, XPS, and LDV. Our data indicates that stored ZnPEG400 nanoparticles maintain physiologically-consistent olfactory enhancement for over 300 days. These engineered nanoparticles support future applications in olfactory research, sensitive detection capabilities, and medicine.

The isolation of PNCs from human and animal blood and the implication of zinc nanoparticle enhancement on olfaction support a biological role for ZnNPs. To evaluate the potential biological role ZnNPs have in the initial events of olfaction, the low molecular filtrate of olfactory mucosa was analyzed for its electrophysiological influence on olfactory neurons. Isolation of the low-molecular-weight filtrate from the olfactory mucosa demonstrated on EOG to provide ZnNP-like enhancement of olfaction. XPS analysis of the low-molecular-weight filtrate was inconclusive for positive identification

of ZnNPs, though literature supports a zinc concentration of 14 µg/dl within the nasal mucus of mice. Commonly used testing methods for zinc are unable to differentiate ionic zinc from any range of zinc nanoparticles. Though limited to electrophysiological comparison, this data further supports a biological role of ZnNPs through indications of the endogenous presence of enhancement capable nanoparticles at the site of action.

The perireceptor environment is mucus based with recent evidence supporting the presence of a microbial community. To evaluate the potential influence ZnNPs may have on the perireceptor environment, multiple bacterial taxa were screened for ZnNP induced growth effects. Bacterial species selected included gram-negative *Escherichia coli* M-17, *Shigella flexneri* and *Salmonella typhimurium* 52096 and gram-positive species *Staphylococcus aureus* ATCC 12600, MRSA-1, *Lactobacillus acidophilus*, *Bacillus subtilis* BSB3, *Bacillus subtilis* BS, and *Bacillus licheniformis*. The screening method involved co-culture with ZnNPs and comparative viability determined through spectrophotometric analysis. Results indicated a differential effect independent of bacterial cell wall structure. The effects on Staphylococcus species, with particular suppression on methicillin resistant *Staphylococcus aureus* (MRSA), and an apparent enhancement of growth in *Bacillus subtilis*, led to a selective study evaluating ZnNP antimicrobial effects in seven strains of MRSA and *Bacillus subtilis*. Results showed that ZnNPs were generally MRSA suppressive in a concentration-dependent manner, with an approximate 33.5% maximum reduction in viability (MRSA-45) ($p<0.05$). Conversely, a general trend of concentration-dependent bacterial growth enhancement is seen primarily in *Bacillus subtilis* at an approximate 18% maximum increase in viability ($p<0.05$).

This differential pattern of activity between a bacterial species of clinical importance in infectivity and antibiotic resistance (MRSA), and a bacterial species utilized as a probiotic for its positive health benefits provides insight into a potential regulatory role that ZnNPs may play in the perireceptor environment.

Understanding the molecular mechanism underlying odorant recognition in the olfactory system and the role that newly discovered ZnNPs may play in that dynamic interaction is important in the context of basic science and advancements in identification of therapeutic targets for application in clinical diseases and disorders associated with loss or dysfunction of smell. Continuing research in the neuroscience of olfaction and nanotechnology may secure future applications of ZnNPs in neurodegenerative medical conditions that involve a loss of smell such as Alzheimer's and Parkinson's, psychological conditions associated with loss of smell such as schizophrenia and depression, occupational health and safety, public health, agricultural production and processing, aromatic technologies related to food and perfume industries, and global security in detection enhancement.

Acknowledgments

The author would like to thank all those who made this work possible through either their direct involvement or through advice and support. Direct involvement from her advisory committee: Dr. Vitaly Vodyanoy, Dr. Iryna Sorokulova, Dr. Edward Morrison and Dr. Robert Judd, she is grateful and honored to have received your guidance and wisdom. The author would like to recognize the contribution of detailed training, patient assistance, comradery and collaboration of co-authors: Oleg Pustovyy, Ludmila Globa, Samantha Hagerty, Shin Muramoto, Yasmine Daniels, William A. MacCrehan, Gheorghe Stan, June W. Lau, and Alex Ducray. The author would like to thank those individuals within the department of Anatomy, Physiology, and Pharmacology whose kindness was greatly appreciated. She would like to thank the teaching staff of the Small Animal Anatomy course and the Veterinary Neuroscience course for their mentorship in the art of teaching. To the author's family, her lifelong friend and husband Brandon and inspiring young daughter Zoey, the author would like state that their influence and her gratitude for them is beyond measure ($p<0.000000001$).

Computer software used: Adobe ® Photoshop, Kodak 1D software, Microcal ™ Origin ® ver. 9.2, Microsoft Office ® Office Word 2015, Microsoft ® Office Excel 2015 Clampfit 10.7; Clampex 10.7.; Molecular imaging performed in Avogadro Software ver. 1.2.0; spectrometric analysis software KC4™ ver. 3.1.

Table of Contents

Abstract ii

Acknowledgments vi

List of Tables xi

List of Figures xii

List of Abbreviations xvii

Chapter 1.0 Introduction 1

Chapter 2.0 Literature Review 6

2.1 Olfactory System Overview and Anatomy 7

2.1.1 Nasal Cavity 7

2.1.2 Main Olfactory Epithelium 12

2.2 Olfactory Receptors 15

2.2.1 Olfactory Receptor Gene Families 20

2.2.2 Gene Expression and Evolution 21

2.2.3 Olfactory Functional Variation Across Organisms 25

2.2.4 Atypical Receptor Expression 27

2.3 Perireceptor Environment 29

2.3.1 Mucus Constituents 29

2.4 Odorants 32

2.5 Neuroprocessing of Olfaction 34

2.5.1 Olfactory Signal Transduction Pathway 34
2.5.2 Olfactory Bulb 38
2.5.3 Higher Brain Center Processing 40
2.6 Prevailing Theories of Olfaction 42
2.7 Zinc Overview 47
2.7.1 Embryogenesis, Development, and Deficiency 48
2.7.2 Metal Ions and Volatile Molecules 49
2.8 Zinc, the Central Nervous System, and Olfaction 50
2.9 Microbiota Overview and in Olfaction 55
2.10 Microbes and Metals 59
2.11 Objectives 61
Chapter 3.0 Physical-Chemical Properties of Zinc Nanoparticles 64
3.1 Abstract 65
3.2 Introduction 66
3.3 Materials and Methods 68
3.4 Results 76
3.5 Discussion 83
3.6 Conclusion 95
Chapter 4.0 Stabilization of Zinc Nanoparticles 97
4.1 Abstract 98
4.2 Introduction 99
4.3 Materials and Methods 102
4.4 Results 107

4.5 Discussion 123
4.6 Associated content 132
4.7 Disclaimer 132
4.8 Appendix 132
Chapter 5.0 Perireceptor Nano-molecular Influence on Olfaction 137
5.1 Abstract 138
5.2 Introduction 139
5.3 Materials and Methods 140
5.4 Results 145
5.5 Discussion 149
5.6 Conclusion 152
Chapter 6.0 Micro-environmental Evaluation of Zinc Nanoparticle Influence 153
6.1 Abstract 154
6.2 Introduction 155
6.3 Materials and Methods 158
6.4 Results 159
6.5 Discussion 169
6.6 Conclusion 175
Chapter 7.0 Conclusions 176
Bibliography 181

List of Tables

Table 2.1 Olfactory Receptor Genes Species Variance 17

Table 2.2 Olfactory Receptor Genes Species Variance in Representative Class I and II Groups 19

Table 3.1 Properties of nanoparticles 79

Table 3.2 Effect of nanoparticles on the odorant responses 82

Table 4.1 Properties of PEG on the surface of zinc nanoparticles 107

Table 4.2 XPS properties of bare and PEGylated zinc nanoparticles, stored at various durations and temperatures 113

Table 4.3 Thermodynamic analysis of oxidation of Zn, ZnPEG400, and ZnPEG1000 nanoparticles 116

Table 5.1. The estimated concentrations of nanoparticles with zinc-like attributes in olfaction enhancement. Significance using ANOVA found between filtrate concentrations at $p<0.05$. 147

Table 6.1 Bacterial screening species chart descriptions. Gram positive-cell wall (G+) and gram-negative cell wall (G-). 170

Table 6.2 Zinc and Zinc Oxide nanoparticle effects on multiple bacterial taxa. Zeta represents available data on zeta potential for the associated zinc or zinc oxide used in the referenced study. Conc. Conversions represents the concentrations extracted from published data and converted for table form. Bacteria refers to species listed without strain specificity. Result describes inhibition/static (bacteriostatic), no significant effect (NSE), or as a reduction in viability equating to inhibition. Dep. refers to a dependency if noted in the reference, concentration versus size dependency. 173

List of Figures

Figure 2.1 Histology of Olfactory Epithelium compared to Respiratory Epithelium. Anti-olfactory marker protein immunofluorescent staining orange (Alexa 555). OMP is selective for mature olfactory sensory neurons 8

Figure 2.2 Main Olfactory Epithelium (MOE) illustration. Illustration by Melissa Singletary 13

Figure 2.3 Histological section of Main Olfactory Epithelium (MOE). Left image hematoxylin and eosin stain (H&E) under high resolution light microscopy (CytoViva). Right image anti-olfactory marker protein (OMP) immunofluorescent tagged orange (Alexa 555) under high resolution dark microscopy (CytoViva) 14

Figure 2.4 Main Olfactory Epithelium (MOE) mucosal surface histological image with anti-olfactory marker protein (OMP) immunofluorescent orange tag (Alexa 555) using high resolution dark field microscopy (CytoViva) 29

Figure 2.5 Ball and stick models of odorants Eugenol, +/- Carvone, and Ethyl Butyrate. Diagrams drawn with Avagadro software 33

Figure 2.6 Illustration of Olfactory Sensory Neuron and depiction of cilia membrane proteins and signal transduction molecules. OBP- Odorant Binding Protein; OR-GPCR Odorant Receptor with trimeric G protein (alpha, beta, and gamma subunits); ACIII- Adenylyl Cyclase III; CNGC- Cyclic Nucleotide Gated Channel; ATP-adenosine tri-phosphate; CaCC- Calcium Activated Chloride Channel; PDE-Phosphodiesterase; RGS- Regulator of G-Proteins; PKA-Phosphokinase A; ORK- Odorant Receptor Kinase; $Na^{+/}$ Ca^{2+} ion transporter NCKX4; NKCC1 ion transporter; CaCm- Calcium calmodulin. Illustration by Melissa Singletary 35

Figure 2.7 Representative EOG recordings from rat olfactory epithelium. The stimuli were of 0.25 s pulses of (1) standard odorant mixture (SOS), (2) odorant mixture + zinc nanoparticles, (3) odorant mixture + copper nanoparticles, (4) odorant mixture + silver nanoparticles, (5) odorant mixture + gold nanoparticles, (6) odorant mixture + platinum nanoparticles, (7) water vapor, (8) standard odorant mixture (SOS), (9/10) odorant mixture + zinc nanoparticles, The concentration of odorant

mixture was 1.6 mmole/L 54

Figure 3.1 Transmission electron microscopy of zinc metal nanoparticles. (a) bar: 5 nm. (b) bar: 2 nm 76

Figure 3.2 Physical characterization of small zinc nanoparticles. a. Atomic force microscope image, 0.01% zinc nanoparticles on mica. 270 nanoparticles with height above 1 nm were detected over a 2.5 μm2 area. b. Size distribution of the particles imaged in a. (Permission from Dovepress # 11575629) 77

Figure 3.3 XPS Zinc nanoparticles. High-resolution XPS analysis showing the Zn 2p3/2 core line, with the Zn peak occurring at a binding energy of 1020.9 eV and the ZnO peak occurring at 1022.5 eV 78

Figure 3.4 Representative EOG recordings from rat olfactory epithelium. The stimuli were of 0.25-s pulses of (1) odorant mixture, (2) odorant mixture +1.2-nm zinc nanoparticles, (3) odorant + 1.2-nm ZnO nanoparticles, (4, 5) water vapor. This is a typical representation of 300 traces 80

Figure 3.5 Representative EOG recordings from rat olfactory and respiratory epithelia. The stimuli were of 0.25-s pulses of odorant with or without nanoparticles. (1) olfactory epithelium, odorant mixture, (2) olfactory epithelium, odorant mixture +small zinc nanoparticles, (3) respiratory epithelium, odorant mixture, (4) respiratory epithelium, the odorant mixture + small zinc nanoparticles 81

Figure 3.6 Graph of relative amplitude in mV for small (1.2 nm) zinc nanoparticles, small (1.2 nm) oxidized zinc nanoparticles, zinc oxide 15 nm, and zinc oxide 70 nm. Statistical significance found between all oxidized zinc nanoparticles (1.2 nm, 15 nm, and 70 nm) and non-oxidized zinc nanoparticles $p < 0.05$ 83

Figure 3.7 Illustration of Zinc Nanoparticles demonstrating hexagonal close packed lattice and 12 core atoms and 47 shell atoms and 1.2 nm. Illustration by Melissa Singletary 87

Figure 4.1 Physical properties of non-PEGylated and PEGylated zinc nanoparticles. (a) AFM images, and (b) histograms showing the size distribution of the nanoparticles. A: Zinc nanoparticles, B: ZnPEG400, C: ZnPEG1000 108

Figure 4.2 Electron microscopy images of Zn, ZnPEG400, and ZnPEG1000 nanoparticles. TEM images (a, c, d) are showing the primarily-elemental zinc nanoparticles at different magnifications, (b) ZnPEG400 nanoparticle showing the metal core and the PEG passivation layer, (e) ZnPEG1000

nanoparticles with negative staining, and (f) ZnPEG1000 magnified from (e). The numbers 1, 2, 3 point to the nanoparticles with visible lattice fringe patterns, indicating their crystallinity. 110

Figure 4.3 XPS spectra. Representative high resolution XPS spectra showing (a) C 1s and (b) Zn 2p3/2 core lines for the freshly prepared bare zinc and PEGylated zinc nanoparticles stored 1 day at 278 K (5 ^{o}C), with the spectra offset to facilitate viewing. The Zn 2p spectra are shown in log-scale. The solid curves indicate the experimentally obtained spectra, with the dotted curves underneath indicating their best-fit chemical components. For the C 1s spectra, from lower to higher binding energy, the components are C-C, C-O, and C=O. For the Zn 2p spectra, the components are Zn and ZnO. For the (a) C 1s plots, the solid vertical line represents the position of the C-C peaks, to which all spectra were calibrated to, with the dotted lines showing the spectral shift of the C-O peaks, which were 286 eV, 286.4 eV, and 286.2 eV for the Zn, ZnPEG400, and ZnPEG1000 systems, respectively. For (b) Zn 2p plots, the solid line represents the position of the Zn peak for the bare Zn system, while the dotted lines show the spectral shift of the ZnO peaks, which were 1024.6 eV, 1025.6 eV, and 1026.0 eV for the Zn, ZnPEG400, and ZnPEG1000 systems, respectively. Each spectrum represents an average of six spectral runs. 112

Figure 4.4 Representative EOG recordings from rat olfactory epithelium. The stimuli were of 0.25 s pulses of (1) odorant mixture, (2) odorant mixture +1.2 nm zinc nanoparticles, (3) odorant mixture + 0.25 mmole/L PEG400, (4) odorant mixture + 0.10 mmole/L PEG1000, (5) water vapor + PEG400, (6) water vapor + PEG1000, and (7) water vapor. The concentration of zinc nanoparticles and odorant mixture were 0.02 nmole/L and 1.6 mmole/L , respectively. The representative set of traces was obtained from 50 EOG traces 118

Figure 4.5 The relative EOG signals as a function of time of storage of zinc nanoparticles. The difference between peak values of EOG evoked by odorant and by non-PEGylated and PEGylated zinc nanoparticles was normalized by the EOG peak evoked by an odorant alone. The relative enhancement by zinc nanoparticles was calculated as described in Materials and methods. 120

Figure 4.6 The relative EOG signals evoked by non-PEGylated and PEGylated zinc nanoparticles a. The relative enhancement by non-PEGylated zinc nanoparticles as a function of ZnO concentration. The difference between peak values of EOG evoked by odorant and by zinc nanoparticles was normalized by the EOG peak evoked by an odorant alone as a function of ZnO concentration that was determined by XPS. The first bar at 3 % of ZnO, corresponds to zinc nanoparticles stored one day at 278 K (5 ^{o}C).

The second and third bars reflect zinc nanoparticles stored for two days at 303 K (30 ^{o}C) and 323 K (50 ^{o}C), at 7.1 % and 7.8 % respectively. The forth bar at 11.5 % of ZnO corresponds to the negative enhancement (inhibition) that was observed with zinc nanoparticles oxidized by percolating air. **b**. The relative EOG enhancement produced by ZnPEG400 nanoparticles after they were stored for one day at 278 K (5 ^{o}C), two days at 303 K (30 ^{o}C) and 323 K (50 ^{o}C), respectively. **c**. The relative EOG enhancement produced by ZnPEG1000 nanoparticles after they were stored for one day at 278 K (5 ^{o}C), two days at 303 K (30 ^{o}C) and 323 K (50 ^{o}C), respectively. 122

Figure 5.1 EOG responses to 1.6 mM odorant (Odorant), 1.6 nM odorant + nanoparticles obtained from olfactory epithelium (Odorant + O_{NPs}), 1.6 nM odorant + nanoparticles obtained from respiratory epithelium (Odorant + R_{NPs}), 1.6 nM odorant + 0.01 nM engineered Zn nanoparticles (Odorant + Zn), and water vapor (Water vapor). 145

Figure 5.2 EOG peak mean values for 18 EOG experiments. ANOVA statistical test of variance showed that all mean values are significantly different at the level of $p<0.05$ [$F(4, 115)=200$, $p=0.0$]. 146

Figure 5.3 Relative EOG peaks as a function of engineered zinc concentration (Ration of EOG peak by (O+Zn)/O. Points are experimental data, line is a linear fit (R-Square=0.997; Intercept=0.99±0.02, Slope=73.6±2.7 1/nm). 147

Figure 5.4 The estimated concentrations of nanoparticles with zinc-like attributes in olfaction enhancement within the olfactory epithelial filtrate (OE) and respiratory filtrate (RE). 148

Figure 5.5 The estimated concentrations of nanoparticles with zinc-like attributes in olfaction enhancement within the olfactory epithelium (OE) and respiratory epithelium (RE) 149

Figure 6.1 Relative viability of screening on multiple bacterial taxa. Results are shown as a mean and standard deviation relative to control growth (100%). Data representative of 24-hour spectrophotometric reading at optical density 595 nm. Bacterial species selected included *Escherichia coli* M-17, *Shigella flexneri, Salmonella typhimurium* 52096, *Staphylococcus aureus* ATCC 12600, MRSA-1, 2, 5, 13, 26, 34 and 45, *Lactobacillus acidophilus, Bacillus subtilis* BSB3, *Bacillus subtilis* BS, and *Bacillus licheniformis* BL. 160

Figure 6.2 MRSA-1 Respective measurement at OD_{595} nm as representation of viability at 24 hours. Statistical significance of reduced bacterial viability with the addition of zinc nanoparticles from total zinc concentrations of 0.1276 ng/µl, 0.225 ng/µl, 0.51 ng/µl, and 0.765 ng/µl at 5, 10, 20, and 30 µl respectively ($p<0.05$). 161

Figure 6.3 MRSA-2 Respective measurement at OD_{595} nm as representation of viability at 24 hours. Statistical significance of reduced bacterial viability with the addition of zinc nanoparticles from total zinc concentrations of 0.225 ng/µl, 0.51 ng/µl, and 0.765 ng/µl at 10, 20, and 30 µl respectively ($p<0.05$). 162

Figure 6.4 MRSA-5 Respective measurement at OD_{595} nm as representation of viability at 24 hours. Statistical significance of reduced bacterial viability with the addition of zinc nanoparticles from total zinc concentration of 0.765 ng/µl at 30 µl ($p<0.05$). Statistical significance of increased relative bacterial viability with the addition of zinc nanoparticles from total zinc concentrations of 0.1276 ng/µl, at 5 µl ($p<0.05$). 163

Figure 6.5 MRSA-13 Respective measurement at OD_{595} nm as representation of viability at 24 hours. Statistical significance of reduced bacterial viability with the addition of zinc nanoparticles from total zinc concentration of 0.765 ng/µl at 30 µl ($p<0.05$). Statistical significance of increased relative bacterial viability with the addition of zinc nanoparticles from total zinc concentrations of 0.1276 ng/µl, at 5 µl ($p<0.05$). 164

Figure 6.6 MRSA-26 Respective measurement at OD_{595} nm as representation of viability at 24 hours. Statistical significance of increased bacterial viability with the addition of zinc nanoparticles at a total zinc concentration of 0.1276 ng/µl, at 5 µl ($p<0.05$). 165

Figure 6.7 MRSA-34 Respective measurement at OD_{595} nm as representation of viability at 24 hours. Statistical significance of reduced bacterial viability with the addition of zinc nanoparticles from total zinc concentrations of 0.225 ng/µl, 0.51 ng/µl, and 0.765 ng/µl at 10, 20, and 30 µl respectively ($p<0.05$). 166

Figure 6.8 MRSA-45 Respective measurement at OD_{595} nm as representation of viability at 24 hours. Statistical significance of reduced bacterial viability with the addition of zinc nanoparticles from total zinc concentrations of 0.225 ng/µl, 0.51 ng/µl, and 0.765 ng/µl at 10, 20, and 30 µl respectively ($p<0.05$). 167

Figure 6.9 BS: *Bacillus subtilis* Respective measurement at OD_{595} nm as representation of viability at 24 hours. Statistical significance of increased bacterial viability with the addition of zinc nanoparticles from total zinc concentration of 0.765 ng/µl, at 30 µl ($p<0.05$). 168

Figure 6.10 Relative viability for MRSA strains 1, 2, 5, 13, 26, 34, and 45 and *Bacillus subtilis* determined by spectrophotometry. Data shown represents runs in triplicates. 169

List of Abbreviations

AC III- Adenylyl Cyclase Type III

AFM- Atomic Force Microscopy

BL- *Bacillus licheniformis*

BS- *Bacillus subtilis*

CaBP- Calcium Binding Protein

cAMP- Cyclic Adenosine Monophosphate

CFU - Colony forming unit

cGMP- Cyclic

CNG- Channel- Cyclic Nucleotide Gated Ion Channel

CNS- Central Nervous System

CNV- Copy number variation

CYP- Cytochrome

EOG- Electroolfactogram

fMRI- Functional magnetic resonance imaging

G- - Gram-negative

G+ - Gram-positive

GABA- Gamma-aminobutyric acid

GBC- Globose Basal Cell

GC-D- Guanyl-cyclase

GDP- Guanosine diphosphate

GG- Grunbergs ganglion

Golf- Olfactory G-Protein

GPCR- G-protein Coupled Receptor

GTP- Guanidine Triphosphate

Gα- Alpha subunit

Gβ- Beta subunit

Gγ- subunit- Gamma subunit

HBC- Horizontal basal cell

IBMX- 3-isobutyl-1-methylxanthine

IETS- Inelastic tunneling spectroscopy

LDV- Laser Doppler Velocimetry

MMP- Metalloproteinase

MOE- Main olfactory epithelium

MRSA- methicillin resistant *Staphylococcus aureus*

NP- Nanoparticle

NSE- No significant effect

OB- Olfactory Bulb

OBP- Odorant Binding Protein

OD_{595} - Optical density at a wavelength of 595 nm

OE- Olfactory Epithelium

OEC- Olfactory ensheathing cell

OMP- Olfactory marker protein

OR- Odorant Receptor/Olfactory Receptor

ORK- Olfactory Receptor Kinase

ORN/OSN- Olfactory Receptor Neuron/Olfactory Sensory Neuron

PDE- Phosphodiesterase

PEG- Polyethylene Glycol

PEG1000- 1000 MW Polyethylene Glycol

PEG400- 400 MW Polyethylene Glycol

PKA- Protein Kinase A

PNCs- Proteon Nucleating Centers

RE- Respiratory Epithelium

RGS2- Regulator of G-protein signaling 2

ROS- Reactive oxygen species

SEM- Scanning Electron Microscopy

SNPs- Single nucleotide polymorphism

SO- Septal organ

SOS- Standard Odorant Suspension

TAARs- Trace amine associated receptors

TEM- Transmission Electron Microscopy

V1R- Vomeronasal receptor type 1

V2R- Vomeronasal receptor type 2

VNO- Vomeronasal organ

XPS- X-ray Photoelectron Microscopy

ZENs- Zinc enriched neurons

ZnNPs- Zinc nanoparticles

ZnO- Zinc oxide

ZnT- Zinc transporter protein

Chapter 1.0 Introduction

The sensory system of olfaction plays a critical physiological function and is a fundamental component of interpreting the environment around us. Smell can alert for danger, such as smoke in the air, can assist in finding food or indicates spoiled foods, support sexual and maternal bonding, increase social behavior, reduce anxiety, and is vividly linked to memories, and emotions (Persuy et al. 2015, Hernandez et al. 2002, Willander and Larsson 2007, Takahashi et al. 2005).

The olfactory sensory neuron, which is the principle functional unit responsible for the first tier of neuronal signaling in smell, sends out feeler cilia on the surface of the olfactory epithelial tissue inside the nose. The initial events that occur on those cilia, at the olfactory receptor, is where the odorants will first engage with the olfactory system leading to the eventual perception of smell. These molecular interactions at the receptor-odorant interface that lead to the recognition of odorant have not been fully elucidated. With innovative technology, a world of interaction on a nano-scale is being explored.

Nanoparticles dancing in the background of a blood sample examined under a high-resolution light microscopy system led to the discovery of naturally present metal nanoparticles in the blood of both humans and animals (Samoylov et al. 2005). Of those metals, only zinc metal nanoparticles were shown to enhance the sense of smell by about 3-fold on electroolfactogram and whole-cell patch clamp (Viswaprakash et al. 2009, Viswaprakash et al. 2006). In small concentrations, effects of zinc nanoparticles (ZnNPs)

on olfaction were dose-dependent and reversible. The particles are spontaneously eliminated from the olfactory mucosa; providing a specific, sensitive, and efficient way of olfactory response control.

Metals play an important role in biology and neurobiology, with significant implications in olfaction through the olfactory bulb and higher cognitive centers (Frederickson and Danscher 1990, Sensi et al. 2009). Zinc is found within the cerebrospinal fluid at concentrations estimated at 31.5 μgL^{-1} (Agarwal and Henkin 1982). Intriguingly, ionic zinc plays a role in secondary and tertiary signaling in olfaction, but when applied to the olfactory epithelium it is inhibitory to olfaction, and in fact, zinc salts are commonly used to induce anosmia in experimental settings (Ishimaru et al. 2000, Smith 1938, Rowe and Smith 1972). This is in contrast to the enhancement seen with ZnNPs.

In an investigation to determine the general location of ZnNP interaction with the transduction pathway in the olfactory sensory neuron, an inhibitor of phosphodiesterase was used to prevent the enzymatic degradation of the second messenger cyclic adenosine monophosphate (cAMP). The intracellular rise of cAMP levels initiates the opening of ion channels and further pathway proteins that lead to an action potential. Arbitrary elevation of cAMP in the absence of an odorant is a method to bypass the GPCR complex at the cellular membrane to produce activation. ZnNPs did not enhance the activation in the presence of the membrane-permeable phosphodiesterase inhibitor, 3-isobutyl-1-methylxanthine (IBMX) (Moore et al. 2012). Based on this lack of enhancement within the transduction cascade post-GPCR complex, we propose that the zinc nanoparticles exert their function at the olfactory receptor level and are engaged in the initial events of

olfaction. This localization supports a described kinetic model of olfactory receptor/odorant/metal interactions (Vodyanoy 2010). The kinetic olfactory model estimated that one metal nanoparticle binds two receptor molecules to make a dimer.

Further *in vivo* evaluation with functional magnetic resonance imaging (fMRI) demonstrated increased activity within the olfactory pathway of higher brain centers to an odorant mixture in the presence of zinc nanoparticles compared to odorant mixture alone (Jia et al. 2012, Jia et al. 2014, Jia et al. 2015). This enhancing effect of zinc nanoparticles is only seen in the presence of odorant and evokes no receptor activation alone. Canine detection dogs at Auburn's training facility were trained to sit awake in an MRI magnet-core to subsequently undergo evaluation of the perception of odorant, particularly in activation of the orbitofrontal cortex in anesthetized versus awake states as well as odorants with and without zinc nanoparticles. A higher degree of activity in the awake state suggested an increased perception of odorant and this was enhanced in the presence of zinc nanoparticles (Jia et al. 2012, Jia et al. 2014, Jia et al. 2015).

The effects can vary with metallic nanoparticles compared to their parent metal or metal salts and have been attributed in part due to the large surface-to-volume ratio. Small metal and metal composite nanoparticles have certain advantages compared to other particles due to their capability to specifically interact with proteins, peptides, and nucleic acids (Hassan and Singh 2014) and ability cross biological barriers (Gidwani and Singh 2014).

Combined, the work in isolated rat olfactory epithelium and in an awake canine model, support an increase in olfactory neuron activation to odorant and increase of the higher cognitive areas involved in the processing of odorant perception. This discovery

opened an unexplored field of nanoparticle interactions with the olfactory receptors and the local epithelial environment surrounding them, including the endogenous nanoparticles within the mucous layer and the normal microbiota.

For odorants to interact with olfactory receptors, they must travel through olfactory epithelial mucus layer and may be influenced during transit by any number of mucus constituents such as microbiota, enzymes, proteins, and metals. The microbiota of the olfactory system is not well established, but emerging work demonstrates a microbial population similar though differing in composition to other mucosal sites. The presence of this community implies that endogenous and exogenous zinc nanoparticles may influence the balance maintained in this system. The antimicrobial effects of zinc are historical and predate current antibiotic methods of bacterial control, particularly in their use of dermatological conditions and ocular therapeutics (Haxthausen and Rasch 1928).

The evaluation of zinc nanoparticles and their role in the initial events of olfaction is coupled with the evaluation of zinc nanoparticles as an application for olfaction enhancement. Characterization and stabilization of the zinc nanoparticles can provide support for a viable translation into exogenous applications and provide insights into further understanding their potential biological mechanism of action through their physical-chemical properties. Furthermore, an appreciation for the influence that zinc nanoparticles in a potential application can have on the microenvironment of the olfactory system can also provide insight into the biological role of zinc nanoparticles in mucosal sites and the consideration for side-effects in homeostatic mucosal conditions when applied exogenously.

This series of studies target characterizing the olfaction enhancing zinc nanoparticles and oxidized zinc nanoparticles by physical-chemical means. Functional evaluation with electrophysiology and determination of chemical composition were performed with EOG, AFM, XPS, TEM, LDV, and ion quantification. Evaluate the use of PEGylation of the zinc nanoparticles using 1000 g/mol or 400 g/mol molecular weight polyethylene glycol (PEG) would afford retention of the olfactory enhancement. The PEGylation is a chemical process involving the passivation of the surface of nanoparticles by PEG, a coiled polymer with multiple ethylene ether units that are soluble in water (Jokerst et al. 2011). The PEGylation apparently decreases the rate of oxidation. It can provide an increased affinity to the target protein and reduced cytotoxicity of nanoparticles (Jokerst et al. 2011). The PEGylation is broadly used for protection of nanoparticles against aggregation in the biological and pharmaceutical applications (Suk et al. 2016, Otsuka, Nagasaki, and Kataoka 2003). Although there are many publications on the PEGylated zinc oxide nanoparticles (Karakoti et al. 2011, Sirelkhatim et al. 2015) this is the first study of PEGylated elemental zinc nanoparticles. We characterized the PEGylated nanoparticles using scanning electron microscopy (SEM), TEM, AFM, XPS, and LDV. This study will evaluate the influence of ZnNPs on a broad spectrum of bacteria co-cultured with four concentrations of small <2nm non-oxidized zinc nanoparticles and a refined strain selection of pathogenic methicillin-resistant *Staphylococcus aureus* (MRSA) in contrast to *Bacillus subtilis*.

Chapter 2.0 Review of Literature

2.1 Olfactory System Overview and Anatomy

2.1.1 Nasal Cavity

From the entrance at the nares, an odorant will travel through the nasal vestibule, past the nasal meatuses on to the ethmoturbinates to reach the sensory cilia of the olfactory epithelium where the odorant will interact with receptors and initiate the cascade of events that lead to the recognition of a smell. The nasal cavity is divided into three main anatomical regions which encompass the nasal vestibule, the respiratory epithelium, and the olfactory epithelium (Craven et al. 2007). There are roles to be played by each part of the pathway and can be species-specific in function.

The skull forms the boney support for the structures that collectively form the upper airways and olfactory system. The passageway is formed by the bilateral incisive bones on its rostroventral surface, laterally to dorsolaterally the walls are formed by the maxillary bone, rostrodorsally by the nasal bone, and the most caudal aspect formed by the ethmoid bone. The ethmoid bone has three parts, including the nasal septum running from caudal to rostral dividing the two nasal passages left to right, the ethmoturbinates (or ethmoid labyrinth), and the osseous cribriform plate with numerous small perforations that communicate directly with the cranium. The caudoventral part of the nasal septum is formed by an osseous bone, the vomer bone, which is part of the roof of the choanae. The choanae form the openings of the left and right nasal cavities to the nasopharyngeal meatus (Howard E. Evans 2013). As the first anatomical feature encountered by an odorant, the structure of the nares influences odorant delivery. There are differences in the gross anatomy of the olfactory system across species, from the blind-ended cavity and

four nostrils of a fish to the dual respiratory-olfactory nasal cavity and two nostrils of most mammals. Two of the four nostrils in teleosts connect to form a one-way system of flow to an olfactory organ. This singular directional flow system for odorant delivery and transportation allows for continuous access to new odors without a delay in the chain (Niimura 2012). The wide distance and lateral positioning of the nares have been implicated in assisting with location and directional cues for some aquatic species particularly useful in low visibility. In canines, the paired nares feature medially located openings with ventrolateral slits that allow for air flow bringing odorants in centrally and an ability to purge the air laterally (Craven, Paterson, and Settles 2010).

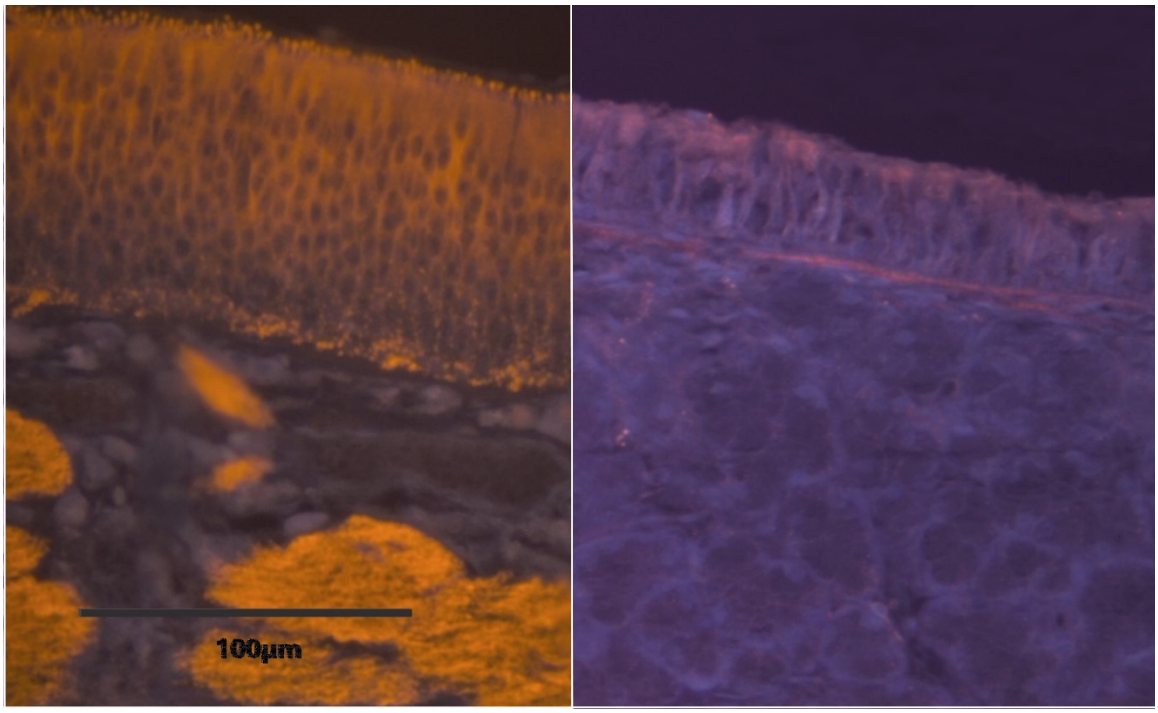

Figure 2.1 Histology of Olfactory Epithelium compared to Respiratory Epithelium. Anti-olfactory marker protein immunofluorescent staining orange (Alexa 555). OMP is selective for mature olfactory sensory neurons.

Odorants first enter the nasal cavity that is lined in the most anterior portion by a stratified squamous epithelium (Randall, Bogdanffy, and Morgan 1987). This passageway, collectively called the vestibule, leads to divisions into meatuses, also referred to as turbinals or concha. These structures include the maxilloturbinal, nasoturbinal and ethmoturbinals which extend from the lateral walls of the nasal cavity and display inward folds. Within the middle nasal vestibule, the three main division in the canine that are generally identified are the dorsal, ventral, and middle meatus on gross anatomical dissection (Moore 1981). The number of meatuses, turbinals or concha vary between species. These structures are modeled to play a role in directing airflow, reducing turbulence, and creating a sub-climate for inspired air to be warmed, humidified and filtered (Menco and Morrison 2003). In mammals, this passageway is a dual-purpose portal of entry for air to bring in odorants to the olfactory system but critically bring in oxygen to the pulmonary system. The upper airway system, including the nasal cavity, larynx and trachea, plays an important role in protecting the vulnerable lower airway system. The respiratory epithelium that begins following a transition from the anterior stratified squamous epithelium and ends in a transition to olfactory epithelium in the posterior aspect. The respiratory epithelium secretes high levels of defensins and antimicrobial peptides within the mucous layer lining. This mucous layer lies atop a stratified columnar epithelium covered in motile cilia. The role of this cilia is to beat rhythmically in a fashion that moves the mucus in a continuous flowing fashion to trap and remove unwanted particles from the inhaled air. This mucous is eventually brought to the nasopharynx where it is discarded into the gastrointestinal tract or is brought forward to the nasal vestibule for removal by sneezing or by a forced blow. Mucosa

provides a microenvironment that is shown to be home to a host of microbes that play a role in immunological protection from competitive inhibition, antimicrobial peptide production, and enzymatic degradation, to innate immune cell priming. The best studied of these mucosal sites is within the gastrointestinal tract followed distantly by the respiratory tract. These studies have neglected to evaluate the olfactory mucosa as a separate system and only recently has a study considered the microbiota of the olfactory system (Francois et al. 2016).

The air with odorant particles are filtered, warmed and humified throughout their passage and continue to the heavily scrolled labyrinth of the ethmotubrinates located in the most caudal aspect of the nasal cavity where odorants will interact with receptors that line the cilia of the olfactory sensory neuron cell in the olfactory mucosa. The orthonasal route of odorant introduction is the "classically" described nasal passageway both passive exposure and active exposure with sniffing. In addition to the orthonasal route, odorants in mammals can be retronasally introduced to the olfactory epithelium. This route is when odorants propagate from the oral cavity through the choanae in the caudodorsal nasopharynx to reach the nasal cavity and olfactory epithelium, thus the OR for recognition (Small et al. 2005).

The olfactory system is one of two main chemosensory systems in mammals along with gustation. It has been evolutionarily conserved and considered the first sensory system to develop evolutionarily and remains the largest gene superfamily in mammals (Niimura 2012, Glusman et al. 2001, Reed 2004, Persuy et al. 2015). There are two main divisions of the olfactory system and two lesser divisions in species such as rodents. The first is responsible for the detection of volatile compounds and is the largest

of the olfactory system, the main olfactory epithelium (MOE). Second is mostly responsible for the detection of pheromones, the vomeronasal organ (VNO). The two smaller described additions to the olfactory system particularly in rodents are Grueneberg's ganglion and the septal organ (SO), also referred to as the Organ of Masera (Rodolfo-Maera 1943). Grueneberg's ganglion (GG) is located separate and isolated from the MOE in the rostrodorsal aspect of the nasal cavity and is suggested to have a thermosensory capacity at sensing coolness (Mamasuew, Breer, and Fleischer 2008) and chemosensory capacity for alarm pheromones (Kikusui et al. 2001). Grueneberg's ganglion has been identified and is present in humans, but the determination of similar function to rodents is not established (Gruneberg 1973). The septal organ is an isolated patch of neuroepithelium located on both the left and right of midline on the caudoventral aspect of the nasal septum and present in rodents and other mammals such as the koala (Kratzing 1984). The function of the SO is thought to serve as an airflow sensor (Ma 2010) and traditional chemosensation similar to the MOE with a much lower number of receptor’s in its repertoire (Grosmaitre et al. 2007).

2.1.2 Main Olfactory Epithelium

The MOE is a pseudostratified ciliated columnar epithelium. Figure 2.2 is a depiction of the MOE and its major cellular components. The sensory cells that are the functional unit of olfaction are the olfactory sensory neurons (OSNs). The OSN is surrounded by supporting (sustentacular) cells that are topped with microvilli and span from the mucosal surface to the basement membrane providing structural integrity to the epithelium. The composition of the epithelial structure includes four principal cells including the support cells, the OSNs, basal cells (OSN stem cells), and the Bowman's glands duct cells (Menco and Morrison 2003, Moran et al. 1982). The basal cells are further categorized as globoid or horizontal basal cells (GBCs and HBCs) (Menco and Morrison 2003). The subepithelial structure is composed of the Bowman's glands acinar cells and glandular bulbs, OSN axon bundles and fascicles, Schwann cells, blood vessels, lymphatic ducts, olfactory ensheathing cells and connective tissue (Ramon-Cueto and Avila 1998). The bowman's glands are the primary secretory gland of the olfactory epithelium with the sustentacular cells also contributing, while the goblet cells represent the principal secretory cells in the respiratory tract (Solbu and Holen 2012). The contents of the mucus and serous secretions from the bowman’s gland are diverse including enzymes, acids, mucopolysaccharides, immune factors, antioxidants, and numerous proteins such as antimicrobial proteins and odorant binding proteins (OBP).

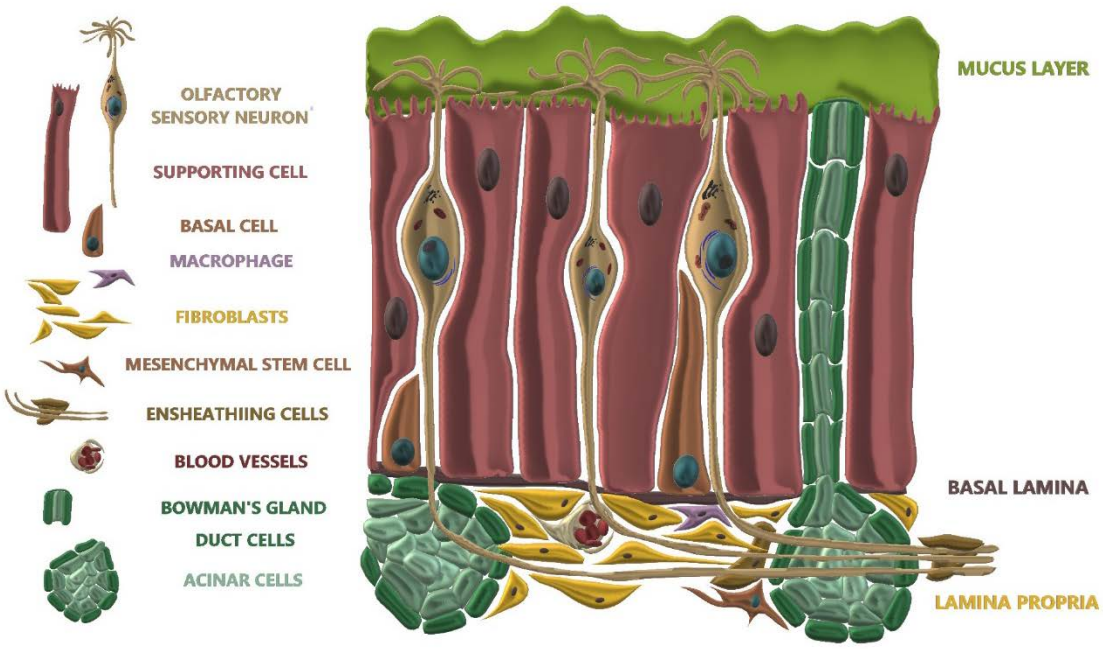

Figure 2.2 Main Olfactory Epithelium (MOE) illustration. Illustration by Melissa Singletary.

The OSNs, also called olfactory receptor neurons (ORN), are true bipolar neurons with a dendrite terminating in approximately 20-30 cilia at the mucosal surface and a single axon that extends to the olfactory bulb (Morrison and Costanzo 1990). The dendritic tree that is formed by the OSN increases the surface area of the receptive field and collectively form the dendritic knob. The increased surface area is estimated at 23 cm^2, which is magnified in consideration of the estimated knob density at up to 60,000 knobs/mm^2 (Doty 1998, Menco and Jackson 1997). The sensory non-motile cilia that form a dendritic knob protrudes into the mucous layer at the mucosal surface allowing for a sampling of the odorants that are dissolved or transported from the inspired air. The soma or cell body then extends a single axon that collectively with all OSN axons form

what is termed the first cranial nerve, the olfactory nerve, classified as a special visceral afferent (SVA) fiber (Doty 1998).

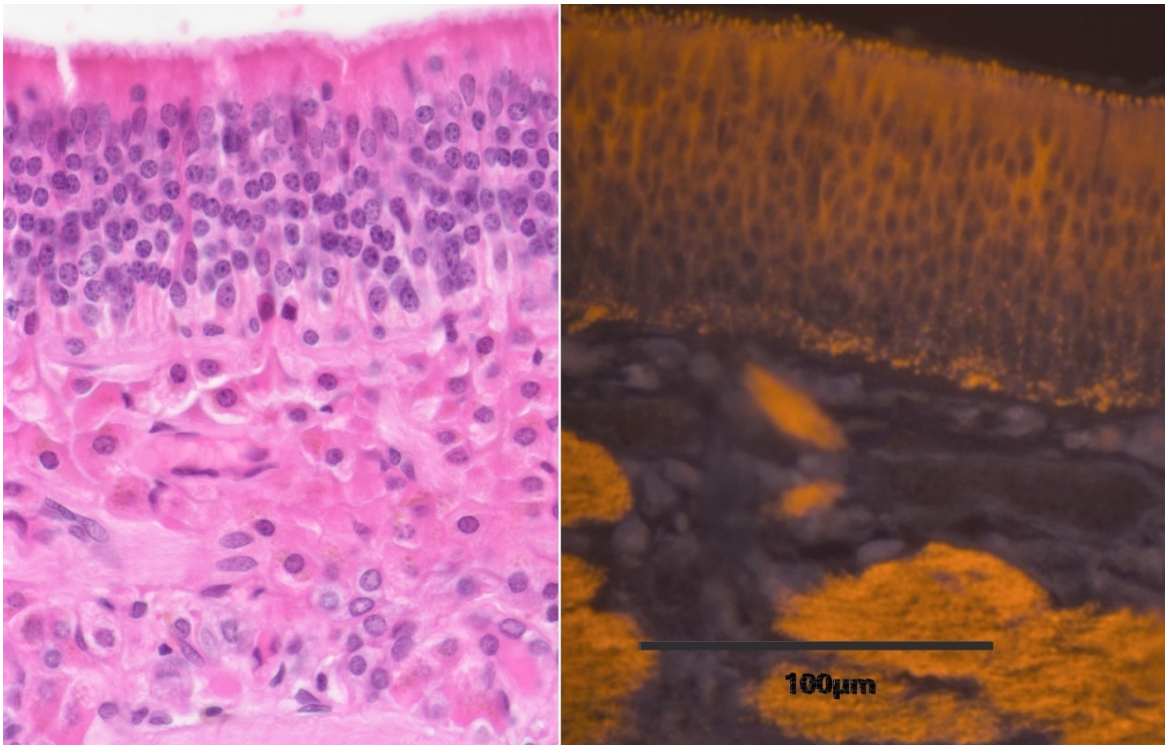

Figure 2.3 Histological section of Main Olfactory Epithelium (MOE). Left image hematoxylin and eosin stain (H&E) under high-resolution light microscopy (CytoViva). Right image anti-olfactory marker protein (OMP) immunofluorescent tagged orange (Alexa 555) under high-resolution dark microscopy (CytoViva).

OSNs are exposed to the external environment on a continual basis. This is a unique feature for this neuron in comparison to the majority of neuron types, and thus requires an ability for this sensory function to recover from injury. The mechanism of olfaction recovery is through a particular cell type, the basal cell, that is an OSN stem cell able to initiate development when needed to replace a damaged OSN. The new OSN will grow a new dendrite to extend to the mucosal surface and a new axon that will navigate

its way through the cribriform plate perforations and find its synaptic target within a glomerulus of the olfactory bulb and reestablish a complete synapse. Metals are essential in cell motility and axonal outgrowth within the extracellular matrix through matrix metalloproteinases (MMPs). This family is important in both physiological and pathological conditions (Ould-Yahoui et al. 2013). The OEC is essential in supporting the migration of the new axons to their target glomeruli, as glial cells the OEC exhibits phenotypic and functional properties onto OSNs and basal cells in the OE to aide in axonal elongation (Ramon-Cueto and Avila 1998).

This regenerative quality of the olfactory sensory neurons allows for the olfactory system to recover an individual OSN within a remarkably quick period of approximately 4-8 weeks in humans with variation seen amongst species (Costanzo 1991). The HBC are round cells located above the basement membrane with a centrally located nucleus and are proposed to represent the tissue stem cells while the GBCs are the proliferative cell population for the OSNs (Suzuki et al. 2013, Mackay-Sim 2010).

2.2 Olfactory Receptors

The olfactory system across species is a critical system well represented by the high number of olfactory odorant receptor (OR) genes present, as abundant as to represent the largest gene superfamily (Persuy et al. 2015) and from 1-3% of the estimated mammalian gene repertoire (Glusman et al. 2001, Reed 2004). The OR gene origins can be traced back to the common ancestor of the phylum Chordata, demonstrating an important role throughout evolution in all vertebrate (Niimura 2012).

This likely reflects the multiple roles and possible undiscovered roles of olfactory receptors and olfactory receptor neurons. Physiologically the olfactory system is involved in critical survival functions such as foraging, feeding, hunting, predator avoidance, spatial orientation, and stress. It also plays a role in the psychological processes of social behaviors, reproduction and maternal bonding (Persuy et al. 2015).

The OR has been identified as a G-protein coupled receptor (GPCR) representing the largest family of GPCRs, the Rhodopsin family. This 7-transmembrane receptor type operates to allow for signal amplification translating very minute detectable amounts of odorant stimuli and transmitting that signal to higher centers in the brain. For the unknown amount of possible odorant molecules that could be encountered and a relative OR specificity, this sensory system requires a complex combinatorial control or code. The combinations of G-proteins present, cellular partners that are present and the odorant itself can create subsequent activated pathway changes. There is a great deal of variation in the number of OR genes across species as well as a diversity of the OR repertoire. An example is in mice where they have a receptor for detecting CO_2, which is odorless to humans that lack this receptor for detection in their repertoire (Hu et al. 2007). Selection pressures have pushed this diversity as the olfactory system works in direct response to its environment. In teleost's such as the Zebrafish, they demonstrate lower OR gene numbers than humans but demonstrate more diversity amongst those numbers than humans (Table 2.1) (Niimura 2012).

Table 2.1 Olfactory Receptor Genes Species Variance

Species	Approx OR Genes	Identified % Pseudogenes	Reference
Human	860	50-60%	((Zozulya, Echeverri, and Nguyen 2001); Gilad, Man et al. 2005)
Mouse	1000	23%	((Young and Trask 2002); Gilad, Man et al. 2005)
Rat	1700	28%	(Young and Trask 2002; Gilad, Man et al. 2005)
Zebrafish	133	12%	(Niimura 2012; Saraiva, Ahuja et al. 2015)
Dog	1100	20%	((Quignon et al. 2003); Niimura 2012)
Pig	1300	9%	(Nguyen et al. 2012)
Primate (Chimpanzee)	813	50-60%	(Gilad, Man et al. 2005; Niimura 2012)
African Elephant	4200	53%	(Niimura, Matsui et al. 2014)
Chicken (*Gallus gallus*)	479	23%	(Steiger, Kuryshev et al. 2009)
Zebra Finch (*Taeniopygia guttata*)	553	40%	(Steiger, Kuryshev et al. 2009)
Green Anole (*Anolis carolinensis)*	156	27%	(Steiger et al. 2009)

Of the OR genes present, there is a portion of them that are categorized as pseudogenes. These are sequences that contain frameshift mutations, nonsense mutations or long deletions. A second category includes the partial sequence of an intact gene, the truncated gene that maintains the potential to become intact upon completion of genome

sequencing. The functional OR gene category typically includes the intact genes and the truncated genes (Niimura 2012). The intact genes are the continuous sequences starting at the initiation codon and ending at the stop codon. They do not display long deletions, and their motifs remain well-conserved. These numbers are not absolute and are approximate as the truncated genes could also represent pseudogenes and intact genes could also be nonfunctional. There is diversity from over 50% of the genes representing pseudogenes in some species such as humans, while less than 10% of the OR genes are representative of pseudogenes (Table 2.1).

The OR genes are further described by their class, broken down into Class I and Class II genes. Class I genes are more conserved and are thought to represent the class of receptors that mostly bind hydrophilic odorants/amino acids. Class I is further classified into groups based on odorant as airborne-detected by α group and water-soluble detected by the δ, ε, ζ, and η groups of Class I. Within Class I β group is thought to detect odorants that are both water soluble and airborne (Niimura 2012). Class II genes are considered to represent hydrophobic odorants that are airborne and include only the γ group. In the conservation of OR genes, mammals retain only the α group of Class I genes in addition to Class II while similarly Xenopus (amphibians) also encode Class I and II genes. However, teleosts encode Class I groups δ, ε, ζ, and η only with no Class II (Table 2.2). The term "fish" genes have been given to the Class I genes due to this selective Class representation. In a phylogenic analysis of zebrafish to mouse OR Class I, Alioto et al. demonstrated that the mice exhibit similar average pairwise identity to the zebrafish families with 27.3 ± 4.8%SD identity. In comparison mouse Class II to zebrafish families 27.7 ± 5.5%SD identity with the difference in mean values not being

significant. They further showed that calculations comparing consensus sequences representing each family yielded similar results (Alioto and Ngai 2005). The conservation of these "fish" genes is seen evolutionarily as the tendency over time to develop pseudogenes in a particular class has been more selectively limited to the Class II genes in comparison to the Class I genes in humans and has been interpreted to mean that these OR genes still have a functional significance in humans (Persuy et al. 2015, Niimura and Nei 2005c, a).

Table 2.2 Olfactory Receptor Genes Species Variance in Representative Class I and II Groups

Species	**α**	**Beta**	**γ**	**δ**	**ε**	**ζ**	**η**
Human	58	-	329	-	-	-	-
Mouse	113	3	947	-	-	-	-
Rat	136	2	1121	-	-	-	-
Zebrafish	-	1	1	62	12	37	38
Dog	161	1	660	-	-	-	-
Primate (Chimpanzee)	64	-	335	-	-	-	-
Chicken (*Gallus gallus*)	10	-	290	-	-	-	-
Zebra Finch (*Taeniopygia guttata*)	2	-	31	-	-	-	-
Green Anole (*Anolis carolinensis)*	1	-	108	-	-	-	-
**Representative of Intact OR Genes*				(Steiger, Kuryshev et al. 2009; Niimura 2012)			

2.2.1 Olfactory Receptor Gene Families

There are four olfactory receptor gene families in mammals, and only one has been discussed thus far, the olfactory (odorant) receptor, OR. This gene family shares their receptor type as a G-protein coupled receptors and includes the vomeronasal receptors, V1R and V2R, and the trace amine-associated receptors (TAARs). The accessory olfactory system, the vomeronasal organ (VNO), operates as an anatomically separate neural pathway in response to pheromones. Not all mammals have a VNO. It is considered degenerate in humans. Pheromones are processed differently than odorants are in the main olfactory system, they are received by one of only 2 vomeronasal receptors (V1Rs and V2Rs) that are expressed on microvillous sensory neurons in the vomeronasal organ that project their axons to the accessory OB (Korsching 2009). The level of diversity amongst OR genes is not appreciated in the VRs.

A novel group of GPCRs that are monogenetically expressed in the vomeronasal organ in a small subset of VNO neurons (~1%) are formyl peptide receptors (FPR) (Riviere et al. 2009). These receptors are also found within cells of the immune system and have been shown to respond to their namesake, formylated peptides, as well as inflammatory associated proteins (Le et al. 2007). Formyl peptides are released by bacteria, which have led to the consideration for these subsets of VNO neurons expressing FPR's to play a role in the detection of infected tissues, interspecies identification of infected induvial and contaminated foods (Riviere et al. 2009).

A subset of OSNs, termed GC-D neurons, will express guanylyl cyclase. These neurons do not display the characteristic cAMP pathway that is common to the OSNs in

the MOE but instead has a cGMP-phosphodiesterase (PDE2A) pathway. This pathway is non-canonical and utilizes cGMP-sensitive CNG's versus cAMP-sensitive CNG's. The information translated to the higher brain centers is communicated via GC-D neuron axons that synapse at the necklace glomeruli in the causal aspect of the olfactory bulb (Juilfs et al. 1997). The receptor is sensitive to urinary peptides, uroguanylin, and guanylin, and possibly carbon dioxide in certain species (Sun et al. 2009, Leinders-Zufall et al. 2007).

2.2.2 Gene Expression and Evolution

There have been two basic principles defined in mammals underlying the establishment of functional architecture within the olfactory system. The first is coined the "one neuron one receptor rule," where each olfactory receptor neuron (OSN) expressing only a single functional OR is tuned to only a specific molecular receptive range. This rule provides that a species can have a repertoire of any number of individual specialized OR's but only one on any given individual OSN. The second basic principle is that convergence of like axons from OSNs converge onto a target glomeruli, meaning that the OSNs expressing a given OR project and converge their axons to a topographically fixed glomerulus on the olfactory bulb (OB) (Korsching 2009). It is reported most consistently that the zebrafish ORs follow the one neuron one receptor rule. However, there are a few reports where exceptions have been noted in goldfish (Sato, Miyasaka, and Yoshihara 2007, Speca et al. 1999).

The signaling pathways and OR and OSN combinations produce an odor coding, providing given populations of olfactory neurons responding to specific odor molecules creating "odor maps" have been used to represent these pathways graphically. To understand the underlying molecular and neural mechanisms of odor detection and processing, the completion of the species and odorant specific maps are key to being able to visualize the pathway. They demonstrate the OR expression and OSN connectivity and can be as detailed to show resolution at the single-cell level. Some of the first maps have been in rabbits and Drosophila olfactory systems where even Drosophila represent the basic principles discussed. These maps demonstrated further insight into the molecular, anatomical, and functional organization of the Drosophila olfactory system (Couto, Alenius, and Dickson 2005). Rodent model axons originate from OSNs expressing a given OR that converge onto a specific pair of glomeruli in the OB, the second basic principle, and have been mapped in these models.

The average length of ORs is around 310 amino acids with several characteristic motifs described. An example motif that is located at the transmembrane region 3 (TM3) and intracellular loop junction between TM3 and TM4 is ‘MAYDRYVAIC.' Inside, the three amino acids in sequence ‘DRY,' which are aspartic acid–arginine–tyrosine happen to be highly conserved amongst the rhodopsin-like GPCRs (Rovati, Capra, and Neubig 2007). Regions that can be involved in ligand binding are suggested to reside where there are multiple alignments described in the mammalian ORs that indicate the extent of conservation as being relatively low such as at TM3 and TM6 (Niimura 2012).

Uniquely the OR genes do not have any introns in their coding regions but often upstream of the coding region will have additional 5´ untranslated exons which can serve

to be alternatively spliced. The use of those non-coding regions can generate multiple mRNA isoforms still resulting in the same end protein, and while this is not a solely unique feature, it is seen commonly in the Rhodopsin GPCRs (Young et al. 2003, Niimura 2012).

Evolutionarily, the OR genes that are located close to one another in what are termed clusters tend to be more closely related. The OR genes tend to be located on almost all chromosomes but are seen clustered together on the chromosomes. It appears to be rare to see a whole gene cluster duplication evolutionarily. Due to this duplication rarity, the OR gene evolution and the overall increase in quantity within species are suggested to be through gene duplication by unequal crossing over resulting in accumulation of mutations leading to an increase in diversity of the sequences of associated duplicates. However, a given OR gene cluster will often contain distantly related genes while OR genes that have a close evolutionary relationship can be found on other chromosomes or clusters (Niimura and Nei 2005b, 2003). Rudd et al. describes a chromosome fission event occurring at an OR gene cluster in the great ape that generated the human chromosomes 14 and 15 (Rudd et al. 2009), which offers that several chromosomal rearrangements could have occurred at the regions of OR gene clusters resulting in the genes in different clusters being shuffled providing these evolutionary OR gene observations. In humans, the OR gene loci are known to be one of the most genetically diverse regions within the genome because it contains many of these duplications and deletions and based on individuality where some have some while others do not.

The OR genes are full of copy number variations (CNVs) which are variations that are seen in the genome structure itself and demonstrate many single nucleotide polymorphisms (SNPs) (Waszak et al. 2010). These variations and SNPs can lead to inactivation of genes which can result in the pseudogenes that are seen ranging from less than 10% to 60% of the total number of OR genes in a given species (Table 2.1) In the study Waszak et al. analysis of 150 individual genomes, there were approximately 15% representing functional OR genes affected by CNVs and approximately 20% of functional OR genes are affected by segregating pseudogenes (Waszak et al. 2010). In various comparative studies amongst a broad range of species, it has been demonstrated a characterization of frequent gene duplications and pseudogenization in the OR genes that lead to drastic changes in the number of genes throughout evolution (Niimura 2012).

In evolutionarily comparing species the orthologs between humans and chimpanzees in OR genes were found to be statistically significantly correlated (De la Cruz et al. 2009). When comparing mice to human OR genes, the clusters are generally well conserved between the two. Mice have quite a bit more OR genes in number than humans (Table 2.1) but share almost the same number of gene clusters that contain 5 or more OR genes (5+ Clusters). This species similarity is possible because the mice clusters contain greater overall numbers in a single cluster than do human cluster, the highest reported in mice was greater than 270 OR genes in one cluster (Niimura and Nei 2005a).

In a study across 13 placental mammals, the mean amino acid sequence identity among the 252 orthologous gene groups (OGGs) found was 81.3% and the median amino acid sequence identity 82.1%. The three OGGs that showed a complete 1:1 orthology

also had the highest identity in amino acid sequence leading the author to the conclusion that these three OGGs were conservative not only in their gene number during evolution, but also in their amino acid sequences making the function of each of these ORs important and likely common to every placental mammal (Niimura, Matsui, and Touhara 2014).

2.2.3 Olfactory Functional Variations Across Organisms

The nose in the fish contains a single type of olfactory organ, the olfactory rosette and lacks the VNO. It includes 3 types of OSNs, the primary two, the ciliated and microvillous cells, and then the minor crypt cells accounting for only a small population within the OE. All cell types innervate the same OB via a tightly fasciculated bundle of olfactory nerves. The primary cells differ from each other in morphology and relative positions in the olfactory epithelium (OE). The ciliated OSNs are situated in the deep layer of the OE, and the microvillous OSNs are in the superficial layer. The ciliated project a long dendrite extending long cilia into the nasal luminal space while the microvillous OSNs project short dendrites that emanate many short microvilli. The minor cell types, the crypt cells are located within the most superficial layer of the OE and have a unique ovoid-shaped cell body that too contains microvilli and submerged short cilia. A profile for the detailed molecular expression in these cells has not been fully developed (Korsching 2009). There are four major groups of odorants that teleosts detect that are water-soluble, they include amino acids, gonadal steroids, bile acids, and prostaglandins (Niimura 2012).

Fish have the crypt cells that are a unique type of OSN and accounts for only a small population within the OE, they are located within the most superficial layer of the OE and have unique ovoid-shaped cell bodies bearing microvilli as well as submerged short cilia. A detailed molecular expression profile has not been clarified for this unique cell including what type of chemosensory receptors are expressed in these cells within the zebrafish (Korsching 2009).

Saraiva, Ahuja et al. generated and analyzed the olfactory transcriptome of the zebrafish and then took the olfactory transcriptome of a mouse for comparison. In their investigation, they looked at the evolutionary relationships in the single olfactory system of teleosts to the dual VNO and OR system of the rodent model and further focused in on the molecular relationships between the two. Overall, they found a high degree of molecular conservation. The orthologs of mouse olfactory cell-specific markers remarkably demonstrated all but a single chemosensory receptor class tested were expressed in the zebrafish olfactory organ. All currently known sensory neuron classes that detect odors and pheromones were tested and demonstrated to be already present in the most recent common ancestor of the teleost's lineage. It was identified that there were conserved and divergent classes of sensory neurons; however, they demonstrated that overall the mouse and zebrafish neural distribution is closely correlated with their chemoreceptor gene repertoire. In summary, they stated to find that the molecular and cellular mechanisms underpinning olfaction in teleost's and mammals are similar despite 430 million years of evolutionary divergence (Saraiva et al. 2015). The zebrafish is phylogenetically found between mammals and insects/worms (Korsching 2009).

Insects have a unique evolutionarily independent olfactory system from mammals, though demonstrating many correlative functional capacities, pathways and processes. In actuality, the odorant receptor in insects belongs to the same family as gustatory receptors (Sato et al. 2008). The odorant receptors for insects are 7-transmembrane proteins inversely embedded within the cell membrane extruding the N-terminus into the cytosol (Benton et al. 2006). The protein receptors in OSNs are ion channels and are shown to require heterodimerization to a secondary odorant receptor protein, Orco for functionality (Silbering and Benton 2010). The odorant receptor protein is present on the sensilla, a hair-like protrusion from the exoskeleton located on insect antenna. The OSN axons are sent to the antennal lobe, which is analogous to the OB in mammals, where then it synapses on respective glomeruli and creates a patterned code and through projection neurons send the information to the mushroom body that is analogous to the piriform cortex in mammals (Vosshall 2001).

2.2.4 Atypical Receptor Expression

Ectopically expressed OR genes are reported to be under evolutionary constraint and with the finding of OR genes expressed in atypical locations through the genome it is thought that ORs may have some additional functions in non-olfactory tissues (De la Cruz et al. 2009). In support of this recent research has shown a role of the OR genes in these atypical areas such as some OR genes expressed in testis, and these ORs are apparently involved in sperm chemotaxis (Spehr et al. 2003). The expression of OR in the arterioles of the eye has been suggested as a function for sensing chemicals within the

eye environment (Pronin et al. 2014). There are reported ORs expressed in the kidney that may modulate renin secretion and regulate blood pressure (Pluznick et al. 2009, Pluznick et al. 2013). Another location with a numerous report of ORs is in enterochromaffin cells and throughout the gut, where it is reported to induce serotonin secretion. Coinciding within the gut ORs were also reported in duodenal enterocytes where some are upregulated in a model of a high-fat diet in obesity-prone rats suggesting a role in the regulation of dietary fat and obesity susceptibility in individuals (Braun et al. 2007, Primeaux, Braymer, and Bray 2013). Chemical sensing, chemotaxis, and cell migration have been implicated as functions of OR in atypical sites, and the skeletal muscle is not an exclusion as they are found to play a role in cell migration and adhesion within the muscles (Griffin, Kafadar, and Pavlath 2009). Numerous reports of OR genes are expressed in various non-olfactory tissues including the tongue, brain, kidney, placenta and more with only a few locations providing evidence of the significance and function in these areas. When these atypical sites express OR proteins, they appear to be regulated by different mechanisms, and ORs display various additional functions compared to the conical nasal local (Persuy et al. 2015).

The regulation of OR gene expression seems to be different in OSNs compared to other cells in the atypical sites discussed. Pulmonary macrophages express OR genes and were reported to play a potential role in response to microbial infection, where it appears to be mediated by bacterially released odorants promoting the macrophage migration and accumulation at the site of infection (Li et al. 2013).

2.3 Perireceptor Environment

2.3.1 Mucus Constituents

The perireceptor environment plays a critical role in signal transduction as it can serve as a limitation or facilitator for odorant delivery to the OR. This environment consists of mucous secretions, enzymes, proteins, microbes, metals, cytokines, immune cells, and odorants.

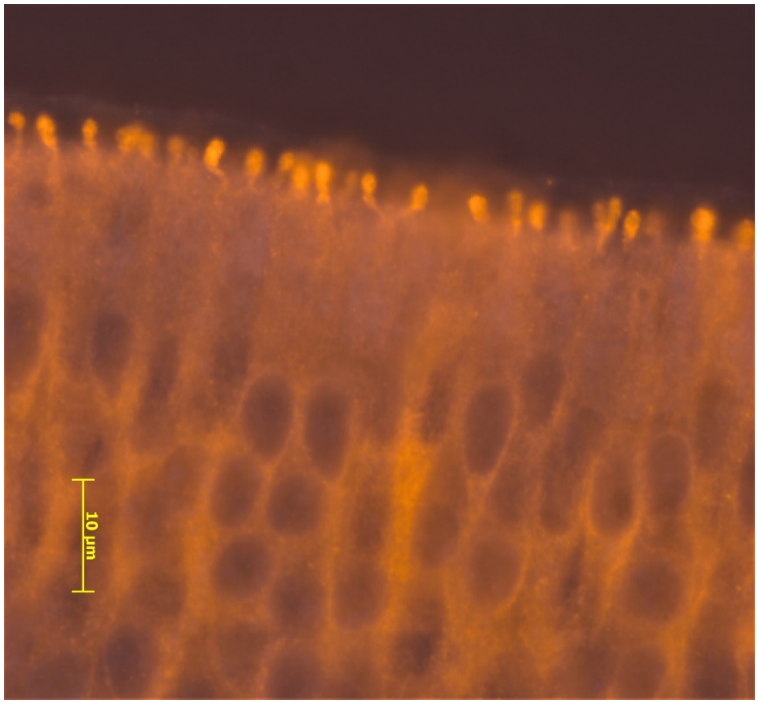

Figure 2.4 Main Olfactory Epithelium (MOE) mucosal surface histological image with anti-olfactory marker protein (OMP) immunofluorescent orange tag (Alexa 555) using high-resolution dark field microscopy (Cytoviva).

The nasal mucus layer is described as ranging from 5 to 30 mm in thickness, while there are no clear distinctions in some reviews between nasal mucus and olfactory mucus due to the contiguous nature of the two epithelia, it is important to distinguish between the two. They represent two distinct regions with varying contributory cells, variation in the microbiota, and varying concentrations of constituents. The properties of the odorant partition coefficient have been shown to influence the odorant deposition patterns in mammals significantly and are described as a "chromatographic separation of odorants along the sensory epithelium" (Rygg, van Duin, and Craven 2013, Nagashima and Touhara 2010).

Enzyme activity within the OE is significant, and enzyme-mediated biotransformation of odorants before OR engagement has been described as well as odorant removal by odor degrading enzymes (ODE)s. The formation of metabolites in the pre-OR mucus interaction, though not 100% effective, create an odorant-metabolite mixture as shown in mice, which emphasized the variation in *in vitro* versus *in vivo* studies of odorant to receptor responses due to the perireceptor environment interactions (Nagashima and Touhara 2010). Bowman's glands secrete high concentrations of cytochrome P450 (CYP), an essential metabolizing enzyme that is also found in high numbers within the liver with activity levels between the two comparable. In addition, other metabolizing enzymes that aid in degradation of xenobiotics secreted by the Bowman's glands include dehydrogenases, oxidases, reductases, carboxylesterases, epoxide hydrolases, uridine diphosphate glucuronyl transferase, glutathione S-transferase, rhodanase, angiotensin-converting enzyme, peptidases, kallikrein, and esterases (Mayer et al. 2009, Ohkubo et al. 1998, Kaliner 1991). These play a crucial role in not only

odorant processing for recognition but as a means for degradation and removal of odorants. In line with this role, the mucus has a high turnover rate.

The extracellular signaling molecule and embryological inducer, sonic hedgehog (Shh) has been found in the nasal mucus and demonstrates a dose-dependent relationship with olfactory function (Henkin et al. 2017).

Of the proteins, odorant binding protein (OBP) is a facilitator for volatile, hydrophobic odorants and assists in the delivery of the odorants to the OR. Humans only have one OBP, while other mammals can have hundreds of variations in OBPs (Briand et al. 2002). The protein family that OBPs belong to are lipocalins and are low molecular-weight proteins with generally low specificity for ligands providing a relatively reversible bind to odorants (Pevsner and Synder 1990, Pelosi 1994).

Immune function and mucosal surfaces are tightly linked throughout the body as a significant line of defense, a location where the outside world meets the body and must, therefore, have considerable defense mechanisms on site. The olfactory mucosa is no exception, with nasal secretions containing immunoglobulins such as IgA, IgM, and IgG (Kaliner 1991). Additionally, there are closely associated innate immune cells and B-lymphocytes, antimicrobial peptides, lysozyme protein, and lactoferrin that provide a defensive role against pathogens (Mellert et al. 1992). The more recently eluded microbiota could also play a role in defense, though no studies have evaluated this directly.

The metal content in the nasal mucus has been reported for copper and zinc ions, magnesium and calcium. Copper was found in concentrations estimated at 40 μM in mice and 16 μg dL^{-1}in humans. While zinc in humans was estimated at 14 μg dL^{-1}, for

magnesium estimates were 1554 µg dL^{-1}, and estimates for calcium at 5303 µg dL^{-1} (Henkin, A., and Martin 2000). There have been no estimations that differentiate from concentrations within nasal mucus and olfactory mucus, though they are continuous, they display distinct characteristics in enzymatic activity and variations in contributory glands. The microbiota of the olfactory system is not well established within the literature. To date, only one published study has evaluated the main olfactory epithelium directly, and a few have commented on findings in the closely associated ethmoid recess in humans (Francois et al. 2016, Yan et al. 2013). However, most available literature has evaluated the nasal cavity in general with a focus on respiratory epithelium. The role that microbes play in olfaction has been assessed from the viewpoint of microbial odorant production, particularly within glands of mammals, that serve as social and behavioral cues.

2.4 Odorants

Odorants detected by the main olfactory epithelium are volatile molecules. They can range in size, charge and associated functional groups with perceptions that result in an aroma, pleasant or unpleasant. The numerous combinations of individual odorant molecules give rise to a vast and unpredictable catalog of aromas that could exist. Figure 2.5 provides example odorants from various classes that were used as a broad-spectrum odorant mixture with multiple OR targets.

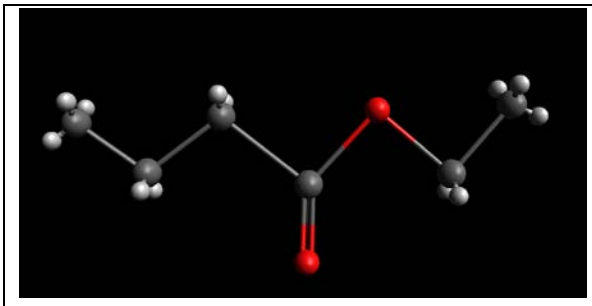

Ethyl Butyrate

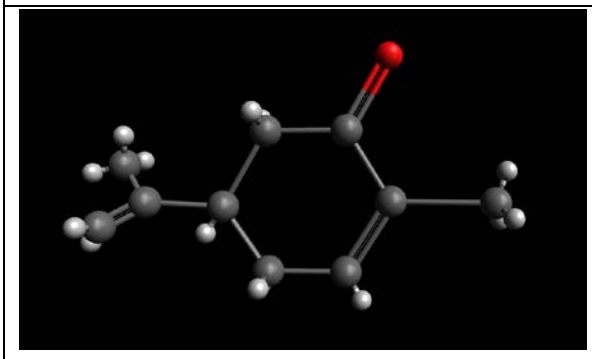

- Carvone

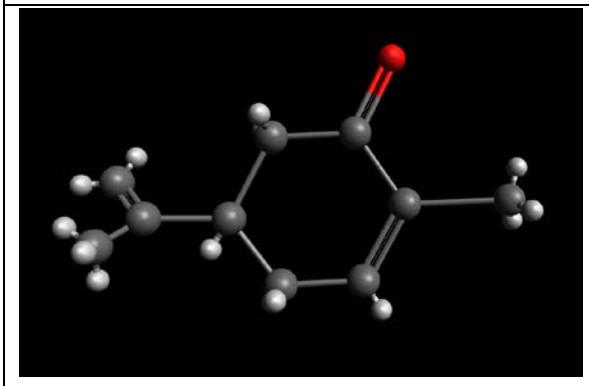

+ Carvone

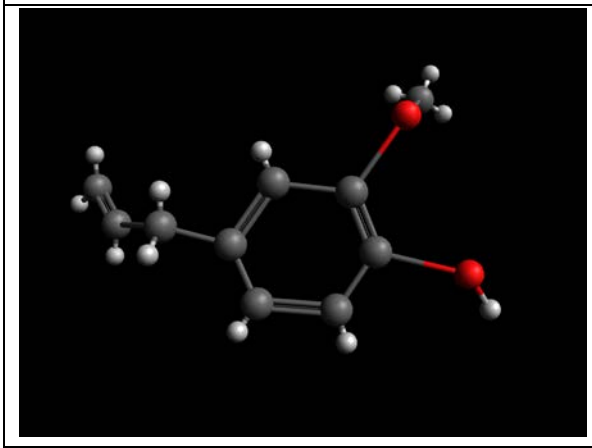

Eugenol

Figure 2.5 Ball and stick models of odorants Eugenol, +/- Carvone, and Ethyl Butyrate.

Diagrams are drawn with Avagadro software.

2.5 Neuroprocessing of Olfaction

2.5.1 Olfactory Signal Transduction Pathway

The odorant (olfactory) receptors (OR) as discussed are G-protein coupled receptors (GPCR). These trimeric G-proteins consist of an alpha, beta and gamma subunit (Firestein 2001, Buck and Axel 1991). The OR are embedded in the membrane of the OSN with high concentrations in the cilia forming the dendritic knob of the neuron. There are approximately between one and fifty sensory cilia per OSN (Morrison and Costanzo 1990). Each OSN expresses only one of over 1,000 OR types. This results in specificity for a single neuron and increased sensitivity by a summation of potentials when multiple OR's are stimulated by the same odorant type resulting in an action potential when the threshold is reached (Firestein 2001). A specific OR is capable of detection in a narrow spectrum to or a broad spectrum of odorant molecules while a specific odorant molecule can activate a variety of ORs at varying levels of intensity and attraction. This blend of sensitivity and specificity variation amongst OR resulting in groups of odorant specific activation that can be overlapping and allow for a more considerable combinatorial coding for more odorant detection possibilities (Persuy et al. 2015).

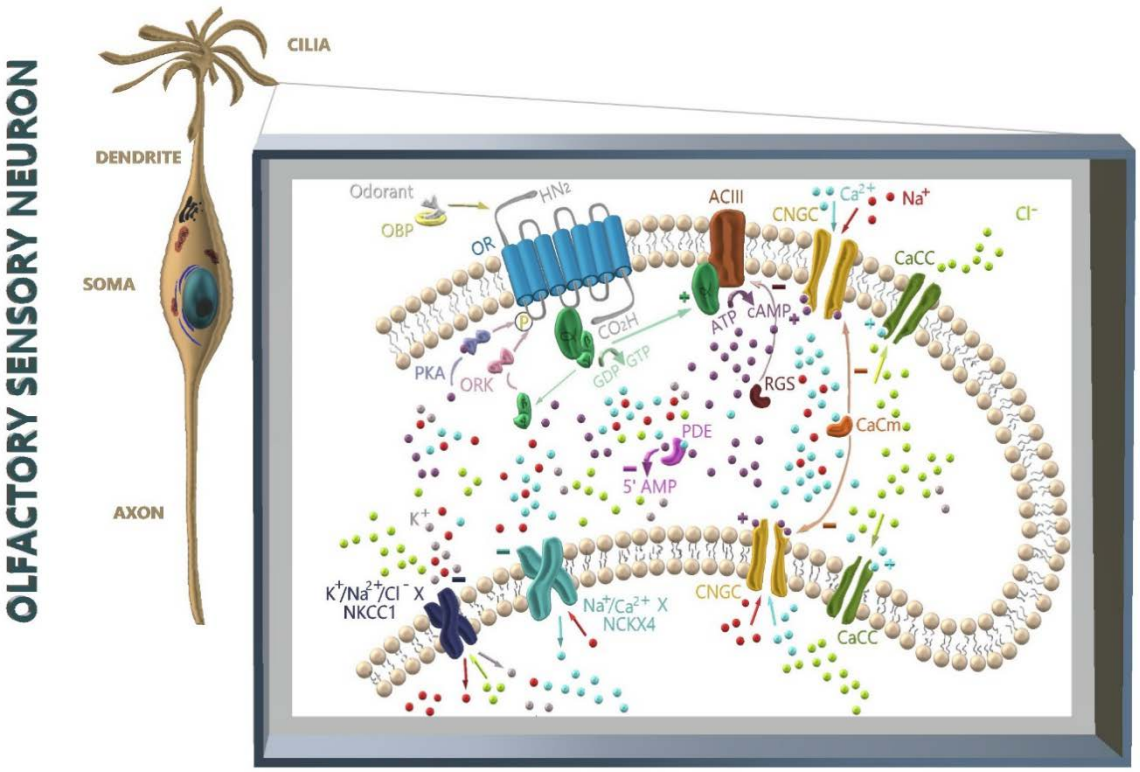

Figure 2.6 Illustration of Olfactory Sensory Neuron and depiction of cilia membrane proteins and signal transduction molecules. OBP- Odorant Binding Protein; OR- GPCR Odorant Receptor with trimeric G protein (alpha, beta, and gamma subunits); ACIII- Adenylyl Cyclase III; CNGC- Cyclic Nucleotide-Gated Channel; ATP- adenosine tri-phosphate; CaCC-Calcium-Activated Chloride Channel; PDE- Phosphodiesterase; RGS-Regulator of G-Proteins; PKA-Phosphokinase A; ORK- Odorant Receptor Kinase ; $Na^{+/}$ Ca^{2+} ion transporter NCKX4; NKCC1 ion transporter; CaCm- Calcium-calmodulin. Illustration by Melissa Singletary.

The resting membrane potential of the OSN is -65mV and threshold typically around -45mV (Firestein 2001). To activate the OR an odorant molecule must bind to the binding pocket of the GPCR and receive the appropriate recognition that will result in a conformational change in the G_{olf} trimeric protein that allows the cytoplasmic end to exchange GDP for GTP and dissociate the $G_{\alpha olf}$ subunit from the G_{β} and G_{γ} subunits. GPCRs are 7-transmembrane receptors that weave from intracellular to extracellular space a total of seven times. The release of the $G_{\alpha olf}$ subunit allows for the interaction of the $G_{\alpha olf}$ with the adenylyl cyclase III (ACIII). Adenylyl cyclase III, in turn, converts intracellular ATP into the cyclic AMP (cAMP) (Firestein 2001). Odorant marker protein (OMP), has been used as a biomarker for OSN maturity, as it is not expressed in basal cells and is expressed in correlation with functional activity. More recently, OMP has been identified as playing a role in the control of the basal cAMP levels (Dibattista and Reisert 2016). The increasing levels of cAMP, approximately 100 cAMP molecules produced per ACIII, allows for at least three collective cAMP molecules to bind to the transmembrane ion channel, cyclic-nucleotide gated channel (CNG) resulting in conformational change and opening. The estimated concentration of CNG's is greater than 2,000/μm^2. The CNG's, in turn, are selective to allow an influx of the positively charged Ca^{2+} and Na^{+} into the cell. This change in voltage across the membrane will further be potentiated by the opening of voltage-gated ion channels that are calcium-activated chloride channels, transmembrane protein TMEM16B, which are proposed to have an association with the calcium-calmodulin precursor calcium-free calmodulin, apocalmodulin (apoCaM) under resting conditions (Yang, Hendrickson, and Colecraft 2014). Their activation allows for an efflux of chloride out of the cell into the

extracellular space (Firestein 2001). This dual flow system provides for relatively quick membrane depolarization.

The environment of the OSN cilia and receptor field is not a typical extracellular space with consistent ion concentrations and stable gradients. Therefore, the OSN has a unique built-in fail safe that aids in depolarization when sodium levels may still be low. This negativity is maintained by the high chloride concentration intracellularly in the OSN cytoplasm compared to the outside milieu. This intracellular chloride gradient provides a mechanism for quick membrane potential depolarization when selective ion channels are opened to the negatively charged molecule and has been termed a Cl^- battery (Firestein 2001). To this point, the chloride efflux is reported to represent 80% of the primary depolarization in the OSN (Lowe and Gold 1993). The re-establishment of this Cl^- gradient in more recent work is thought to be the function of ion transporter NKCC1 (Haering et al. 2015). The NKCC1 ion transporter is a sodium, potassium, chloride symporter transporting 1 Na+ and 1K+ per 2 Cl^- (Haering et al. 2015). The ciliary calcium is also redistributed to the extracellular space by $Na^{+/}$ Ca^{2+} extrusion through the transporter NCKX4 (Stephan et al. 2012). This re-establishment of gradients is the repolarization phase which starts with a hyperpolarization state temporarily where the cell is refractory to a stimulus while it resets itself.

The mechanism by which there is feedback internally within the cell membrane is multifactorial. With the influx of calcium during depolarization reaches a threshold when it can act directly on the ion channels through calcium-calmodulin binding that decreases the ion channel sensitivity to cAMP thereby dampening the response and elevating the threshold for required stimulus intensity for subsequent excitation. Regulator of G-

protein signaling (RGS) additionally reduces levels of cAMP through means of inhibiting further production by direct inhibition of adenylyl cyclase III activity. In particular, when RGS2 was inhibited experimentally, it resulted in downregulation of signal transduction in the neuronal membrane (Sinnarajah et al. 2001). This ability of the olfactory system to have multiple methods to modulate the response to stimulus threshold is also utilized as a mechanism for changing the gain and adaptation by adjusting the OSN sensitivity (Kurahashi and Menini 1997, Reisert and Matthews 2000, Firestein 2001). Increased levels of cAMP activate phosphokinase A (PKA) which serves to phosphorylate the receptor thereby inhibiting its function. PKA works alongside odorant receptor kinase (ORK) to achieve this through cAMP activation of the G-protein beta-gamma subunits. The calcium-calmodulin serves a second function in activation of phosphodiesterase (PDE) within the cytoplasm. The PDE, once active, will degrade or break down the cAMP to restore the nominal cAMP levels found with basal expression (Firestein 2001).

The action potential is potentiated down the axon to reach its monosynaptic second neuron target in the olfactory bulb. The OSN utilizes glutamate as its primary excitatory neurotransmitter (Berkowicz, Trombley, and Shepherd 1994).

2.5.2 Olfactory Bulb

OSN axons project from their soma within the olfactory epithelium to respectively associated glomeruli within the olfactory bulb. The glomeruli are selective for individual OR's allowing for collections of OSN axons expressing the same OR to bundle as axon fascicles and innervate selective glomeruli. Main cell types of the

olfactory bulb include the mitral cell neuron, tufted cell neuron, peri-glomerular cells and granular cells. Approximately 25,000 axons per glomeruli according to studies in rabbits and about 1,800 glomeruli per bulb reaching 3,600 glomeruli total (Firestein 2001). The olfactory bulb can be considered laminated with six distinct layers. The first layer, the axon fiber layer from the OSN axonal projections entering the OB. The second is the glomerular/peri-glomerular layer. The third lamination is the external plexiform layer, which is cell-sparse with mostly dendrodendritic synapse and tufted cells. The fourth layer is the mitral cell layer and represents the primary signal output for the previous layers. The fifth layer is the internal plexiform layer with sparse synaptic activity and low numbers of cells. The innermost and sixth layer is the granular layer with granular interneuron cells that form the core of the olfactory bulb serving as the second site of progenitor cells within the olfactory system outside of the basal cells within the OE (Sarnat and Flores-Sarnat 2017, Sarnat and Yu 2016).

This one-receptor-one-neuron rule also relates to associated specific receptor glomeruli. The glomeruli are located on the outer layer of the olfactory bulb as sphere-like structures where the OSN axon synapses on the mitral and tufted cells of the OB. The mitral cells are the primary output cell followed by the tufted cells of the olfactory bulb and are glutaminergic neurons utilizing the neurotransmitter glutamate as an excitatory chemical signal. Approximately 50 mitral and tufted cells are responsive to a single glomerulus. These glomeruli, which are the synaptic collection of OSN axons and receptor-specific mitral and tufted cells, are surrounded by the periglomerular cells. These interneurons are intrinsic in their activity to the OB with dendrodendritic synapses to the glomeruli and associated cells. These surrounding periglomerular cells are

predominately gabaminergic and dopaminergic neurons acting on NMDA receptors of the mitral and tufted cell axons and function in inhibition within and between glomeruli (Ohm, Muller, and Braak 1991, Ohm et al. 1990). The granular cells within the innermost layer function in inhibition within and between mitral and tufted cells through gabaminergic neurotransmitters on NMDA receptors. These unique interneurons also have dendrodendritic synapses with the mitral and tufted cells and lack an axon with no extrinsic connection from the OB (Hirata et al. 2006). The olfactory bulb is the site within the CNS with the highest concentration of dendrodendritic synapses (Hayashi 1999, Kaba and Keverne 1992). The reciprocal contact between the mitral cell and the granular cell is such that direction of stimulation mitral to granular excites while granular to mitral inhibits (Kosaka et al. 1985). Estimates of 50-100 inhibitory granular cells per mitral cell are reported (Hirata et al. 2006).

2.5.3 Higher Brain Center Processing

The output information from the olfactory bulb is sent from the mitral and tufted cell axons toward the higher cognitive brain areas through the olfactory peduncle, the connection between the olfactory bulb and the basilar forebrain (Brunjes, Kay, and Arrivillaga 2011). The areas of the brain receiving direct input from the olfactory bulb output axons are collectively termed the olfactory cortex. These include the anterior olfactory nucleus (AON), the tenia tecta, the olfactory tubercle (OT), the piriform cortex (PC), the cortical amygdaloid nucleus, the periamygdaloid cortex, and the entorhinal cortex (Zelano and Sobel 2005, Price, Slotnick, and Revial 1991). The AON is the most

rostral region of the olfactory cortex and has a large number of commissural fibers that project contralateral and ipsilateral information to the piriform cortices (Zelano and Sobel 2005, Brunjes, Illig, and Meyer 2005). Uniquely, the olfactory sensory system does not directly communicate with the thalamus and has direct connections to the higher brain centers. All other sensory systems require thalamocortical processing. Studies have suggested that the olfactory bulb cortex functions in a similar capacity to the thalamus (Sarnat, Flores-Sarnat, and Wei 2017, Zelano and Sobel 2005). The majority of OB output is directed toward the PC. The PC projects to the dorsomedial nucleus of the thalamus, orbitofrontal cortex, and a significant role in the top-down control as feedback projections to the OB. The PC lacks a neocortical organization with only three layers but is highly associative lacking a topographic organization. The elaborate topographical spatial patterns of the glomeruli of the OB are lost in the projections to the PC, which demonstrate a more divergent-convergent profile (Wiegand et al. 2011, Miyamichi et al. 2011). The entorhinal cortex is the connection pathway to the hippocampus and is considered relevant to studies in the memory associations with olfaction. The entorhinal cortex receives input from multiple areas of the olfactory tract and functions in feedback to the OB (Zelano and Sobel 2005). The amygdala carries the input to projections into the hypothalamus and feedback to the OB. This is the area of the olfactory cortex that is most studied for its involvement in emotion as part of the limbic system (Zelano and Sobel 2005, Sullivan et al. 2015). The only area of the olfactory cortex not known to directly send feedback synaptic information to the olfactory bulb is the olfactory tubercle. The olfactory tubercle projects to the dorsomedial nucleus of the thalamus and thought to

play a role in reward and motivation due to its strong reciprocal connections to the nucleus accumbens, ventral tegmentum, and pallidum (Heimer 2003, Ikemoto 2007).

The feedback that majority of the olfactory cortex and the orbitofrontal cortex provide to the olfactory bulb is a source of adaptation and habituation that can occur in the sense of olfaction. Adaptation has been classified as peripheral versus central adaption. Peripheral adaptation occurs due to a decreased neural response in the pre-glomerular tract and central adaptation as a decreased neural response in the post-glomerular tract (Pellegrino et al. 2017). Habituation, on the other hand, is considered by Rankin et al. “defined as a behavioral response decrement that results from repeated stimulation and that does not involve sensory adaption/sensory fatigue or motor fatigue” (Rankin et al. 2009). This is further expanded upon by Pellegrino et al. that includes the consideration of adaptation as the "neural processes (peripheral and cerebral) that constitute this decrease in behavioral response" (Pellegrino et al. 2017). This adaptation can occur after as little as two repetitions of an intense odor stimulus where perception is diminished through the electrical activity at the OSN level is not (Hummel, Knecht, and Kobal 1996, Hummel, Mojet, and Kobal 2006).

2.6 Prevailing Theories of Olfaction

In the field of olfaction, there is a debate regarding the molecular model between the lock and key model of “shape” theory and the waves of “vibrational” theory. Tests have been conducted across species from the American honeybee to humans. The classic theory of shape is seen as the mainstream theory as no experimental evidence has been

demonstrated to support vertebrate olfactory receptor vibrational theory. However, there are inconsistencies with the shape theory that have led to suggestions of a modified "receptor ligand-docking theory" (Block et al. 2017) and inconsistencies with the vibrational theory that have led to the "swipe card" theory (Brookes, Horsfield, and Stoneham 2012b).

Many receptor-ligand interactions throughout biological systems involve a lock and key fit for recognition and subsequent receptor activation. This is the basis for the "shape" theory of olfaction (Amoore, Palmieri, and Wanke 1967). However, due to the exponential quantity of differing odorants that can be encountered the simple one key one lock concept does not suffice and requires a pattern of responses with varying affinities which are based on intermolecular interactions (Askim, Mahmoudi, and Suslick 2013).

Of our senses, photoreceptors have been shown to respond to electromagnetic oscillations of light in vision and hair cells to the frequencies of sound in audition. The olfactory receptor is a GPCR and considered rhodopsin-like. Rhodopsin GPCRs represent the family of receptors that rods and cones of vision. Lucia Turin in the 1990's reinvigorated and reimagined the different vibrational theories proposed previously from Dyson in the 1930's and Wright in the 1950's involved in odorant recognition in olfaction (Dyson 1938, Wright 1954). Turin's model proposes that olfactory receptors respond to the vibrational frequencies of individual odorant molecules as compared to the molecular shape. His model requires an electron donor for biological transduction and the proposed mechanism was quantum inelastic electron tunneling. He supports the vibrational theory of olfaction through modeling and psychochemical testing (Turin 1996). Certain molecules are capable of very similar shapes while varied in vibrational

frequencies. Deuteration is the process of chemically exchanging hydrogen to deuterium thus creating an isotope of an odorant. Deuterium is one of two hydrogen isotopes and varies in having a reduced mass compared to representative hydrogen and demonstrates pronounced differences in vibrational frequencies (Kushto and Jagodzinski 1998). Therefore, deuterated molecules can be examined for qualitative differences with similar structures though altered vibrational frequencies. Enantiomers are molecular mirror images that possess identical vibrational frequencies but differ in shape and have been used for selective testing as their perceptions have been shown to differ thus supporting an element of odorant recognition beyond vibration alone (Brookes, Horsfield, and Stoneham 2009).

The controversial debate amongst "shape" theory and "vibrational" theory have led to a multi-disciplinary evaluation of the validity of quantum electron tunneling and has resulted in mathematically based support for the vibrational concept. However, with the findings concerning both enantiomers and isotopes there emerged the "Swipe-Card" theory as a modified model that recognizes molecular shape and odorant vibrations (Brookes, Horsfield, and Stoneham 2012b).

There are few published papers regarding studies conducted in the vibrational theory model of olfaction and include eleven currently identified. The species tested in these identified papers include American Honeybee, *Drosophila*, and Humans. With variation between species, this is an area where careful consideration of the variability is important. The data is reported in various ways through each paper as different measures and methods were used between studies and subjects. The studies utilizing human trials and or human *in vitro* methods included Block et al. in 2015, Gane et al. in 2013 and

Haffeden et al. in 2001. Block et al. compared human and mouse ORs *in vitro* between cells lines in their responses to deuterated and undeuterated isotopomers odorants. Conceptually isotopomers differ in their vibrational frequencies, though are identical in their ground-state conformations. In this report, no differences in the receptor response *in-vitro* between odorants and receptor pairs (Block et al. 2015). Gane et al. performed human perception study *in vivo* using deuterated and undeuterated isotopomers odorants and found a significance in subject-distinction between odorants (Gane et al. 2013). Haffenden et al. used analogues of benzaldehyde with trained panelists in a duo-trio test showing a significant difference with benzaldehyde-d_6. This was reported to be associated with shifts in absorption frequencies while modeling suggests molecularly maintained shape supporting a vibrational model (Haffenden, Yaylayan, and Fortin 2001). Keller et al. in a brief communication reported using a psychophysical test for olfaction showed that acetophenone and deuterated acetophenone were indistinguishable in their panel of human subjects, though admittedly training or experience could result in different outcomes within the test if repeated and concluded that "molecular vibrations alone cannot explain the perceived smell of an odorous molecule" (Keller and Vosshall 2004).

Higher representative studies for the vibrational theory are reported within insects. Trails involving the Honey Bee were reported by Wright et al. Paoli et al. in 2016 reported on differential odor coding between isotopomers in honeybees. The neuronal activation maps generated were distinct between deuterated isoforms of naturally occurring odorants summarizing that "other features, such as molecular vibrations, may contribute to odor signal transduction" (Paoli et al. 2016). Gronenberg et

al. evaluated deuterated isotopes in honeybees and learning with the proboscis extension reflex to condition the distinction between odorants. They successfully showed that honeybees readily learn to discriminate between the deuterated and non-deuterated compounds supporting intra-molecular vibrational contributions to odorant discrimination (Gronenberg et al. 2014). Trails involving the *Drosophila* fly were reported to support the vibrational theory in individual studies. Bittner et al. used acetophenone as a test case to suggest that isotopomers provided different odorant qualities and concluded that inelastic tunneling of the vibrational model in olfaction might play a role in the discrimination between isotopomers, though it is not generally spectroscopic in total (Bittner et al. 2012). Drimyli et al. demonstrated a conserved differential response of electrophysiological antennae measurement amplitudes to aldehydes, alcohols, ketones, nitriles, and their deuterated isotopologues, concluding that their results, "strongly suggest that Drosophilid olfactory receptors are activated by molecular vibrations." (Drimyli et al. 2016). Franco et al. performed deuterated odorant studies that demonstrated *Drosophila* differentiation between isotopic odorant recognition and further ability to condition selectivity between isotopic odorants supporting a molecular vibration sensing odorant recognition component (Franco et al. 2011).

Considerations for species differences are significant concerning insects versus mammalians as the ORs are distinct between the two. Evolutionary independence is seen between insects and mammal ORs, though similarities are noted in the olfactory receptor review. Insects display a 7-transmembrane protein that is inversely embedded within the cell membrane and N-terminus located in the cytosol, in comparison to mammalian

GPCRs with the N-terminus located in the extracellular space (Benton et al. 2006). Protein receptors in insect OSNs are ion channels and not considered direct correlates to the mammalian GPCRs (Silbering and Benton 2010). These differences are important in the interpretation of insect-based studies and translation to mammalian olfaction. The second consideration between studies of insect olfaction is the consideration of sensitivity and odorant preparation. A study by Paoli et al. in 2017 demonstrated that a minute impurity of only 0.0006% was sufficient to activate a strong odorant evoked response in *Drosophila* to benzaldehyde-d_5. This highlighted the need for purified odorants by gas-chromatographic purification processes to ensure there is no confounding activation between two odorants when results for selectivity are desired (Paoli et al. 2017).

2.7 Zinc Overview

Zinc is categorized as an essential trace element and is found ubiquitously throughout all biological system (International Zinc Nutrition Consultative et al. 2004). Estimates are that the human body contains between 2 to 4 grams of zinc total, though serum measurements alone are not sufficient to represent total body zinc (Ollig et al. 2016). Zinc is highly protein bound, utilizing albumin in particular, within circulation and majority stored intracellularly. Zinc stores have not been described in the body, but rather zinc is utilized significantly within skeletal muscles and bone, representing over 80% of total body zinc and demonstrating high turnover especially with normal osteogenesis (Iyengar 1998). Zinc is unusually versatile as a transition metal which displays physiochemical properties that make it ideal for utilization in the body such as

the capability to assume multiple coordination numbers and dynamic geometries that gives zinc stereochemical adaptability (Vallee and Falchuk 1993). Zinc is not subject to oxido-reductive reactions under physiological conditions, which make it better biologically compatible due to being relatively non-toxic. This adaptability allows zinc to serve as a cofactor for over 300 enzymes, which are found across all six enzyme classes including oxidoreductases, hydrolases, lyases, transferases, isomerases, and ligases (Rink and Gabriel 2000). Zinc is further found to stabilize proteins, facilitating their folding by zinc chelation with the amino acid cysteine and histidine for the formation of zinc fingers with a finger-like motif. Zinc can modulate cellular functions through participation in multiple signaling processes within cells, in particular at selective synaptic clefts (Colvin et al. 2010, Maret 2014). Specifically, zinc is required for gene expression, proliferation, DNA and RNA synthesis, and apoptosis (Kloubert and Rink 2015).

Due to the lack of zinc storage pools in the body, regular intake is required to maintain homeostasis. The circulating zinc is estimated to complete about 150 cycles per day. Zinc is released from food during the digestive process and taken up in intestines. The absorption method has been shown to be relative to the amount of zinc present in food and is saturable. At high levels, zinc can be absorbed passively through a paracellular route and specific transporters and transcellular at normative levels (McMahon and Cousins 1998).

2.7.1 Embryogenesis, Development and Deficiency

Development is an intricate series and compilation of events that lead to a final composed system. In this manner, there are critical time points or windows where the right molecules have to be in the right vicinity at the right stage for the appropriate maturation or step in development to be achieved. Zinc has a role in many of these processes that are necessary for appropriate and intended development. The roles that zinc plays in DNA and RNA transcription, metabolism and endocrine function lead to the basis of the role that zinc plays in growth and development. However, the primary mechanisms are unknown, but in deficient zinc levels in pregnancy are associated with intrauterine growth retardation, characteristically low birthweights, hindered neurobehavioral development, and preterm deliveries (Tamura et al. 2000). Zinc deficiency is associated with skin disorders, gastrointestinal disruption, growth stunting, weight loss, mood changes, behavioral changes, neurological deficits, loss of smell and taste acuity. The vast role that zinc plays within the body eludes to the consequences of deficiency.

2.7.2 Metal Ions and Volatile Molecules

Odorants most widely perceived by mammals are volatile molecules. As volatile molecules, their interactions with metal ions can reasonably change the characteristics of the odorant and thereby change its perception or array or receptor sensitivity and specificity. The relationship of volatile odorant ligand inclination for coordination to metallic ions to the strength of perceived odorant is directly proportional. A stronger ligand for metal ions correlates with a stronger odor. The particular volatile molecule

classes that fit into this strong correlation are thiols, amines, and isonitriles (Block et al. 2017). From the late 1970's the idea that metals and metal ions, in particular, could play a role in olfaction has been considered, though not evaluated substantially. It was posed first by Robert Crabtree that copper ions may play a role through a proposed OR metalloprotein (Crabtree 1978). Jack Day also suggested that transition metals could serve in the odorant recognition (olfaction) of certain functional groups (Day 1978). Metalloproteins are a ubiquitously found joining of metallic ions and proteins within the body that are dependent for function. To the point, it is reported that almost half of all enzymes must be associated with a metal for function (Anzellotti and Farrell 2008, Waldron et al. 2009).

2.8 Zinc, the Central Nervous System, and Olfaction

The term “metalloneurochemistry” has become a field of study over the last two decades that dive into the interactions between metals and the nervous system (Lippard 2014). A significant portion of the focus in this relatively newer field has been on metals such as zinc, iron, copper, and manganese as they can serve as co-factors in various proteins and enzymes. However, a recognition of the presence and need for a better understanding of the role zinc specifically plays within the central nervous system has led to a significant effort toward characterizing and developing better tools to evaluate zinc. The role that zinc plays in signal transduction in the central nervous system (CNS) is still under considerable exploration. Zinc ions are found in large concentrations within certain areas of the CNS such as the olfactory bulb, hippocampus, hypothalamus, and

cerebral cortex. The concentration is mostly in the glomerular and granular layers and considered mobile within neurons (Frederickson and Danscher 1990, Sensi et al. 2009). The measurable quantity within the cerebrospinal fluid is estimated at 31.5 mg L^{-1} (Agarwal and Henkin 1982). The abundance of zinc found within the brain suggests a significant role in normal homeostatic function, and in the absence of appropriate zinc levels in deprivation states, correspondingly zinc is not uniformly depleted from the body during times of deficiency. The first stage tissues for zinc depletion are the peripheral sites such as bone, testes, and plasma (Jackson, Jones, and Edwards 1982). Glutamate is an excitatory neurotransmitter and is utilized by the OSN, mitral and tufted neurons of the olfactory system and zinc is co-released at the synaptic cleft with glutaminergic neurons contributing to the signaling. The method is exocytosis similar to that of the neurotransmitters, though the target and functional role that these zinc ions play in the neuronal signaling is not described. Zinc deficiency is associated with signs of hyposmia and anosmia, and this may play a role in that clinical observation.

The requirement for zinc in biological function and the lack of a zinc storage pool within the body require a level of regulatory controls for homeostasis. ZIP proteins (Zrt/Irt-like proteins) are zinc importers that can facilitate the intracellular uptake of zinc, in particular, the expression is upregulated when extracellular levels of zinc are increased as a mechanism of toxicity reduction (Emmetsberger et al. 2010). Zinc exporters and zinc-binding proteins work to lower intracellular zinc levels to maintain homeostasis as intracellular levels are elevated. Such proteins are the metal-ion sequestering protein, metallothionein (MT-III), that binds to an excess of zinc in a redox-dependent manner within the cytoplasmic domain and can export the ions as a cellular protective mechanism

(Nakashima and Dyck 2009). The function of MT-III can be compromised with the presence of reactive oxygen species (ROS) by interfering with the zinc binding capacity of the protein (Sensi et al. 2009). The method of transport utilized by zinc transporters (ZnT) is through ion containing vesicle formation that can undergo exocytosis or be stored separately from the cytoplasm (Arus et al. 2013). There are two ZnT's represented in neurons, the neuronal specific ZnT3 and the plasma membrane-associated neuronal ZnT1. ZnT1 is able to associate with the subunits of ligand-gated ion channels that bind zinc in the NMDA receptor (Mellone et al. 2015). The regulation and significance of zinc in sensory signaling in olfaction are seen with glutaminergic zinc-enriched neurons (ZENs) that are present in high densities in the olfactory bulb. An analogous zinc response to electrical stimulation in axons within the OB were evaluated with the zinc probe ZP1 that selectively labels intracellular zinc and quantifies vesicle exocytosis and release through a decrease in signal (Blakemore et al. 2013). This link between zinc release and olfactory neuronal activation is compounded by the zinc response at the olfactory mucosa with zinc inhibiting olfaction, and the underlying mechanisms are not well eluded.

The role that metals can play in receptology, neurotransmission, and physiology within the central nervous system and within specifically the olfactory system are relatively understudied. Suslick et al. 2013, proposed a shuttlecock mechanism for the function of zinc or copper at the GPCR 4-5 loop which increases sensitivity to thiols and amines providing assisted activation of the olfactory receptor that allows for odorant binding and suggests the OR could serve as a metalloprotein (Wang, Luthey-Schulten, and Suslick 2003).

Metal nanoparticles were found in human and animal blood as proteon nucleating center (PNCs) (Samoylov et al. 2005). The isolated metals included gold, silver, platinum, zinc, and copper (Figure 2.7). The PNCs were sized between 1 and 2 nm, but only the small zinc PNCs were able to demonstrate a significant impact on the function of ORs at a three-fold enhancement in OR response to odorant. This enhancement was not found in the absence of odorant and further not found with zinc ions (Viswaprakash et al. 2009).

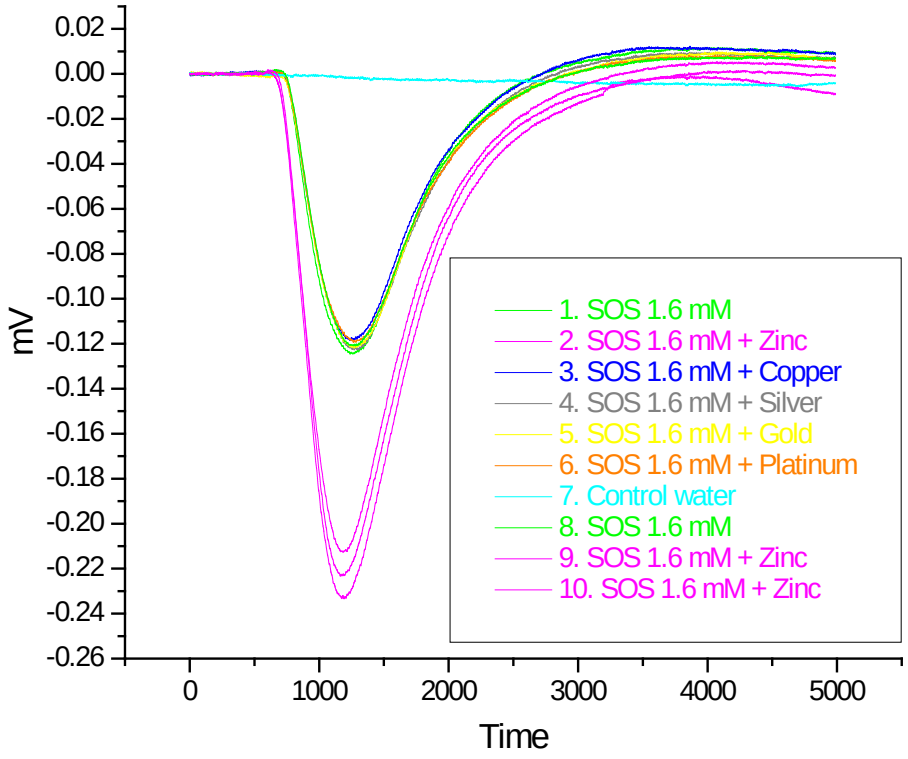

Figure 2.7 Representative EOG recordings from rat olfactory epithelium. The stimuli were of 0.25 s pulses of (1) standard odorant mixture (SOS), (2) odorant mixture + zinc nanoparticles, (3) odorant mixture + copper nanoparticles, (4) odorant mixture + silver nanoparticles, (5) odorant mixture + gold nanoparticles, (6) odorant mixture + platinum nanoparticles, (7) water vapor, (8) standard odorant mixture (SOS), (9/10) odorant mixture + zinc nanoparticles. The concentration of odorant mixture was 1.6 mmole/L.

Zinc ions, in contrast, have been used historically as a means to induce anosmia as they are suggested to may block the c-AMP dependent transduction channels thus preventing calcium influx and subsequent signal transduction cascade (Ishimaru et al. 2000)Kramer and Molokanova 2001), activation of cAMP-specific phosphodiesterase (Percival et al. 1997), inhibition of adenylyl cyclase (Klein et al. 2004) and $G_{\alpha s}$-protein

(Gao et al. 2005). Indeed, replacing the zinc nanoparticles capable of olfaction enhancement with zinc ions effectively reversed the enhancing effects as measured on EOG.

2.9 Microbiota Overview and in Olfaction

The essence of living exists in a delicate balance that maintains homeostasis allowing for organism health, function, growth and survival. An organism exists within the environment and is in constant contact with the microorganisms found within that environment. Microbes are found on all mucosal surfaces in the body through environmental exposures throughout life that lead to selective colonization's. The adult intestine contains microbiota that are ten times the number of human cells found within the body (Xu and Gordon 2003). This incredible, 10^{14} number of bacterial cells correlates to the amount of genetic material represented by this population, more than 5 million genes total ranging from 500 to 1,000 differing species making up this microbiome (Human Microbiome Project 2012b, a). The diversity and quantity of microbes found in the gut are particularly highest within the distal colon in humans and stratification occurs due to the differences in pH, gut motility and gut transit time (Cook et al. 2012). Three dominant phyla comprising approximately 75% of all microbiota found in studies of fecal samples in humans include *Firmicutes, Bacteriodetes*, and *Actinobacteria* (Gibson and Roberfroid 2008). The gut is a critical body system and is home to this diverse population that can be non-pathogenic symbionts contributing to homeostasis, opportunistic pathogens and also obligate pathogenic causes of disease and disorder (Sommer and Backhed 2013). The balance of the microbiota is not only a

species-specific one but is also specific to each individual, such as no two individuals will have an identical make up of microbiota (Human Microbiome Project 2012b). The effects of microbiota on the host are strain specific and not general to all phyla, genus or species itself (Lee et al. 2015). The development of this microbiota occurs over time and changes with age, diet, sex, lifestyle, and environment (Zapata and Quagliarello 2015, Singh and Manning 2016, Odamaki et al. 2016). The most substantial factor affecting this balance is the diet (de Vos and de Vos 2012).

The role of the gut microbiota in health is a field of study that is fast growing, and with newer technologies and experimental models, the field is expanding. The interaction of microbes in health in the gut has been demonstrated to be important in many host functions. One of the primary functions shown included nutrient metabolism, as non-digestible carbohydrates and proteins are broken down by the microbes in the gut to primarily short-chain fatty acids and amines respectively that the host would otherwise be unable to utilize in the absence of the microbes (Jacobs et al. 2009). It is in this way that the dietary intake is maximized nourishing the microbiota and providing a health benefit to the host.

Another area of function in the host-microbe interactions has been found of great importance in the immune system development and priming particularly through experiments in germ-free mice models demonstrating a conditioned tolerance and level of immune homeostasis (Arrieta and Finlay 2012). Physiologically the gut microbiota has been shown to be important in critical developmental periods for gut development (Sommer and Backhed 2013).

In the studies of various bacterial strains and microbial effects on the host, behavioral effects were examined and a link between the gut-brain-microbiota axis as a bidirectional neurohumoral communication network developed (Collins, Surette, and Bercik 2012, McLean et al. 2012). The ability for specific strains of bacteria to produce neurotransmitters such as serotonin and gamma-aminobutyric acid (GABA) is a proposed role in some of the brain-gut communication and modulatory function with therapeutic potential (Patterson et al. 2014).

Within these roles mentioned and the many other roles lie the potential for disruption of homeostasis and disorder under abnormal conditions when the microbiota are not maintained. In this state of dysbiosis, the microflora's role in the immune system for tolerance and homeostasis is unbalanced and can contribute to many issues including inflammatory conditions such as inflammatory bowel disease and allergic responses such as asthma (Sanders et al. 2013). When homeostasis is not maintained within the organism, it can hold the potential for prolonged states of normal processes functioning abnormally, such as chronic inflammation, that can lead to the development of cancer (Blumberg and Powrie 2012).

With conditions in dysbiosis contributing to diseases, such as inflammatory bowel disease, the progression, and pathology of disease lends the microbiota itself as possible therapeutic targets with rebalancing strategies such as probiotic treatments (Sanders et al. 2013, Moraes-Filho and Quigley 2015). With the diversity of individualized naturally acquired microbiota, the therapeutic developments will need to address the strain-specific variation and provide evidence-based targeted therapies. Understanding the roles and

functions of the diversity of microflora has vast implications and applications in adjunct therapies for the treatment of disease and disorders.

The nasal cavity and the respiratory system is significant in its microbial-host interplay. The lower respiratory tract is vulnerable due to a delicate alveolar network, and the most caudal nasal cavity where the olfactory epithelium is located is a potential point of entry to the central nervous system (CNS) as OSNs are unique in their direct communication and direct monosynaptic connection to the OB within the telencephalon. This is a feature that has been described in infectious and toxicological investigations. Viruses with the capability to enter the CNS via the olfactory neurons include diseases of significant importance in human health such as rabies, poliomyelitis, and pseudorabies (Lafay et al. 1991, Mulder et al. 1996, Flexner and Clark 1912). Additional viruses of importance that utilize receptor cell incorporation and trans-neuronal transport in intranasal exposure are Adenoviruses, Borna virus, Equine Herpesvirus, Influenza A, Canine Distemper, and Vesicular Stomatitis virus (Barnett, Cassell, and Perlman 1993, Zhao, Otaki, and Firestein 1996, Morales et al. 1988, Rudd, Cattaneo, and von Messling 2006, Narita et al. 2001, Aronsson et al. 2003).

The nasal microbiota is described by Abramson et al in canines in 1976 with results of predominantly *Enterococci* and *Staphylococci* and the observation that location composition differed with a 46% incidence of Gram-negative rods on the inferior nasal portion sampled (Abramson et al. 1976). This led to another study by Abramson et al in 1980 on the anterior and superior regions of the canine nares with results of a difference in microbial population from *Streptococci, Clostridia, and Staphylococci* anteriorly, low recovery superiorly mostly with *Bacillus sp*. cultured (Abramson, Isenberg, and

McDermott 1980). The profiling of the microbiota throughout the nasal passages has overlooked the microbiota of the olfactory system and it is not well established. The recognition of the distinct microenvironment of the olfactory system has led to emerging work in mice that demonstrates a similar core biome as seen with many mucosal sites, with the two dominant phyla composing *Firmicutes* (30-70%) and *Bacteroidetes* (15-60%), followed by *Proteobacteria* (5-25%) and *Actinobacteria* (<10%) in descending abundance respectively (Francois et al. 2016). In a study with humans, an indirect evaluation of the olfactory-adjacent region of the nasal mucosa, the three dominant phyla were markedly different in their ratios with *Actinobacteria* (50%), *Firmicutes* (24%), and *Proteobacteria* (20%) and less than 3% from *Bacteroidetes* (Yan et al. 2013). The three dominant phyla comprising approximately 75% of all microbiota found in studies of fecal samples in humans include *Firmicutes, Bacteroidetes,* and *Actinobacteria* (Gibson and Roberfroid 2008). There is great variation amongst species due to the nasal passage anatomical variations, in addition to genetic, environmental, behavioral, and individual differences. There is room for further investigation into the microbiota of the olfactory system directly and the potential relationships it has with the homeostasis and function of odorant detection and local immunity.

2.10 Metals and Microbes

Zinc has played an antimicrobial role in medicine and agricultural management for decades and even predates modern antibiotics as a means of microbial control. The

initial appreciation for zinc was in preparations for wound and dermatological conditions as well as in ophthalmology in ocular therapeutics (Haxthausen and Rasch 1928).

Toxicity has been associated with ionic zinc in the state of Zn^{2+} and for formulations with salts such as zinc sulfate and zinc gluconate (Hamidovic 2015, Duncan-Lewis, Lukman, and Banks 2011). A study of zinc neurotoxicity focused on the salts associated with the zinc and found that the toxicity level was salt-linked (Pavlica, Gaunitz, and Gebhardt 2009). Categorizing the effects using concentrations ranging from 0.05–0.3 mM placed citrate and sulfate at the highest, orotate acetate, chloride, and gluconate as moderate and histidinate the lowest (Pavlica, Gaunitz, and Gebhardt 2009). Across studies evaluating preparations with salts a 0.01% neurotoxicity cutoff in animal studies is established (Hansen et al. 1994).

Use of zinc nanoparticles in more recent years has been as zinc oxide primarily. The zinc oxide nanoparticles are used as drug carriers and in medical devices for their antimicrobial properties and antibiofilm formation (Coughlan et al. 2008, Holt et al. 2018). Directly using zinc to mitigate gastrointestinal disease is seen with the supplementation of zinc in animal feeds as well as in children and susceptible individuals throughout third world countries (Stensland et al. 2015, Lazzerini and Wanzira 2016). Studies of the antimicrobial effects of zinc nanoparticles have been limited to nanoparticles sized ≥3nm and as zinc oxide nanoparticles. These studies have shown a spectra of size-based antimicrobial effects with the smaller size having a greater capacity for microbial suppression, though generally suppressive across doses (Emami-Karvani and Chehrazi 2011, Raghupathi, Koodali, and Manna 2011).

The use of toxicity data from zinc across preparations, oxidation levels, and size are lacking in continuity. The concentration used with this study on the olfactory tissue is 0.02 nmole/L zinc nanoparticles, equal to 1.3076 e^{-10} % and falls exponentially below the 0.01% neurotoxicity cutoff. The differential effects of ionic zinc to zinc nanoparticles on olfactory sensory neurons indicates the expected toxicities within the microenvironment of the olfactory system may also be inconsistent with the ionic zinc or zinc oxide studies. Further studies to evaluate the effects that zinc nanoparticles have on the microbial community could serve as an indicator of the biological role that zinc nanoparticles may play that is divergent from the effects of ionic zinc, zinc salts, and zinc oxides.

2.11 Objectives

This project is to understand the fundamental role of zinc metal nanoparticles in the initial events of olfaction, their nano-level interactions, and micro-environmental influences.

1. The first aim of this work involved characterizing the physical-chemical properties and mechanisms of zinc nanoparticle enhancement of olfaction. Methods used in support of this aim included zinc nanoparticle production though underwater high-voltage discharge method and nanoparticle evaluation through transmission and scanning electron microscopy (TEM and SEM), atomic force microscopy (AFM), X-ray photoelectron spectroscopy (XPS), and laser Doppler velocimetry (LDV). Each of these techniques allows us to view the nanoparticle structure, to determine their size distribution, their oxidative state, and measure the particle zeta potential respectively.

This information further allows for calculations to determine the electron shell and core make-up of the nanoparticle. Characterizing the zinc nanoparticle with peak influence on olfaction enhancement allows for further consideration in reproducibility for potential applications and in understanding the biological role in olfaction.

2. A second aim utilizes polyethylene glycol as a nanoparticle coating to physiologically preserve the zinc nanoparticles olfaction enhancement capabilities over time and heat exposure. Methods involved techniques to characterize their physiochemical properties included TEM, SEM, AFM, XPS, and LDV to provide a comparison with bare zinc nanoparticles. This application based development supports reproducibility and storage stability of zinc nanoparticles through a non-toxic, digestible coating preserving olfaction enhancing physiological properties.

3. A third aim was to isolate and physiologically characterize endogenous nanoparticle filtrate isolated from olfactory epithelial and respiratory epithelial tissues. Methods used in the accomplishment of this aim include tissue isolation, homogenization, and serial filtration to result in an ultra-fine filtrate. Electrophysiological evaluation utilized EOG on isolated OE evoked by standard odorant mixture with either OE or RE filtrate and baseline without filtrate.

4. A fourth aim is to describe the micro-environmental influence of zinc nanoparticles in their interactions with microbiota. Methods to evaluate the influence of zinc nanoparticles include co-culturing of zinc nanoparticles with multiple bacterial taxa in liquid media for spectrophotometric analysis as a viability assay. Using this technique allows for an understanding of the effects the presence of zinc nanoparticles have on the ability of bacterial species to grow under a series of concentrations.

This research is important and significant in uncovering the mechanisms of olfactory sensory receptor zinc nanoparticle enhancement. There is a gap in knowledge defining the molecular mechanisms involved in olfaction, and this work may contribute to closing that gap. Continuing research in the neuroscience of olfaction and technology may secure future applications in neurodegenerative medical conditions that involve a loss of smell such as Alzheimer's and Parkinson's, psychological conditions associated with loss of smell such as schizophrenia and depression, occupational health and safety, public health, agricultural production and processing, aromatic technologies related to perfume industries, and global security in detection enhancement.

Chapter 3.0 Physical-chemical properties of zinc nanoparticle olfaction enhancement[1]

[1] A portion of this chapter is published: Hagerty, S., Y. Daniels, M. Singletary, O. Pustovyy, L. Globa, W. A. MacCrehan, S. Muramoto, G. Stan, J. W. Lau, E. E. Morrison, I. Sorokulova, and V. Vodyanoy. 2016a. "After oxidation, zinc nanoparticles lose their ability to enhance responses to odorants." Biometals 29 (6):1005-1018. doi: 10.1007/s10534-016-9972-y.

3.1 Abstract

Zinc nanoparticles were isolated from human and animal blood in the form of proteon nucleating centers (PNCs). Characterization of these nanoparticles demonstrated a true nanoscale size of 1 to 2 nm and a crystal lattice fringe consistent with metallic zinc. Unique to these zinc nanoparticles was the capacity to enhance the electrical response of olfactory sensory neurons to odorants by three-fold. This enhancement was dependent on the presence of odorant and was reversed when zinc ions were applied versus the zinc nanoparticles. Laboratory reproduction aimed at a nanoscale metallic zinc nanoparticle duplication was developed using the underwater electrical discharge method. The laboratory produced zinc nanoparticles exhibited the same electrophysiological enhancement in olfactory sensory neurons with a 3-fold amplification as measured by whole cell patch clamp and electroolfactogram (EOG). Characterization of the zinc nanoparticles in size distribution, the degree of oxidation, structure, ion concentration, and an assessment of the charge stability of the dispersed system is needed to establish the stability of the zinc nanoparticles and provide further insight into their potential mechanism of action. Electrical responses of olfactory sensory neurons to odorants were examined in the presence of zinc nanoparticles of differing degrees of oxidation. A subset of the laboratory zinc nanoparticles was subjected to oxidation by percolation and analyzed by atomic force microscopy for size distribution, X-ray photoelectron spectroscopy for elemental composition, transmission electron microscopy (TEM) for structural analysis, suspension analysis for zinc ion quantification, and laser doppler velocimetry for the zeta potential. Zinc nanoparticles were 1.2±0.3 nm in diameter consisting of 94% non-oxidized zinc atoms, a hexagonal close pack lattice crystal

structure, high surface atom percentage at 80%, and a zeta potential of -42.4 ± 4.8 (SE) mV, which all support a highly stable and chemically reactive configuration. The small zinc nanoparticles significantly enhanced electrical responses on EOG. Oxidation of zinc nanoparticles at varying sizes including the small zinc nanoparticles (1.2 nm) and ZnO standard samples in nanoscale (15 nm and 70 nm) did not produce enhancement on EOG. This loss of enhancement capability was independent of size, high surface to volume ratio, and ion concentration. Instead, this olfaction enhancement in response to odorant would suggest physical state play a significant role in the mechanism of action.

3.2 Introduction

Zinc metal nanoparticles (ZnNPs) are present in human and animal blood. The endogenous and engineered ZnNPs were found to significantly enhance olfactory responses to the odorant by about 3-fold as measured by single cell measurements with whole cell patch-clamp or collective olfactory tissue measurements through electroolfactogram (EOG) (Viswaprakash et al. 2009, Viswaprakash et al. 2006). Zinc nanoparticles create no odor effects alone but increase the odor response if mixed with an odor. In small concentrations, effects are dose-dependent and reversible. The particles are spontaneously eliminated from the olfactory mucosa; providing a specific, sensitive, and efficient way of olfactory response control. Some other metal nanoparticles such as copper, gold, and silver do not present the results observed for zinc. Gold and silver nanoparticles created a transient enhancement, while copper nanoparticles did not affect the relative EOG amplitude, but prolonged the overall stability of the signals (Viswaprakash et al. 2009). When zinc nanoparticles were replaced by Zn^{+2} ions at the

same concentrations, a decrease in receptor neuron response was recorded. When the enzymatic decomposition of the second messenger cyclic adenosine monophosphate (cAMP) was eliminated by the membrane-permeable phosphodiesterase inhibitor 3-isobutyl-1-methylxanthine (IBMX), the increased ciliary cAMP levels rose above threshold resulting in membrane depolarization which produced EOG signals that were not enhanced by the addition of zinc nanoparticles (Moore et al. 2012). Based on these findings, we determined that zinc nanoparticles function at the olfactory receptor level and are engaged in the initial events of olfaction.

A kinetic model of olfactory receptor/odorant/metal interactions based upon experimental results described a stoichiometry of metal nanoparticles and receptors, and the mode of their action (Vodyanoy 2010). The kinetic olfactory model estimated that one metal nanoparticle binds two receptor molecules to make a dimer. A canine detector model was utilized in an effort to translate the receptor potentials at the olfactory epithelium to higher cognition brain center perception. Awake and anesthetized canines were exposed to odorant alone and odorant plus zinc nanoparticles while live-recordings obtained in functional magnetic resonance imaging unit (fMRI). Our canine fMRI results indicate that the addition of zinc nanoparticles results in a significant increase of brain excitation in response to odorants. This is consistent with the increase in excitation of olfactory sensory neurons observed in response to higher vs. lower concentrations of odorants (Jia et al. 2012, Jia et al. 2014, Jia et al. 2015). We also found that zinc nanoparticles enhanced sensitivity to odor intensity with no effect on odor valence perception. These results agree well with our *in vitro* electrophysiological results. The fact that zinc nanoparticle enhancement was seen in awake dogs, both young and mature

cell cultures (Viswaprakash et al. 2010), and dissected olfactory epithelium (OE) coupled with endogenous zinc nanoparticle isolation in live animals' blood (Samoylov et al. 2005), reveals the suggested significance of this enhancement for the initial events in olfaction. This study targets characterizing the olfaction enhancing zinc nanoparticles and oxidized zinc nanoparticles by physical-chemical means. Functional evaluation with electrophysiology and determination of chemical composition were performed with EOG, AFM, XPS, TEM, LDV, and ion quantification.

3.3 Materials and Methods

3.3.1 Animals

Animals used in this project were cared for by the Division of Laboratory Animal Health of Auburn University assuring compliance with all applicable regulations. The primary regulations governing the care and use of animals utilized in research and teaching include the following: the Animal Welfare Act, the NIH-PHS Policy, the Guide for the Care and Use of Laboratory Animals, and the Guide for the Care and Use of Agricultural Animals in Agricultural Research and Teaching. The protocol was approved by the Auburn University Institutional Animal Care and Use Committee (AU IACUC) committee. Active efforts were made to avoid exposing animals to discomfort, pain, or injury. Adult male Sprague–Dawley rats (Envigo, Dublin, VA) weighing 250 g to 300 g were used.

3.3.2 Metal nanoparticles

Metal nanoparticles were produced by a modified method (Tokushige, Nishikiori, and Ito 2010, Kruyt 1952). The system consists of a water container, having a high-voltage generator connected to two metal electrodes submerged in water. By controlling the voltage and distance between electrodes, the plasma created underwater produces a very fine dispersion of the metal into nanoparticles. Two metal electrodes (Alfa Aesar, 99.9999%) of 2 mm diameter are positioned in a large Pyrex jar ≈ 7 mm below the gas-water interface at the distance between electrodes of ≈ 0.5 cm. 750 mL of LC-MS grade water (Omnisolv) are used in this procedure. Before the experiment, to remove dissolved oxygen, the water was heated up to boiling point and boiled until the large vapor bubbles appeared. The water then cooled to 298.15 K (25 ^{o}C) and for 20 minutes percolated with nitrogen gas produced by evaporation of liquid nitrogen. The jar filled with nitrogen gas was placed in the water bath with running water to prevent overheating. An alternating voltage of 15 kV and 60Hz, was applied to the electrodes, and the electric discharge was sustained for 1 h. The water suspension was collected in a 1 L glass beaker and placed in the refrigerator for 12 h to allow large metal particles to sediment. Suspended particles were separated from the sediment and subjected to centrifugation at 147,099.75 m/s^2 (15,000 g_n) for 2 h at 298.15 K (25 ^{o}C). After centrifugation, the pellet was discarded, and the supernatant was subjected to further centrifugations to produce fractions of nanoparticles enriched in particles of particular sizes. The centrifuge speed and time to separate nanoparticles by size was estimated with Stock's equation.

$$U=g_n d^2(D-\rho)/18\eta,$$

where U was the rate of sedimentation, g_n – acceleration, d – diameter of the nanoparticle, D, and ρ are densities of metal and water, respectively, and η is the viscosity of water.

Zinc nanoparticles were size-selected for 1 nm to 2 nm diameters. These were prepared by the electrical discharge method as described above, a part of the small zinc nanoparticles was oxidized by percolating air through the suspension of nanoparticles for 20 min at 313.15 K (40 ^{o}C). The air for the oxidation procedure was obtained by evaporation of liquid air. Zinc oxide nanoparticles provided by NIST with nominal diameters of 15 nm and 70 nm (Black et al. 2012, Cline et al. 2013) were also used in olfactory experiments.

The particle suspensions were analyzed similarly to methods described previously (Samoylov et al. 2005, Vodyanoy et al. 2016, Daniels, MacCrehan, and Vodyanoy 2015). The total concentration of metal in suspension was measured by atomic absorption spectra (GTW Analytical Services), and the particle size and number determined by the atomic force microscopy (AFM). The crystallinity of small nanoparticles was analyzed by the Transmission Electron Microscopy (TEM). The degree of nanoparticle oxidation was obtained from the X-ray photon spectroscopy (XPS).

3.3.3 Zn^{2+} ion concentration in suspensions of nanoparticles

Zinc ion concentration was measured in the zinc and zinc oxide nanoparticle water suspension. The concentration of Zn^{2+} ions in suspensions of small zinc nanoparticles was measured before and after oxidation. Zn^{2+} measurements were carried

out with duplicate samples. Zinc ion levels were measured using the Colorimetric Zinc Ion Quantitation Kit (AAT Bioquest, Sunnyvale, CA) according to the manufacturer's instructions. Optical density values were measured at 620 nm using a microplate reader (Bio-Tek, Winooski, VT). The zinc ion concentration of the sample was determined by comparison of experimental mean values with curves generated by standards, supplied with the assay. The minimum detectable concentration of the assay was 0.1 μmole/L.

3.3.4 TEM

TEM was performed using an FEI Titan at 300 kV. A few microliters of air-dried droplets of the Zn NP suspension were spread onto a holey carbon substrate on copper TEM grids. Fringes widths were measured on different nanoparticles, and the Miller-Bravais indices of the crystalline structures were calculated using the Crystallography lab software (Gu, Furuharaa, and Zhang 2016).

3.3.5 AFM

Images of metal nanoparticles were taken by Bruker MultiMode 8 (Santa Barbara, CA) atomic force microscope in Tapping® (intermittent-contact) mode, using PPP-SEIH Nanosensors (Neuchatel, Switzerland) AFM probes; the nominal values specified by the vendor for the force constant and the resonance frequency of these probes are 15 N/m and 130 kHz, respectively. The AFM calibration was verified before measurements on

crystallographic 6H-SiC (0001) steps. From the topographical micrographs of these steps, the AFM calibration was found to be within 3% accuracy of the nominal height (0.75 nm) of SiC single half-monolayers. The AFM imaging was used to measure the size distribution of particles. Monolayers of zinc nanoparticles were prepared on a mica substrate for all measurements by depositing and evaporating a small amount of 0.01% nanoparticles water suspension on freshly cleaved mica surfaces.

3.3.6 XPS

XPS was used to make quantitative spectroscopic measurements of the elemental composition of the nanoparticles' surfaces. The Kratos Axis Ultra delay-line detector (DLD) instrument in the hybrid mode used a monochromatic Al Kα1,2 x-ray source (hυ = 1486.6 eV). The stoichiometry of the Zn and ZnO components were determined from the high-resolution spectra of Zn 2p (1017 eV to 1057 eV) and were acquired using a pass energy of 40 eV with an energy resolution of 0.1 eV. A Gaussian distribution was used for peak fitting, with a full width at half maximum (FWHM) constraint of 1.7 eV which was obtained from the C 1s peak located at 285 eV (BE). Water suspensions containing zinc and zinc oxide nanoparticles were deposited separately on silicon wafers and allowed to evaporate during pump down to minimize oxidation. To examine the stability of zinc metal nanoparticles, the particles were stored at 5 ^{o}C for 317 days, and XPS measurements were made at the beginning and the end of the storage.

3.3.7 Zeta potential

Zeta potentials of the nanoparticles in water suspension were measured with a Zetasizer Nano ZSP (Malvern Instruments, Worcestershire, UK) by the LDV technique (Hagerty et al. 2016a). The average of six sequential runs was obtained. Zeta potentials were estimated by Henry's equation:

$$\zeta=3\eta\mu/2\varepsilon F(k\alpha)$$

in which ζ is the zeta potential, η is the viscosity, μ is the electrophoretic mobility, ε is the dielectric constant of the medium and $F(k\alpha)$ is Henry's function, which equals 1.5 using the Smoluchowski equation (Jachimska, Wasilewska, and Adamczyk 2008).

3.3.8 Odorants

Odorants were purchased from Sigma-Aldrich. An odorant mixture containing 1.6 mmole/L each of ethyl butyrate, eugenol, and (+) and (–) carvone in water was mixed with a vortex and stored in a dark glass bottle until the experiment.

3.3.9 Delivery of odorants and metal nanoparticles

For stimulation, a 0.25 s pulse of the odorant mixture at 55158 N/m^2 (8 psi) was formed by a computer-controlled Pneumatic PicoPump PV800 (World Precision Instruments, Sarasota, FL). A pulse of positive pressure drove the odorant into a glass nozzle directed at the olfactory epithelium. The residual odorant was cleared by air

between each stimulus application. The odorant pulse patterns were initiated manually at predetermined time intervals or automatically by computer. The automatic computer routine was composed of 0.25 s pulses at 20 s and 60 s intervals for EOG recording. One series of 10 pulses at 20 s intervals constituted one ‘‘EOG recording’’. Thus, in the automatic regime, the single EOG recording had a duration of 200 s and could correspond to 10 response traces. These recordings were repeated as many times as needed to cover a desirable number of pulses and duration for a single experiment. A nanoparticle suspension was mixed with odorant solutions to make final nanoparticle concentrations of 0.02 nmole/L. During the puff, the odorant vapor containing metal nanoparticles was delivered to the OE surface. We showed that delivery of metal nanoparticles by the water vapor and the liquid suspension produced an efficient transfer of particles to the olfactory epithelium (Viswaprakash et al. 2009). The odorants and nanoparticles delivered by the water vapors were perceived by live animals (Jia et al. 2014, Jia et al. 2016).

3.3.10 Electrophysiology

Our measurements are based on Electroolfactography (EOG) (Viswaprakash et al. 2009). The method utilizes Axon Instrument MultiClamp 700A amplifier and 1322A DigiData acquisition system.

Rat septal olfactory mucosa was dissected out and placed in a perfusion chamber such that the basal portions were immersed in physiological buffer (containing 137 mmole/L NaCl, 5.3 mmole/L KCl, 4.2 mmole/L $NaHCO_3$, 0.4 mmole/L KH_2PO_4, 3.4

mmole/L Na_2HPO_4, 1.3 mmole/L $CaCl_2$, 0.2 mmole/L $MgSO_4$, and 5.6 mmole/L D-glucose at pH 7.4), while the epithelial surface with olfactory cilia was exposed to air. Patch electrodes of approximately 24 μm tip opening areas filled with the same physiological buffer were connected to a patch-clamp amplifier to detect responses from the olfactory epithelium. Once contact between the electrode and the surface of the olfactory epithelium was formed, air puffs of the odorant mixture were applied. Zinc metal or metal oxide particles were added to the odorant mixture. Odor responses over the time course of several minutes were recorded after being amplified by a patch-clamp amplifier and filtered at 2 kHz to 5 kHz. The stimuli were given by 3 sequences. The sequence I was composed of the pulses (1) odorant mixture, (2) odorant mixture +small zinc nanoparticles, (3) odorant mixture + 15-nm ZnO nanoparticles, (4) odorant mixture + 70-nm ZnO nanoparticles, (5) 15-nm ZnO nanoparticles, (6) 70-nm ZnO nanoparticles, and (7) water vapors. The sequence II contained pulses of (1) odorant mixture, (2) odorant mixture +small zinc nanoparticles, (3) odorant + small ZnO nanoparticles, (4, 5) water vapor. The sequence pulses III was applied to the olfactory and respiratory epithelia and composed of (1) odorant mixture, (2) odorant mixture +small zinc nanoparticles.

At one contact, 3 to 5 repetitions of EOG recording of 10 traces each were collected. After completion of EOG recording in the first contact, the electrode was moved to another area of the olfactory epithelium, and a new contact was made to generate 3-5 repetitions of EOG recording. EOG were collected from 3 to 5 regions of the epithelium and experiments were replicated with 2-3 epithelia for each sequence of pulses.

3.4 Results

3.4.1 TEM

Zinc metal nanoparticles are shown in Figure 3.1, as TEM micrographs. The TEM micrographs reveal nanoparticles with diameters of approximately 2 nm to 5 nm in size showing crystal lattice fringes. Fringes corresponding to metallic zinc core.

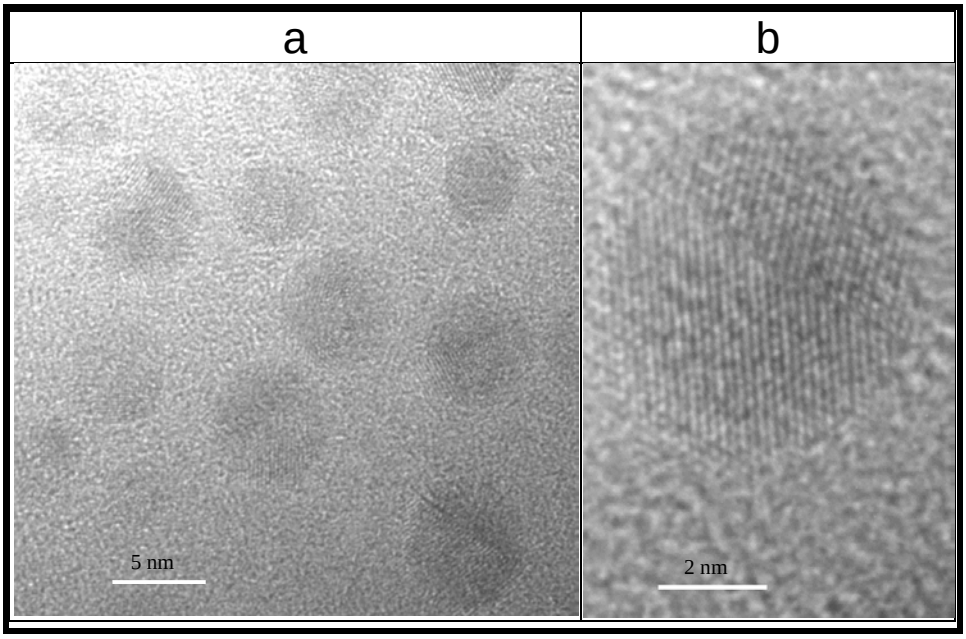

Figure 3.1 Transmission electron microscopy of zinc metal nanoparticles. (a) bar: 5 nm. (b) bar: 2 nm.

3.4.2 AFM and XPS

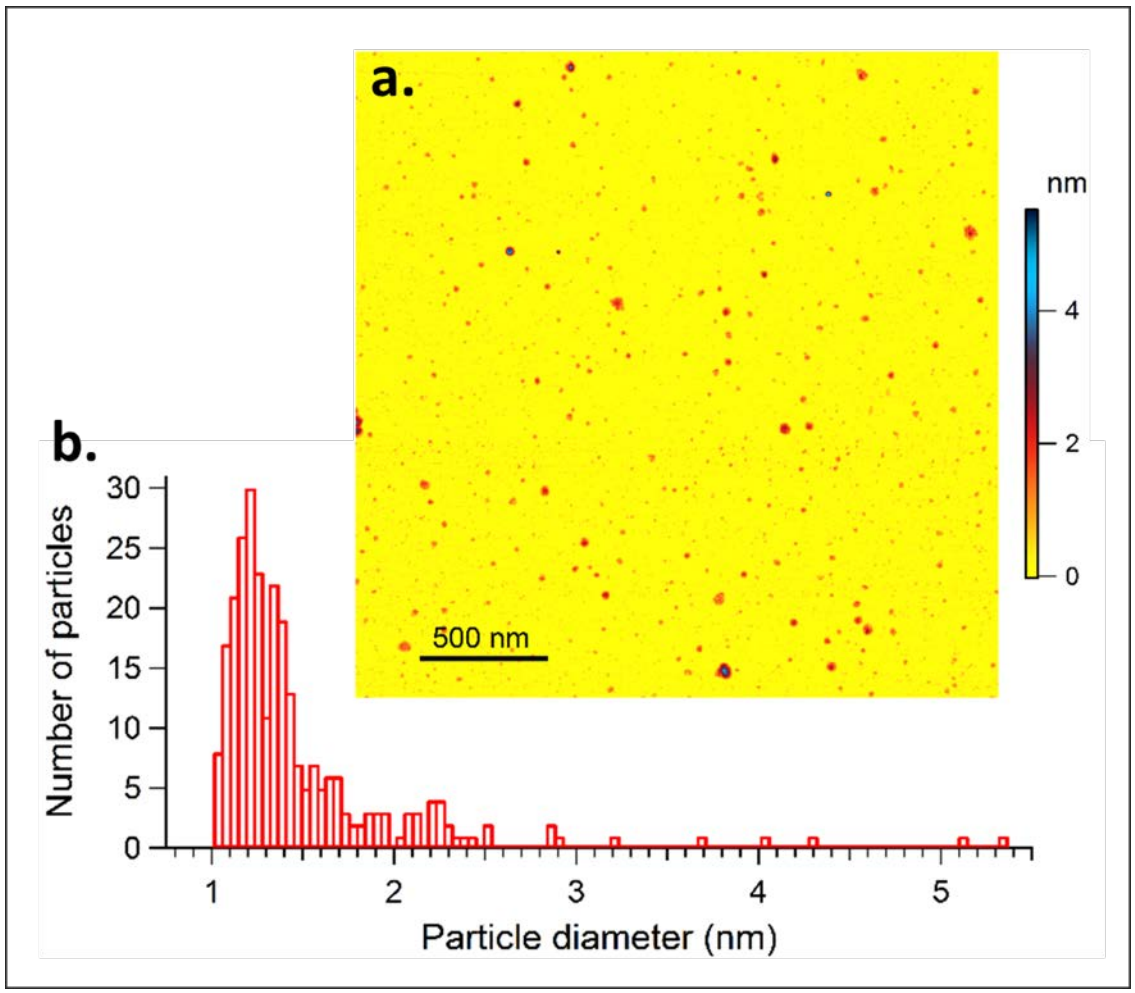

Figure 3.2 Physical characterization of small zinc nanoparticles. a. Atomic force microscope image, 0.01% zinc nanoparticles on mica. 270 nanoparticles with height above 1 nm were detected over a 2.5 μm2 area. b. Size distribution of the particles imaged in a. (Permission from Dovepress # 11575629)

Figure 3.2 exhibits the physical properties of zinc nanoparticles prepared by high-voltage discharge. AFM showed the size distributions of Zn nanoparticles, with average diameters of 1.2±0.3 nm (Figure 3.2 a). A histogram (Figure 3.2 b) shows a distribution with a relatively high peak around the average value (the standard deviation [SD] was

calculated from the bell distribution around the peak) and the tail up to 6 nm. Figure 3.3 displays the XPS of freshly prepared (3 days old) 1.2 nm zinc nanoparticles. The XPS analysis of the Zn $2p_{3/2}$ core line revealed that metallic zinc nanoparticles were oxidized to a minimal extent, where the relative atomic concentrations of Zn and ZnO species were determined to be (93.9±3.4 (SD)) % and (6.1±3.4 (SD)) %, respectively. These data reveal that about 94% of metal atoms were not oxidized. In contrast, the 1.2 nm zinc oxide nanoparticles were found to contain smaller concentrations of metallic zinc (88.5±2.1 (SD)) % and a higher concentration of oxidized zinc (11.5±2.1 (SD)) %, respectively.

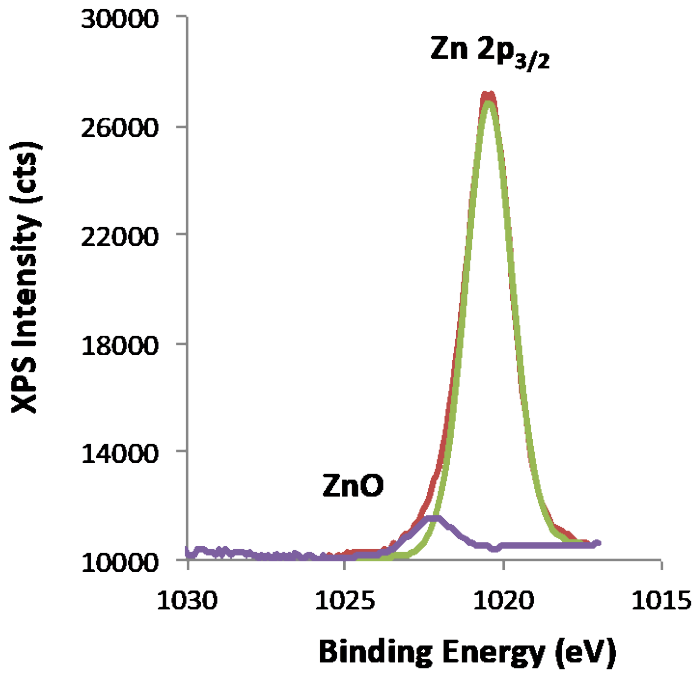

Figure 3.3 XPS Zinc nanoparticles. High-resolution XPS analysis showing the Zn 2p3/2 core line, with the Zn peak occurring at a binding energy of 1020.9 eV and the ZnO peak occurring at 1022.5 eV.

Table 3.1 Properties of nanoparticles

Sample	Size, nm	[1]S/V ratio nm^{-1}	Total Number Of atoms	Number of atoms in shell	[2]f	[3]Zn^{2+}ion] μmole/L	% Oxidized	% non-oxidized
Zn	1.2	5.00	59	47	0.80	4.8±0.5	6.1±3.4	93.9±3.4
ZnO	1.2	5.00	76	62	0.82	1.0±0.20	11.5±2.1	88.5±2.1

1- Surface to volume ratio, 2 - Fraction of surface atoms, 3 - Concentration of Zn2+ions in the stimuli suspension before application to olfactory epithelium (mean value ± SD).

3.4.3 Zn^{2+} ion concentration in suspensions of nanoparticles

The Zn^{2+} ion levels are given in Table 3.1 The Zn^{2+} ion concentrations are presented as mean values ± standard deviation (SD). The zinc ion concentration in the suspension of 1.2 nm zinc nanoparticles is more than 4 times greater than that of 1.2 nm zinc oxide. The zinc ion concentration in all ZnO suspensions varies between 1 μmole/L and 13 μmole/L, while the relative amplitude of EOG evoked by the odorant+suspensions changes only by 0.1%.

3.4.5 Zeta potential

Zeta potentials were selectively evaluated for the subset of zinc nanoparticles capable of olfactory enhancement. Therefore the 1.2 nm non-oxidized zinc nanoparticles in water suspension were measured to assess the electric potential at the slipping plane between the inner stern layer and the diffuse layer. Results of six runs measured the zeta potential at -42.4 ± 4.8 (SE) mV for zinc nanoparticles.

3.4.6 Odorant responses to Oxidation

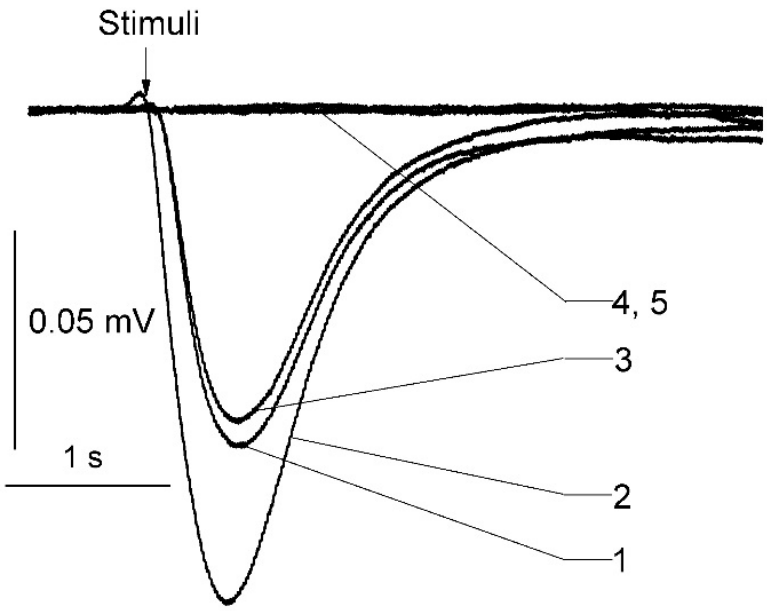

Figure 3.4 Representative EOG recordings from rat olfactory epithelium. The stimuli were of 0.25-s pulses of (1) odorant mixture, (2) odorant mixture +1.2-nm zinc nanoparticles, (3) odorant + 1.2-nm ZnO nanoparticles, (4, 5) water vapor. This is a typical representation of 300 traces.

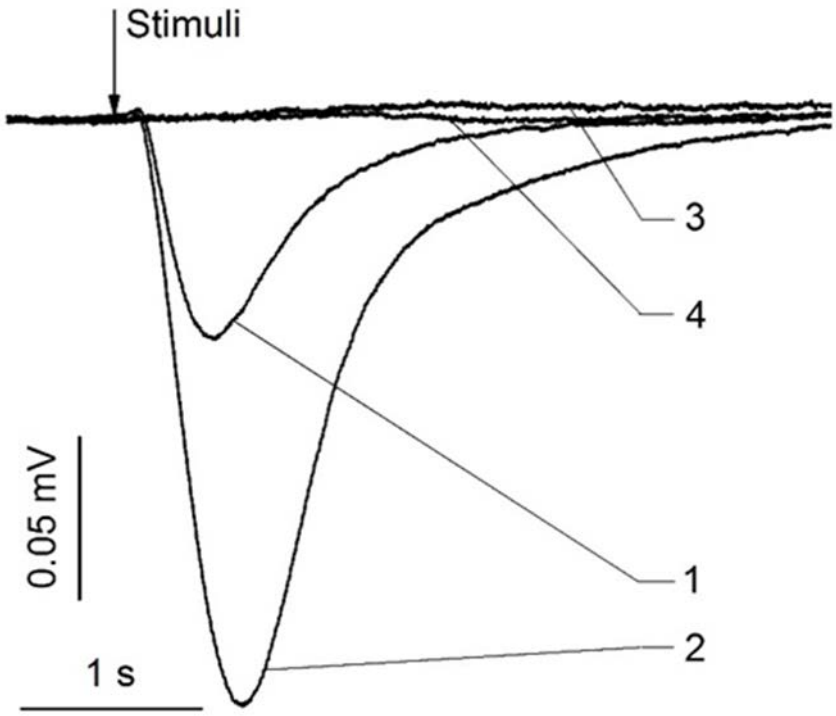

Figure 3.5 Representative EOG recordings from rat olfactory and respiratory epithelia. The stimuli were of 0,25-s pulses of odorant with or without nanoparticles. (1) olfactory epithelium, odorant mixture, (2) olfactory epithelium, odorant mixture +small zinc nanoparticles, (3) respiratory epithelium, odorant mixture, (4) respiratory epithelium, odorant mixture +small zinc nanoparticles.

Representative EOG recordings depicted in Figure 3.4 shows odorant responses modified by 1.2 nm zinc nanoparticles. The relative peak amplitudes are given in Table 3.2. Only non-oxidized zinc nanoparticles enhance odorant responses. The oxidized nanoparticles manifested a slight decrease of the EOG amplitude when they were mixed with odorants. The EOG signals evoked by ZnO nanoparticles with water vapor (no odorants) were minuscule and not much different from the EOG responses to water vapor (Table 3.2, Figure 3.4, traces 5-7). The control experiments with respiratory epithelium show no response to the odorant and a mixture of odorant with zinc metal nanoparticles (Figure 3.5).

Table 3.2 Effect of nanoparticles on the odorant responses

[1]Stimuli	Nanoparticle Size, nm	[2]Relative amplitude
Zn + odorant	1.2	1.46±0.032
ZnO + odorant	1.2	0.82±0.017
ZnO + odorant	15	0.88±0.014
ZnO + odorant	70	0.85±0.019

1 – Excitation of EOG by 1. 6 mM odorant vapor + 0.2 nM of nanoparticles,
2 – Relative amplitude of the EOG peak evoked by the stimuli to the EOG peak evoked by odorant alone ($p<0.05$).

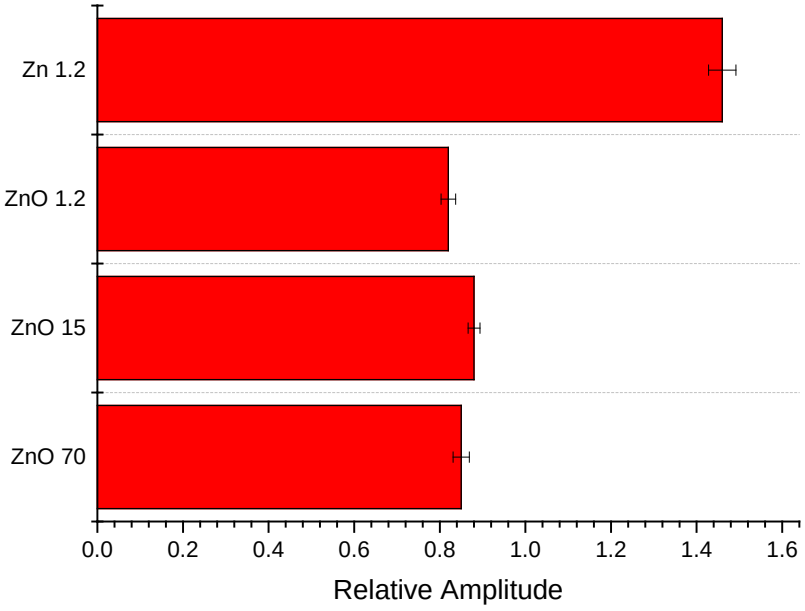

Figure 3.6 Graph of relative amplitude in mV for small (1.2 nm) zinc nanoparticles, small (1.2 nm) oxidized zinc nanoparticles, zinc oxide 15 nm, and zinc oxide 70 nm. Statistical significance found between all oxidized zinc nanoparticles (1.2 nm, 15 nm, and 70 nm) and non-oxidized zinc nanoparticles $p < 0.05$.

3.5 Discussion

Metals and the field of neurobiology are intertwined, and zinc plays a central role. Zinc is specifically found in high concentrations in the neurobiology of olfaction within the olfactory bulb and higher cognitive center (Frederickson and Danscher 1990, Sensi et al. 2009). Measuring zinc levels is difficult using most available techniques to differentiate between total zinc and zinc nanoparticles of varying sizes, in particular our nanoscale zinc at <2 nm, therefore, most studies evaluating the distribution of zinc in the

brain were studied by methods that cannot discriminate between zinc ions and zinc metal particles (Takeda 2001, Takeda et al. 1997). The zinc content in whole rat blood is ≈100 μmole/L. (Fugano), but Zn^{2+} ion concentrations in the neuronal extracellular fluid are estimated to be 0.15 μole/L (Takeda 2000). The intracellular free Zn^{2+} ion concentration in neurons is estimated to be ≈1 nM (Canzoniero, Sensi, and Choi 1997). The physiological role of the endogenous Zn^{2+} ions in the olfactory sensory neurons is not very clear. However, added zinc ions at concentrations 20 μmole/L can inhibit the stimulatory GTP-binding protein of adenylyl cyclase (Gao, Du, and Patel 2005), an important component of the initial events of olfactory signal transduction. The physiological role of endogenous Zn^{2+} ions is well studied in the neurons of the olfactory bulb. Localized to synaptic terminals, zinc ions can be released by membrane depolarization and can reach extracellular synaptic concentrations of 100–300 μM. The released zinc modulates neuronal excitability under normal conditions (Horning, Blakemore, and Trombley 2000, Horning and Trombley 2001).

The collective data of enhanced EOG responses to an odorant with engineered 1.2 nm zinc nanoparticles as they correspond to endogenous zinc nanoparticles found within human and animal blood (Samoylov et al. 2005) and these naturally occurring nanoparticles in physiologically analogous fashion also enhance olfactory responses (Viswaprakash et al. 2009). Further, translation of this electrophysiological data at the epithelial level to not only anesthetized but canine in a fully awake state also experienced enhancement of olfactory pathway regions in the high brain centers under fMRI imaging with the addition of zinc nanoparticles to odorant (Jia et al. 2016), this enhancement is significant for the initial events in olfaction.

The sensory system of olfaction is significant across species, but in mammals, it begins with the function of bringing air and its volatile odorant particulates by a sniffing mechanism into the nasal vestibule and to make contact with the olfactory epithelium. The odorant molecules come into contact with the mucus layer of the olfactory epithelium where it encounters numerous compounds, one of which can be an olfactory binding protein (OBP) that aides in the transportation of the odorant molecule to the receptor sites (Lancet and Pace 1987, Buck and Axel 1991). With the right receptor-odorant binding it initiates an intracellular cascade of signal transduction events, including the G-protein-dependent production of second messenger molecules by adenylyl cyclase (Breer 2003a, b) leading to the opening of ion channels and the passing of ion currents (Zufall, Firestein, and Shepherd 1991). This process triggers an action potential in the olfactory receptor neurons (ORNs) (Lancet and Benarie 1993) that projects directly to the olfactory bulb (OB) (Harel, Carmel, and Lancet 2003). The signal is then transmitted to the anterior olfactory nucleus, piriform cortex, periamygdaloid cortex, and entorhinal cortex via olfactory stria (Castiglioni et al. 2011). The phosphodiesterase activity in the cilia is accounted for rapid termination of the olfactory response by degrading odor-induced second messenger molecules (cAMP) (Boekhoff and Breer 1992, Firestein, Darrow, and M. 1991).

The enhancement of EOG responses to odorant by the zinc metal nanoparticles and inability to facilitate olfaction by addition to odorant zinc oxide nanoparticles may have a dual nature. The oxidation of zinc nanoparticles may change a physical state of the metal, but also could result in a production of zinc ions (Wöll 2007) that would inhibit olfactory responses. The inhibition by zinc ions may occur due to blocking cyclic-

nucleotide-gated-channels (Kramer and Molokanova 2001), activation of cAMP-specific phosphodiesterase (Percival et al. 1997), inhibition of adenylyl cyclase (Klein et al. 2004) and $G_{\alpha s}$-protein (Gao et al. 2005). Our results, however, show no correlation between the relative amplitude of the EOG peak and the concentration of Zn^{2+}-ions (Table 3.1 and 3.2). 1.2 nm zinc nanoparticles increase responses to odorant by a factor of 1.46 (Table 3.2). When these zinc nanoparticles were oxidized, they were not able to enhance responses to the odorant. This inability to enhance response to odorant is difficult to attribute to the inhibitory actions of zinc ions. The concentration of Zn^{2+} ions that go together with oxidized zinc nanoparticles is five times smaller than that accompanied non-oxidized zinc when the strong enhancement observed. Additionally, The Zn^{2+}ion concentration in all ZnO suspensions changes by 13 folds, while the relative amplitude of EOG evoked by the odorant+ZnO suspensions varies only by 0.1%. These data suggest that after oxidation, the changed physical state of zinc rather than the changed valence state is a nature of the ZnO nanoparticles failure to enhance olfactory odorant responses.

The TEM images reveal round nanoparticles of various diameters. The high-resolution images of zinc metal nanoparticles show lattice fringes which indicate that zinc nanoparticles are crystals. Within the uncertainty of our measurements, we found that the typical fringes of 0.21 nm and 0.17 nm correspond to [01$\underline{1}$1] and [01$\underline{1}$2] directions for the hexagonal close-packed crystal lattice of metal zinc. The results are consistent with those obtained for zinc nanowires and nanorod (Chen et al. 2007, Lu et al. 2016).

Figure 3.7 Illustration of Zinc Nanoparticles demonstrating hexagonal close packed lattice and 12 core atoms and 47 shell atoms and 1.2 nm. Illustration by Melissa Singletary.

The AFM and XPS spectra of small zinc nanoparticle reveal that they are 1.2 nm in diameter and consisted of more than 94 % of non-oxidized zinc atoms (Figure 3.7). The production of nanometer-sized metallic particles suggests the assembly of a significant number of metal atoms. The crystal structure of metallic zinc has a hexagonal close-packed lattice with a constant a=b=0.266 nm and c=0.495 nm. The unit cell contains 6 atoms and has a volume of 0.0912 nm^3 (Yoo and Wei 1967).

The total volume of the 1.2-nm particle is

$$V_{tot} = \frac{4}{3}\pi(0.6)^3 = 0.904\ nm^3$$

Then, the total number of atoms in the 1.2-nm zinc nanoparticle is estimated to be

$$N_{tot} = \frac{0.904 \times 6}{0.0912} = 59\ atoms$$

To estimate the number of atoms in the shell of 1.2-nm zinc nanoparticles, we find the volume of the shell as a difference between V_{tot} and V_{core} , where

$$V_{core} = \frac{4}{3}\pi(0.6 - \frac{0.495}{2})^3 = 0.183\ nm^3$$

$$V_{shell} = 0.904 - 0.183 = 0.721\ nm^3$$

Then the number of atoms in the shell,

$$N_{shell} = \frac{0.721 \times 6}{0.0912} = 47\ atoms$$

The number of atoms in the core

$$N_{core} = \frac{0.183 \times 6}{0.0912} = 12\ atoms$$

One of the remarkable properties of small metal nanoparticles is their stability in water and in blood plasma (Samoylov et al. 2005). It was discovered that metal nanoparticles with a particular number of atoms in a cluster have added stability. These atom numbers are associated with particular particle sizes, the number of shells, and percentage of surface atoms. To be expected, the higher the number of atoms, the more shells and the larger diameter of the particle while simultaneously a lower percentage of surface atoms. Atom numbers of 13, 55, 147, 309, 561, and 923 are so-called ‘‘magic numbers" of atoms. At 13, a single shell and less than 1 nm diameter are expected with a significant number of surface atoms over 90%. From 13 to 55 the shell number increases to 2 and diameter is expected to increase to approximately 1.4 nm and display an estimated 76% of surface atoms (Aiken and Finke 1999b). These nanoparticles designated as full-shell nanoparticles that are constructed by successively packed layers of metal atoms around a single metal atom (Aiken and Finke 1999a, Khanna, Rao, and

Jena 2002). The percolation of air through the suspension of 1.2 nm zinc nanoparticles for 20 min at 313.15 K caused a modest reduction of non-oxidized zinc atoms to 88% showing a significant resistance to oxidation. Similar resistance to atmospheric oxidation was observed in the chemically synthesized metallic zinc nanocrystals explained in part by the unique crystalline surface properties of the anisotropic nanoparticles (Mai et al. 2013a). The estimated 12 atoms of the core and the total 59 atoms of the 1.2 nm zinc nanoparticle are in close agreement with the "magic number" full-shell nanoparticles with 13 and 55 atoms. Each metal atom has the maximum number of nearest neighbors, which imparts some degree of extra stability to full-shell clusters (Aiken and Finke 1999a, Jena, Khanna, and Rao 1996).

The crystal structure of our zinc nanoparticles was a hexagonal close-packed lattice, and similarly, the zinc oxide also has a hexagonal close-packed lattice. The zinc oxide constants were a=b=0.325 nm and c=0.520 nm. The more prevalent form of zinc oxide found is with the wurzite structure. Assuming we have the more prevalent form, it then has two zinc and two oxygen atoms per unit cell, making a total of 4 atoms per cell and a volume of 0.0475 nm^3 (Morkoç and Özgur 2009).

The measured zeta potential of the zinc nanoparticles at -42.4 ± 4.8 (SE) mV informs that the zinc nanoparticles aggregate to a far lesser degree as the electrostatic repulsion between adjacent zinc nanoparticles experience electrostatic repulsion between each other due to like charge. The high range of zeta potential is indicative of a reasonable level of stability in solution with suggested resistance to breaking or flocculating in suspension over storage conditions.

The surface atoms of the 1.2 nm zinc nanoparticle account for 80% of all atoms, while the surface of the 1.2 nm zinc oxide nanoparticle contains 82% of all atoms (Table 3.1). Two standardized zinc oxide compounds of 15 nm zinc oxide and 70 nm zinc oxide were used for comparison and had 10% and 2.3% respectively of all atoms at the surface shell (Table 3.1). The high surface-volume ratio and fraction surface atoms are important to give a zinc nanoparticle the ability to bind olfactory receptor proteins and create dimers necessary for the active olfactory receptor-G-protein dimers (Vodyanoy 2010, Moore et al. 2012, Jia et al. 2015), though are more representative of nanoparticle size than oxidation state as the shell atoms were similar at 1.2 nm in size irrespective of oxidation, while at 15 nm and 70 nm zinc oxide nanoparticles are significantly reduced. We propose that endogenous zinc nanoparticles supply a particular quantity of functional receptor dimers that can be activated by the odorant and take part in the generation of the olfactory signal. The remainder of the monomeric receptors remain primarily inactive and do not contribute to the odorant-induced olfactory response. When the olfactory epithelium is exposed to a mixture of zinc nanoparticles and the same odorant, additional receptor dimers are recruited and established in the plasma membrane by joining pairs of previously unbound receptors. The appearance of new dimerized receptors increases the available, receptive field to respond to the odorant and results in an increase of the odorant-induced olfactory response.

Olfactory receptors belong to the 7-transmembrane receptor superfamily of proteins that have seven domains spanning the plasma membrane a total of seven times resulting in three intracellular loops with a carboxyl terminus and three extracellular loops with an amino-terminal end and coupled intracellularly with G-proteins (Buck and

Axel 1991). This GPCR is transmembrane in olfactory cilia with a plasma membrane thickness estimated at 5 nm (Mitra et al. 2004). Considering the membrane thickness and GPCR density in the OSN cilia, zinc nanoparticles (< 5 nm) capacity to bind two of these complexes is compatible with this membrane topology and thickness. A general high surface surface-to-volume ratio in nanoparticles lends a higher degree to membrane interaction and with the significant 80% of atomic concentration in the outer nanoparticle shell the 1.2 nm zinc nanoparticles should render receptor coupling efficiently.

The enhancement of the olfactory response by zinc nanoparticles is significant in consideration of the Luca Turin's model that suggests an inelastic electron tunneling spectroscopy (IETS) mechanism for discriminating odors (Turin 1996). In the IETS model, an electron donor is required for receptor activation through an odorant evoked inelastic tunneling of an electron between a donor (D) and acceptor (A) within the receptor. The points D and A are different in energy by $\hbar\omega_o$ (phonon energy), to ensure that tunneling of an electron takes place only if the energy is absorbed by an odorant's phonon. Turin hypothesizes that electron tunneling results in the G-protein dissociation, which subsequently triggers the olfactory signal cascade. We proposed that the active electron donor in Turin's model of olfaction could be the zinc nanoparticles described (Brookes, Horsfield, and Stoneham 2012a, Jia et al. 2015, Vodyanoy 2010).

It had been predicted that nanoparticles within the diameter range 1 nm to 10 nm would likely exhibit quantum-mechanical properties (Alivisatos 1996). The arising physical properties are not those of bulk metal nor those of molecular compounds. However, these properties are highly determined by the particle size, interparticle distance, and shape of the nanoparticles (Brust and Kiely 2002). The quantum size effect

is manifested if the de Broglie wavelength of the valence electrons is of the same order as the size of the particle itself. Subsequently, the particles act electronically as zero-dimensional quantum dots (or quantum boxes) highly relevant to quantum-mechanical principles. In nanoparticles, there is a gap between the valence band and the conduction band, in contrast to bulk metals. Single-electron tunnel transitions occur between a donor and acceptor.

If the electrostatic energy, $E_{el} = e^2/2C$, is larger than the thermal energy, $E_T = kT$. where C is electric capacitance, e – elementary charge, k – Boltzmann coefficient, T – absolute temperature (Daniel and Astruc, 2004).

The capacitance of 2 nm metal particle, $C=4\pi\varepsilon\varepsilon_o r$, where ε is the relative dielectric constant of the receptor protein, (Simonson and Brooks 1996), the ε_o is the vacuum dielectric constant 8.85×10^{-12}, and r=1 nm.

$$C=4\pi\times9\times8.85\times10^{-12}\times10^{-9}=1.0\times10^{-18}\text{ F.}$$

$$E_{el}=(1.6\times10^{-19})^2/(2\times1.0\times10^{-18})=1.15\times10^{-19}\text{ CV}=79.6\text{ meV}$$

That is significantly higher than the thermal energy at 25 ^oC.

$$E_T=1.38\times10^{-23}\times298=4.11\times10^{-21}\text{ J}=25.6\text{ meV}$$

Therefore, metal nanoparticles with a diameter smaller than 6 nm satisfy the condition of the single-electron transfer. The single-electron tunnel transition was experimentally observed with ~1 nm quantum dot at room temperature (Barreiro, van der Zant, and Vandersypen 2012). Taken in total, there is the reasonable feasibility of our hypothesis of small zinc nanoparticles serving as an electron donor in Turin's vibrational model of olfaction (Turin 1996).

Discontinuous size effects were experimentally observed in physics of small metal particles studied by the surface plasmon resonance, in the chemistry of supramolecular structures and molecular recognition, and in the biology of DNA-metal nanoparticle assemblies and sensors (reviewed in (Daniel and Astruc 2004)). Based on this theoretical and known experimental evidence of the discontinuous size effects, we believe that our experimental results confirm the size influence and surface composition of zinc metal nanoparticles on the enhancement of olfactory odorant responses.

An evaluation of concentration dependency of odorant-stimulated olfactory sensory neuron shows that one zinc nanoparticle binds two receptor molecules to produce a dimer (Vodyanoy 2010). Additionally, there is useful information provided by immunoprecipitation, fluorescence resonance energy transfer, and bioluminescence resonance energy transfer (BRET) that's certainly a fraction of cilia olfactory receptors makes homodimers (Bush 2008, Hall 2009, Sanz and Pajot-Augy 2013, Wade et al. 2011) the same as the rhodopsin homodimerization in optic disc membranes discovered by atomic force microscopy (Fotiadis et al. 2003b, a). We hypothesize that a single receptor cannot be stimulated by the odorant. Instead, only if it is coupled with another receptor with the assistance of a zinc nanoparticle, it can take part in signal transduction. It has been shown by immunogold electron microscopy that only a fraction of the olfactory receptors produces dimers, while all of those other receptors happen to be in the monomer state (Fukutani et al. 2012). Therefore, the enhancement of the olfactory signal by zinc nanoparticles could have a simple explanation. The endogenous zinc nanoparticles produce a particular quantity of operational receptor dimers that can be evoked by the odorant and take part in the origination of the olfactory signal. The rest of

the monomeric receptors remain passive and do not input into the odorant-evoked olfactory response. If the olfactory epithelium is challenged with a mixture of zinc nanoparticles and the same odorant, new receptor dimers are made by connecting pairs of formerly unbound receptors. The input of new receptor dimers will then cause a rise of the odorant-evoked olfactory response.

Recently, zinc nanoparticles were shown to enhance rat olfactory odorant responses used in the bio-electronic nose (Zhang et al. 2016). Zinc nanoparticles are not only metal particles that are capable enhancing olfactory odorant response. Exposure to 0.45 μg/L nanosilver suspension led to increased Crucian carp EOG responses, whereas exposure to 45 μg/L silver nanoparticle suspension and silver ion solution resulted in suppressing EOG signals (Bilberg et al. 2011). Other studies confirm toxicity of silver nanoparticles and silver ions (Bilberg et al. 2010, Farmen et al. 2012). Intranasal zinc sulfate irrigation in mmol/L concentrations in rodents was shown to destroy olfactory receptors (Burd 1993, Matulionis 1975). In contrast, zinc nanoparticles did not manifest toxicity at the fractions of nmol/L concentrations are not toxic to astrocytes (Vodyanoy et al. 2016).

There are other methods to facilitate olfactory responses. Down-regulation of any step in the olfactory signal transduction cascade could contribute to termination of odorant-evoked responses. The receptor phosphorylation (Boekhoff and Breer 1992), inactivation of G-protein (Simon, Strathmann, and Gautam 1991), reduction of adenylyl cyclase activity (Sklar, Anholt, and Snyder 1986), and activation of phosphodiesterase (Borisy et al. 1992) could cause a decrease in intracellular cAMP concentrations, and consecutively would reduce the olfactory response. Therefore, inhibition of this down-

regulation would cause the enhancement of an olfactory response. Indeed, the existence of inhibitory $G_{\alpha i}$-subunits in olfactory cilia and the adenylyl cyclase enhancement in the presence of $G_{\alpha i}$-antibody were demonstrated (Sinnarajah et al. 1998). Similarly, the inhibition of RGS2 proteins downregulates signal transduction in olfactory neurons by inhibiting activation of adenylyl cyclase. The whole cell patch-clamp experiments demonstrated the enhancement of odorant responses by inhibition of RGS2 proteins by RGS2 antibodies (Sinnarajah et al. 2001). Also, the deactivation of the phosphodiesterase by the IBMX increased cAMP levels in olfactory cilia (Moore et al. 2012). The above enhancement methods are based upon the biochemical intervention that is difficult to implement in live animals. Whereas, the enhancement of odorant responses by zinc nanoparticles was demonstrated in wholly unrestrained conscious dogs (Jia et al. 2016).

3.6 Conclusions

The physio-chemical characterization of zinc nanoparticles demonstrated a crystalline structure of zinc metal nanoparticles on transmission electron microscopy (TEM), an average size of 1.2 nm on atomic force microscopy (AFM), with 94% non-oxidized on X-ray Photoelectron Spectroscopy (XPS), a zeta potential of -48 mV, an 80% surface volume, and physiological capability of olfactory enhancement.

The physio-chemical characterization of laboratory oxidized zinc nanoparticles established from a subset of the average size of 1.2 nm zinc nanoparticles demonstrated

an increased level of oxidation at 12% oxidized atoms with XPS, no significant change in surface atoms, and the loss of the physiological capability of olfaction enhancement.

The standard 15 nm zinc oxide nanoparticles and 70 nm zinc oxide nanoparticles exhibited an inverse size to surface atom ratio, with lower surface atoms corresponding to higher nanoparticle diameter, and a similar loss of physiological capability of olfactory enhancement with small oxidized zinc nanoparticles.

The overall features of non-oxidized, 1.2 nm zinc nanoparticles exhibit a reasonable level of stability and high chemical reactivity. This in combination with the biologically relevant zinc nanoparticles found in human and animal blood supports a role within the initial events of olfaction, possibly serving as an electron donor in the vibrational theory of olfaction.

Chapter 4.0 Stabilization of zinc nanoparticles[1]

[1] This chapter is published: Singletary M, Hagerty S, Muramoto S, Daniels Y, MacCrehan WA, Stan G, et al. (2017) PEGylation of zinc nanoparticles amplifies their ability to enhance olfactory responses to odorant. PLoS ONE 12(12): e0189273. https://doi.org/10.1371/journal.pone.0189273

PEGylation of zinc nanoparticles amplifies their ability to enhance olfactory responses to odorant

Melissa Singletary[1], Samantha Hagerty[1], Shin Muramoto[2], Yasmine Daniels[2], William A MacCrehan[2], Gheorghe Stan[2], June W. Lau[2], Oleg Pustovyy[1], Ludmila Globa[1], Edward E. Morrison[1], Iryna Sorokulova[1], and Vitaly Vodyanoy[1*]

[1] Department of Anatomy, Physiology and Pharmacology, Auburn University College of Veterinary Medicine, Auburn, Alabama, USA

[2] Material Measurement Laboratory, National Institute of Standards and Technology, Gaithersburg, Maryland, USA

*Corresponding Author: Vitaly Vodyanoy, 109 Greene Hall, Auburn University, Auburn, AL 36849, USA, e-mail: vodyavi@auburn.edu; tel.; +1-334-844-5405.

4.1 Abstract

Olfactory responses are intensely enhanced with the addition of endogenous and engineered primarily-elemental small zinc nanoparticles (NPs). With aging, oxidation of these Zn nanoparticles eliminated the observed enhancement. The design of a polyethylene glycol coating to meet storage requirements of engineered zinc nanoparticles is evaluated to achieve maximal olfactory benefit. The zinc nanoparticles were covered with 1000 g/mol or 400 g/mol molecular weight polyethylene glycol (PEG). Non-PEGylated and PEGylated zinc nanoparticles were tested by electroolfactogram with isolated rat olfactory epithelium and odorant responses evoked by the mixture of eugenol, ethyl butyrate and (±) carvone after storage at 278 K (5 ^{o}C),

303 K (30 ºC) and 323 K (50 ºC). The particles were analyzed by atomic force microscopy, transmission electron microscopy, X-ray photoelectron spectroscopy, and laser Doppler velocimetry. Our data indicate that stored ZnPEG400 nanoparticles maintain physiologically-consistent olfactory enhancement for over 300 days. These engineered nanoparticles support future applications in olfactory research, sensitive detection, and medicine.

4.2 Introduction

Metal nanoparticles have been isolated from the blood of several vertebrate species, leading to investigations regarding their role within the olfactory system (Samoylov et al. 2005). Among the group of elemental metals, zinc demonstrated a significant enhancement of olfactory responses to odorant stimulation not seen with copper, gold, or silver (Viswaprakash et al. 2009). Zinc nanoparticles were engineered using a high-voltage electrical discharge method. For electrophysiology, the olfactory epithelium (OE) was surgically removed from adult Sprague-Dawley rats, and whole cell patch-clamp and electroolfactogram (EOG) were evoked by a headspace vapor of a 1.6 mmole/L standard odorant solution of ethyl butyrate, eugenol, and ±carvone with or without zinc nanoparticles to be tested (Viswaprakash et al. 2009). By these *ex vivo* experiments, enhancement was found to be dose-dependent, specific, and reversible. In conjunction with *ex vivo* analyses of sensory neurons in the rodent OE, we noninvasively analyzed *in vivo* cognitive effects on the brain regions associated with olfaction of non-anesthetized dogs using functional magnetic resonance imaging (fMRI). These studies

indicated that engineered zinc nanoparticles added to odorant caused a significant rise of olfactory associated brain activity (Jia et al. 2016).

In a comparison of engineered zinc nanoparticles of various sizes and states of oxidation, the highest olfactory enhancement was noted for nanoparticles measuring approximately 1.2 nm in diameter and in the primarily-elemental state, while oxidation inhibited the enhancement (Hagerty et al. 2016b). However, the enhancement declined over time. Therefore, improvement of the nanoparticles was necessary. In this work, we tested the hypothesis that PEGylation of the zinc nanoparticles using 1000 g/mol or 400 g/mol molecular weight polyethylene glycol (PEG) would afford retention of the olfactory enhancement. The PEGylation is a chemical process involving the passivation of the surface of nanoparticles by PEG, a coiled polymer with multiple ethylene ether units that are soluble in water (Jokerst et al. 2011). The PEGylation apparently decreases the rate of oxidation. It can provide an increased affinity to the target protein and reduced cytotoxicity of nanoparticles (Jokerst et al. 2011). The PEGylation is broadly used for protection of nanoparticles against aggregation in the biological and pharmaceutical applications (Suk et al. 2016, Otsuka, Nagasaki, and Kataoka 2003). Although there are many publications on the PEGylated zinc oxide nanoparticles (Karakoti et al. 2011, Sirelkhatim et al. 2015) this is the first study of PEGylated elemental zinc nanoparticles.

Small metal and metal composite nanoparticles have certain advantages compared to other particles due to their capability to specifically interact with proteins, peptides, and nucleic acids (Hassan and Singh 2014) and serve as important players in nanoparticle-based drugs (Erickson 2012), as metal electrocatalysts (McKone et al. 2013), in immune quantum dots (Hoshino et al. 2009), by crossing biological barriers

(Gidwani and Singh 2014), and many other applications in nanomedicine (Kogan et al. 2007).

The protection of metal nanoparticles from rapid oxidation and improvement of their biophysical and biochemical properties for better interactions with receptors, compatibility of the particle-cell interface, and reduced toxicity, is important for their potential clinical outcome (Anand et al. 2017, Hassan and Singh 2014, Xie et al. 2015).

We characterized the PEGylated nanoparticles using scanning electron microscopy (SEM), transmission electron microscopy (TEM), atomic force microscopy (AFM), X-ray photoelectron spectroscopy (XPS), and laser Doppler velocimetry (LDV).

The overall goal of this work was to protect zinc nanoparticles from oxidation and preserve their physiological properties to enhance olfactory responses to odorants over the long storage and elevated temperatures.

The future outcome of this work could provide an improvement in the individual sense of smell in conditions such as Alzheimer's and Parkinson's, which demonstrate olfaction deficits (Association 2017). In early Alzheimer's olfactory deficits are a preclinical sign that worsens with the disease progression (Bahuleyan and Singh 2012, Mesholam et al. 1998). Alzheimer's disease affects an estimated 5.5 million Americans as of 2017 and is the 10th leading cause of death in the United States (Association 2017). We hope that future treatments with zinc nanoparticles acting on the olfactory receptor level at minimal concentrations could reverse the loss of smell and improve emotional well-being and quality of life.

4.3 Materials and Methods

To characterize the properties of zinc nanoparticles under varying conditions, two sets of experimental settings were utilized: (1) Non-PEGylated and PEGylated zinc nanoparticles were stored at 283 K (5 ^{o}C) and then employed, along with a standard odorant mixture in EOG olfactory experiments over a storage period of 317 days. (2) Non-PEGylated and PEGylated zinc nanoparticles were subjected to accelerated aging at temperatures of 303 K (30 ^{o}C) and 323 K (50 ^{o}C) for 2 days before the EOG experiments that followed directly after storage.

4.3.1 Preparation of PEGylated Zn nanoparticles

Zinc nanoparticles of ~1.2 nm in size were prepared by a high-voltage electrical discharge method (Kruyt 1952). The of polyethylene glycol solutions of molecular weight 1000 g/mol or 400 g/mol (Sigma-Aldrich), PEG1000 or PEG400, respectively, were added to the nanoparticle suspension to make 1% w/v of PEGs. The suspensions were heated to 40 ^{o}C, purged with N_2 obtained from liquid nitrogen, and maintained at these conditions for 20 minutes. The suspension was sonicated at 19 W, 40 kHz for 20 min.

4.3.2 TEM

TEM was carried out utilizing an FEI Titan operated at 80 kV and 300 kV. Small drops of the zinc nanoparticle water suspension were deposited onto a QUANTIFOIL® Holey Carbon Film on copper TEM grids. Widths of the interference fringes were measured and the Miller-Bravais indices of the crystalline structures were estimated by the Crystallography lab software (Gu, Furuharaa, and Zhang 2016).

4.3.3 AFM

Metal nanoparticles were imaged by Bruker MultiMode 8 (Santa Barbara, CA) atomic force microscope in Tapping® (intermittent-contact) mode. Further details of AFM measurements are described in (Hagerty et al. 2016a).

4.3.4 XPS

XPS was utilized to measure atomic composition of the nanoparticles' surfaces. The Kratos Axis Ultra delayline detector (DLD) instrument in the hybrid mode used a monochromatic Al Kα1, 2 X-ray source (hυ = 1486.6 eV) as described in (Hagerty et al. 2016a). The ratio of the Zn and ZnO were obtained from the high-resolution spectra of Zn 2p (1017 eV to 1057 eV) and were measured with the energy resolution of 0.1 eV. Water suspensions of the nanoparticles were spread onto the gold-coated silicon wafers, and evaporated during evacuation of the system.

4.3.5 Zeta potential

Zeta potentials of the nanoparticles in water suspension were measured with a Zetasizer Nano ZSP (Malvern Instruments, Worcestershire, UK) by the LDV technique (Hagerty et al. 2016a). The average of six sequential runs were obtained. Zeta potentials were estimated by Henry's equation:

$$\zeta=3\eta\mu/2\varepsilon F(k\alpha)$$

in which ζ is the zeta potential, η is the viscosity, μ is the electrophoretic mobility, ε is the dielectric constant of the medium and $F(k\alpha)$ is Henry's function, which equals 1.5 using the Smoluchowski equation (Jachimska, Wasilewska, and Adamczyk 2008).

4.3.6 Odorants

Odorants were obtained from Sigma-Aldrich. An odorant mixture of 1.6 mmole/L each of ethyl butyrate, eugenol, and (+) and (–) carvone in water was prepared with a vortex mixer and stored in a dark glass container at 283K (5 ^{o}C).

4.3.7 Delivery of odorants and metal nanoparticles

During experiment, a 0.25 s pulse of the odorant mixture at 55158 N/m^2 (8 psi) was generated by a computer-controlled Pneumatic PicoPump PV800 (World Precision Instruments, Sarasota, FL). A pulse of positive pressure pushed the odorant into a glass nozzle toward the OE. The computer controlled odorant delivery was comprised of 0.25 s

pulses at 20 s and 60 s times for EOG data collection. The single EOG recording took 200 s and contained 10 response traces. A nanoparticle suspension was combined with odorant solutions to reach a final nanoparticle concentration of 0.02 nmole/L. During the pulse of delivery, the vapor of odorant with metal nanoparticles was transferred to the OE surface (Viswaprakash et al. 2009).

4.3.8 Animals

The animal protocol was approved by the Auburn University Institutional Animal Care and Use Committee (AU IACUC). Adult male Sprague–Dawley rats (Envigo, Dublin, VA) weighing ~300 g were used. EOG olfactory experiments over a storage period of 317 days were carried out with different animals as described in (Viswaprakash et al. 2009, Hagerty et al. 2016a).

4.3.9 Electrophysiology

We used electroolfactography (EOG) (Ottoson 1971). The instrumentation included Axon Instrument MultiClamp 700A amplifier and 1322A DigiData acquisition system. Rat OE was dissected out and positioned in a perfusion chamber such that the basal parts were immersed in physiological solution, while the olfactory cilia ware positioned in the water/air interface. Glass electrodes of ≈ 24 μm tip opening were linked to the amplifier to record signals from the OE. After connection between the electrode and the OE was made, air pulse of the odorant mixture was applied and a continuous EOG signal was recorded as function of time. All olfactory experiments were performed

ex vivo. The primarily-elemental or PEGylated zinc nanoparticles were delivered with the odorant mixture. The relative enhancement of olfactory responses by zinc nanoparticles were calculated as $(EOG_{O+Zn}-EOG_O)/EOG_O$, where EOGo was the peak of electrical response evoked by the odorant alone, and EOG_{O+Zn} was the peak response stimulated by the mixture of the odorant and Zn nanoparticles. Similarly, the relative enhancements by ZnPEG400 and ZnPEG1000 were determined as $(EOG_{O+ZnPEG400}-EOG_O)/EOG_O$ and $(EOG_{O+ZnPEG1000}-EOG_O)/EOG_O$, respectively. Further details of the method were described in (Hagerty et al. 2016a, Viswaprakash et al. 2009).

4.3.10 Statistical analysis

Data averaging, ANOVA, t-test, curve fitting, and graph plotting were carried out using Origin 2015 (Northampton, MA) and 2010 Microsoft Excel.

4.4 Results

4.4.1 Properties of PEG on the surface of zinc nanoparticles

Zinc nanoparticles were engineered from metal bars by an electrolysis method (Hagerty et al. 2016b) and were PEGylated with 400 g/mol or 1000 g/mol molecular weight polyethylene glycol (S1 Supporting Information), and referred hereafter as ZnPEG400 and ZnPEG1000, respectively. The properties of the PEG molecules on the nanoparticle surface are shown in Table 4.1. PEG400, with 14 fewer monomers than PEG1000, was predicted to form a thinner coating on the surface of zinc nanoparticles (S1 Supporting Information).

Table 4.1 Properties of PEG on the surface of zinc nanoparticles

Property	ZnPEG400	ZnPEG1000	Reference
Area per PEG single chain, nm^2	1.3	2.91	(Butterworth, Illum, and Davis 2001)
Number of monomers in PEG	9	23	S1 Supporting Information
Thickness of PEG layer, nm	1.3	2.3	S1 Supporting Information

4.4.2 AFM

Fig 4.1 demonstrates the physical properties of non-PEGylated and PEGylated zinc nanoparticles. AFM showed the diameter distributions of zinc nanoparticles, with mean sizes of 1.2 ± 0.3 (SD) nm (Figs 4.1 A, a and b). Fig 4.1 A, b shows the histogram with a peak around the mean value. Similarly, the size distributions of ZnPEG400 and

ZnPEG1000 revealed the average diameter of 1.4±0.4 (SD) nm for both formulations. (Figs 4.1, B, b, and C, b).

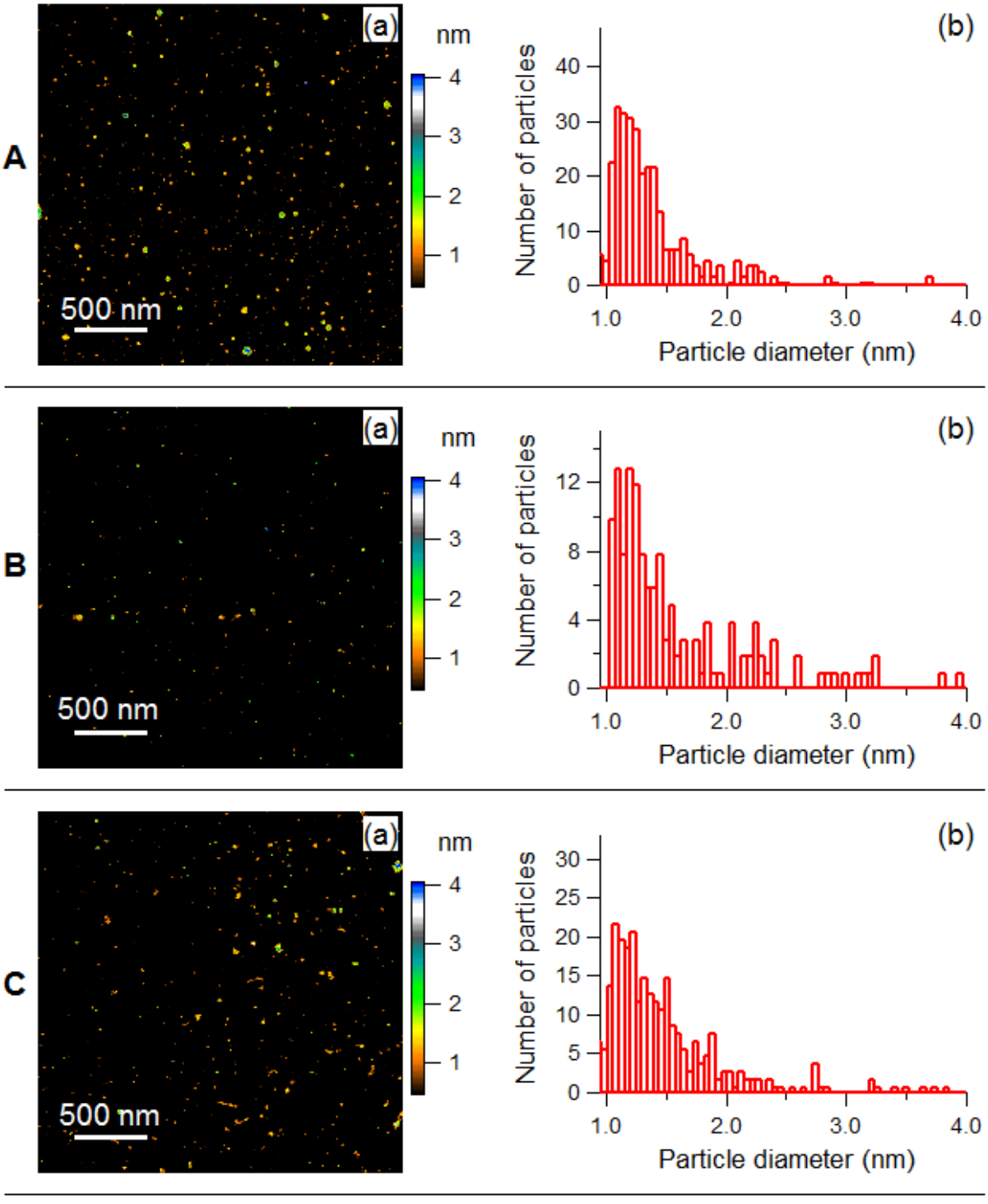

Fig 4.1 Physical properties of non-PEGylated and PEGylated zinc nanoparticles. (a) AFM images, and (b) histograms showing the size distribution of the nanoparticles. A: Zinc nanoparticles, B: ZnPEG400, C: ZnPEG1000.

4.4.3 TEM

Fig 4.2 summarizes the electron microscopy images of Zn, ZnPEG400, and ZnPEG1000 nanoparticles. Panels a and b show TEM micrographs of Zn and ZnPEG400 nanoparticles, respectively. Both particles show lattice fringes. Panels c and d provide TEM images of zinc nanoparticles also showing their crystalline character. Panel e illustrates TEM image of ZnPEG1000 nanoparticles. Arrows show layers surrounding nanoparticles that are presumed to be coatings of PEG1000. Panel f depicts the enlarged dashed square shown in panel e. Within the uncertainty of our data accuracy, we determined that the characteristic fringes of 0.21 nm and 0.17 nm found in both non-PEGylated and PEGylated zinc nanoparticles match the (011) and (012) vectors for the hcp crystal lattice of zinc. Larger than average size particles are shown to emphasize the crystal fringes.

4.4.4 XPS

The non-PEGylated and PEGylated zinc nanoparticles were subjected to four experimental conditions: 1. Freshly prepared nanoparticles stored for 1 day at of 278 K (5

^{o}C); 2. Particles stored for 317 days at 278 K (5 ^{o}C); 3. Particles stored for 2 days at the temperature of 303 K (30 ^{o}C); and 4. Particles stored for 2 days at 323 K (50 ^{o}C). Physical analyses of all the samples were performed immediately after the end of each of the exposure conditions to minimize any changes in chemistry.

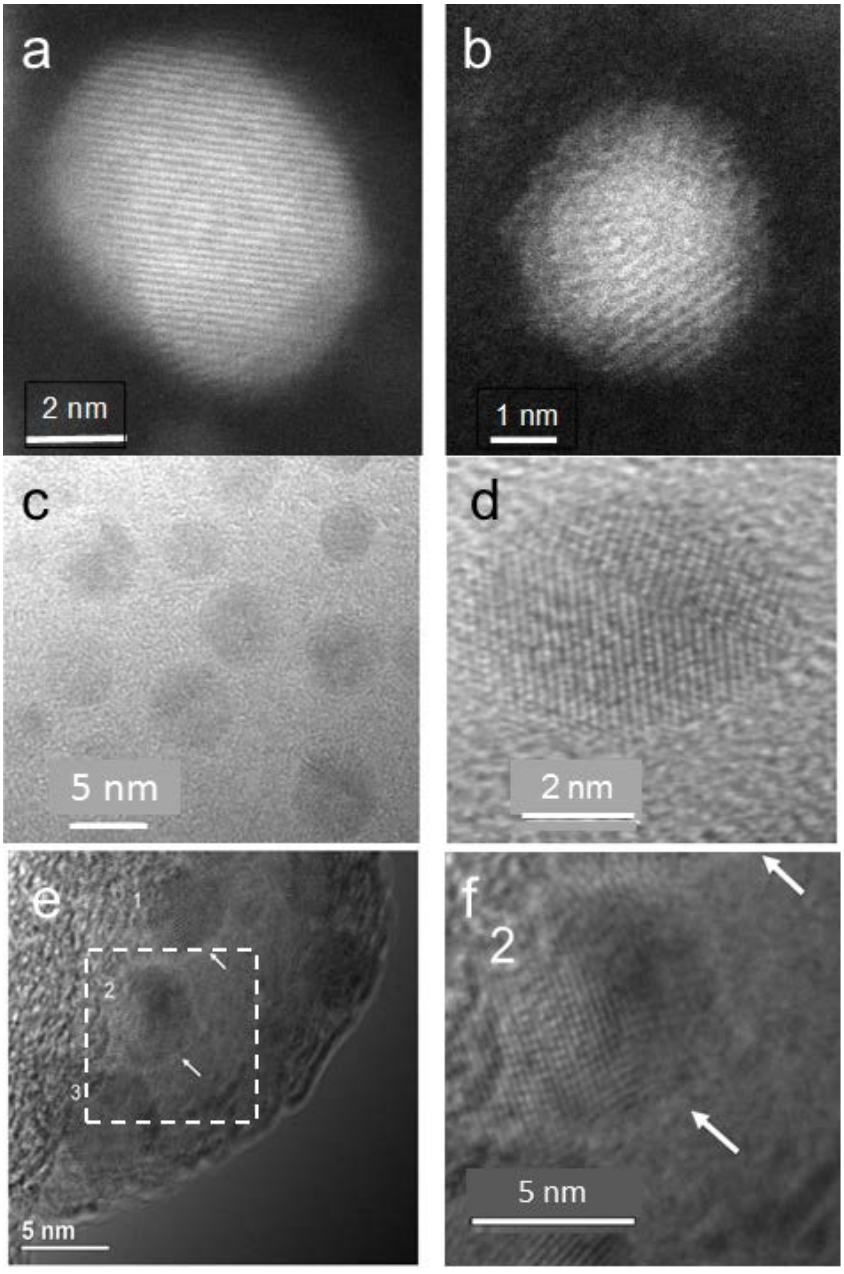

Fig 4.2 Electron microscopy images of Zn, ZnPEG400, and ZnPEG1000 nanoparticles. TEM images (a, c, d) are showing the primarily-elemental zinc nanoparticles at different magnifications, (b) ZnPEG400 nanoparticle showing the metal core and the PEG passivation layer, (e) ZnPEG1000 nanoparticles with negative staining, and (f) ZnPEG1000 magnified from (e). The numbers 1, 2, 3 point to the nanoparticles with visible lattice fringe patterns, indicating their crystallinity.

Fig 4.3 shows the representative XPS spectra obtained for freshly prepared zinc and PEGylated zinc nanoparticles stored 1 day at 278 K (5 ^{o}C). A summary of the XPS data for non-PEGylated and PEGylated zinc nanoparticles for all four experimental conditions is shown in Table 4.2. The spectra were calibrated using the adventitious carbon C 1s peak at a binding energy of 284.6 eV, which allowed the identification of the following chemical species at their respective binding energies: hydrocarbon (C-C≈285 eV), ether (C-O, ≈286.1), carboxyl (C=(OH), ≈288.1) (Ferro, Dal Colle, and De Battisti 2005), zinc (Zn $2p_{3/2}$, ≈1021.8 eV) (Naumkin et al. 2012, Deroubaix and Marcus 1992) and ZnO (Zn $2p_{3/2}$, ≈1024 eV) (Mai et al. 2013b). The rise in the amplitude of C-O peak and the reduction in the binding energy of Zn $2p_{3/2}$ peaks in the ZnPEG400 and PEG1000 samples confirmed the successful PEGylation of zinc nanoparticles. The Zn $2p_{3/2}$ band shown that metallic zinc nanoparticles were oxidized only slightly, where the concentrations of Zn and ZnO were found to be 97.0 ± 0.8 (SD) % and 3.0 ± 0.8 (SD) %, respectively (Table 4.2, 278 K, 1 day). Interestingly, the PEGylation process caused a significant increase in the concentration of oxidized zinc atoms, where the interaction

with PEG400 (278 K, 1 day) resulted in an increase of ZnO concentration from 3.0±0.8 (SD) % to 10.5±4.0 % ($t(5)=4.93$, $p=0.004$), while in the case of PEG1000, the ZnO concentration increased to 12.0±3.8 % ($t(5)=6.47$, $p=0.001$).

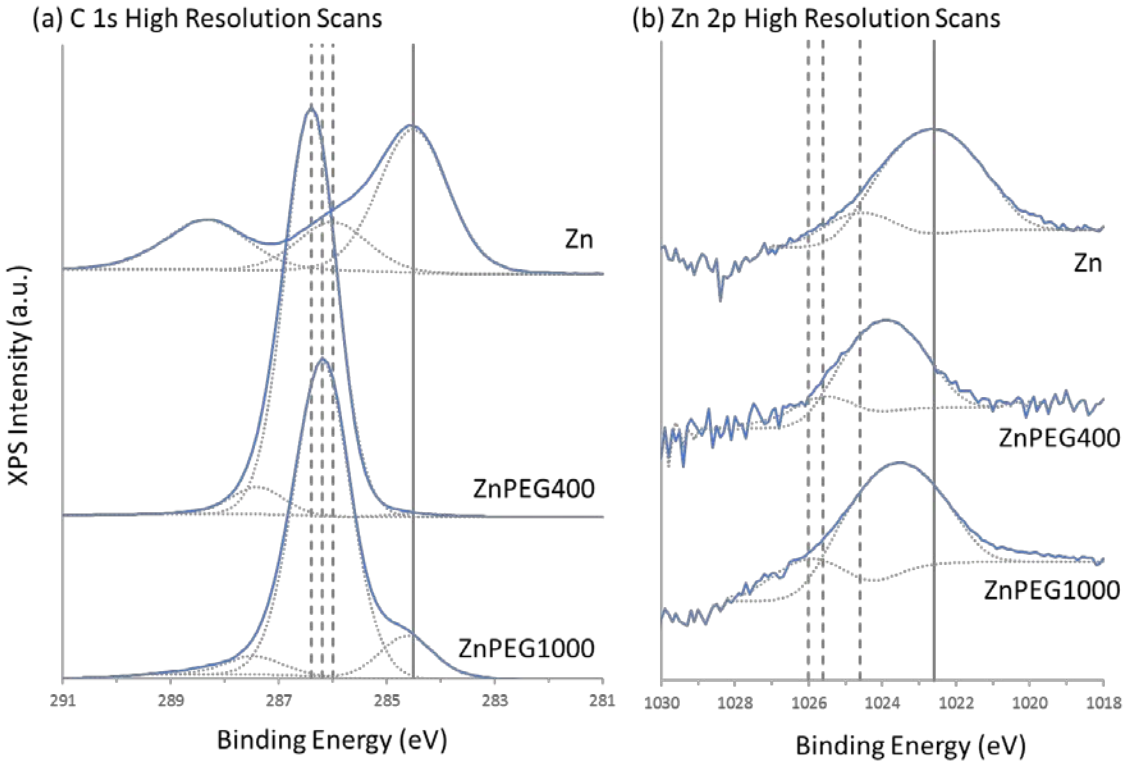

Fig 4.3 XPS spectra. Representative high resolution XPS spectra showing the (a) C 1s and (b) Zn 2p3/2 core lines for the freshly prepared bare zinc and PEGylated zinc nanoparticles stored 1 day at 278 K (5 ^{o}C), with the spectra offset to facilitate viewing. The Zn 2p spectra are shown in log-scale. The solid curves indicate the experimentally obtained spectra, with the dotted curves underneath indicating their best-fit chemical components. For the C 1s spectra, from lower to higher binding energy, the components are C-C, C-O, and C=O. For the Zn 2p spectra, the components are Zn and ZnO. For the (a) C 1s plots, the solid vertical line represents the position of the C-C peaks, to which all

spectra were calibrated to, with the dotted lines showing the spectral shift of the C-O peaks, which were 286 eV, 286.4 eV, and 286.2 eV for the Zn, ZnPEG400, and ZnPEG1000 systems, respectively. For (b) Zn 2p plots, the solid line represents the position of the Zn peak for the bare Zn system, while the dotted lines show the spectral shift of the ZnO peaks, which were 1024.6 eV, 1025.6 eV, and 1026.0 eV for the Zn, ZnPEG400, and ZnPEG1000 systems, respectively. Each spectrum represents an average of six spectral runs.

Table 4.2 XPS properties of bare and PEGylated zinc nanoparticles, stored at various durations and temperatures

Sample	T K	Time days	Survey			High Resolution Zn 2p			
			O1s %	C 1s %	Zn2p %	BE eV	Zn %	BE eV	ZnO %
Zn	278	1	27.8 ± 2.3	70.5 ± 1.7	1.8 ± 0.1	**1021.8**	**97.0 ± 0.8**	**1024.6**	**3.0 ± 0.8**
ZnPEG400	278	1	32.3 ± 0.5	67.4 ±0.7	0.3 ± 0.1	**1022.0**	**89.5 ± 4.0**	**1023.8**	**10.5 ± 4.0**
ZnPEG1000	278	1	30.3 ± 0.9	69.6 ± 2.1	0.1 ± 0.0	**1021.9**	**88.0 ± 3.8**	**1023.5**	**12.0 ± 3.8**
Zn	278	317	38.4 ± 1.0	60.2 ± 1.5	1.4 ± 0.1	**1021.9**	**96.0 ± 1.0**	**1023.7**	**4.0 ± 1.0**
ZnPEG400	278	317	31.5 ± 0.1	68.4 ± 0.1	0.1 ± 0.0	**1022.2**	**75.9 ± 8.2**	**1023.9**	**24.1 ± 8.2**
ZnPEG1000	278	317	31.1 ± 0.3	68.0 ± 0.4	0.9 ± 0.2	**1021.9**	**86.1 ± 0.5**	**1024.2**	**13.9 ± 0.5**
Zn	303	2	24.5 ± 4.1	75.1 ± 0.6	0.4 ± 0.1	**1021.7**	**92.2 ± 3.5**	**1024.1**	**7.8 ± 3.5**
ZnPEG400	303	2	23.2 ± 4.4	76.6 ± 3.0	0.2 ± 0.0	**1022.0**	**93.0 ± 2.8**	**1023.7**	**7.0 ± 2.8**
ZnPEG1000	303	2	24.6 ± 5.4	75.2 ± 5.2	0.2 ± 0.1	**1021.8**	**94.2 ± 5.6**	**1023.4**	**5.8 ± 5.6**
Zn	323	2	38.3 ± 5.3	60.8 ± 3.5	0.9 ± 0.3	**1021.0**	**92.9 ± 3.3**	**1023.3**	**7.1 ± 3.3**
ZnPEG400	323	2	27.7 ± 4.6	72.1 ± 6.8	0.2 ± 0.1	**1021.9**	**88.6 ± 2.6**	**1023.7**	**11.4 ± 2.6**
ZnPEG1000	323	2	21.8 ± 3.5	77.9 ± 2.7	0.3 ± 0.1	**1021.7**	**92.7±1.6**	**1024.0**	**7.3±1.6**

Table 2 (continued).

Sample	T K	Time days	Survey			High Resolution C 1s					
			O1s %	C 1s %	Zn2p %	BE eV	C-C %	BE eV	C-O %	BE eV	C=O(OH) %
Zn	278	1	27.8 ± 2.3	70.5 ± 1.7	1.8 ± 0.1	284.3	66.2 ± 2.9	286.2	22.6 ± 1.5	288.5	11.2 ± 1.7
ZnPEG400	278	1	32.3 ± 0.5	67.4 ±0.7	0.3 ± 0.1	285.0	3.7 ± 2.1	286.9	92.0 ± 3.0	288.5	4.3 ± 1.0
ZnPEG1000	278	1	30.3 ± 0.9	69.6 ± 2.1	0.1 ± 0.0	283.2	3.0 ± 0.6	286.7	94.5 ± 0.6	290.2	2.6 ± 0.0
Zn	278	317	38.4 ± 1.0	60.2 ± 1.5	1.4 ± 0.1	284.4	60.2 ± 0.9	285.8	18.6 ± 0.7	288.1	21.2 ± 0.5
ZnPEG400	278	317	31.5 ± 0.1	68.4 ± 0.1	0.1 ± 0.0	285.0	0.9 ± 0.2	287.0	92.8 ± 0.9	288.0	6.3 ± 0.8
ZnPEG1000	278	317	31.1 ± 0.3	68.0 ± 0.4	0.9 ± 0.2	285.1	11.5 ± 2.4	286.7	83.5 ± 1.9	288.0	5.0 ± 0.8
Zn	303	2	24.5 ± 4.1	75.1 ± 0.6	0.4 ± 0.1	284.4	60.8 ± 6.8	286.5	31.5 ± 4.0	289.2	7.7 ± 4.0
ZnPEG400	303	2	23.2 ± 4.4	76.6 ± 3.0	0.2 ± 0.0	284.4	38.9 ± 15.0	286.8	56.9 ± 15.3	288.8	4.2 ± 0.5
ZnPEG1000	303	2	24.6 ± 5.4	75.2 ± 5.2	0.2 ± 0.1	284.4	39.2 ± 14.9	286.6	55.7 ± 14.9	288.6	5.1 ± 1.1
Zn	323	2	38.3 ± 5.3	60.8 ± 3.5	0.9 ± 0.3	284.2	65.6 ± 14.7	285.9	20.6 ± 8.8	288.2	13.8 ± 6.1
ZnPEG400	323	2	27.7 ± 4.6	72.1 ± 6.8	0.2 ± 0.1	284.4	35.2 ± 10.7	286.9	62.6 ± 12.7	283.7	2.2 ± 0.1
ZnPEG1000	323	2	21.8 ± 3.5	77.9 ± 2.7	0.3 ± 0.1	284.4	50.5 ± 15.7	286.5	43.7 ± 15.4	288.6	5.8 ± 0.8

BE refers to the binding energy of the peak, and % refers to the relative atomic composition of the elements normalized to the elements shown below, within their respective scans (i.e., Survey, High Resolution Zn 2p and C 1s).

The XPS survey scan of the freshly prepared non-PEGylated and PEGylated zinc nanoparticles (Table 4.2, 278 K, 1 day) showed the concentration of the O 1s and C 1s species to be 27.8±2.3 % and 70.5±1.7 % , respectively, which significantly changed to 32.3±0.5 %($t(5)=4.28$, $p=0.003$) and 67.4±0.7 % ($t(5)=3.77$, $p=0.005$) for ZnPEG400, respectively. The values of O 1s and C 1s for ZnPEG1000 were 30.3±0.9 % ($t(5)=2.26$, $p=0.0053$) and 69.6±2.1 % ($t(5)=0.74$, $p=0.48$), respectively (there were no statistically significant changes for ZnPEG1000).

ZnPEG400 after 317 days of storage, showed the higher level of ZnO of 24.1±8.2% ZnO compared to 10.5±4.0% ($t(5)=3.45$, $p=0.008$) for the freshly prepared ZnPEG400, as shown in Table 4.2.

Very different XPS results were observed for ZnPEG1000 after storage. The concentration C-O group showed a modest decrease from 94.5±0.6 % to 83.5±1.9 % ($t(5)=12.3$, $p=0.0001$), but a sensible increase in the C-C concentration from 3.0±0.6 % to 11.5±2.4 % ($t(5)=7.68$, $p=0.0001$). The concentration of ZnO for this condition were 12.0±3.8 % and 13.9±0.5 % ($t(5)=1.11$, $p=0.3$) showed no significant difference. These data suggest no significant changes in the electronic structure of both Zn and PEG1000 after the initial PEGylation.

4.4.5 Arrhenius activation energies of oxidation

Oxidation of the zinc nanoparticles was observed under storage at different temperatures and duration, as evidenced by the increase of ZnO components in Table 4.2. Using an apparent concentration of primarily- elemental zinc as a function of time and

storage temperature, the Arrhenius activation energies of oxidation were estimated (Segel 1975) by equation (S6) (S1 Supporting Information) and shown in Table 4.3.

Table 4.3 Thermodynamic analysis of oxidation of Zn, ZnPEG400, and ZnPEG1000 nanoparticles

Particle	T °C	Estimated activation energy, E_a kJ.mol^{-1}	Reference
Zn, 1.2 nm	5-50	113	Present work
Zn foil, 0.126 mm	300-400	119	(Moore and Lee 1951)
ZnO powder, oxygen desorption	86-97	96	(Hideo, Masanobu, and Tadashi 1965)
Molten Zn	600-700	104	(Cope 1961)
ZnPEG400, 1.4 nm	5-50	15.5	Present work
ZnPEG1000, 1.4 nm	5-50	34.9	Present work
Pd/Fe nanoparticles, 60-100 nm	20-35	39.47	(Wang, Le, et al. 2015)
Pd/FePEG200	20-35	38.66	(Wang, Le, et al. 2015)

4.4.6 Zeta potential

The change in the physical properties of zinc nanoparticles after PEGylation is also confirmed by alteration of the zeta potential. The PEG binding resulted in a sharp reduction of zeta potential in water. Zeta potential showed values of -42.4 ± 4.8 (SE) mV, -26.1 ± 2.5 (SE) mV ($t(7)=7.96$, $p=0.0001$), and -27.5 ± 2.5 (SE) mV ($t(7)=7.28$, $p=0.0001$) for Zn, ZnPEG400, and ZnPEG1000 nanoparticles, respectively.

4.4.7 Enhancement of odorant response by PEGylated nanoparticles

The initial experiments were carried out with the freshly prepared non-PEGylated and PEGylated zinc nanoparticles. Representative electroolfactograms showing effects of PEG400 and PEG1000 without zinc nanoparticles and recorded from the rat OE are shown in Fig 4.4. The EOG responses evoked by PEG400 and PEG1000 without odorant mixture are very small and hardly can be distinguished from the EOG signal of water. This result is consistent with polyethylene glycol being odorless (Gomes, Liteplo, and Meek 2003). The EOG evoked by the odorant mixture with zinc nanoparticles (trace 2) shows a strong enhancement compared to the signal induced by the odorant mixture alone (trace 1). Combining odorants with ZnPEG400 and ZnPEG1000 results in the lower signals depicted by the traces 3 and 4, respectively. The mean values of seven measurements of the relative responses to the odorant mixtures with Zn, ZnPEG400, and ZnPEG1000 were 2.69±0.11, 0.821±0.05, and 0.310±0.04, respectively. An analysis of variance showed that at the 0.05 level, the means were significantly different, $F(2, 18)=1900$, $p=0.000$, indicating that the freshly prepared Zn nanoparticles were superior to ZnPEG400 and ZnPEG1000, and ZnPEG400 with odorant produced larger relative responses than ZnPEG1000 with odorant.

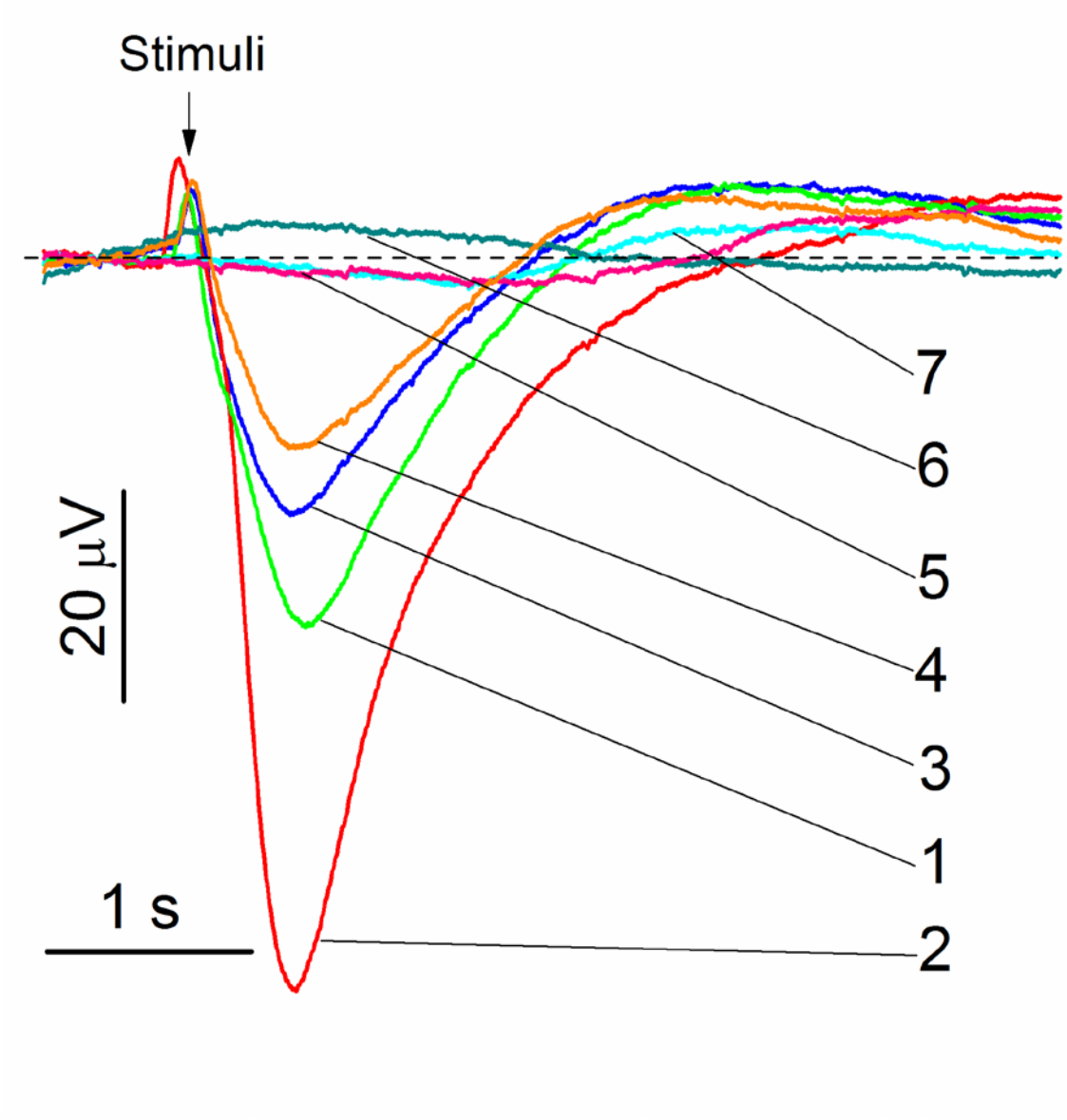

Fig 4.4 Representative EOG recordings from rat olfactory epithelium. The stimuli were of 0.25 s pulses of (1) odorant mixture, (2) odorant mixture +1.2 nm zinc nanoparticles, (3) odorant mixture + 0.25 mmole/L PEG400, (4) odorant mixture + 0.10 mmole/L PEG1000, (5) water vapor + PEG400, (6) water vapor + PEG1000, and (7) water vapor. The concentration of zinc nanoparticles and odorant mixture were 0.02 nmole/L and 1.6 mmole/L , respectively. The representative set of traces was obtained from 50 EOG traces.

The olfactory responses to odorant mixed with PEG400 or PEG1000 were tested systematically over the period of 317 days. As evidenced by the foregoing data, the freshly prepared Zn nanoparticles outperformed both ZnPEG400 and ZnPEG1000. However, as analysis of variance showed, at the level of 0.05, there was no significant difference between the relative olfactory responses to Zn, ZnPEG400, and ZnPEG1000 nanoparticles ranging from 3 days to 64 days of storage ($F_{3\ days}(2, 25)=0.64$, $p=0.54$; $F_{5\ days}(2, 69)=2.53$, $p=0.087$; $F_{18\ days}(2, 30)=0.92$, $p=0.41$); $F_{58\ days}(2, 12)=1.14$, $p=0.35$; and $F_{64\ days}=(2, 21)=3.12$, $p=0.065$). Only after 280 days and 317 days of storage we observed the significant difference between the relative olfactory responses to Zn, ZnPEG400, and ZnPEG1000 nanoparticles ($F_{280\ days}(2, 48)=90$, $p=0.000$; $F_{317\ days}(2, 36)=149$, $p=0.000$). Following 280 days of storage, ZnPEG400 provided the highest enhancement followed by Zn and then ZnPEG1000. Near the end of the storage time, the mixture odorant and ZnPEG1000 caused a decrease of the EOG signal compared to the signal generated by the odorant alone (Fig 4.5).

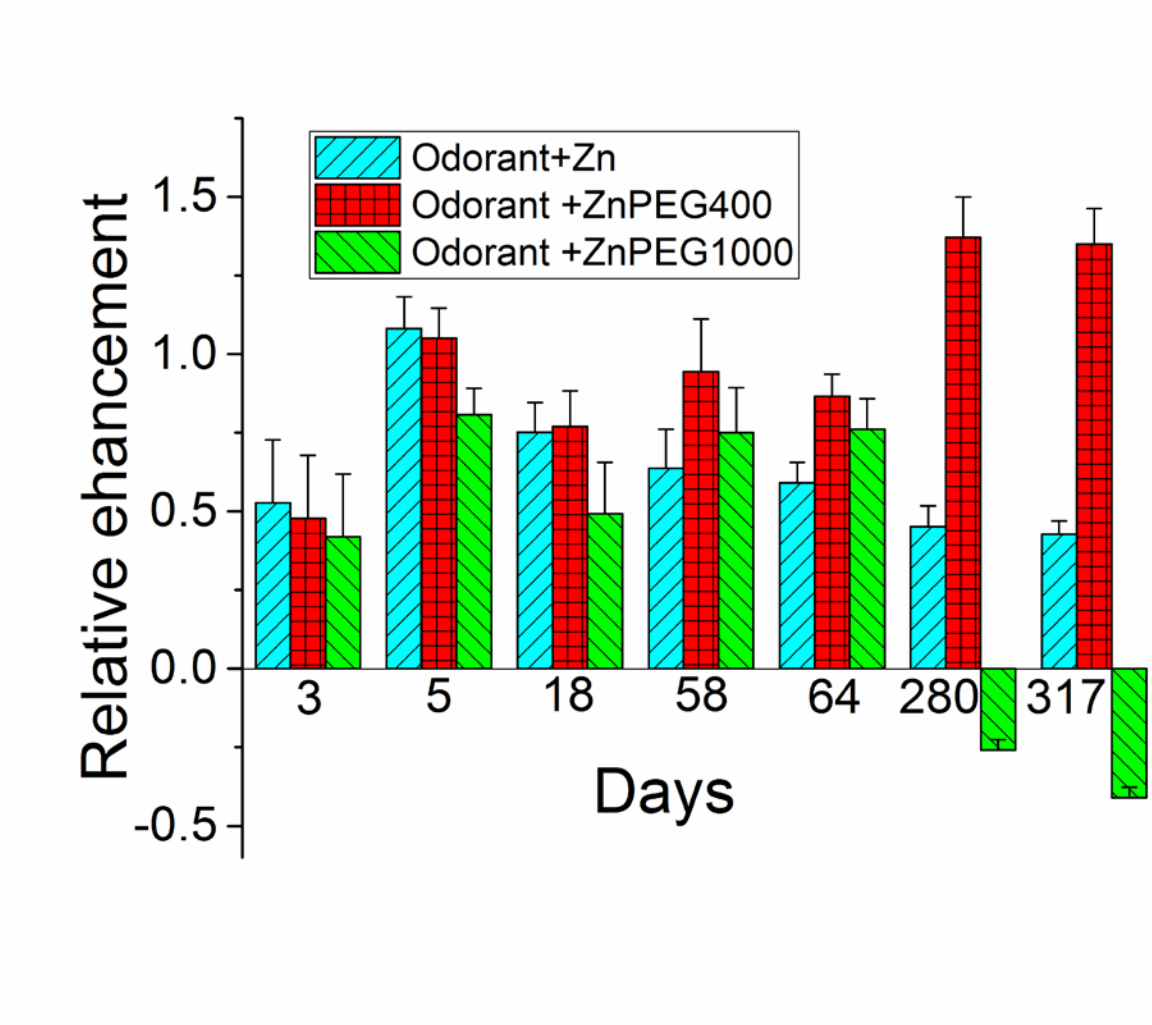

Fig 4.5 The relative EOG signals as a function of time of storage of zinc nanoparticles. The difference between peak values of EOG evoked by odorant and by non-PEGylated and PEGylated zinc nanoparticles was normalized by the EOG peak evoked by an odorant alone. The relative enhancement by zinc nanoparticles was calculated as described in Materials and methods.

To characterize effects of thermally-enhanced formation of ZnO on the odorant responses, we analyzed the effects of non-PEGylated and PEGylated zinc nanoparticles stored for two days at an elevated temperature. Fig 4.6 shows the relative enhancement of responses to odorants as the function ZnO concentration determined by XPS and temperature. The relative olfactory enhancement by the zinc nanoparticles declined sharply from 55% to -7 %, when the ZnO concentration increased from 3.0% to 11.5 % (Fig 4.6 a). The enhancement with ZnPEG1000 did not show the obvious dependence on the ZnO concentration but it strongly declined with the temperature (Fig 4.6 c). The enhancement with ZnPEG400 (Fig 4.6 b) appeared not to be very sensitive to zinc oxidation and temperature.

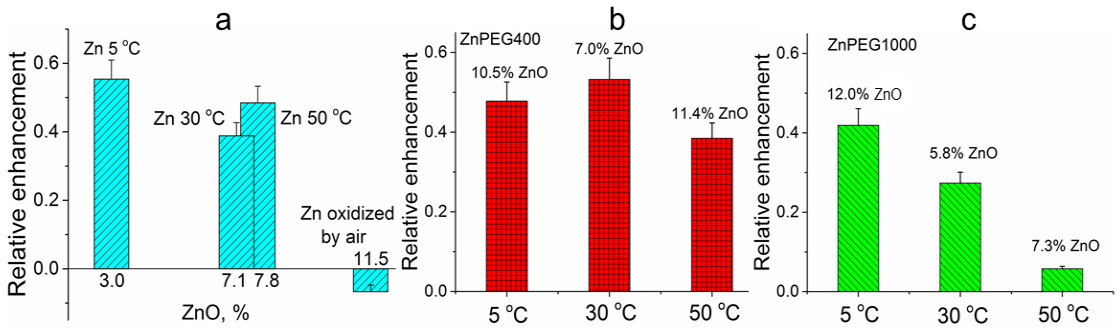

Fig 4.6 The relative EOG signals evoked by non-PEGylated and PEGylated zinc nanoparticles. a. The relative enhancement by non-PEGylated zinc nanoparticles as a function of ZnO concentration. The difference between peak values of EOG evoked by odorant and by zinc nanoparticles was normalized by the EOG peak evoked by an odorant alone as a function of ZnO concentration that was determined by XPS. The first bar at 3 % of ZnO, corresponds to zinc nanoparticles stored one day at 278 K (5 ^{o}C). The second and third bars reflect zinc nanoparticles stored for two days at 303 K (30 ^{o}C) and 323 K (50 ^{o}C), at 7.1 % and 7.8 % respectively. The forth bar at 11.5 % of ZnO corresponds to the negative enhancement (inhibition) that was observed with zinc nanoparticles oxidized by percolating air. **b**. The relative EOG enhancement produced by ZnPEG400 nanoparticles after they were stored for one day at 278 K (5 ^{o}C), two days at 303 K (30 ^{o}C) and 323 K (50 ^{o}C), respectively. **c**. The relative EOG enhancement produced by ZnPEG1000 nanoparticles after they were stored for one day at 278 K (5 ^{o}C), two days at 303 K (30 ^{o}C) and 323 K (50 ^{o}C), respectively.

4.5 Discussion

4.5.1 Characterization of PEGylated zinc nanoparticles

The crystalline structure of zinc nanoparticles revealed in this work is consistent with those obtained for zinc nanowires and nanorods (Chen et al. 2007, Lu et al. 2016). The equivalence of the zinc lattices and core lattices of PEGylated zinc nanoparticles indicates that PEGylating maintains the crystalline nature of the metal particles. To further analyze physical properties of the non-PEGylated and PEGylated zinc nanoparticles, XPS was utilized for study of nanoparticles in the variety of experimental conditions.

The decrease in the binding energy of Zn $2p_{3/2}$ peaks in the ZnPEG400 and PEG1000 nanoparticles and the rise in the amplitude of the XPS C-O peak indicated that PEGylation of zinc nanoparticles was successful. The Zn $2p_{3/2}$ band shown that metallic zinc nanoparticles were oxidized only slightly, where the concentrations of Zn and ZnO were found to be 97.0 ± 0.8 (SD) % and 3.0 ± 0.8 (SD) %, respectively (Table 4.2, 278 K, 1 day).

The interaction of the PEG molecules and zinc nanoparticles had a remarkable effect on the binding energies of carbon and zinc. Bonding of the molecules onto the nanoparticles was associated with an increase in the binding energy of the C-O bond, and a corresponding decrease in the ZnO binding energy. For the nanoparticles held at 278 K for 1 day (Table 4.2), for example, the C-O binding energy increased from 286.2 eV to 286.9 eV (by roughly 0.7 eV) while the ZnO binding energy decreased by 0.9 eV when

the nanoparticles were covered by PEG400. A similar shift in binding energies were observed for the nanoparticles covered in PEG1000. We speculate that the PEG molecules are interacting with the zinc atoms in such a way that the electronic structure of the nanoparticles is affected, and a conjugated electron system is produced (Mason 1983). It is likely that long polymer chains increase the withdrawal of electron charge and electronic stability, which subsequently increases the binding energy of the C and O elements within the chain (Duan et al. 2016). Conversely, the polymer chains may act as a passivation layer that leads to a reduction in binding energy because of the fact that the zinc nanoparticles are acting as electron donors, which has been observed for platinum nanoparticles below 7 nm in size (Qiu et al. 2006).

The highest shift in binding energy was observed for ZnPEG400 nanoparticles stored at 278 K for 317 days (Table 4.2). The binding energy of the C-O component increased by 0.9 eV relative to the control value of 286.2 eV, and a corresponding decrease in binding energy of 0.7 eV was seen for ZnO. Similar shifts in binding energy were also observed for PEGylated zinc nanoparticles exposed to elevated temperatures of 303 K (30 ^{o}C) and 323 K (50 ^{o}C). These observations point to the covalent binding of PEG to the engineered zinc nanoparticles, with similar binding energy shifts observed after PEGylation of MoS_2 nanoflakes (Wang, Li, et al. 2015, Feng et al. 2015), Gadolinium oxide thin film and nanoparticles (Guay-Bégin et al. 2012), and gold nanorods (Thierry et al. 2009).

The value of the activation energy for the oxidation of zinc nanoparticles agrees well with that obtained by the oxidation of zinc foil (Moore and Lee 1951), the oxygen desorption from ZnO powder, and the oxidation of molten zinc (Cope 1961). After

PEGylation, zinc nanoparticles showed reduction of the activation energy, with the binding of PEG400 producing a larger energy reduction compared to PEG1000. No literature was available for comparison of the activation energy of the PEGylated zinc nanoparticles. However, a decrease in the activation energy was reported when 60-100 nm Pd/Fe nanoparticles underwent PEGylation (Wang, Le, et al. 2015).

The reduction of the nanoparticle surface charge after PEGylation may explain an increased affinity to target proteins (Jokerst et al. 2011).

4.5.2 Enhancement of odorant response by PEGylated nanoparticles

Previously, we showed that primarily-elemental zinc nanoparticles strongly enhanced responses to odorants, while zinc nanoparticles oxidized by air did not enhance but slightly inhibited the responses (11.5% ZnO compared to 3.0% for the primarily-elemental nanoparticle) (Hagerty et al. 2016b). The olfactory enhancement of approximately 140% using ZnPEG400 after 317 days of storage was not an anticipated result based on the higher level of ZnO of 24.1% ZnO compared to 10.5% for the freshly prepared ZnPEG400, as shown in Table 2. Although no significant change in the C-O concentration was observed, the C-C concentration decreased from 3.7% to 0.9%. The increase in the observed level of ZnO in this case does not imply a high level of oxidized zinc atoms, but rather seems to reveal that there is a formation of a unique conjugated electron system between the zinc nanoparticles and PEG400 molecules that may be responsible for the increase in olfactory response.

To explain the mechanism of enhancement and inhibition by ZnPEG400 and ZnPEG1000, respectively, it is essential to consider what has been discovered about the olfactory enhancement by zinc nanoparticles.

We have reported that two molecules of olfactory receptor binds a single zinc nanoparticle to create a dimer (Vodyanoy 2010). We suggested that the odorant cannot activate a single receptor. When two receptors bind to an endogenous zinc nanoparticle, the created dimer participate in signal transduction. The remaining receptors are monomeric (Fukutani et al. 2012). Consequently, the dimerization mechanism enabled by the zinc nanoparticles provides an explanation for the olfactory enhancement. When the OE is exposed to a mix of the odorant and engineered zinc nanoparticles, the nanoparticles link previously unconnected receptors and create new dimers. The enhancement of olfactory response is therefore explained by the contribution of the created dimers in the signal transduction.

The olfactory enhancement by zinc nanoparticles is significant in consideration of Luca Turin's vibrational hypothesis that proposed an inelastic electron tunneling spectroscopy (IETS) mechanism for discriminating odorants (Turin 1996). The model needs a donor of electrons, and it is rational to propose that zinc nanoparticles become electron donors (Vodyanoy 2010, Brookes, Horsfield, and Stoneham 2012a, Jia et al. 2016, Hagerty et al. 2016b). Therefore, zinc nanoparticles play a dual role in the enhancement of olfaction: they increase the concentration of receptor dimers and serve as electron donors for the tunnel electron transport.

The addition of the ZnPEG400 nanoparticles to odorant at the end of 317 days of storage at 278 K (5 ^{o}C) resulted in the highest relative EOG enhancement that was larger than enhancement by the un-PEGylated zinc nanoparticles. This amplified enhancement can be explained by the increased binding affinity to olfactory receptors in part due to the reduction of the surface charge as it was manifested by the reduction of zeta potential and because of the increase of hydrophobicity (Mu et al. 2014). Additionally, XPS data indicate covalent binding between PEG400 and zinc nanoparticles that may cause oxidative coupling between the PEG molecules and zinc atoms on the surface of zinc nanoparticles. The combined electron system may be more efficient in donating electrons than non-PEGylated zinc nanoparticles and therefore contributed to the amplified olfactory enhancement. The signal amplification effects for combined electron system was reported for PEGylated electrodes (Doneux, Cherif, and Buess-Herman 2016, Doneux et al. 2016, Hotchen et al. 2015, Nekoueian et al. 2015). Furthermore, the estimated transmission probability of electron transfer through the PEG400 layer was larger than that for the PEG1000 (S1 Supporting Information). All the above properties of ZnPEG400 (increased binding affinity, combined zinc-PEG electron system, and favorable electron transmission probability) provide an explanation for the amplified olfactory enhancement compared to non-PEGylated zinc nanoparticles.

The XPS analysis of the ZnPEG1000 after long storage indicated that in contrast to ZnPEG400 data, zinc nanoparticles and PEG1000 did not produce a conjugated electron system, and therefore they do not have the advantage of facile electron donation compared to non-PEGylated zinc. This observation may be explained by the length, viscosity, and rigidity of PEGs. PEG400 with ~9 monomer repeats (as opposed to ~23

repeats in PEG1000) has a lower viscosity and rigidity than those of PEG1000 (Wang et al. 2009). With the lower viscosity and rigidity, the PEG 400 can enable a more intimate interaction with the olfactory sensory receptors. Moreover, being a shorter molecule the PEG400 produced a thinner layer around the zinc nanoparticle. The estimated transmission probability of electron transfer through the PEG400 layer was approximately 4 times higher than that of the PEG1000 (S1 Supporting Information). The PEG400 layer, therefore, can provide the sufficient electron transfer for the olfactory transaction, while PEG1000 is much less efficient. ZnPEG1000 nanoparticles showed negative relative EOG signals post 280 days incubation because they compete with the endogenous zinc nanoparticles for binding sites in the olfactory receptors. The ZnPEG1000 nanoparticles occupied the receptor binding sites that were intended for endogenous zinc nanoparticles. This binding resulted in the receptor dimers that were not capable of triggering the signal transaction because zinc nanoparticles could not transfer electrons through the PEG1000 layers. Thus, the produced signal evoked by the odorant with ZnPEG1000 nanoparticles will be smaller than the signal evoked by the odorant alone (Fig 4.5).

The relative enhancement of zinc nanoparticles had a non-monotonic dependence on the time of storage. The freshly prepared particles had the highest enhancement. The enhancement declined on day 3 and then increased again on day 5 (Fig 4.5). This non-monotonic behavior cannot be explained through the animal to animal variability. The amplitude of the electrical signals varies from cell to cell and from animal to animal (Firestein, Picco, and Menini 1993). The EOG measured at the different contact points of OE may have a different amplitude. However, the earlier measurements showed that the

correctly normalized relative values of the epithelial electrical signals were conserved amongst the single animal and different animals of the same age and breed (Scott and Scott-Johnson 2002, Ottoson 1956). This fact allowed the use of different animals to quantitatively characterize initial olfactory events. We previously used this approach to characterize the effects of different odorants at various concentrations and evaluate the effects of zinc nanoparticles (Viswaprakash et al. 2009). We further showed that the cultured olfactory neurons initially obtained from different mouse pups also conserved the EOG kinetic properties of the neurons at the same age. For these cultured neurons, we also showed that zinc nanoparticles enhanced EOG responses of both younger and older cultures (Viswaprakash et al. 2010).

We speculate that non-monotonic dependence of an olfactory enhancement by zinc nanoparticles can be attributed to the time-dependent changes in the electronic structure of the nanoparticles related to the relaxation and diffusion of atoms. Indeed, taking into the account that the self-diffusion coefficient of zinc in the single zinc crystal at 278 K is 7.7×10^{-22} m^2/s (Banks 1941), it would take ≈31 h to move a zinc atom the distance of 1.2 nm. This time is consistent with the time of the initial decline in the relative olfactory enhancement. Zinc nanoparticles of 1.2 nm in diameter contain ~59 zinc atoms (47 atoms in the shell and 12 atoms in core) (Hagerty et al. 2016b). The freshly prepared zinc nanoparticles may be all in the non-oxidized state and produce the maximal olfactory enhancement. The present XPS data showed that in one day, 3% of zinc atoms of the primarily-elemental zinc nanoparticles, or ≈2 atoms are ZnO. Being in the shell of nanoparticles, ZnO may cause an initial decline in the olfactory enhancement.

After a further storage, zinc atoms diffused from the shell to the core and no longer interacted with olfactory receptors. The detrimental effect of ZnO on olfactory enhancement could be similar to that reported for cancer cells treated with the non-thermal atmospheric-pressure plasma particles that caused cell death by alteration of antioxidant activity (Kaushik et al. 2014). Likewise, the polymeric membrane with ZnO particles is described to offer antibacterial activity (Nasajpour et al. 2018). The non-monotonic dependence on particle size, shape, support, composition, and oxidation state was found in the catalytic properties of metal nanoparticles (Cuenya 2010) and the effects of metal nanoparticles on biological systems (LB. 2014).

The mechanism of the amplified enhancement by PEG400 coating of zinc nanoparticles exposed to elevated temperatures is similar to that of the enhancement by ZnPEG400 nanoparticles subjected to long-term storage at 278 K (5 ^{o}C). The XPS spectra of ZnPEG400 subjected to elevated temperature showed similar features to the Nanoparticles stored for longer times. These observations provide evidence for the large number of covalently bound species and production of a conjugated electron system of zinc nanoparticles and PEG400 molecules. The mechanism of the amplified enhancement produced by the ZnPEG400 after heating are similar to those described for these particles after prolonged storage. Although PEG reduces oxidation of elemental zinc both for 400 g/mol and 1000 g/mol molecules, the PEG1000 coating causes a considerable increase in the coating thickness which consequently reduces the enhancement of the odorant response.

We can conclude that small ~1.2 nm diameter non-oxidized primarily-elemental zinc nanoparticles produced enhancement of responses to odorants, as verified by physiological experiments, whereas air-oxidized zinc nanoparticles inhibits olfaction. When the zinc nanoparticles were covered with thin layers of polyethylene glycol of molecular weight 400 g/mol and 1000 g/mol (ZnPEG400 and ZnPEG1000), the PEGylation preserved the nanoparticles from oxidation while conserving their crystalline structure. PEGylation maintains the ability of the zinc nanoparticles to enhance the olfactory response to the odorant. The polyethylene glycol molecules by themselves produced a small olfactory response inhibition when delivered with the odorant, and did not produce a noticeable effect when applied without odorant. The ZnPEG400 nanoparticles continued to manifest the amplified enhancement of odorant response even after a 300-days storage at 278 K (5 ^{o}C), while ZnPEG1000 nanoparticles produced an inhibition under the same conditions. ZnPEG400 withstood two-day storage at 303 K (30 ^{o}C) and 323 K (50 ^{o}C) and evoked the adequate enhancement of olfaction, but ZnPEG1000 showed a reduced enhancement at the same conditions. The PEG400 appeared to be far better for preservation of properties of zinc nanoparticles for long term storage and elevated temperatures. The enhancement and inhibition of olfaction by zinc nanoparticles preserved by PEGylation were consistent with Turin's model of olfaction. The novelty of this work is that biocompatible and safe PEG400 coat of zinc nanoparticles provides both preservation of particles and amplification of olfactory enhancement. Future olfactory experiments with the intranasal delivery of protected zinc nanoparticles to a transient chemically acquired anosmic rodent model and a cognitively

impaired Alzheimer's rodent model will test the pre-clinical validity of smell enhancement described in this work.

4.6 Associated content

S1 Supporting Information

The S1 Supporting Information show details of methods and calculations.

4.7 Disclaimer

Certain commercial equipment, instruments, or materials are identified in this paper to specify the experimental procedure adequately. Such identification is not intended to imply recommendation or endorsement by the National Institute of Standards and Technology, nor is it intended to imply that the materials or equipment identified are necessarily the best available for the purpose.

4.8 Appendix

4.8.1 Supplemental Information

Striking Image

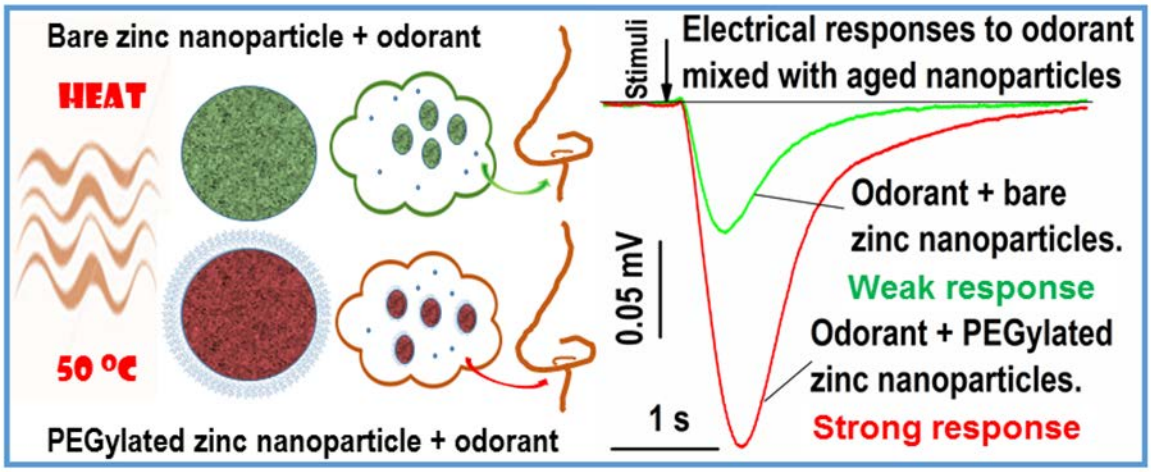

Figure 4.7 Summary image of heat influence on zinc nanoparticles olfaction enhancement with and without PEGylation.

4.7.2 Number of monomers in poly-ethylene glycols (PEGs)

The structural molecular formula of PEG is

$$H\text{-}(O\text{-}CH_2\text{-}CH_2)_n\text{-}OH$$

The molecular mass of the polymer is a sum of masses of H, OH and N×(mass of the monomer)

=18 + N×44. Therefore, the number of monomers in the PEG with a molecular mass of M is equal

N=(M-18)/44.

Consequently, the number of monomers in PEG400=(400-18)/44≈9 and in PEG1000=(1000-18)/44≈23.

4.8.3 Thickness of the PEG layer on the surface of nanoparticle

Using the area per PEG single chain of a surface of a nanoparticle (Butterworth, Illum, and Davis 2001) the estimate of the PEG layer thickness (L) can be done by the following equations(Perry et al. 2012):

$$L = \frac{Na^{5/3}}{D^{2/3}}, \quad (1S)$$

Where a=0.35 nm is a length of a single PEG monomer, D – the distance between the PEG's chains defined by the equation:

$$D = 2\sqrt{\frac{A}{\pi}} \quad (2S)$$

Where A=1.28 nm^2 for the PEG400, and A=2.91 nm^2 for the PEG1000.

From equations (1S) and (2S) follows that L_{400}=1.32 nm and L_{1000}=2.28 nm.

4.8.4 The transmission probability of electron transfer through the PEG layer

The transmission probability T of electron with energy E, mass m through the potential barrier of height U_o and thickness L can be approximated by the equations (Griffiths 1995):

$$T = \frac{16E(U_o - E)}{U_o^2}\exp(-2\alpha L) \quad (3S)$$

Where $\alpha = \sqrt{\frac{2m(U_o - E\}}{h^2}}$

(4S)

h is Plank's constant.

For zinc nanoparticles of 1.2 nm in diameter, the electron energy (E) was estimated to be 79.6 meV (Hagerty et al. 2016b). The potential barrier of PEG layer (U_o) varies depending of method between 0.1 and 0.2 eV(Smolne, Weber, and Buback 2016, Sannaningannavar, Navati, and Ayachit 2016, Kabra et al. 2015). The transmission

probability (*T*) of electron through PEG400 layer of L=1.32 nm and U_o=0.101 eV (Kabra et al. 2015) is calculated by equations 3S and 4S.

$$\frac{16E(U_o-E)}{U_o^2}=\frac{16(0.0796eV)(0.101eV-0.0796eV)}{(0101\ eV)^2}=2.6718$$

$$\alpha L=(1.32\times10^{-9}m)\times\sqrt{\frac{2(9.11\times10^{-31}kg)(0.101eV-0.0796eV)(1.6\times10^{-19}J/eV)}{(1.055\times10^{-34}J.s)^2}}=0.99295$$

The transmission probability then for PEG400 layer

T_{400}=2.6718exp[-2(0.99295)]= 0.36673.

Similar calculations for 1.2 nm zinc nanoparticle covered with PEG1000 layer give T_{1000}=0.08652.

The transmission probability is a strong function of the potential barrier (U_o). For example, when U_o=0.2eV(Smolne, Weber, and Buback 2016, Sannaningannavar, Navati, and Ayachit 2016) , *T*400 and *T*1000 are 0.0345 and 0.00112, respectively.

4.8.5 Energy of activation of zinc nanoparticle oxidation

The Arrhenius equation (Segel 1976) can be used to express the temperature dependence of the first-order activation kinetics:

$$k = Ae^{-\frac{E_a}{RT}} \qquad (5S)$$

where *R* is the universal gas constant, E_a represents the apparent activation energy, and *A* -- the pre-exponential Arrhenius factor. Taking the logarithm of Eq. (5S) yields:

$$\log k = -\frac{E_a}{2.303R}\times\frac{1}{T}+\log A \qquad (6S)$$

If the logarithm of k in Eq. (5S) is plotted against the reciprocal of temperature, 1/T, then the slope of this graph yields the activation energy (E_a), the thermal activation level of transitions from not-oxidized to oxidized atoms.

Chapter 5.0 Perireceptor Nano-molecular Influence on Olfaction

5.1 Abstract

Metals are found to play a role in multiple facets of biology, and some, such as zinc are critical and found ubiquitously throughout biological organisms. Metal nanoparticles such as copper, gold, and zinc have been isolated from human and animal blood. Of those, zinc nanoparticles (ZnNPs) have been shown to enhance responses of the olfactory sensory neurons to odorants by about three-fold. Characterization of the physiochemical properties of zinc nanoparticles determined that only small (1.2 nm), non-oxidized, primarily elemental zinc nanoparticles were capable of olfaction enhancement. This tissue level enhancement in combination with perception studies in awake canines with fMRI demonstrates an *ex vivo* and *in vivo* enhancement of olfaction and higher cognitive processing of olfaction with the addition of zinc nanoparticles to odorant. In line with that fact, metals have been found in mucosal sites in the body including within the olfactory system. To evaluate the potential biological role ZnNPs have in the initial events of olfaction, the nano-composition of the perireceptor environment was analyzed for its electrophysiological influence on olfactory neurons. Isolation of the nano-molecular substrate from the olfactory mucosa demonstrated on EOG to provide ZnNPs-like enhancement of olfaction. XPS analysis of the nano-filtrate was inconclusive for positive identification of ZnNPs, though literature supports a zinc concentration of 14 μg/dl within the nasal mucus of mice. Available studies do not differentiate between ionic zinc and zinc metal nanoparticles. Though limited to an electrophysiological comparison, this data further supports a biological role of ZnNPs

through indications of the endogenous presence of enhancement capable nanoparticles at the site of action.

5.2 Introduction

The interplay of metals and biology has a component established in neurobiology, with many implications in the sensory system of olfaction in the olfactory bulb and higher cognitive centers (Frederickson and Danscher 1990, Sensi et al. 2009). Zinc is found within the cerebrospinal fluid at concentrations estimated at 31.5 $\mu g/L^{-1}$ (Agarwal and Henkin 1982). Ionic zinc applied to the olfactory epithelium is inhibitory to olfaction and zinc salts are commonly used to induce anosmia in experimental settings (Ishimaru et al. 2000, Smith 1938, Rowe and Smith 1972). Zinc particles were identified in human and animal blood that was in the nanoscale (1-2 nm) and non-ionic that evoked significant enhancement in combination with odorant in the olfactory sensory neuron (Viswaprakash et al. 2009, Viswaprakash et al. 2006).

The described *ex vivo* experiments showed an enhancement that was dose-dependent, specific, and reversible. In conjunction with *ex vivo* analyses of sensory neurons in the rodent OE, an investigation into the perception and higher processing in the olfactory pathway was conducted in a canine model. Functional magnetic resonance imaging (fMRI) was performed on awake and anesthetized canines exposed to odorants with and without zinc nanoparticles. This method analyzed *in vivo* cognitive effects on the brain regions associated with olfaction and results concluded that an increase of olfactory associated higher brain center activity was recorded with the addition of zinc nanoparticles to odorant (Jia et al. 2016).

However, the commonly used methods for determining zinc status do not differentiate between zinc ions and zinc nanoparticles and these studies have demonstrated a differential response based on size, oxidation, and state of zinc in olfaction (Takeda 2001, Takeda et al. 1997, Hagerty et al. 2016b). Presence of zinc nanoparticles (ZnNPs) within the olfactory epithelium (OE) and respiratory epithelium (RE) has not been reported. This study examined the electrophysiological properties of endogenous nanoparticles obtained from the OE and RE compared to engineered ZnNPs on responses the olfactory sensory neuron to odorant.

5.3 Materials and Methods

5.3.1 Animal Model

Animals used in this project were cared for by the Division of Laboratory Animal Health of Auburn University in compliance with all applicable regulations. The protocol was approved by the AU IACUC committee. The animals were provided standardized conditions and housing arrangement with two animals per cage for socialization and continual free access to food and water with enrichment toys. Their care was in accordance with primary regulations governing the care and use of animals. Those policies include the Animal Welfare Act (AWA), Guide for the Care and Use of Laboratory Animals, NIH-PHS Policy, and the Guide for the Care and Use of Agricultural Animals in Agricultural Research and Teaching. Efforts were taken to explicitly avoid the exposure of the animals to discomfort, pain, and/or injury. Animals

were adult, male, approximate weight of 250 g to 300 g, Sprague–Dawley rats acquired from Envigo, Dublin, VA. Rats were chosen as the model for experimentation based on the foundation of replace, reduce and refine. The rat as a model for olfaction is well represented in literature due to its ease of tissue access and stable viability of olfactory epithelial electrical activity and continued neuron function following isolation for periods of time up to an hour.

5.3.2 Epithelial Tissue Extracts

Olfactory Epithelial Filtrate for EOG

Obtaining of extra-fine extracts from olfactory epithelium. Olfactory and respiratory epithelia were surgically removed from 4 males, 250 g, Sprague D. rats were pooled in ice-cold Ringer solution, ground in the glass-in-glass sterile tissue homogenizer and filtered consecutively with 30- and 3-kDa Centricon filters (Millipore). The filtrate was mixed with odorant for testing in EOG experiments

Respiratory Epithelial Filtrate for EOG

Obtaining of extra-fine extracts from olfactory epithelium. Olfactory and respiratory epithelia were surgically removed from 4 males, 250 g, Sprague D. rats were pooled in ice-cold Ringer solution, ground in the glass-in-glass sterile tissue homogenizer and filtered consecutively with 30- and 3-kDa Centricon filters (Millipore). The filtrate was mixed with odorant for testing in EOG experiments.

5.3.3 Zinc Nanoparticles

Underwater High-Voltage Discharge Method

Metal nanoparticles were produced by a modified method (Tokushige, Nishikiori, and Ito 2010, Kruyt 1952) as described in methods, Chapter 2 (Hagerty et al. 2016b). Zinc nanoparticles were size-selected for <2 nm diameter and characterized as described Chapter 3.

5.3.4 Electroolfactogram

Electrophysiology is measured by electroolfacotgram. The basis is on measurements of the potential of a collection of OSNs within a given area of the pipette tip, method based on Electroolfactography (EOG) described previously (Viswaprakash et al. 2009). The method utilizes Axon Instrument MultiClamp 700A amplifier and 1322A DigiData acquisition system.

Microsurgical removal of olfactory septal mucosa from the rodent model, rat, is placed in a perfusion chamber that allows for basal cellular immersion in physiological buffer solution and epithelial surface exposure to air where olfactory receptors are in highest density on the OSN cilia. Buffer solution contains 137 mmole/L NaCl, 5.3 mmole/L KCl, 4.2 mmole/L $NaHCO_3$, 0.4 mmole/L KH_2PO_4, 3.4 mmole/L Na_2HPO_4, 1.3 mmole/L $CaCl_2$, 0.2 mmole/L $MgSO_4$, and 5.6 mmole/L D-glucose at pH 7.4.

Electrodes are pulled fresh with an approximate tip diameter of 24 μm. The patch electrode is filled with physiological buffer of the same composition as immersion

solution. Electrodes are attached to a patch-clamp amplifier to detect responses from the olfactory epithelium. Contact is established between the electrode and tissue surface, and tissue is stabilized. Once stabilization is achieved, air puffs of the odorant mixture were applied. Odorant mixtures of laboratory zinc for positive control, water vapor for negative control, odorant alone for baseline, OE nanoparticle filtrate added to odorant mixture, and RE nanoparticle filtrate added to odorant mixture. Odor responses over the time course of several minutes were recorded after being amplified by a patch-clamp amplifier and filtered at 2 kHz to 5 kHz.

5.3.5 Odorants

Odorants were obtained from Sigma-Aldrich. An odorant mixture of 1.6 mmole/L each of ethyl butyrate, eugenol, and (+) and (–) carvone in water was prepared with a vortex mixer and stored in a dark glass container at 283K (5 ^{o}C).

5.3.6 Delivery of odorants and metal nanoparticles

During the experiment, a 0.25 s pulse of the odorant mixture at 55158 N/m^2 (8 psi) was generated by a computer-controlled Pneumatic PicoPump PV800 (World Precision Instruments, Sarasota, FL). A pulse of positive pressure pushed the odorant into a glass nozzle toward the OE. The computer controlled odorant delivery was comprised of 0.25 s pulses at 20 s and 60 s times for EOG data collection. The single EOG recording took 200 s and contained 10 response traces. A nanoparticle suspension was combined with odorant solutions to reach a final nanoparticle concentration of 0.02 nmole/L.

During the pulse of delivery, the vapor of odorant with metal nanoparticles was transferred to the OE surface (Viswaprakash et al. 2009). Three mixtures were developed with OE nanoparticle filtrate, RE nanoparticle filtrate, and laboratory produced small zinc nanoparticles as characterized in Chapter 2.

5.3.7 Statistics and Software

Software used for analysis include Clampex 10.7; Clampfit 10.7., Microsoft Office ® Office Word 2015, Microsoft ® Office Excel 2015, 2010. Data averaging, ANOVA, t-test, curve fitting, and graph plotting were carried out using Microcal ™ Origin ® ver. 9.2 (Northampton, MA).

5.4 Results

5.4.1 Odorant responses to Endogenous filtrate

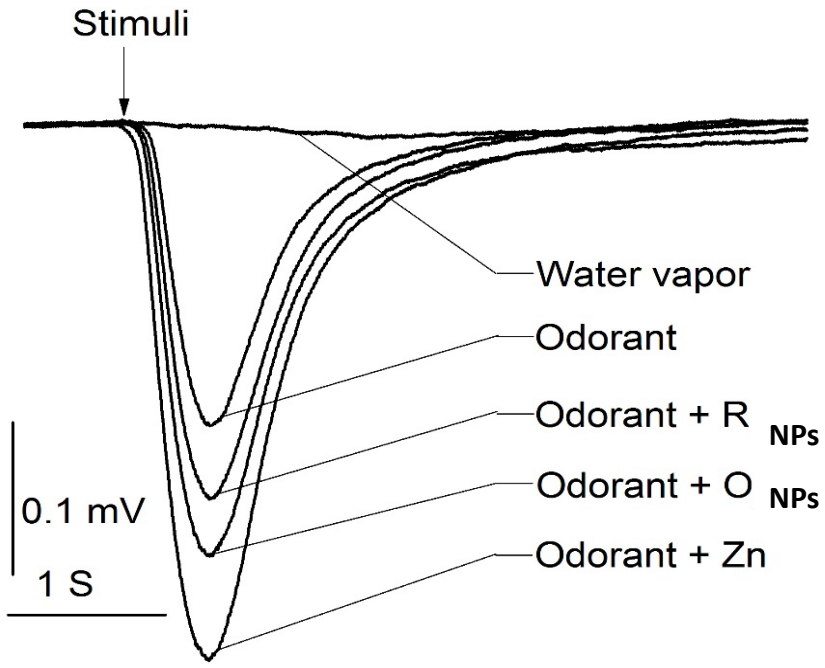

Figure 5.1 EOG responses to 1.6 mM odorant (Odorant), 1.6 nM odorant + nanoparticles obtained from olfactory epithelium (Odorant + O_{NPs}), 1.6 nM odorant + nanoparticles obtained from respiratory epithelium (Odorant + R_{NPs}), 1.6 nM odorant + 0.01 nM engineered Zn nanoparticles (Odorant + Zn), and water vapor (Water vapor).

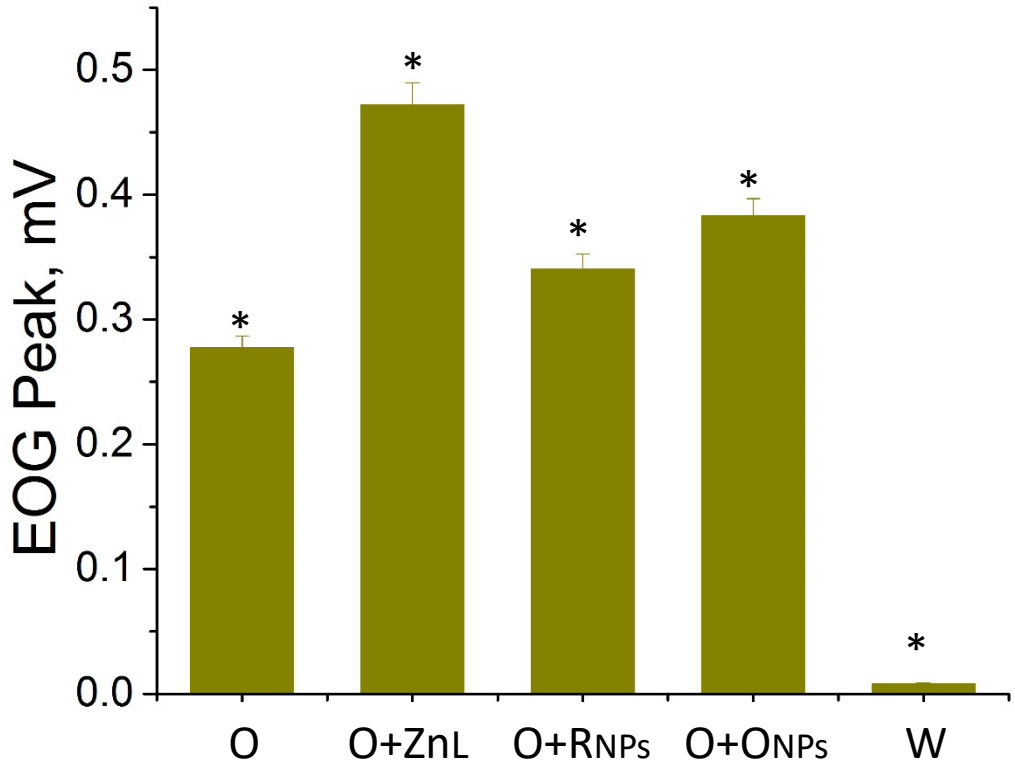

Figure 5.2 EOG peak mean values for 18 EOG experiments. ANOVA statistical test of variance showed that all mean values are significantly different at the level of $p<0.05$ [$F(4, 115)=200$, $p=0.0$].

The response as measured by EOG demonstrated the engineered ZnNPs, OE and RE filtrates mixed with odorant evoked higher olfactory responses compared to the response induced by odorant alone.

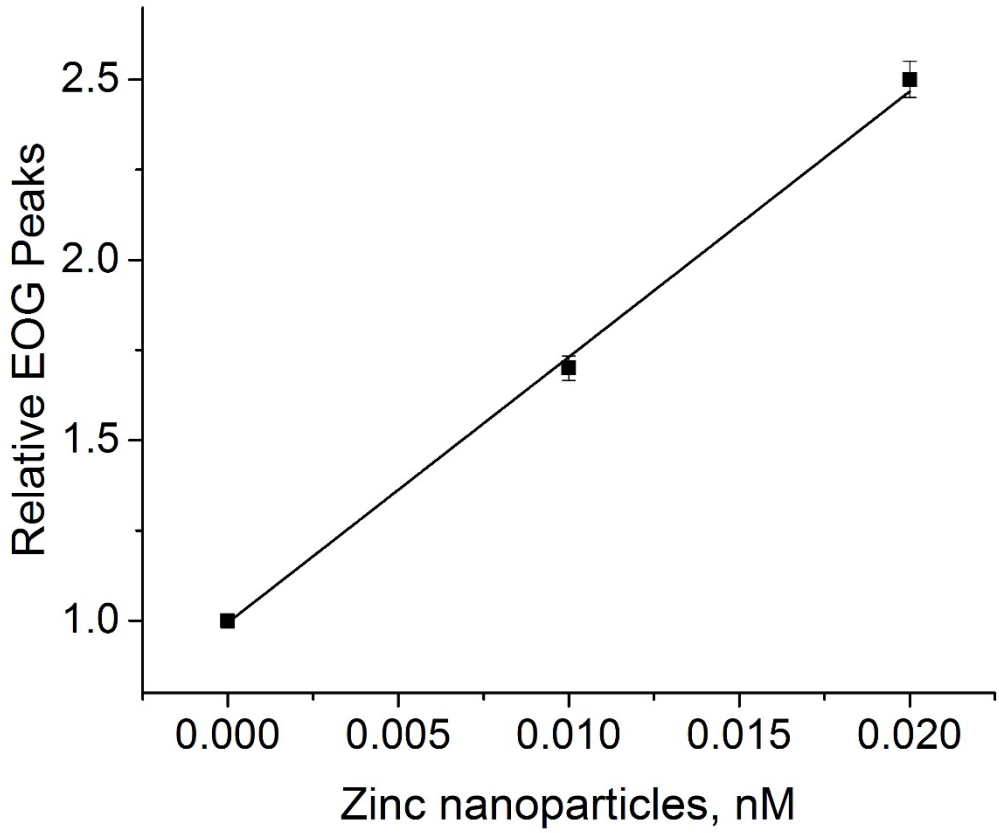

Figure 5.3 Relative EOG peaks as a function of engineered zinc concentration (Ration of EOG peak by (O+Zn)/O. Points are experimental data, and line is a linear fit (R-Square=0.997; Intercept=0.99±0.02, Slope=73.6±2.7 1/nm).

Using the plot in Figure 5.3 as a calibration curve, we estimated the concentration of zinc nanoparticles in the olfactory and respiratory suspensions, and in the olfactory and respiratory epithelia, shown in Table 5.1.

Table 5.1. Concentration Estimates

Tissue	Filtrate Concentration			Tissue Concentration		
OE	5.3×10^{-3}	$\pm 5 \times 10^{-4}$	nM	10.3	± 1.0	nM
RE	2.7×10^{-3}	$\pm 5 \times 10^{-4}$	nM	7.9	± 1.5	nM

Table 5.1. The estimated concentrations of nanoparticles with zinc-like attributes in

olfaction enhancement. Significance using ANOVA found between filtrate concentrations at $p<0.05$.

The concentrations of estimated zinc nanoparticles in OE and OR extracts are, $5.3x10^{-3} \pm 5x10^{-4}$ nM and $2.7x10^{-3} \pm 5x10^{-4}$ nM, respectively (Table 5.1, Figure 5.4).

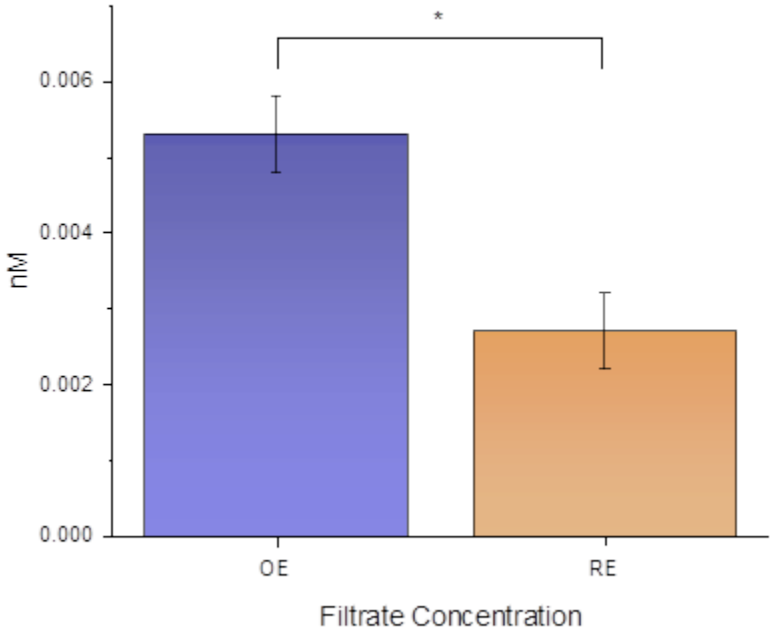

Figure 5.4 The estimated concentrations of nanoparticles with zinc-like attributes in olfaction enhancement within the olfactory epithelial filtrate (OE) and respiratory filtrate (RE).

The concentrations of zinc nanoparticles in OE and OR are, 10.3 ± 1.0 nM and 7.9 ± 1.5 nM, respectively (Table 5.1, Figure 5.5).

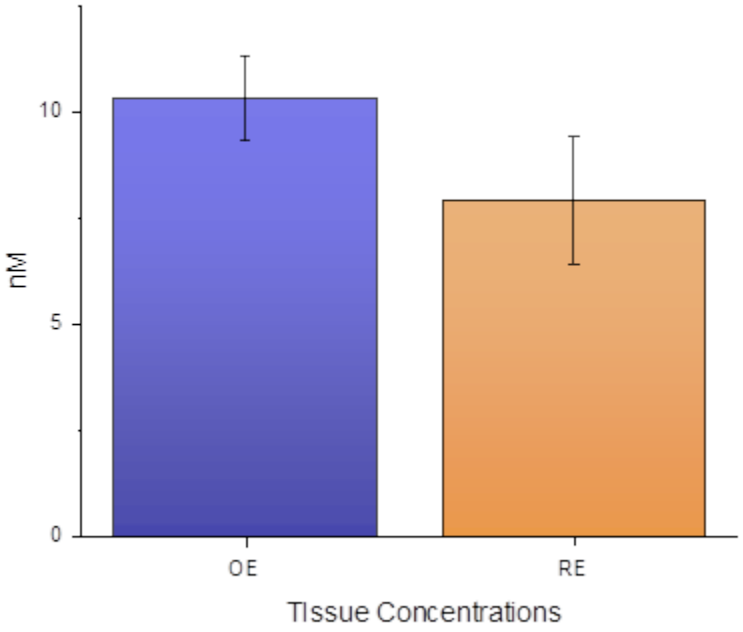

Figure 5.5 The estimated concentrations of nanoparticles with zinc-like attributes in olfaction enhancement within the olfactory epithelium (OE) and respiratory epithelium (RE).

According to (Frederickson et al. 2006), the extracellular concentration of zinc is in the range 5-25 nM.

5.5 Discussion

The presence of ZnNPs within the body may have physiological significance. To determine the role of ZnNPs in olfaction, many questions still have to be answered. However, the presence of olfaction enhancing nanoparticles within the OE and RE suggests a physiological role in the initial events of olfaction at the receptor level. The

nanoparticle action in this study on EOG is analogous to that with zinc nanoparticles described previously.

Concentrations of tissue level zinc were consistent with previously reported extracellular zinc concentrations (Frederickson et al. 2006). The difference seen in OE and RE in solution of nanoparticle filtrate coincided with an increase in EOG response to odorant. This result is fitting with the functional requirement of zinc nanoparticles in olfaction in our proposed model of receptor dimerization and potential to serve as an electron donor in the vibrational theory of olfaction. The respiratory and olfactory epithelium is adjacent to a transitional zone, with shared mucus constituents in this transitional area. However, the cellular components that contribute to the mucus layer where the metals are present and would be required to have interaction with the receptor for physiological function are unique in the olfactory system. The bowman's glands contribute to the mucus and serous secretions that differ in composition from the nasal mucus. The mucus contains a diverse collection of enzymes, acids, mucopolysaccharides, immune factors, antioxidants, and numerous proteins such as antimicrobial proteins and odorant binding proteins (OBP) (Solbu and Holen 2012, Mira 1963, Briand et al. 2002, Mellert et al. 1992). Zinc ions have been found in the mucus layer are estimated at concentrations of 14 μg dL^{-1} in humans (Henkin, A., and Martin 2000). The comparison of zinc ions to zinc nanoparticles physiologically in the olfactory system has indicated a differential effect with zinc ions inhibiting EOG signals in the OE and zinc nanoparticles enhancing EOG signals above normal baseline in the presence of odorant (Ishimaru et al. 2000, Smith 1938, Rowe and Smith 1972). Zinc levels in the mucus layer do not differentiate between zinc ions and zinc nanoparticles (Takeda 2001,

Takeda et al. 1997). Other metal nanoparticles, such as gold, platinum, silver, and copper, were tested in olfaction with EOG and did not display the same enhancement as seen with zinc nanoparticles (Viswaprakash et al. 2009). The data in this study of olfaction enhancement capabilities in RE and OE nanoparticle filtrate suggests that physiologically the active molecule is not ionic zinc, oxidized zinc, or other metal nanoparticles found in human and animal blood strengthening the argument for an endogenous zinc nanoparticle component to the OE.

Using electrophysiology as a comparative tool for a functional substance of similarity to the characterized zinc metal nanoparticles capable of olfaction enhancement, a zinc analogous nanoparticle solution was recovered from both olfactory epithelium primarily and respiratory epithelium to a lesser degree. The presence of zinc nanoparticles in the olfactory epithelium is critical to support the proposed biological function of endogenous zinc nanoparticles in the initial role of olfaction. A proposed role through receptor dimerization and action as a potential electron donor in the vibrational theory of olfaction. This data supports the endogenous presence of an olfaction enhancing capable molecule, suggestive of endogenous zinc nanoparticles.

Zinc nanoparticles are found in human and animal, which lends to the consideration that zinc nanoparticles could hold the potential to be ubiquitous throughout the body and present in the mucus layer of the OE at the site of action for the zinc nanoparticles used in EOG studies. The consistent finding of total zinc in the CNS and higher concentrations in the olfactory system, though not evaluated, could contain a portion of zinc metal nanoparticles undifferentiated by the testing method. The significant difference in the biological behavior of ions to nanoparticles for zinc

highlights the need for a more accessible means to differentiate between ions and nanoparticles. This ease of differentiation is particularly important as the use of nanoparticles in medicine and production is increasing.

5.6 Conclusions

The nanoparticle filtrate from the OE produced the highest significant enhancement of olfactory sensory neuron response to odorant. The nanoparticle filtrate from the RE also produced a significant enhancement in olfactory sensory neuron response to odorant to a lesser level than OE which is consistent with a biological function of significance within the OE for odorant receptor activation.

The difficulty in differentiating zinc ions to zinc nanoparticles in a biologically homogenized sample with traditional techniques is tremendous. However, the electrophysiological results are comparable to laboratory produced zinc nanoparticles, the consecutive filtering to a fine level of nanoscale filtrate, and the background of selectivity for olfaction enhancement to small (1.2 nm), non-oxidized, zinc primarily metal state nanoparticles, suggests a zinc nanoparticle-like molecule endogenously present within the olfactory epithelium.

Chapter 6.0 Micro-environmental evaluation of the olfactory system and influence of zinc nanoparticles

6.1 Abstract

Studies on the effects of zinc in the body and as an antimicrobial have examined ionic zinc (Zn^{2+}) and oxidized zinc nanoparticles (ZnO-NPs) with size ≥3 nm. Publications report ZnO-NPs exhibit strong to moderate toxicity to the Gram-positive *Bacillus subtilis* and methicillin-resistant *Staphylococcus aureus* (MRSA). No studies evaluating the antimicrobial effects of small (<2 nm size) non-oxidized zinc nanoparticles (ZnNPs) antimicrobial effects have been conducted. In the present study, the growth of Gram-positive and Gram-negative pathogenic, conditionally pathogenic, and non-pathogenic bacteria were evaluated. Bacterial species selected included Gram-negative *Escherichia coli* M-17, *Shigella flexneri* and *Salmonella typhimurium* 52096 and Gram-positive species *Staphylococcus aureus* ATCC 12600, methicillin-resistant *Staphylococcus aureus* (MRSA), *Lactobacillus acidophilus, Bacillus subtilis* BSB3, *Bacillus subtilis* BS, and *Bacillus licheniformis* BL. A second test evaluated seven different MRSA strains and *B. subtilis* were cultured with small non-oxidized ZnNPs 1.2 nm. Relative growth patterns were determined by spectrophotometric analysis at a 24-hour time point. Results included an observed trend that non-oxidized ZnNPs were generally MRSA suppressive, with an approximate 34% maximum reduction in viability ($p<0.05$). Conversely, observing growth for *B. subtilis* with an approximate 18% maximum increase in viability ($p<0.05$). These initial results display a possible differential pattern of effects to reported Zn antimicrobial activity with Zn^{2+} and ZnO. The results are consistent with differential effects of ZnO-NPs, Zn^{2+}, and ZnNPs on epithelial tissue of the olfactory system. Further evaluation is needed to determine the

mechanism of action for the effects of small non-oxidized zinc nanoparticle on the growth multiple bacterial taxa.

6.2 Introduction

Zinc is an essential micronutrient, it is required for multiple biological processes. The metal zinc is considered relatively non-toxic to humans (Fosmire 1990). There are benefits attributed to zinc, such as neuroprotection, as well as toxicities which are different based on the zinc salt (Pavlica, Gaunitz, and Gebhardt 2009, Pavlica and Gebhardt 2010). Zinc and zinc compounds are commonly used in products such as zinc oxide and zinc oxide nanoparticles in sunscreens due to its UV protective effects (Rai, Shanmuga, and Srinivas 2012). Zinc oxide nanoparticles are also used as drug carriers and in medical devices for their antimicrobial properties and antibiofilm formation (Coughlan et al. 2008, Holt et al. 2018).

The antimicrobial effects of zinc are historical and predate current antibiotic methods of bacterial control, particularly in their use of dermatological conditions and ocular therapeutics (Haxthausen and Rasch 1928). The use of bacitracin, which is a mixture of cyclic peptides produced by specific *Bacillus subtilis* strains, combined with zinc salts, have been used historically as a topical "antibiotic" with strong Gram-positive spectrum (Gross, Johnson, and Lafferty 1956, Johnson, Anker, and Meleney 1945). The relevance of zinc at mucosal sites is supported by zinc oxide and zinc salts in feed-additives as a significant means of reducing diarrhea in animals (Stensland et al. 2015).

In cases of human medicine and zinc supplementation, zinc is now listed as a recommended therapy for diarrhea in children in third world countries by the World

Health Organization (Lazzerini and Wanzira 2016). Foodborne pathogens are of significant concern for population health. The antibiotic repertoire is no longer expanding, but the antibiotic-resistant strains of pathogens are. The CDC reports that approximately 33% of individuals carry *S. aureus* in their nasal passage and 2% of individuals carry methicillin-resistant *S. aureus* (MRSA) strains (Graham, Lin, and Larson 2006).

There are other bacteria of consideration in the nasal passageway that have been identified as potential agents that utilize the olfactory neural network as a point of entry that can lead to meningitis, though are not the predominant bacterial species isolated in meningitis; these include *E. coli, S. aureus,* and rarely *Salmonella* spp. (Thigpen et al. 2011, Greenhow et al. 2014). These are most commonly associated with previous nasopharyngeal or sinus colonization, at-risk groups including immunosuppressed or post-neurosurgical groups suggesting an opportunistic entry into the central nervous system (Thigpen et al. 2011, Greenhow et al. 2014).

The recognition that microbiota in mammals and the environment play a critical role in homeostasis is a growing field. *Bacillus subtilis* is an important environmental bacteria that is found in soils and vegetation serving as an important regulator in soil balance and selective biological plant disease control agent (Hsueh et al. 2015). In mammalian therapeutics, *Bacillus* species are known to produce enzymes (digestive and lytic), essential amino acids and vitamins, over 200 antibiotics, and prevented heat-stress related adverse effects when used as a probiotic (Moore et al. 2014).

Odorants brought to the olfactory epithelium may traverse the mucous layer interacting with microbiota, enzymes, proteins, and metals. The microbiota of the

olfactory system is not well established, but emerging work demonstrates a similar core biome in mice, with the two dominant phyla composing *Firmicutes* (30-70%) and *Bacteroidetes* (15-60%), followed by *Proteobacteria* (5-25%) and *Actinobacteria* (<10%) in descending abundance respectively (Francois et al. 2016). In a study with humans, an indirect evaluation of the olfactory-adjacent region of the nasal mucosa, the three dominant phyla were markedly different in their ratios with *Actinobacteria* (50%), *Firmicutes* (24%), and *Proteobacteria* (20%) and less than 3% from *Bacteroidetes* (Yan et al. 2013). The three dominant phyla comprising approximately 75% of all microbiota found in studies of fecal samples in humans include *Firmicutes*, *Bacteroidetes*, and *Actinobacteria* (Gibson and Roberfroid 2008). These results indicate a similar core biome, with a variation in the ratios of phyla isolation. There is significant individual variation, collection site variation, environmental factors, and collection methods that can account for this variation. Other work in our lab suggests that there is a significant difference in the bacterial composition between the respiratory epithelium, the ethmoturbinates, and the main olfactory epithelium (unpublished data). The presence of a microbiotal community in the olfactory system indicates a microenvironment that can be influenced by xenobiotics, proteins, enzymes, and metals that can be found within the mucus layer.

The development of bacitracin from *Bacillus subtilis* peptides is a recognition of the contributory attributes of the bacterial products that can be harnessed for biological advantage (Gross, Johnson, and Lafferty 1956, Johnson, Anker, and Meleney 1945). The combinatory effects of zinc salts with the antimicrobial properties of a bacterial antimicrobial peptide demonstrate the cooperative potential for microbiota and zinc

metals biologically. The effects of zinc directly on *Bacillus subtilis* and various bacterial taxa have not evaluated small sized <2nm non-oxidized zinc nanoparticles, like those found in human and animal blood (Viswaprakash et al. 2009, Viswaprakash et al. 2006). This study will asses a broad spectrum of bacteria co-cultured with four concentrations of small sized <2nm non-oxidized zinc nanoparticles and a selection of seven pathogenic methicillin-resistant *Staphylococcus aureus* (MRSA) strains in contrast to *Bacillus subtilis*.

6.3 Materials and Methods

6.3.1 Test-cultures

The test-cultures used in this experiment were obtained from the stock culture collection used in previous work at Auburn University College of Veterinary Medicine (Auburn, AL). Maintenance of the stock culture collection is at a standard -20ºC in an NZY supplement medium with 25% v/v glycerol.

6.3.2 Growth Assays

A 1% inoculum from bacteria grown overnight in NZY at 37ºC was sub-cultured in NZY for 2 hours at 37ºC and 100 µl bacteria suspension was dispensed in 96-well plate according to a scheme. NZY blank and bacteria with distilled water mid-log phase were used as controls. Plate incubation for 24-hours and spectrophotometric reading at 595 nm conducted. Bacterial species selected included *Escherichia coli* M-17, *Shigella*

flexneri, *Salmonella typhimurium* 52096, *Staphylococcus aureus* ATCC 12600, MRSA-1, 2, 5, 13, 26, 34 and 45, *Lactobacillus acidophilus*, *Bacillus subtilis* BSB3, *Bacillus subtilis* BS, and *Bacillus licheniformis* BL. Performed in duplicates and triplicates. Using one-way ANOVA for analysis with Fisher's test at a significance of $p<0.05$.

6.3.3 Dark Field Microscopy

Morphological characterization of the cultures was done with a high-resolution CitoViva microscope.

6.3.4 Statistics

Software used for analysis include Microsoft Office ® Office Word 2015, Microsoft ® Office Excel 2015, 2010, and spectrometric analysis software KC4™ ver. 3.1. Data averaging, ANOVA, t-test, and graph plotting were carried out using Microcal ™ Origin ® ver. 9.2 (Northampton, MA).

6.4 Results

Total zinc concentration determined for the stock sample was measured at 0.765 mg/L (0.765 ng/µl). Sample sizes represent total zinc at 3.83 ng, 7.65 ng, 15.3 ng, 23 ng at 5, 10, 20, and 30 µl respectively. The total volume of dilution at 30 µl resulted in concentrations of 0.1276 ng/µl, 0.225 ng/µl, 0.51 ng/µl, and 0.765 ng/µl at 5, 10, 20, and 30 µl respectively.

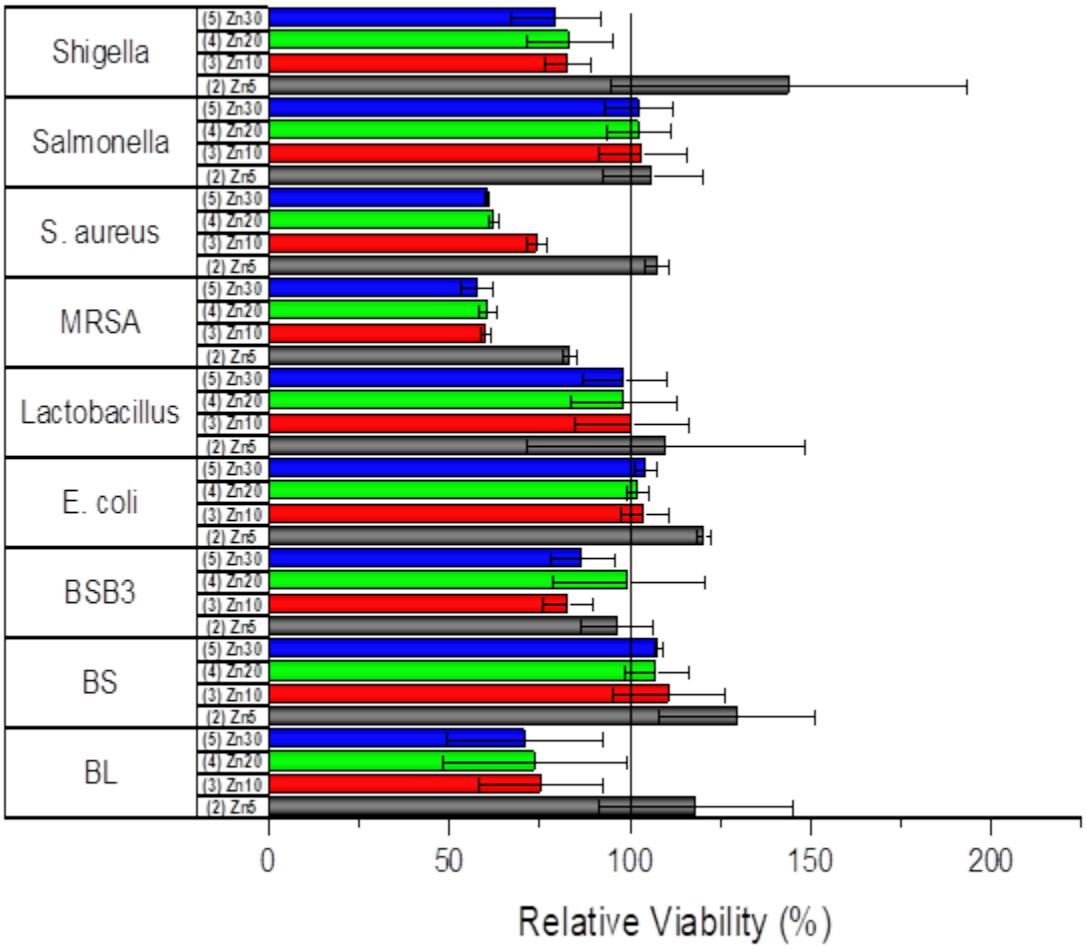

Figure 6.1 Relative viability of different bacterial taxa. Results are shown as a mean and standard deviation relative to control growth (100%). Data representative of 24-hour spectrophotometric reading at optical density 595 nm. Bacterial species selected included *Escherichia coli* M-17, *Shigella flexneri, Salmonella typhimurium* 52096, *Staphylococcus aureus* ATCC 12600, MRSA-1, 2, 5, 13, 26, 34 and 45, *Lactobacillus acidophilus, Bacillus subtilis* BSB3, *Bacillus subtilis* BS, and *Bacillus licheniformis* BL.

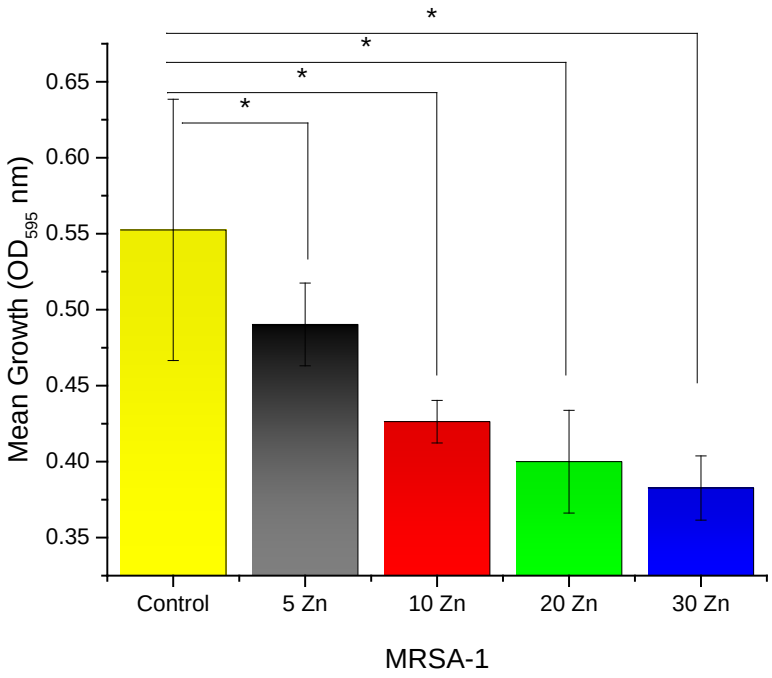

Figure 6.2 Viability of MRSA-1 at different concentration of Zn nanoparticles. Statistical significance of reduced bacterial viability with the addition of zinc nanoparticles from total zinc concentrations of 0.1276 ng/µl, 0.225 ng/µl, 0.51 ng/µl, and 0.765 ng/µl at 5, 10, 20, and 30 µl respectively.

($p<0.05$).

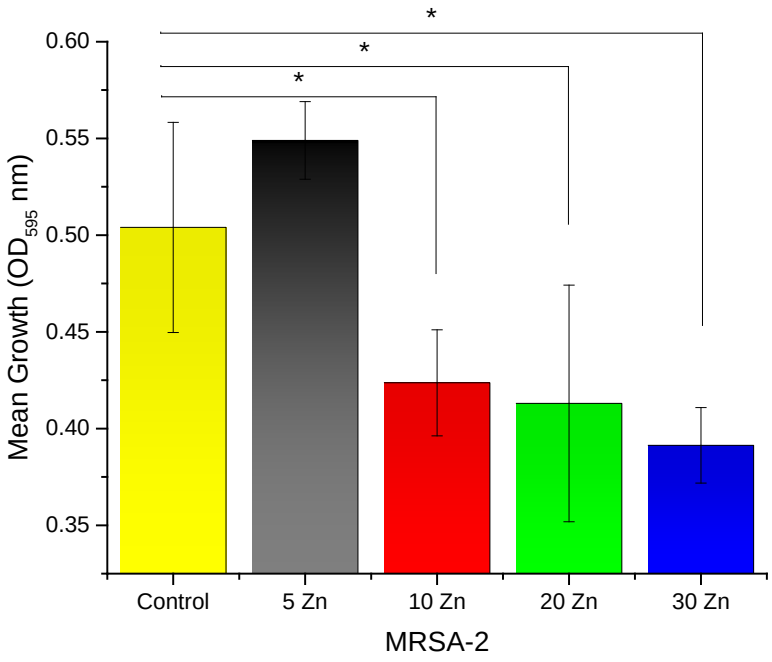

Figure 6.3 Viability of MRSA-2 at different concentration of Zn nanoparticles. Statistical significance of reduced bacterial viability with the addition of zinc nanoparticles from total zinc concentrations of 0.225 ng/µl, 0.51 ng/µl, and 0.765 ng/µl at 10, 20, and 30 µl respectively ($p<0.05$).

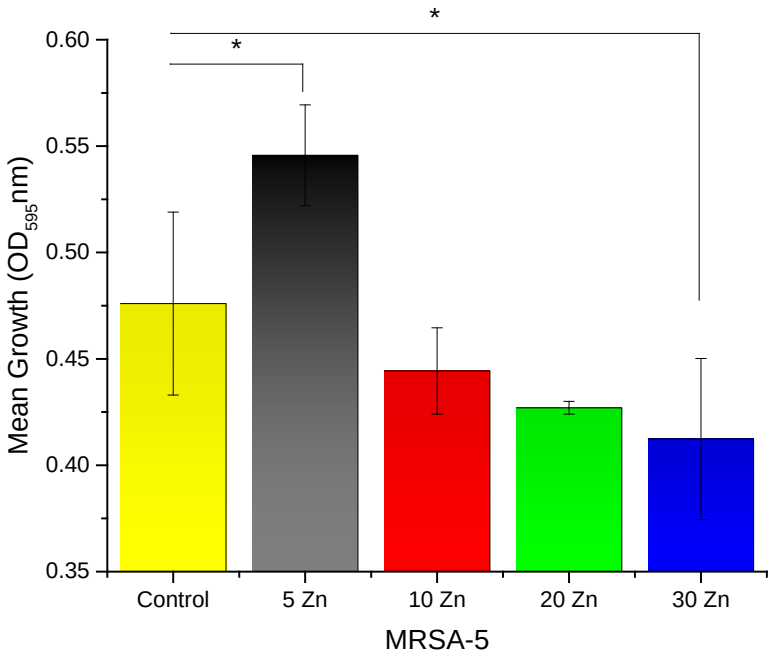

Figure 6.4 Viability of MRSA-5 at different concentration of Zn nanoparticles. Statistical significance of reduced bacterial viability with the addition of zinc nanoparticles from total zinc concentration of 0.765 ng/µl at 30 µl ($p<0.05$). Statistical significance of increased relative bacterial viability with the addition of zinc nanoparticles from total zinc concentrations of 0.1276 ng/µl, at 5 µl ($p<0.05$).

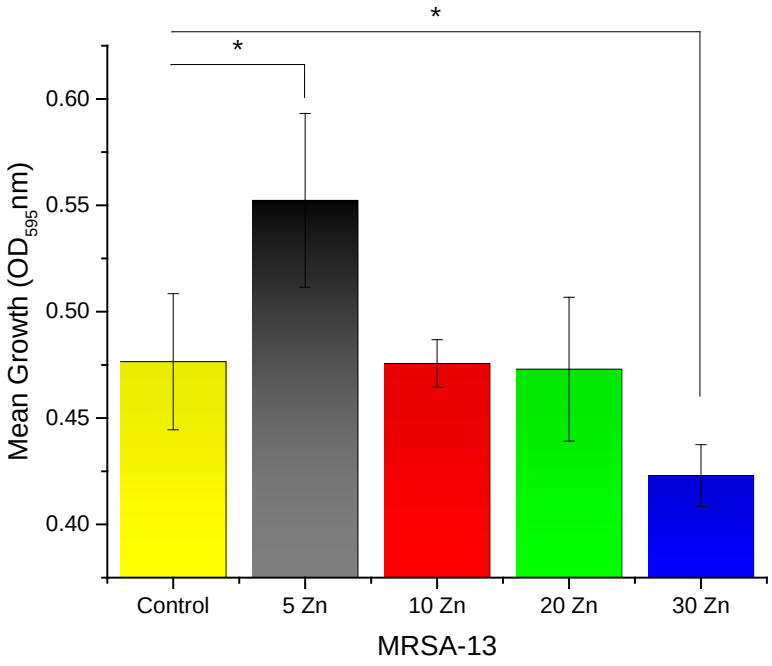

Figure 6.5 Viability of MRSA-13 at different concentration of Zn nanoparticles. Statistical significance of reduced bacterial viability with the addition of zinc nanoparticles from total zinc concentration of 0.765 ng/µl at 30 µl ($p<0.05$). Statistical significance of increased relative bacterial viability with the addition of zinc nanoparticles from total zinc concentrations of 0.1276 ng/µl, at 5 µl ($p<0.05$).

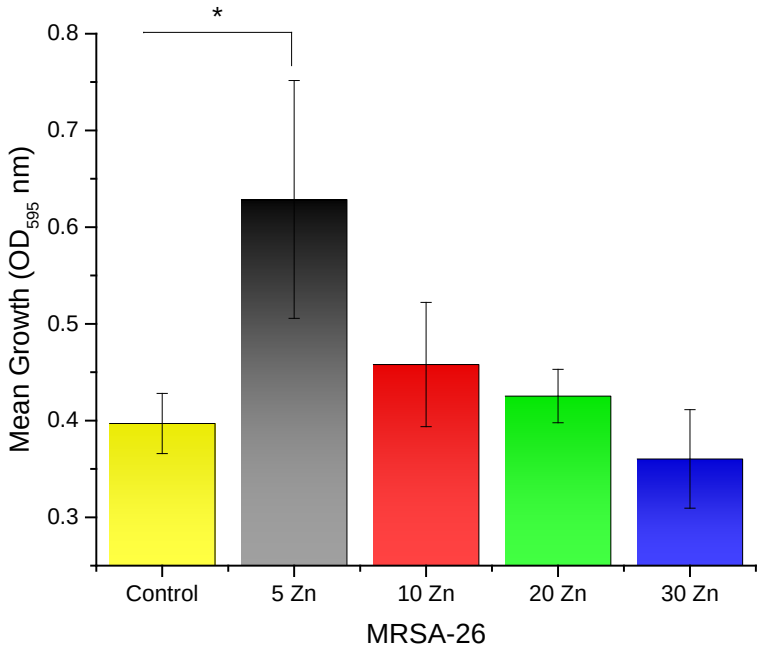

Figure 6.6 Viability of MRSA-26 at different concentration of Zn nanoparticles. Statistical significance of increased bacterial viability with the addition of zinc nanoparticles at a total zinc concentration of 0.1276 ng/µl, at 5 µl ($p<0.05$).

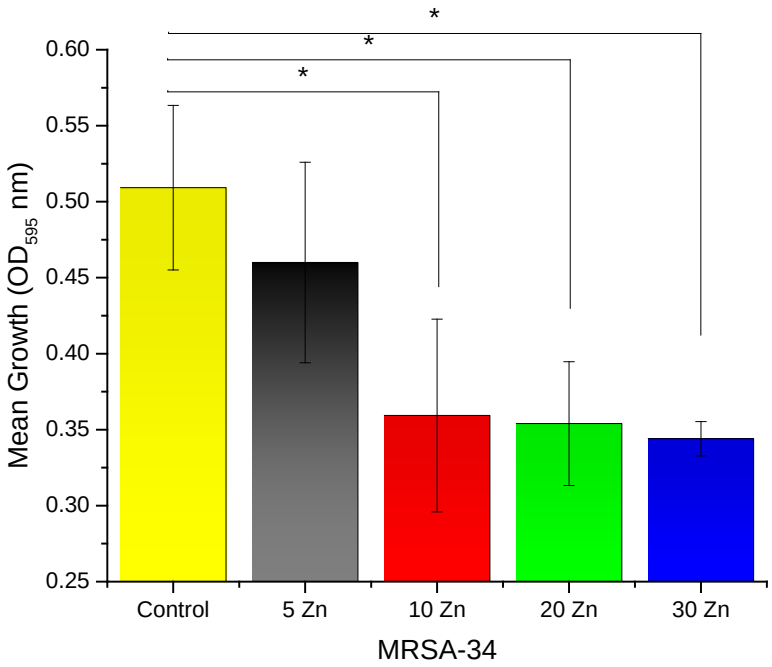

Figure 6.7 Viability of MRSA-34 at different concentration of Zn nanoparticles. Statistical significance of reduced bacterial viability with the addition of zinc nanoparticles from total zinc concentrations of 0.225 ng/µl, 0.51 ng/µl, and 0.765 ng/µl at 10, 20, and 30 µl respectively ($p<0.05$).

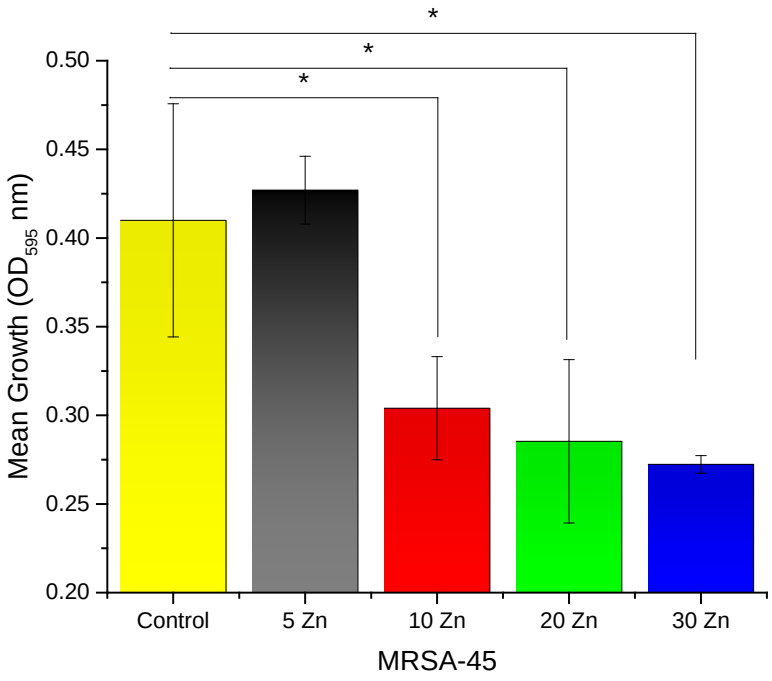

Figure 6.8 Viability of MRSA-45 at different concentration of Zn nanoparticles. Statistical significance of reduced bacterial viability with the addition of zinc nanoparticles from total zinc concentrations of 0.225 ng/µl, 0.51 ng/µl, and 0.765 ng/µl at 10, 20, and 30 µl respectively ($p<0.05$).

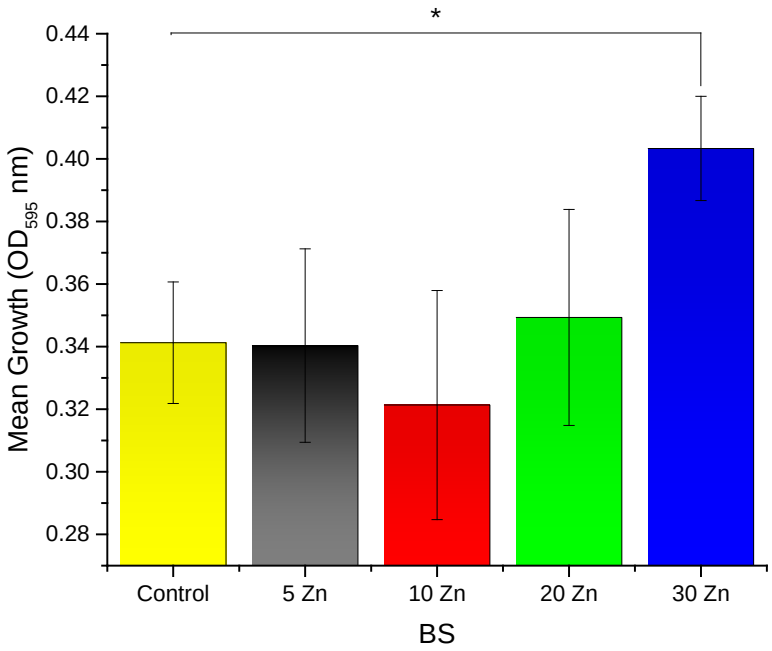

Figure 6.9 Viability of *Bacillus subtilis* at different concentration of Zn nanoparticles. BS: *Bacillus subtilis*. Statistical significance of increased bacterial viability with the addition of zinc nanoparticles from total zinc concentration of 0.765 ng/µl, at 30 µl ($p<0.05$).

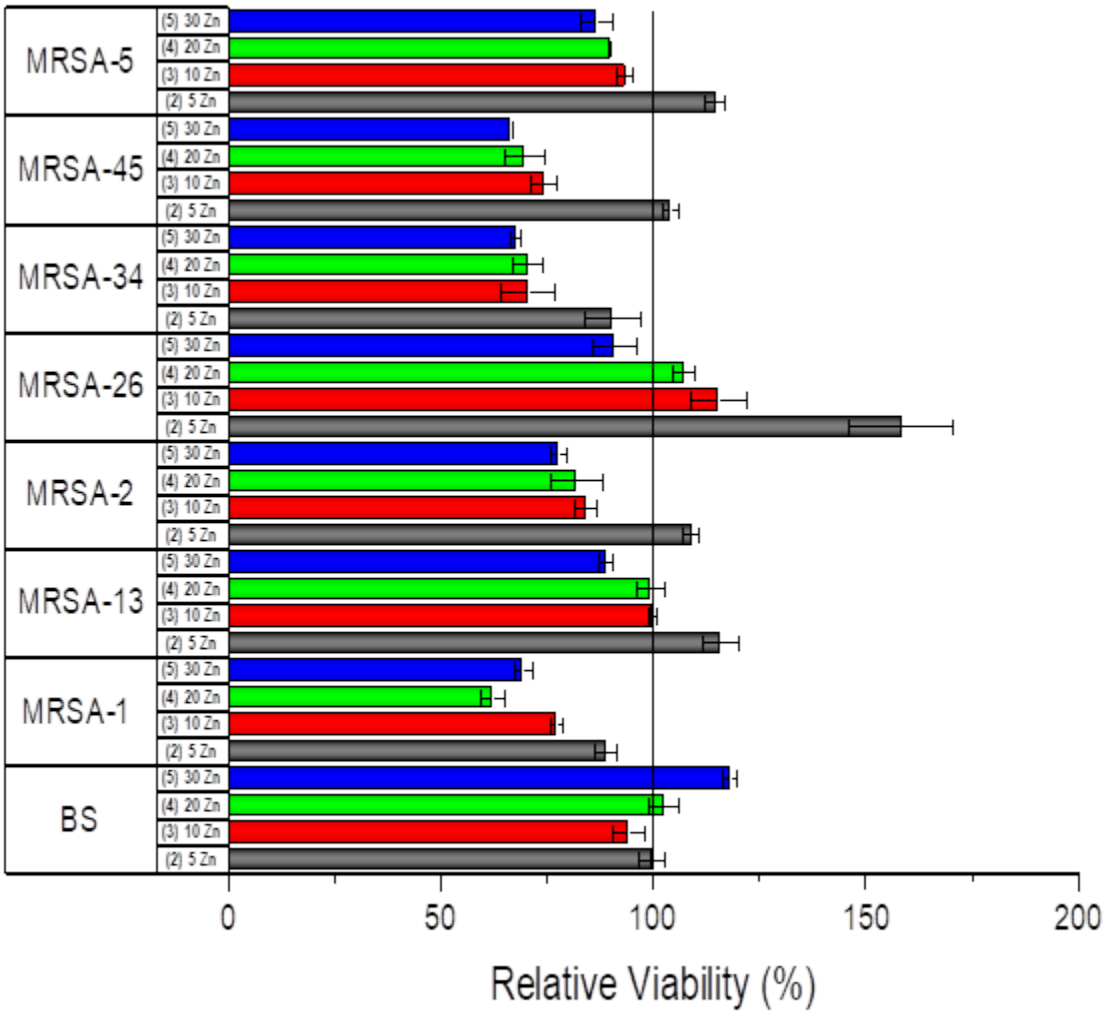

Figure 6.10 Relative viability for MRSA strains and *Bacillus subtilis.* Data shown represents runs in triplicates.

6.5 Discussion

The preliminary screening for across multiple bacterial taxa covered Gram-negative bacteria, Gram-positive bacteria, conditionally pathogenic bacterial species, and primarily commensal bacterial species. The ZnNPs were characterized in previous work (Ch. 3) and were non-oxidized, primarily-elemental, and 1.2 nm in size.

The ZnNPs had no effect on *Salmonella typhimurium* 52096, at the lowest concentration *Shigella flexneri* growth was stimulated and the higher concentrations inhibited 17-32 % of *Shigella flexneri* cells. ZnNPs at all concentrations inhibited 17-43% of MRSA cells in the screening evaluation, though at the lowest concentration stimulated the growth of *Staphylococcus aureus* ATCC 12600. While ZnNPs at higher concentrations inhibited *Staphylococcus aureus* ATCC 12600 26-40%. ZnNPs stimulated the growth of *Escherichia coli* M-17 and *Lactobacillus acidophilus*. ZnNPs stimulate the growth of *Bacillus subtilis* and at lower concentrations also stimulate the growth of *Bacillus licheniformis.* At higher concentrations, ZnNPs inhibit 25-29% of *Bacillus licheniformis* cells.

Bacteria	Phyla	Family	Wall	Primary
Escherichia coli	Proteobacteria	Enterobacteriaceae	G-	Non-pathogenic
Shigella flexneri	Proteobacteria	Enterobacteriaceae	G-	Pathogenic
Salmonella typhimurium	Proteobacteria	Enterobacteriaceae	G-	Pathogenic
Staphylococcus aureus	Firmicutes	Staphylococcacae	G+	Conditionally Pathogenic
Lactobacillus acidophilus	Firmicutes	Lactobacillacae	G+	Non-pathogenic
Bacillus subtilis	Firmicutes	Bacillacae	G+	Non-pathogenic
Bacillus licheniformis	Firmicutes	Bacillacae	G+	Non-pathogenic

Table 6.1 Bacterial species used in the study. Gram-positive cell wall (G+) and Gram-negative cell wall (G-).

These findings are not correlated to bacterial cell wall structure, as there are differential effects between Gram-positive bacteria and no general suppression or enhancement attributable to a cellular wall component.

Results included an observed trend that ZnNPs were generally MRSA suppressive in a concentration-dependent manner, with a broad in total 35% maximum reduction in viability ($p<0.05$). Individual strains demonstrated varying levels of susceptibility to ZnNP induced growth retardation, though a reverse concentration-dependent effect was found in *B. subtilis* as the higher concentration appeared to enhance bacterial growth ($p<0.05$).

A significant difference was found between the means of *B. subtilis* and MRSA strains, with the exception of MRSA-45 ($p<0.05$). Irrespective of bacterial taxa, concentrations of zinc nanoparticles at 0.1276 ng/µl, at 5 µl, displayed an overall increase or no effect on relative viability across taxa. The 0.225 ng/µl, 0.51 ng/µl, and 0.765 ng/µl at 10, 20, and 30 µl respectively, displayed an overall decrease in relative viability across taxa with the considerable exception of *B. subtilis*.

All MRSA strains showed reduced viability. Our results for MRSA-1 were significant in each concentration from 11.2% to 30.7% in reduced relative bacterial viability. Our results show a maximum reduction in viability with MRSA-2 at 22.3%, MRSA-5 at 13.3%, MRSA-13 at 11.2, MRSA-34 at 32.4%, and MRSA-45 at 33.5%. MRSA-26 displayed a maximum reduction in viability at 9.23%, but not achieving statistical significance possibly attributable to a higher SD. In contrast, we found that *B.subtilis* had a significant maximum enhancement in relative viability at 18.19 %.

Suppression of growth in all bacterial isolates of MRSA at 0.765 ng/µl (30µl) with significance reached in 6 out of 7 strains evaluated. However, significant enhancement in growth was detected at the same concentration of ZnNPs in *B. subtilis*.

Multiple strains, MRSA-5, MRSA-13, and MRSA-26, displayed growth enhancement at the lower concentration and reversal effect at higher concentrations.

The general trend of concentration-dependent bacterial growth enhancement is seen primarily in *Bacillus subtilis* at an approximate 18% maximum increase in viability. A general concentration-dependent suppressive trend is seen across MRSA strains demonstrating an approximate 33.5% peak maximum reduction in viability (MRSA-45) ($p<0.05$).

Table 6.2 compares multiple studies of the antimicrobial effects of zinc as zinc oxide nanoparticles and non-oxidized zinc nanoparticles in varying sizes and concentrations. In work by Singaraveian et al. 2017 they report evaluating the antimicrobial action of zinc nanoparticles that were not oxidized and their size reported as, "in nanoscale regime" at concentrations of 50, 80, and 120 µg/ml. The study found a concentration-dependent response with rising inhibition at elevated concentrations with *S. aureus*, *E. coli*, and *Pseudomonas aeruginosa* but no effect on *Enterococcus faecalis* (R Singaravelan 2017). This study attributes the effects to their measured negative zeta potential of -11 mV (R Singaravelan 2017).

Zinc	Size	Zeta	Conc. Conversions	Bacteria	Result	Dep.	Reference
ZnNP	"Nano-Scale"	-11mV	50-180ng/µl	*E. coli*	Inhibition	Conc.	(R Singaravelan 2017)
				S. aureus	Inhibition		
				E. faecalis	NSE		
				P. aeruginosa	Inhibition		
ZnO	3nm		19.5ng/µl	*E. coli*	NSE	Conc.	(Emami-Karvani and Chehrazi 2011)
			19.5ng/µl	*S. aureus*	NSE		
			1,000ng/µl	*E. coli*	bacteriostatic		
			500ng/µl	*S. aureus*	bacteriostatic		
			10,000 ng/µl	*E. coli*	bacteriostatic		
			10,000 ng/µl	*S. aureus*	bactericidal		
ZnO	35-80nm		5-100ppm	*B. subtilis*	bacteriostatic		(Hsueh et al. 2015)
ZnO	12nm		6mM	*S. aureus*	<10% viability	Size	(Raghupathi, Koodali, and Manna 2011)
	25nm		6mM	*S. aureus*	~40% viability		
	88nm		6mM	*S. aureus*	~60% viability		
	212nm		6mM	*S. aureus*	~80% viability		
ZnO	8nm		1mM	*S. aureus*	~5% viability	Size	(Jones et al. 2008)
			5mM	*B. subtilis*	~5% viability		
	12nm		3mM	*E. coli*	~0% viability		
ZnNP	1.2nm	-42mV	0.1276ng/µl	MRSA	NSE to Enhancement	Conc.	Current Study
			0.225ng/µl	MRSA	Inhibition		
			0.51ng/µl	MRSA	Inhibition		
			0.765ng/µl	MRSA	Inhibition		
			0.1276ng/µl	*B. subtilis*	NSE	Conc.	
			0.225ng/µl	*B. subtilis*	NSE		
			0.51ng/µl	*B. subtilis*	NSE		
			0.765ng/µl	*B. subtilis*	Enhancement		

Table 6.2 Zinc and Zinc Oxide nanoparticle effects on multiple bacterial taxa. Zeta- zeta potential for the associated zinc or zinc oxide. Conc. Conversions- the concentrations extracted from published data and converted. NSE- no significant effect. Dep.- dependency concentration (Conc) versus size dependency (Size).

Work by Raghupathi et al. demonstrated a size-dependent effect of zinc oxide nanoparticles. Showing an inverse relationship as the inhibition of bacterial growth in *S.*

aureus was increased with decreasing nanoparticle size (Raghupathi, Koodali, and Manna 2011). Furthermore, their group evaluated the contribution of Zn^{2+} toward the growth inhibition by comparing the Zn^{2+} concentration released in solution of ZnO nanoparticle colloidal suspension. They determined that the release of free Zn^{2+} ions in solution were low enough not to be the main factor contributing to the ZnO nanoparticle antimicrobial activity (Raghupathi, Koodali, and Manna 2011).

The size-dependent effects of zinc oxide nanoparticles are in line with the general higher activity in comparison to their parent metals primarily attributed to a higher surface area. This is supported by the physiochemical attributes of zinc nanoparticles used in this study high surface-to-volume ratio and higher surface atoms at 80%, which implies a high chemical reactivity. There is a lack of literature evaluating zinc nanoparticles less than 3nm and their effects on the microenvironment of the microbiota or microbes in general, even more so a lack of evaluating non-oxidized zinc nanoparticles.

Most testing methods do not differentiate zinc into its sub-forms including zinc nanoparticles versus ionic zinc. The zinc estimates in nasal mucus are 0.014ng/µl, in comparison to the effective concentration in this study, there is not an adequate concentration for significant antimicrobial effect. However, these estimates of zinc concentrations do not differentiate zinc from nanoparticles and location of mucus sampling is not specific to the olfactory mucosa where concentrations are estimated to be higher. The results of our study showed that non-oxidized zinc nanoparticles influence the growth of multiple bacterial taxa and could be influencing the microbiota at the level of the olfactory epithelium. This alludes to a need for further evaluation into this heavy

metal sub-set and their potential biological importance.

6.6 Conclusion

Our results display a differential pattern of effects to reported Zn antimicrobial activity with ionic Zn^{2+}, zinc oxide (ZnO) and ZnO nanoparticles. The general trend displayed suppressive activity against MRSA and general *B. subtilis* enhancement in a concentration-dependent manner.

This differential effect is significant in consideration of general suppression in pathogenic bacterial strains with multi-drug resistance, while a simultaneous sparing of inhibition on commensal bacterial considered primarily beneficial.

The results are consistent with differential effects of ZnO-NPs, Zn^{2+}, and ZnNPs on epithelial tissue of the olfactory system. The data support a potential role of ZnNPs in the perireceptor regulation of microbial populations in the olfactory system.

Further evaluation is needed to determine the mechanism of action for small non-oxidized zinc nanoparticle growth effects on multiple bacterial taxa and in relative microbiota subsets.

Chapter 7.0 Conclusions

The physio-chemical characterization of zinc nanoparticles demonstrated a crystalline structure of zinc metal nanoparticles on transmission electron microscopy (TEM), an average size of 1.2 nm on atomic force microscopy (AFM), with 94% non-oxidized on X-ray Photoelectron Spectroscopy (XPS), a zeta potential of -48 mV, an 80% surface volume, and physiological capability of olfactory enhancement.

The physio-chemical characterization of laboratory oxidized zinc nanoparticles established from a subset of the average size of 1.2 nm zinc nanoparticles demonstrated an increased level of oxidation at 12% oxidized atoms with XPS, no significant change in surface atoms, and the loss of the physiological capability of olfaction enhancement.

The standard 15 nm zinc oxide nanoparticles and 70 nm zinc oxide nanoparticles exhibited an inverse size to surface atom ratio, with lower surface atoms corresponding to higher nanoparticle diameter, and a similar loss of physiological capability of olfactory enhancement with small oxidized zinc nanoparticles.

The overall features of non-oxidized, 1.2 nm zinc nanoparticles exhibit a good level of stability and high chemical reactivity. This in combination with the biologically relevant zinc nanoparticles found in human and animal blood supports a role within the initial events of olfaction, possibly serving as an electron donor in the vibrational theory of olfaction.

When the zinc nanoparticles were covered with thin layers of polyethylene glycol of molecular weight 400 g/mol and 1000 g/mol (ZnPEG400 and ZnPEG1000), the PEGylation preserved the nanoparticles from oxidation while conserving their crystalline structure.

PEGylation maintains the ability of the zinc nanoparticles to enhance the olfactory response to the odorant while the polyethylene glycol molecules alone inhibits the olfactory response.

The ZnPEG400 nanoparticles continued to manifest the amplified enhancement of odorant response even after 300-days storage at 278 K (5 ^{o}C), while ZnPEG1000 nanoparticles produced an inhibition under the same conditions.

ZnPEG400 withstood two-day storage at 303 K (30 ^{o}C) and 323 K (50 ^{o}C) and evoked the adequate enhancement of olfaction, but ZnPEG1000 showed a reduced enhancement at the same conditions.

The PEG400 appeared to be far better for the preservation of properties of zinc nanoparticles for long-term storage and elevated temperatures. The enhancement and inhibition of olfaction by zinc nanoparticles preserved by PEGylation were consistent with Turin's model of olfaction.

The novelty of this work is that biocompatible and safe PEG400 coat of zinc nanoparticles provides both preservation of particles and amplification of olfactory enhancement.

The nanoparticle filtrate from the OE produced the highest significant enhancement of olfactory sensory neuron response to odorant. The nanoparticle filtrate from the RE also produced a significant enhancement in olfactory sensory neuron response to odorant to a lesser level than OE which is consistent with a biological function of significance within the OE for odorant receptor activation.

The difficulty in differentiating zinc ions to zinc nanoparticles in a biologically homogenized sample with traditional techniques is tremendous. However, the electrophysiological results are comparable to laboratory produced zinc nanoparticles, the consecutive filtering to a fine level of nanoscale filtrate, and the background of selectivity for olfaction enhancement to small (1.2 nm), non-oxidized, zinc primarily metal state nanoparticles, suggests a zinc nanoparticle-like molecule endogenously present within the olfactory epithelium.

The results in the microenvironmental influence of zinc nanoparticles display a differential pattern of effects in the multiple bacterial taxa evaluated compared to reported Zn antimicrobial activity with ionic Zn^{2+}, zinc oxide (ZnO) and ZnO nanoparticles. Our results display a differential pattern of effects to reported Zn antimicrobial activity with ionic Zn^{2+}, zinc oxide (ZnO) and ZnO nanoparticles. The general trend displayed suppressive activity against MRSA and general *B. subtilis* enhancement in a concentration-dependent manner.

This differential effect is significant in consideration of general suppression in pathogenic bacterial strains with multi-drug resistance, while a simultaneous sparing of inhibition on commensal bacterial considered primarily beneficial.

The results are consistent with differential effects of ZnO-NPs, Zn^{2+}, and ZnNPs on epithelial tissue of the olfactory system. The data support a potential role of ZnNPs in the perireceptor regulation of microbial populations in the olfactory system.

7.1 Future Work

Future olfactory experiments with the intranasal delivery of protected zinc

nanoparticles to a transient chemically acquired anosmic rodent model and a cognitively impaired Alzheimer's rodent model will test the pre-clinical validity of smell enhancement described in this work.

Further characterization of the isolated nanoparticle filtrate from the OE and RE are needed to confirm the presence of zinc nanoparticles. Transmission electron microscopy and energy-dispersive X-ray spectroscopy are needed.

Olfactory microbiotal community composition determination is needed. Further evaluation of the *in vivo* effects that zinc nanoparticles have on the microbiota will provide a greater understanding of their microenvironmental influence.

References

Abramson, A. L., R. F. D'Amato, H. D. Isenberg, and W. H. Pryor. 1976. "Microbiology of the canine nasal cavities." *Ann Otol Rhinol Laryngol* 85 (3 pt 1):394-7. doi: 10.1177/000348947608500312.

Abramson, A. L., H. D. Isenberg, and L. M. McDermott. 1980. "Microbiology of the canine nasal cavities." *Rhinology* 18 (3):143-50.

Agarwal, R. P., and R. I. Henkin. 1982. "Zinc and copper in human cerebrospinal fluid." *Biological Trace Element Research* 4 (2):117-124. doi: 10.1007/bf02783252.

Aiken, J. D., and R. G. Finke. 1999a. "A review of modern transition-metal nanoclusters: their synthesis, characterization, and applications in catalysis." *Journal of Molecular Catalysis a-Chemical* 145 (1-2):1-44.

Aiken, John D., and Richard G. Finke. 1999b. "A review of modern transition-metal nanoclusters: their synthesis, characterization, and applications in catalysis." *Journal of Molecular Catalysis A: Chemical* 145 (1):1-44. doi: https://doi.org/10.1016/S1381-1169(99)00098-9.

Alioto, T. S., and J. Ngai. 2005. "The odorant receptor repertoire of teleost fish." *BMC Genomics* 6:173. doi: 10.1186/1471-2164-6-173.

Alivisatos, A. P. 1996. "Semiconductor Clusters, Nanocrystals, and Quantum Dots." *Science* 271 (5251):933-937. doi: 10.1126/science.271.5251.933.

Amoore, J. E., G. Palmieri, and E. Wanke. 1967. "Molecular Shape and Odour - Pattern Analysis by Papa." *Nature* 216 (5120):1084-&. doi: DOI 10.1038/2161084a0.

Anand, Avnika Singh, Dipti N. Prasad, Shashi Bala Singh, and Ekta Kohli. 2017. "Chronic exposure of zinc oxide nanoparticles causes deviant phenotype in Drosophila melanogaster." *Journal of Hazardous Materials* 327:180-186. doi: https://doi.org/10.1016/j.jhazmat.2016.12.040.

Anzellotti, A. I., and N. P. Farrell. 2008. "Zinc metalloproteins as medicinal targets." *Chem Soc Rev* 37 (8):1629-51. doi: 10.1039/b617121b.

Aronsson, F., B. Robertson, H. G. Ljunggren, and K. Kristensson. 2003. "Invasion and persistence of the neuroadapted influenza virus A/WSN/33 in the mouse olfactory system." *Viral Immunol* 16 (3):415-23. doi: 10.1089/088282403322396208.

Arrieta, M. C., and B. B. Finlay. 2012. "The commensal microbiota drives immune homeostasis." *Front Immunol* 3:33. doi: 10.3389/fimmu.2012.00033.

Arus, D., A. Dancs, N. V. Nagy, and T. Gajda. 2013. "A comparative study on the possible zinc binding sites of the human ZnT3 zinc transporter protein." *Dalton Transactions* 42 (33):12031-12040. doi: 10.1039/c3dt50754h.

Askim, J. R., M. Mahmoudi, and K. S. Suslick. 2013. "Optical sensor arrays for chemical sensing: the optoelectronic nose." *Chem Soc Rev* 42 (22):8649-82. doi: 10.1039/c3cs60179j.

Association, Alzheimer's. 2017. "2017 Alzheimer's disease facts and figures." *Alzheimer's & dementia : the journal of the Alzheimer's Association.* (13:325-73.).

Bahuleyan, B., and S. Singh. 2012. "Olfactory memory impairment in neurodegenerative diseases." *J Clin Diagn Res* 6 (8):1437-41. doi: 10.7860/JCDR/2012/3408.2382.

Banks, F. R. 1941. "The measurement of self-diffusion in zinc." *Physical Review* 59 (4):376-381. doi: DOI 10.1103/PhysRev.59.376.

Barnett, E. M., M. D. Cassell, and S. Perlman. 1993. "Two neurotropic viruses, herpes simplex virus type 1 and mouse hepatitis virus, spread along different neural pathways from the main olfactory bulb." *Neuroscience* 57 (4):1007-25.

Barreiro, Amelia, Herre S. J. van der Zant, and Lieven M. K. Vandersypen. 2012. "Quantum Dots at Room Temperature Carved out from Few-Layer Graphene." *Nano Letters* 12 (12):6096-6100. doi: 10.1021/nl3036977.

Benton, R., S. Sachse, S. Michnick, and L. Vosshall. 2006. "Atypical membrane topology and heteromeric function of Drosophila odorant receptors in vivo." *Chemical Senses* 31 (5):A5-A5.

Berkowicz, D. A., P. Q. Trombley, and G. M. Shepherd. 1994. "Evidence for glutamate as the olfactory receptor cell neurotransmitter." *J Neurophysiol* 71 (6):2557-61. doi: 10.1152/jn.1994.71.6.2557.

Bilberg, K., H. Malte, T. Wang, and E. Baatrup. 2010. "Silver nanoparticles and silver nitrate cause respiratory stress in Eurasian perch (Perca fluviatilis)." *Aquat. Toxicol.* 96 (2):159-65. doi: 10.1016/j.aquatox.2009.10.019.

Bilberg, Katrine, Kjell B. Døving, Kristian Beedholm, and Erik Baatrup. 2011. "Silver nanoparticles disrupt olfaction in Crucian carp (Carassius carassius) and Eurasian perch (Perca fluviatilis)." *Aquatic Toxicology* 104 (1–2):145-152. doi: 10.1016/j.aquatox.2011.04.010.

Bittner, E. R., A. Madalan, A. Czader, and G. Roman. 2012. "Quantum origins of molecular recognition and olfaction in Drosophila." *J Chem Phys* 137 (22):22A551. doi: 10.1063/1.4767067.

Black, D., J.J. Ritter, J. E. Bonevich, A. Henins, and J.P. Cline. 2012. "Nanocrystalline zinc oxide powder for x-ray diffraction metrology." *ADV X RAY ANAL* 56:61-70.

Blakemore, L. J., E. Tomat, S. J. Lippard, and P. Q. Trombley. 2013. "Zinc released from olfactory bulb glomeruli by patterned electrical stimulation of the olfactory nerve." *Metallomics* 5 (3):208-213. doi: 10.1039/c3mt20158a.

Block, E., V. S. Batista, H. Matsunami, H. Zhuang, and L. Ahmed. 2017. "The role of metals in mammalian olfaction of low molecular weight organosulfur compounds." *Nat Prod Rep* 34 (5):529-557. doi: 10.1039/c7np00016b.

Block, E., S. Jang, H. Matsunami, S. Sekharan, B. Dethier, M. Z. Ertem, S. Gundala, Y. Pan, S. Li, Z. Li, S. N. Lodge, M. Ozbil, H. Jiang, S. F. Penalba, V. S. Batista, and H. Zhuang. 2015. "Implausibility of the vibrational theory of olfaction." *Proc Natl Acad Sci U S A* 112 (21):E2766-74. doi: 10.1073/pnas.1503054112.

Blumberg, R., and F. Powrie. 2012. "Microbiota, disease, and back to health: a metastable journey." *Sci Transl Med* 4 (137):137rv7. doi: 10.1126/scitranslmed.3004184.

Boekhoff, I., and H. Breer. 1992. "Termination of second messenger signaling in olfaction." *Proceedings of the National Academy of Sciences of the United States of America* 89 (2):471-474.

Borisy, FF, GV Ronnett, AM Cunningham, D Juilfs, J Beavo, and SH Snyder. 1992. "Calcium/calmodulin-activated phosphodiesterase expressed in olfactory receptor neurons." *The Journal of Neuroscience* 12 (3):915-923.

Braun, T., P. Voland, L. Kunz, C. Prinz, and M. Gratzl. 2007. "Enterochromaffin cells of the human gut: sensors for spices and odorants." *Gastroenterology* 132 (5):1890-901. doi: 10.1053/j.gastro.2007.02.036.

Breer, H. 2003a. "Olfactory receptors: molecular basis for recognition and discrimination of odors." *Analytical and Bioanalytical Chemistry* 377 (3):427-433.

Breer, H. 2003b. "Sense of smell: recognition and transduction of olfactory signals." *Biochemical Society Transactions* 31:113-116.

Briand, L., C. Eloit, C. Nespoulous, V. Bezirard, J. C. Huet, C. Henry, F. Blon, D. Trotier, and J. C. Pernollet. 2002. "Evidence of an odorant-binding protein in the human olfactory mucus: location, structural characterization, and odorant-binding properties." *Biochemistry* 41 (23):7241-52.

Brookes, J. C., A. P. Horsfield, and A. M. Stoneham. 2009. "Odour character differences for enantiomers correlate with molecular flexibility." *J R Soc Interface* 6 (30):75-86. doi: 10.1098/rsif.2008.0165.

Brookes, J. C., A. P. Horsfield, and A. M. Stoneham. 2012a. "The Swipe Card Model of Odorant Recognition." *Sensors* 12 (11):15709-15749. doi: 10.3390/s121115709.

Brookes, J. C., A. P. Horsfield, and A. M. Stoneham. 2012b. "The swipe card model of odorant recognition." *Sensors (Basel)* 12 (11):15709-49. doi: 10.3390/s121115709.

Brunjes, P. C., K. R. Illig, and E. A. Meyer. 2005. "A field guide to the anterior olfactory nucleus (cortex)." *Brain Res Brain Res Rev* 50 (2):305-35. doi: 10.1016/j.brainresrev.2005.08.005.

Brunjes, P. C., R. B. Kay, and J. P. Arrivillaga. 2011. "The mouse olfactory peduncle." *J Comp Neurol* 519 (14):2870-86. doi: 10.1002/cne.22662.

Brust, Mathias, and Christopher J. Kiely. 2002. "Some recent advances in nanostructure preparation from gold and silver particles: a short topical review." *Colloids and*

Surfaces A: Physicochemical and Engineering Aspects 202 (2–3):175-186. doi: http://dx.doi.org/10.1016/S0927-7757(01)01087-1.

Buck, L., and R. Axel. 1991. "A Novel Multigene Family May Encode Odorant Receptors - a Molecular-Basis for Odor Recognition." *Cell* 65 (1):175-187.

Burd, G. D. 1993. "Morphological-study of the effects of intranasal zinc-sulfate irrigation on the mouse olfactory epithelium and olfactory-bulb." *Microsc Res Tech* 24 (3):195-213. doi: 10.1002/jemt.1070240302.

Bush, Cristina F. 2008. "Olfactory Receptor Dimerization." Ph.D., Graduate Division of Biological and Biomedical Sciences, Emory University.

Butterworth, M. D., L. Illum, and S. S. Davis. 2001. "Preparation of ultrafine silica- and PEG-coated magnetite particles." *Colloids and Surfaces A: Physicochemical and Engineering Aspects* 179 (1):93-102. doi: http://dx.doi.org/10.1016/S0927-7757(00)00633-6.

Canzoniero, L. M., S. L. Sensi, and D. W. Choi. 1997. "Measurement of intracellular free zinc in living neurons." *Neurobiol Dis* 4 (3-4):275-9. doi: 10.1006/nbdi.1997.0160.

Castiglioni, A. J., N. N. Remis, E. N. Flores, and J. Garcia-Anoveros. 2011. "Expression and vesicular localization of mouse Trpml3 in stria vascularis, hair cells, and vomeronasal and olfactory receptor neurons." *J Comp Neurol* 519 (6):1095-114. doi: 10.1002/cne.22554.

Chen, Yong Jun, Bo Chi, Hong Zhou Zhang, Hua Chen, and Ying Chen. 2007. "Controlled growth of zinc nanowires." *Materials Letters* 61 (1):144-147. doi: http://dx.doi.org/10.1016/j.matlet.2006.04.044.

Cline, J. P., M. Leoni, D. Black, A. Henins, J. E. Bonevich, P. S. Whitfield, and P. Scardi. 2013. "Crystalline domain size and faulting in the new NIST SRM 1979 zinc oxide." *Powd Diffr* 28 (SupplementS2):S22-S32. doi: doi:10.1017/S0885715613001188.

Collins, S. M., M. Surette, and P. Bercik. 2012. "The interplay between the intestinal microbiota and the brain." *Nat Rev Microbiol* 10 (11):735-42. doi: 10.1038/nrmicro2876.

Colvin, R. A., W. R. Holmes, C. P. Fontaine, and W. Maret. 2010. "Cytosolic zinc buffering and muffling: their role in intracellular zinc homeostasis." *Metallomics* 2 (5):306-17. doi: 10.1039/b926662c.

Cook, M. T., G. Tzortzis, D. Charalampopoulos, and V. V. Khutoryanskiy. 2012. "Microencapsulation of probiotics for gastrointestinal delivery." *J Control Release* 162 (1):56-67. doi: 10.1016/j.jconrel.2012.06.003.

Cope, J. O. 1961. "Kinetics of the oxidation of molten zinc." *Transactions of the Faraday Society* 57 (0):493-503. doi: 10.1039/TF9615700493.

Costanzo, R. M. 1991. "Regeneration of olfactory receptor cells." *Ciba Found Symp* 160:233-42; discussion 243-8.

Coughlan, A., D. Boyd, C. W. Douglas, and M. R. Towler. 2008. "Antibacterial coatings for medical devices based on glass polyalkenoate cement chemistry." *J Mater Sci Mater Med* 19 (12):3555-60. doi: 10.1007/s10856-008-3519-x.

Couto, A., M. Alenius, and B. J. Dickson. 2005. "Molecular, anatomical, and functional organization of the Drosophila olfactory system." *Curr Biol* 15 (17):1535-47. doi: 10.1016/j.cub.2005.07.034.

Crabtree, R. H. 1978. "Copper(I) - Possible Olfactory Binding-Site." *Journal of Inorganic & Nuclear Chemistry* 40 (7):1453-1453. doi: Doi 10.1016/0022-1902(78)80071-2.

Craven, B. A., T. Neuberger, E. G. Paterson, A. G. Webb, E. M. Josephson, E. E. Morrison, and G. S. Settles. 2007. "Reconstruction and morphometric analysis of the nasal airway of the dog (Canis familiaris) and implications regarding olfactory airflow." *Anat Rec (Hoboken)* 290 (11):1325-40. doi: 10.1002/ar.20592.

Craven, B. A., E. G. Paterson, and G. S. Settles. 2010. "The fluid dynamics of canine olfaction: unique nasal airflow patterns as an explanation of macrosmia." *J R Soc Interface* 7 (47):933-43. doi: 10.1098/rsif.2009.0490.

Cuenya, B. R. 2010. "Synthesis and catalytic properties of metal nanoparticles: Size, shape, support, composition, and oxidation state effects." *Thin Solid Films* 518 (12):3127-3150. doi: 10.1016/j.tsf.2010.01.018.

Daniel, M. C., and D. Astruc. 2004. "Gold nanoparticles: assembly, supramolecular chemistry, quantum-size-related properties, and applications toward biology, catalysis, and nanotechnology." *Chem Rev* 104 (1):293-346. doi: 10.1021/cr030698+ [doi].

Daniels, Yasmine C., William A. MacCrehan, and Vitaly Vodyanoy. 2015. "Characterization of Olfactory-Enhancing Zinc Metal Nanoparticles." IEEE International Conference on Nanotechnology, Rome, Italy, July 27-30.

Day, Jack C. 1978. "New nitrogen bases with severe steric hindrance due to flanking tert-butyl groups. cis-2,6-Di-tert-butylpiperidine. Possible steric blocking of olfaction." *The Journal of Organic Chemistry* 43 (19):3646-3649. doi: 10.1021/jo00413a003.

De la Cruz, O., R. Blekhman, X. Zhang, D. Nicolae, S. Firestein, and Y. Gilad. 2009. "A signature of evolutionary constraint on a subset of ectopically expressed olfactory receptor genes." *Mol Biol Evol* 26 (3):491-4. doi: 10.1093/molbev/msn294.

de Vos, W. M., and E. A. de Vos. 2012. "Role of the intestinal microbiome in health and disease: from correlation to causation." *Nutr Rev* 70 Suppl 1:S45-56. doi: 10.1111/j.1753-4887.2012.00505.x.

Deroubaix, G., and P. Marcus. 1992. "X-RAY PHOTOELECTRON-SPECTROSCOPY ANALYSIS OF COPPER AND ZINC-OXIDES AND SULFIDES." *Surface and Interface Analysis* 18 (1):39-46. doi: 10.1002/sia.740180107.

Dibattista, M., and J. Reisert. 2016. "The Odorant Receptor-Dependent Role of Olfactory Marker Protein in Olfactory Receptor Neurons." *Journal of Neuroscience* 36 (10):2995-3006. doi: 10.1523/Jneurosci.4209-15.2016.

Doneux, Thomas, Linda Yahia Cherif, and Claudine Buess-Herman. 2016. "Controlled Tuning of the Ferri/Ferrocyanide Electron Transfer at Oligo (Ethylene Glycol)-Modified Electrodes." *Electrochimica Acta* 219:412-417. doi: 10.1016/j.electacta.2016.10.005.

Doneux, Thomas, Alexis de Ghellinck, Eleonore Triffaux, Nicolas Brouette, Michele Sferrazza, and Claudine Buess-Herman. 2016. "Electron Transfer Across an Antifouling Mercapto-hepta(ethylene glycol) Self-Assembled Monolayer." *Journal of Physical Chemistry C* 120 (29):15915-15922. doi: 10.1021/acs.jpcc.5b12260.

Doty, RL. 1998. *Textbook of Clinical Neurology*. Edited by Pappert EJ. Goltz CG., *Cranial Nerve I. Olfaction*. Philadelphia: Saunders.

Drimyli, E., A. Gaitanidis, K. Maniati, L. Turin, and E. M. Skoulakis. 2016. "Differential Electrophysiological Responses to Odorant Isotopologues in Drosophilid Antennae." *eNeuro* 3 (3). doi: 10.1523/ENEURO.0152-15.2016.

Duan, Chunhui, Robin E. M. Willems, Jacobus J. van Franeker, Bardo J. Bruijnaers, Martijn M. Wienk, and Rene A. J. Janssen. 2016. "Effect of side chain length on the charge transport, morphology, and photovoltaic performance of conjugated polymers in bulk heterojunction solar cells." *Journal of Materials Chemistry A* 4 (5):1855-1866. doi: 10.1039/C5TA09483F.

Duncan-Lewis, C. A., R. L. Lukman, and R. K. Banks. 2011. "Effects of zinc gluconate and 2 other divalent cationic compounds on olfactory function in mice." *Comp Med* 61 (4):361-5.

Dyson, G.M. 1938. "The Scientific basis of odour." *Chemistry & Industry* 57:647-651.

Emami-Karvani, Z., and P. Chehrazi. 2011. "Antibacterial activity of ZnO nanoparticle on gram-positive and gram-negative bacteria." *African Journal of Microbiology Research* 5 (12):1368-1373.

Emmetsberger, J., M. M. Mirrione, C. Zhou, M. Fernandez-Monreal, M. M. Siddiq, K. M. Ji, and S. E. Tsirka. 2010. "Tissue Plasminogen Activator Alters Intracellular Sequestration of Zinc through Interaction with the Transporter ZIP4." *Journal of Neuroscience* 30 (19):6538-6547. doi: 10.1523/Jneurosci.6250-09.2010.

Erickson, B. E. 2012. "Mapping Nanotech Drugs' Landscape." *Chemical & Engineering News* 90 (36):46-+.

Farmen, E., H. N. Mikkelsen, O. Evensen, J. Einset, L. S. Heier, B. O. Rosseland, B. Salbu, K. E. Tollefsen, and D. H. Oughton. 2012. "Acute and sub-lethal effects in juvenile Atlantic salmon exposed to low mug/L concentrations of Ag nanoparticles." *Aquat Toxicol* 108:78-84. doi: 10.1016/j.aquatox.2011.07.007.

Feng, W., L. Chen, M. Qin, X. Zhou, Q. Zhang, Y. Miao, K. Qiu, Y. Zhang, and C. He. 2015. "Flower-like PEGylated MoS2 nanoflakes for near-infrared photothermal cancer therapy." *Sci Rep* 5:17422. doi: 10.1038/srep17422.

Ferro, Sergio, Maurizio Dal Colle, and Achille De Battisti. 2005. "Chemical surface characterization of electrochemically and thermally oxidized boron-doped diamond film electrodes." *Carbon* 43 (6):1191-1203. doi: http://dx.doi.org/10.1016/j.carbon.2004.12.012.

Firestein, S. 2001. "How the olfactory system makes sense of scents." *Nature* 413 (6852):211-218.

Firestein, S., C. Picco, and A. Menini. 1993. "The Relation between Stimulus and Response in Olfactory Receptor-Cells of the Tiger Salamander." *Journal of Physiology-London* 468:1-10.

Firestein, Stuart , Bruce Darrow, and Shepherd Gordon M. 1991. "Activation of the sensory current in salamander olfactory receptor neurons depends on a G protein-mediated cAMP second messenger system." *Neuron* 6 (5):825-835.

Flexner, Simon, and Paul F. Clark. 1912. "A note on the mode of infection in epidemic poliomyelitis." *Proceedings of the Society for Experimental Biology and Medicine* 10 (1):1-2. doi: 10.3181/00379727-10-1.

Fosmire, G. J. 1990. "Zinc toxicity." *Am J Clin Nutr* 51 (2):225-7.

Fotiadis, Dimitrios, Yan Liang, Slawomir Filipek, David A. Saperstein, Andreas Engel, and Krzysztof Palczewski. 2003a. "Atomic-force microscopy: rhodopsin dimers in native disc membranes." *Nature (London, United Kingdom)* 421 (6919):127-128.

Fotiadis, Dimitrios, Yan Liang, Slawomir Filipek, David A. Saperstein, Andreas Engel, and Krzysztof Palczewski. 2003b. "Is rhodopsin dimeric in native retinal rods? Reply." *Nature (London, United Kingdom)* 426 (6962):31.

Franco, M. I., L. Turin, A. Mershin, and E. M. Skoulakis. 2011. "Molecular vibration-sensing component in Drosophila melanogaster olfaction." *Proc Natl Acad Sci U S A* 108 (9):3797-802. doi: 10.1073/pnas.1012293108.

Francois, A., D. Grebert, M. Rhimi, M. Mariadassou, L. Naudon, S. Rabot, and N. Meunier. 2016. "Olfactory epithelium changes in germfree mice." *Sci Rep* 6:24687. doi: 10.1038/srep24687.

Frederickson, C. J., and G. Danscher. 1990. "Zinc-Containing Neurons in Hippocampus and Related Cns Structures." *Progress in Brain Research* 83:71-84.

Frederickson, C. J., L. J. Giblin, A. Krezel, D. J. McAdoo, R. N. Muelle, Y. Zeng, R. V. Balaji, R. Masalha, R. B. Thompson, C. A. Fierke, J. M. Sarvey, M. de Valdenebro, D. S. Prough, and M. H. Zornow. 2006. "Concentrations of extracellular free zinc (pZn)(e) in the central nervous system during simple anesthetization, ischemia and reperfusion." *Experimental Neurology* 198 (2):285-293.

Fukutani, Yosuke, Jun Ishii, Keiichi Noguchi, Akihiko Kondo, and Masafumi Yohda. 2012. "An improved bioluminescence-based signaling assay for odor sensing with a yeast expressing a chimeric olfactory receptor." *Biotechnology and Bioengineering* 109 (12):3143-3151. doi: 10.1002/bit.24589.

Gane, S., D. Georganakis, K. Maniati, M. Vamvakias, N. Ragoussis, E. M. Skoulakis, and L. Turin. 2013. "Molecular vibration-sensing component in human olfaction." *PLoS One* 8 (1):e55780. doi: 10.1371/journal.pone.0055780.

Gao, X. L., Z. Y. Du, and T. B. Patel. 2005. "Copper and zinc inhibit G alpha(s) function." *Journal of Biological Chemistry* 280 (4):2579-2586.

Gibson, Glenn R., and M. B. Roberfroid. 2008. *Handbook of prebiotics*. Boca Raton: CRC Press.

Gidwani, M., and A. V. Singh. 2014. "Nanoparticle enabled drug delivery across the blood brain barrier: in vivo and in vitro models, opportunities and challenges." *Curr Pharm Biotechnol* 14 (14):1201-12.

Glusman, G., I. Yanai, I. Rubin, and D. Lancet. 2001. "The complete human olfactory subgenome." *Genome Res* 11 (5):685-702. doi: 10.1101/gr.171001.

Gomes, R., R. Liteplo, and M.E. Meek. 2003. *Ethylene Glycol: Human Health Aspects (Concise International Chemical Assessment Documents), Concise International Chemical Assessment Documents (Book 45)*. Ottawa, Canada: World Health Organization.

Graham, P. L., 3rd, S. X. Lin, and E. L. Larson. 2006. "A U.S. population-based survey of Staphylococcus aureus colonization." *Ann Intern Med* 144 (5):318-25.

Greenhow, T. L., Y. Y. Hung, A. M. Herz, E. Losada, and R. H. Pantell. 2014. "The changing epidemiology of serious bacterial infections in young infants." *Pediatr Infect Dis J* 33 (6):595-9. doi: 10.1097/inf.0000000000000225.

Griffin, C. A., K. A. Kafadar, and G. K. Pavlath. 2009. "MOR23 promotes muscle regeneration and regulates cell adhesion and migration." *Dev Cell* 17 (5):649-61. doi: 10.1016/j.devcel.2009.09.004.

Griffiths, David J. 1995. *Introduction to Quantum Mechanics*. Upper Saddle River, New Jersey: Prentice Hall.

Gronenberg, W., A. Raikhelkar, E. Abshire, J. Stevens, E. Epstein, K. Loyola, M. Rauscher, and S. Buchmann. 2014. "Honeybees (Apis mellifera) learn to discriminate the smell of organic compounds from their respective deuterated isotopomers." *Proc Biol Sci* 281 (1778):20133089. doi: 10.1098/rspb.2013.3089.

Grosmaitre, X., L. C. Santarelli, J. Tan, M. Luo, and M. Ma. 2007. "Dual functions of mammalian olfactory sensory neurons as odor detectors and mechanical sensors." *Nat Neurosci* 10 (3):348-54. doi: 10.1038/nn1856.

Gross, H. M., W. A. Johnson, and G. J. Lafferty. 1956. "Bacitracin. III. Formulatory characteristics of zinc bacitracin." *J Am Pharm Assoc Am Pharm Assoc* 45 (7):447-9.

Gruneberg, H. 1973. "A ganglion probably belonging to the N. terminalis system in the nasal mucosa of the mouse." *Z Anat Entwicklungsgesch* 140 (1):39-52.

Gu, X.-F., T. Furuharaa, and W.-Z. Zhang. 2016. "PTCLab: free and open-source software for calculating phase transformation crystallography." *Journal of applied crystallography* 49:1-8.

Guay-Bégin, Andrée-Anne, Pascale Chevallier, Luc Faucher, Stéphane Turgeon, and Marc-André Fortin. 2012. "Surface Modification of Gadolinium Oxide Thin Films and Nanoparticles using Poly(ethylene glycol)-Phosphate." *Langmuir* 28 (1):774-782. doi: 10.1021/la202780x.

Haering, C., N. Kanageswaran, P. Bouvain, P. Scholz, J. Altmuller, C. Becker, G. Gisselmann, J. Waring-Bischof, and H. Hatt. 2015. "Ion transporter NKCC1, modulator of neurogenesis in murine olfactory neurons." *J Biol Chem* 290 (15):9767-79. doi: 10.1074/jbc.M115.640656.

Haffenden, L. J. W., V. A. Yaylayan, and J. Fortin. 2001. "Investigation of vibrational theory of olfaction with variously labelled benzaldehydes." *Food Chemistry* 73 (1):67-72. doi: Doi 10.1016/S0308-8146(00)00287-9.

Hagerty, S., Y. Daniels, M. Singletary, O. Pustovyy, L. Globa, W. A. MacCrehan, S. Muramoto, G. Stan, J. W. Lau, E. E. Morrison, I. Sorokulova, and V. Vodyanoy. 2016a. "After oxidation, zinc nanoparticles lose their ability to enhance responses to odorants." *Biometals* 29 (6):1005-1018. doi: 10.1007/s10534-016-9972-y.

Hagerty, Samantha, Yasmine Daniels, Melissa Singletary, Oleg Pustovyy, Ludmila Globa, William A. MacCrehan, Shin Muramoto, Gheorghe Stan, June W. Lau, Edward E. Morrison, Iryna Sorokulova, and Vitaly Vodyanoy. 2016b. "After oxidation, zinc nanoparticles lose their ability to enhance responses to odorants." *Biometals* 29 (6):1005-1018.

Hall, Randy A. 2009. "Olfactory Receptor Interactions with other receptors." *Ann. N.Y. Acad. Sci.* 1170:147-149.

Hamidovic, A. 2015. "Position on zinc delivery to olfactory nerves in intranasal insulin phase I-III clinical trials." *Contemp Clin Trials* 45 (Pt B):277-80. doi: 10.1016/j.cct.2015.08.011.

Hansen, L. F., M. Hammer, S. H. Petersen, and G. D. Nielsen. 1994. "Effects of intranasal ZnSO4 irrigation on olfactory and trigeminal cues." *Physiol Behav* 55 (4):699-704.

Harel, D., L. Carmel, and D. Lancet. 2003. "Towards an odor communication system." *Computational Biology and Chemistry* 27 (2):121-133.

Hassan, S., and A. V. Singh. 2014. "Biophysicochemical perspective of nanoparticle compatibility: a critically ignored parameter in nanomedicine." *J Nanosci Nanotechnol* 14 (1):402-14.

Haxthausen, H., and C. Rasch. 1928. "SOME REMARKS ON THE BACTERICIDAL PROPERTIES OF ZINC OXIDE." *British Journal of Dermatology* 40 (12):497-501. doi: 10.1111/j.1365-2133.1928.tb13640.x.

Hayashi, Y. 1999. "[Metabotropic glutamate receptor: its ligands and function in the olfactory system]." *Nihon Yakurigaku Zasshi* 113 (2):73-83.

Heimer, L. 2003. "A new anatomical framework for neuropsychiatric disorders and drug abuse." *Am J Psychiatry* 160 (10):1726-39. doi: 10.1176/appi.ajp.160.10.1726.

Henkin, R. I., S. Hosein, W. A. Stateman, A. B. Knoppel, and M. Abdelmeguid. 2017. "Improved smell function with increased nasal mucus sonic hedgehog in hyposmic patients after treatment with oral theophylline." *Am J Otolaryngol* 38 (2):143-147. doi: 10.1016/j.amjoto.2016.11.010.

Henkin, R.I. , Doherty A., and B.M. Martin. 2000. *New frontiers in immunobiology*. Edited by Jan E Veldman; Desiderio Passàli; David J Lim. The Hague; Netherlands: Kugler Publications ; Library Research Associates [distributor].

Hernandez, H., N. Serafin, A. M. Terrazas, P. G. Marnet, G. Kann, J. A. Delgadillo, and P. Poindron. 2002. "Maternal olfaction differentially modulates oxytocin and prolactin release during suckling in goats." *Horm Behav* 42 (2):232-44.

Hideo, Watanabe, Wada Masanobu, and Takahashi Tadashi. 1965. "The Activation Energy for Oxygen Desorption from Zinc Oxide Surfaces." *Japanese Journal of Applied Physics* 4 (12):945.

Hirata, T., M. Nakazawa, S. Yoshihara, H. Miyachi, K. Kitamura, Y. Yoshihara, and M. Hibi. 2006. "Zinc-finger gene Fez in the olfactory sensory neurons regulates development of the olfactory bulb non-cell-autonomously." *Development* 133 (8):1433-43. doi: 10.1242/dev.02329.

Holt, B., S. Gregory, T. A. Sulchek, S. Yee, and M. D. Losego. 2018. "Aqueous zinc compounds as residual antimicrobial agents for textiles." *ACS Appl Mater Interfaces*. doi: 10.1021/acsami.7b15871.

Horning, M. S., and P. Q. Trombley. 2001. "Zinc and copper influence excitability of rat olfactory bulb neurons by multiple mechanisms." *Journal of Neurophysiology* 86 (4):1652-1660.

Horning, Michelle S., Laura J. Blakemore, and Paul Q. Trombley. 2000. "Endogenous mechanisms of neuroprotection: role of zinc, copper, and carnosine." *Brain Res* 852 (1):56-61. doi: http://dx.doi.org/10.1016/S0006-8993(99)02215-5.

Hoshino, A., S. Hanada, N. Manabe, T. Nakayama, and K. Yamamoto. 2009. "Immune Response Induced by Fluorescent Nanocrystal Quantum Dots <emphasis emphasistype="italic">In Vitro</emphasis> and <emphasis

emphasistype="italic">In Vivo</emphasis>." *IEEE Transactions on NanoBioscience* 8 (1):51-57. doi: 10.1109/TNB.2009.2016550.

Hotchen, Christopher E., Ian J. Maybury, Geoffrey W. Nelson, John S. Foord, Philip Holdway, and Frank Marken. 2015. "Amplified electron transfer at poly-ethylene-glycol (PEG) grafted electrodes." *Physical Chemistry Chemical Physics* 17 (17):11260-11268. doi: 10.1039/C5CP01244A.

Howard E. Evans, Alexander de Lahunta. 2013. *Miller's Anatomy of the Dog*. E-book: Elsevier Health Sciences.

Hsueh, Y. H., W. J. Ke, C. T. Hsieh, K. S. Lin, D. Y. Tzou, and C. L. Chiang. 2015. "ZnO Nanoparticles Affect Bacillus subtilis Cell Growth and Biofilm Formation." *PLoS One* 10 (6):e0128457. doi: 10.1371/journal.pone.0128457.

Hu, J., C. Zhong, C. Ding, Q. Chi, A. Walz, P. Mombaerts, H. Matsunami, and M. Luo. 2007. "Detection of near-atmospheric concentrations of CO2 by an olfactory subsystem in the mouse." *Science* 317 (5840):953-7. doi: 10.1126/science.1144233.

Human Microbiome Project, Consortium. 2012a. "A framework for human microbiome research." *Nature* 486 (7402):215-21. doi: 10.1038/nature11209.

Human Microbiome Project, Consortium. 2012b. "Structure, function and diversity of the healthy human microbiome." *Nature* 486 (7402):207-14. doi: 10.1038/nature11234.

Hummel, T., M. Knecht, and G. Kobal. 1996. "Peripherally obtained electrophysiological responses to olfactory stimulation in man: electro-olfactograms exhibit a smaller degree of desensitization compared with subjective intensity estimates." *Brain Res* 717 (1-2):160-4.

Hummel, T., J. Mojet, and G. Kobal. 2006. "Electro-olfactograms are present when odorous stimuli have not been perceived." *Neurosci Lett* 397 (3):224-8. doi: 10.1016/j.neulet.2005.12.048.

Ikemoto, S. 2007. "Dopamine reward circuitry: two projection systems from the ventral midbrain to the nucleus accumbens-olfactory tubercle complex." *Brain Res Rev* 56 (1):27-78. doi: 10.1016/j.brainresrev.2007.05.004.

International Zinc Nutrition Consultative, Group, K. H. Brown, J. A. Rivera, Z. Bhutta, R. S. Gibson, J. C. King, B. Lonnerdal, M. T. Ruel, B. Sandtrom, E. Wasantwisut, and C. Hotz. 2004. "International Zinc Nutrition Consultative Group (IZiNCG) technical document #1. Assessment of the risk of zinc deficiency in populations and options for its control." *Food Nutr Bull* 25 (1 Suppl 2):S99-203.

Ishimaru, T., T. Tsukatani, T. Miwa, and M. Furukawa. 2000. "Zinc modulates the electro-olfactogram of the frog." *Auris Nasus Larynx* 27 (3):257-60.

Iyengar, G. V. 1998. "Reevaluation of the trace element content in Reference Man." *Radiation Physics and Chemistry* 51 (4):545-560. doi: https://doi.org/10.1016/S0969-806X(97)00202-8.

Jachimska, B, M Wasilewska, and Z. Adamczyk. 2008. "Characterization of Globular Protein Solutions by Dynamic Light Scattering, Electrophoretic Mobility, and Viscosity Measurements." *Langmuir* 24:6866-6872.

Jackson, M. J., D. A. Jones, and R. H. T. Edwards. 1982. "Tissue Zinc Levels as an Index of Body Zinc Status." *Clinical Physiology* 2 (4):333-343. doi: DOI 10.1111/j.1475-097X.1982.tb00038.x.

Jacobs, D. M., E. Gaudier, J. van Duynhoven, and E. E. Vaughan. 2009. "Non-digestible food ingredients, colonic microbiota and the impact on gut health and immunity: a role for metabolomics." *Curr Drug Metab* 10 (1):41-54.

Jena, P., S. N. Khanna, and B. K. Rao. 1996. "Stability and electronic structure of cluster assembled materials." In *Cluster Assembled Materials*, 1-25.

Jia, H, O Pustovyy, P Waggoner, RJ Beyers, J Schumacher, J Barrett, E Morrison, RL Gillette, TS Denney, VJ Vodyanoy, and G Deshpande. 2012. "Functional MRI of the Olfactory System in Awake and Anesthetized Dogs." 20th annual meeting of the International Society for Magnetic Resonance in Medicine, Melbourne, Australia.

Jia, H., O. M. Pustovyy, P. Waggoner, R. J. Beyers, J. Schumacher, C. Wildey, J. Barrett, E. Morrison, N. Salibi, T. S. Denney, V. J. Vodyanoy, and G. Deshpande. 2014. "Functional MRI of the olfactory system in conscious dogs." *PLoS One* 9 (1):e86362. doi: 10.1371/journal.pone.0086362.

Jia, H., O. M. Pustovyy, Y. Wang, P. Waggoner, R. J. Beyers, J. Schumacher, C. Wildey, E. Morrison, N. Salibi, T. S. Denney, V. J. Vodyanoy, and G. Deshpande. 2016. "Enhancement of Odor-Induced Activity in the Canine Brain by Zinc Nanoparticles: A Functional MRI Study in Fully Unrestrained Conscious Dogs." *Chem Senses* 41 (1):53-67. doi: 10.1093/chemse/bjv054.

Jia, Hao, Oleg M. Pustovyy, Yun Wang, Paul Waggoner, Ronald J. Beyers, John Schumacher, Chester Wildey, Edward Morrison, Nouha Salibi, Thomas S. Denney, Vitaly J. Vodyanoy, and Gopikrishna Deshpande. 2015. "Enhancement of Odor-Induced Activity in the Canine Brain by Zinc Nanoparticles: A Functional MRI Study in Fully Unrestrained Conscious Dogs." *Chemical Senses*. doi: 10.1093/chemse/bjv054.

Johnson, B. A., H. Anker, and F. L. Meleney. 1945. "Bacitracin: A New Antibiotic Produced by a Member of the B. Subtilis Group." *Science* 102 (2650):376-7. doi: 10.1126/science.102.2650.376.

Jokerst, Jesse V., Tatsiana Lobovkina, Richard N. Zare, and Sanjiv S. Gambhir. 2011. "Nanoparticle PEGylation for imaging and therapy." *Nanomedicine (London, England)* 6 (4):715-728. doi: 10.2217/nnm.11.19.

Jones, N., B. Ray, K. T. Ranjit, and A. C. Manna. 2008. "Antibacterial activity of ZnO nanoparticle suspensions on a broad spectrum of microorganisms." *Fems Microbiology Letters* 279 (1):71-76. doi: 10.1111/j.1574-6968.2007.01012.x.

Juilfs, D. M., H. J. Fulle, A. Z. Zhao, M. D. Houslay, D. L. Garbers, and J. A. Beavo. 1997. "A subset of olfactory neurons that selectively express cGMP-stimulated phosphodiesterase (PDE2) and guanylyl cyclase-D define a unique olfactory signal transduction pathway." *Proceedings of the National Academy of Sciences of the United States of America* 94 (7):3388-3395. doi: DOI 10.1073/pnas.94.7.3388.

Kaba, H., and E. B. Keverne. 1992. "Analysis of synaptic events in the mouse accessory olfactory bulb with current source-density techniques." *Neuroscience* 49 (2):247-54.

Kabra, Komal, Anil A. Sonkamble, Kunal H. Wananje, Ashok C. Kumbharkhane, and Arvind V. Sarode. 2015. "Dynamics of polymer matrix in non-polar solvent Using TDR Technique." *BIONANO FRONTIER Vol. 8 (3) December 2015* 8 (3):378-380.

Kaliner, M. A. 1991. "Human Nasal Respiratory Secretions and Host Defense." *American Review of Respiratory Disease* 144 (3):S52-S56. doi: DOI 10.1164/ajrccm/144.3_pt_2.S52.

Karakoti, Ajay S., Soumen Das, Suntharampillai Thevuthasan, and Sudipta Seal. 2011. "PEGylated Inorganic Nanoparticles." *Angewandte Chemie International Edition* 50 (9):1980-1994. doi: 10.1002/anie.201002969.

Kaushik, N. K., N. Kaushik, D. Park, and E. H. Choi. 2014. "Altered Antioxidant System Stimulates Dielectric Barrier Discharge Plasma-Induced Cell Death for Solid Tumor Cell Treatment." *Plos One* 9 (7). doi: ARTN e103349 10.1371/journal.pone.0103349.

Keller, A., and L. B. Vosshall. 2004. "A psychophysical test of the vibration theory of olfaction." *Nat Neurosci* 7 (4):337-8. doi: 10.1038/nn1215.

Khanna, S. N., B. K. Rao, and P. Jena. 2002. "Magic numbers in metallo-inorganic clusters: Chromium encapsulated in silicon cages." *Physical Review Letters* 89 (1):016803.1-016803.4. doi: 016803 10.1103/PhysRevLett.89.016803.

Kikusui, T., S. Takigami, Y. Takeuchi, and Y. Mori. 2001. "Alarm pheromone enhances stress-induced hyperthermia in rats." *Physiol Behav* 72 (1-2):45-50.

Kloubert, V., and L. Rink. 2015. "Zinc as a micronutrient and its preventive role of oxidative damage in cells." *Food Funct* 6 (10):3195-204. doi: 10.1039/c5fo00630a.

Kogan, Marcelo J., Ivonne Olmedo, Leticia Hosta, Ariel R Guerrero, Luis Javier Cruz, and Fernando Albericio. 2007. "Peptides and metallic nanoparticles for biomedical applications." *Nanomedicine* 2 (3):287-306. doi: 10.2217/17435889.2.3.287.

Korsching, S. 2009. "The molecular evolution of teleost olfactory receptor gene families." *Results Probl Cell Differ* 47:37-55. doi: 10.1007/400_2008_11.

Kosaka, T., Y. Hataguchi, K. Hama, I. Nagatsu, and J. Y. Wu. 1985. "Coexistence of immunoreactivities for glutamate decarboxylase and tyrosine hydroxylase in some neurons in the periglomerular region of the rat main olfactory bulb: possible coexistence of gamma-aminobutyric acid (GABA) and dopamine." *Brain Res* 343 (1):166-71.

Kratzing, J. E. 1984. "The anatomy and histology of the nasal cavity of the koala (Phascolarctos cinereus)." *J Anat* 138 (Pt 1):55-65.

Kruyt, H.R. 1952. *Colloid Science*. Vol. VI. New York: Elsevier.

Kurahashi, T., and A. Menini. 1997. "Mechanism of odorant adaptation in the olfactory receptor cell." *Nature* 385 (6618):725-729.

Kushto, G. P., and P. W. Jagodzinski. 1998. "Vibrational spectra and normal coordinate analysis of 4-(dimethylamino)benzaldehyde and selected isotopic derivatives." *Spectrochim Acta A Mol Biomol Spectrosc* 54A (6):799-819.

Lafay, F., P. Coulon, L. Astic, D. Saucier, D. Riche, A. Holley, and A. Flamand. 1991. "Spread of the CVS strain of rabies virus and of the avirulent mutant AvO1 along the olfactory pathways of the mouse after intranasal inoculation." *Virology* 183 (1):320-30.

Lancet, D., and N. Benarie. 1993. "Olfactory Receptors." *Current Biology* 3 (10):668-674.

Lancet, D., and U. Pace. 1987. "The Molecular-Basis of Odor Recognition." *Trends in Biochemical Sciences* 12 (2):63-66.

Lazzerini, Marzia, and Humphrey Wanzira. 2016. "Oral zinc for treating diarrhoea in children." *Cochrane Database of Systematic Reviews* (12). doi: 10.1002/14651858.CD005436.pub5.

LB., Boldyreva. 2014. "The physical aspect of the effects of metal nanoparticles on biological systems. ." *Nanomaterials and Nanosciences.* 2(1) (Spin supercurrents.).

Le, Y. Y., J. M. M. Wang, X. L. Liu, Y. Kong, X. W. Hou, L. F. Ruan, and H. W. Mou. 2007. "Biologically active peptides interacting with the G protein-coupled formylpeptide receptors." *Protein and Peptide Letters* 14 (9):846-853. doi: Doi 10.2174/092986607782110211.

Lee, H. K., S. H. Choi, C. R. Lee, S. H. Lee, M. R. Park, Y. Kim, M. K. Lee, and G. B. Kim. 2015. "Screening and Characterization of Lactic Acid Bacteria Strains with Anti-inflammatory Activities through in vitro and Caenorhabditis elegans Model

Testing." *Korean J Food Sci Anim Resour* 35 (1):91-100. doi: 10.5851/kosfa.2015.35.1.91.

Leinders-Zufall, T., R. E. Cockerham, S. Michalakis, M. Biel, D. L. Garbers, R. R. Reed, F. Zufall, and S. D. Munger. 2007. "Contribution of the receptor guanylyl cyclase GC-D to chemosensory function in the olfactory epithelium." *Proceedings of the National Academy of Sciences of the United States of America* 104 (36):14507-14512. doi: 10.1073/pnas.0704965104.

Li, J. J., H. L. Tay, M. Plank, A. T. Essilfie, P. M. Hansbro, P. S. Foster, and M. Yang. 2013. "Activation of olfactory receptors on mouse pulmonary macrophages promotes monocyte chemotactic protein-1 production." *PLoS One* 8 (11):e80148. doi: 10.1371/journal.pone.0080148.

Lippard, S. J. 2014. "Metalloneurochemistry: An overview and mobile zinc signaling in sensory perception." *Abstracts of Papers of the American Chemical Society* 248.

Lowe, G., and G. H. Gold. 1993. "Nonlinear amplification by calcium-dependent chloride channels in olfactory receptor cells." *Nature* 366 (6452):283-6. doi: 10.1038/366283a0.

Lu, C., Y. Cheng, Q. Pan, X. Tao, B. Yang, and G. Ye. 2016. "One-dimensional Growth of Zinc Crystals on a Liquid Surface." *Sci Rep* 6:19870. doi: 10.1038/srep19870.

Ma, M. 2010. "Multiple Olfactory Subsystems Convey Various Sensory Signals." In *The Neurobiology of Olfaction*, edited by A. Menini. Boca Raton (FL).

Mackay-Sim, A. 2010. "Stem cells and their niche in the adult olfactory mucosa." *Archives Italiennes De Biologie* 148 (2):47-58.

Mai, Nguyen T., Trinh T. Thuy, Derrick M. Mott, and Shinya Maenosono. 2013a. "Chemical synthesis of blue-emitting metallic zinc nano-hexagons." *CrystEngComm* 15 (33):6606-6610. doi: 10.1039/C3CE40801A.

Mai, Nguyen T., Trinh T. Thuy, Derrick M. Mott, and Shinya Maenosono. 2013b. "Chemical synthesis of blue-emitting metallic zinc nano-hexagons." *Cryst Eng Comm* 15 (33):6606-6610. doi: 10.1039/C3CE40801A.

Mamasuew, K., H. Breer, and J. Fleischer. 2008. "Grueneberg ganglion neurons respond to cool ambient temperatures." *Eur J Neurosci* 28 (9):1775-85. doi: 10.1111/j.1460-9568.2008.06465.x.

Maret, W. 2014. "Zinc in the biosciences." *Metallomics* 6 (7):1174. doi: 10.1039/c4mt90021a.

Mason, M. G. 1983. "Electronic structure of supported small metal clusters." *Physical Review B* 27 (2):748-762.

Matulionis, D. H. 1975. "Ultrastructural study of mouse olfactory epithelium following destruction by ZnSO4 and its subsequent regeneration." *Am J Anat* 142 (1):67-89. doi: 10.1002/aja.1001420106.

Mayer, U., A. Kuller, P. C. Daiber, I. Neudorf, U. Warnken, M. Schnolzer, S. Frings, and F. Mohrlen. 2009. "The proteome of rat olfactory sensory cilia." *Proteomics* 9 (2):322-34. doi: 10.1002/pmic.200800149.

McKone, James R., Bryce F. Sadtler, Caroline A. Werlang, Nathan S. Lewis, and Harry B. Gray. 2013. "Ni–Mo Nanopowders for Efficient Electrochemical Hydrogen Evolution." *ACS Catalysis* 3 (2):166-169. doi: 10.1021/cs300691m.

McLean, P. G., G. E. Bergonzelli, S. M. Collins, and P. Bercik. 2012. "Targeting the microbiota-gut-brain axis to modulate behavior: which bacterial strain will translate best to humans?" *Proc Natl Acad Sci U S A* 109 (4):E174; author reply E176. doi: 10.1073/pnas.1118626109.

McMahon, R. J., and R. J. Cousins. 1998. "Mammalian zinc transporters." *J Nutr* 128 (4):667-70.

Mellert, T. K., M. L. Getchell, L. Sparks, and T. V. Getchell. 1992. "Characterization of the Immune Barrier in Human Olfactory Mucosa." *Otolaryngology-Head and Neck Surgery* 106 (2):181-188.

Mellone, M., S. Pelucchi, L. Alberti, A. A. Geneazzani, M. Di Luca, and F. Gardoni. 2015. "Zinc transporter-1: a novel NMDA receptor-binding protein at the postsynaptic density." *Journal of Neurochemistry* 132 (2):159-168. doi: 10.1111/jnc.12968.

Menco, B. P. M., and J. E. Jackson. 1997. "A banded topography in the developing rat's olfactory epithelial surface." *Journal of Comparative Neurology* 388 (2):293-306.

Menco, Bert Ph. M. , and Edward E. Morrison. 2003. "Morphology of the Mammalian Olfactory Epithelium: Form, Fine Structure, Function, and Pathology." In *Handbook of Olfaction and Gustation*, edited by Richard L. Doty, 17-49. New York: Marcel Dekker, Inc.,.

Mesholam, R. I., P. J. Moberg, R. N. Mahr, and R. L. Doty. 1998. "Olfaction in neurodegenerative disease: a meta-analysis of olfactory functioning in Alzheimer's and Parkinson's diseases." *Arch Neurol* 55 (1):84-90.

Mira, E. 1963. "Oxidative and Hydrolytic Enzymes in Bowman's Glands." *Acta Otolaryngol* 56:706-14.

Mitra, Kakoli, Iban Ubarretxena-Belandia, Tomohiko Taguchi, Graham Warren, and Donald M. Engelman. 2004. "Modulation of the bilayer thickness of exocytic pathway membranes by membrane proteins rather than cholesterol." *Proceedings of the National Academy of Sciences of the United States of America* 101 (12):4083-4088. doi: 10.1073/pnas.0307332101.

Miyamichi, K., F. Amat, F. Moussavi, C. Wang, I. Wickersham, N. R. Wall, H. Taniguchi, B. Tasic, Z. J. Huang, Z. He, E. M. Callaway, M. A. Horowitz, and L. Luo. 2011. "Cortical representations of olfactory input by trans-synaptic tracing." *Nature* 472 (7342):191-6. doi: 10.1038/nature09714.

Moore, C. H., O. Pustovyy, J. C. Dennis, T. Moore, E. E. Morrison, and V. J. Vodyanoy. 2012. "Olfactory responses to explosives associated odorants are enhanced by zinc nanoparticles." *Talanta* 88:730-733. doi: 10.1016/j.talanta.2011.11.024.

Moore, T., L. Globa, O. Pustovyy, V. Vodyanoy, and I. Sorokulova. 2014. "Oral administration of Bacillus subtilis strain BSB3 can prevent heat stress-related adverse effects in rats." *J Appl Microbiol* 117 (5):1463-71. doi: 10.1111/jam.12606.

Moore, W. J. 1981. *The mammalian skull / W. J. Moore, Biological structure and function ; 8.* Cambridge [Eng.] ; New York: Cambridge University Press.

Moore, Walter J., and James K. Lee. 1951. "Kinetics of the formation of oxide films on zinc foil." *Transactions of the Faraday Society* 47 (0):501-508. doi: 10.1039/TF9514700501.

Moraes-Filho, J. P., and E. M. Quigley. 2015. "THE INTESTINAL MICROBIOTA AND THE ROLE OF PROBIOTICS IN IRRITABLE BOWEL SYNDROME: a review." *Arq Gastroenterol* 52 (4):331-8. doi: 10.1590/S0004-28032015000400015.

Morales, J. A., S. Herzog, C. Kompter, K. Frese, and R. Rott. 1988. "Axonal transport of Borna disease virus along olfactory pathways in spontaneously and experimentally infected rats." *Med Microbiol Immunol* 177 (2):51-68.

Moran, D. T., J. C. Rowley, 3rd, B. W. Jafek, and M. A. Lovell. 1982. "The fine structure of the olfactory mucosa in man." *J Neurocytol* 11 (5):721-46.

Morkoç, Hadis, and Ümit Özgur. 2009. *Zinc Oxide: Fundamentals, Materials and Device Technology*. Weinheim: WILEY-VCH Verlag GmbH & Co. KGaA.

Morrison, Edward E., and Richard M. Costanzo. 1990. "Morpholgy of the Human Olfactory Epithelium." *THE JOURNAL OF COMPARITIVE NEUROLOGY* 297:1-13.

Mu, Qingxin, Guibin Jiang, Lingxin Chen, Hongyu Zhou, Denis Fourches, Alexander Tropsha, and Bing Yan. 2014. "Chemical Basis of Interactions Between Engineered Nanoparticles and Biological Systems." *Chemical reviews* 114 (15):7740-7781. doi: 10.1021/cr400295a.

Mulder, W., J. Pol, T. Kimman, G. Kok, J. Priem, and B. Peeters. 1996. "Glycoprotein D-negative pseudorabies virus can spread transneuronally via direct neuron-to-neuron transmission in its natural host, the pig, but not after additional inactivation of gE or gI." *J Virol* 70 (4):2191-200.

Nagashima, A., and K. Touhara. 2010. "Enzymatic conversion of odorants in nasal mucus affects olfactory glomerular activation patterns and odor perception." *J Neurosci* 30 (48):16391-8. doi: 10.1523/JNEUROSCI.2527-10.2010.

Nakashima, A. S., and R. H. Dyck. 2009. "Zinc and cortical plasticity." *Brain Research Reviews* 59 (2):347-373. doi: 10.1016/j.brainresrev.2008.10.003.

Narita, M., A. Uchimura, M. Kawanabe, H. Fukushi, and K. Hirai. 2001. "Invasion and spread of equine herpesvirus 9 in the olfactory pathway of pigs after intranasal inoculation." *J Comp Pathol* 124 (4):265-72. doi: 10.1053/jcpa.2000.0461.

Nasajpour, A., S. Ansari, C. Rinoldi, A. S. Rad, T. Aghaloo, S. R. Shin, Y. K. Mishra, R. Adelung, W. Swieszkowski, N. Annabi, A. Khademhosseini, A. Moshaverinia, and A. Tamayol. 2018. "A Multifunctional Polymeric Periodontal Membrane with Osteogenic and Antibacterial Characteristics." *Advanced Functional Materials* 28 (3). doi: ARTN 1703437 10.1002/adfm.201703437.

Naumkin, Alexander V., Anna Kraut-Vass, Stephen W. Gaarenstroom, and Cedric J. Powell. 2012. NIST X-ray Photoelectron Spectroscopy Database. Washington: NIST.

Nekoueian, Khadijeh, Christopher E. Hotchen, Mandana Amiri, Mika Sillanpaa, Geoffrey W. Nelson, John S. Foord, Philip Holdway, Antoine Buchard, Stephen C. Parker, and Frank Marken. 2015. "Interfacial Electron-Shuttling Processes across KolliphorEL Monolayer Grafted Electrodes." *Acs Applied Materials & Interfaces* 7 (28):15458-15465. doi: 10.1021/acsami.5b03654.

Nguyen, D. T., K. Lee, H. Choi, M. K. Choi, M. T. Le, N. Song, J. H. Kim, H. G. Seo, J. W. Oh, K. Lee, T. H. Kim, and C. Park. 2012. "The complete swine olfactory subgenome: expansion of the olfactory gene repertoire in the pig genome." *BMC Genomics* 13:584. doi: 10.1186/1471-2164-13-584.

Niimura, Y. 2012. "Olfactory receptor multigene family in vertebrates: from the viewpoint of evolutionary genomics." *Curr Genomics* 13 (2):103-14. doi: 10.2174/138920212799860706.

Niimura, Y., A. Matsui, and K. Touhara. 2014. "Extreme expansion of the olfactory receptor gene repertoire in African elephants and evolutionary dynamics of orthologous gene groups in 13 placental mammals." *Genome Res* 24 (9):1485-96. doi: 10.1101/gr.169532.113.

Niimura, Y., and M. Nei. 2003. "Evolution of olfactory receptor genes in the human genome." *Proc Natl Acad Sci U S A* 100 (21):12235-40. doi: 10.1073/pnas.1635157100.

Niimura, Y., and M. Nei. 2005a. "Comparative evolutionary analysis of olfactory receptor gene clusters between humans and mice." *Gene* 346:13-21. doi: 10.1016/j.gene.2004.09.025.

Niimura, Y., and M. Nei. 2005b. "Evolutionary changes of the number of olfactory receptor genes in the human and mouse lineages." *Gene* 346:23-8. doi: 10.1016/j.gene.2004.09.027.

Niimura, Y., and M. Nei. 2005c. "Evolutionary dynamics of olfactory receptor genes in fishes and tetrapods." *Proc Natl Acad Sci U S A* 102 (17):6039-44. doi: 10.1073/pnas.0501922102.

Odamaki, T., K. Kato, H. Sugahara, N. Hashikura, S. Takahashi, J. Z. Xiao, F. Abe, and R. Osawa. 2016. "Age-related changes in gut microbiota composition from newborn to centenarian: a cross-sectional study." *BMC Microbiol* 16 (1):90. doi: 10.1186/s12866-016-0708-5.

Ohkubo, K., J. N. Baraniuk, R. Hohman, M. Merida, L. B. Hersh, and M. A. Kaliner. 1998. "Aminopeptidase activity in human nasal mucosa." *Journal of Allergy and Clinical Immunology* 102 (5):741-750. doi: Doi 10.1016/S0091-6749(98)70013-2.

Ohm, T. G., H. Muller, and E. Braak. 1991. "Calbindin-D-28k-like immunoreactive structures in the olfactory bulb and anterior olfactory nucleus of the human adult: distribution and cell typology--partial complementarity with parvalbumin." *Neuroscience* 42 (3):823-40.

Ohm, T. G., H. Muller, N. Ulfig, and E. Braak. 1990. "Glutamic-acid-decarboxylase-and parvalbumin-like-immunoreactive structures in the olfactory bulb of the human adult." *J Comp Neurol* 291 (1):1-8. doi: 10.1002/cne.902910102.

Ollig, Johanna, Veronika Kloubert, Inga Weßels, Hajo Haase, and Lothar Rink. 2016. "Parameters Influencing Zinc in Experimental Systems in Vivo and in Vitro." *Metals* 6 (3):71.

Otsuka, H., Y. Nagasaki, and K. Kataoka. 2003. "PEGylated nanoparticles for biological and pharmaceutical applications." *Advanced Drug Delivery Reviews* 55 (3):403-419. doi: 10.1016/S0169-409x(02)00226-0.

Ottoson, D. 1956. "Analysis of the Electrical Activity of the Olfactory Epithelium." *Acta Physiologica Scandinavica* 35:7-83.

Ottoson, David. 1971. "The Electro-Olfactogram: A Review of Studies on the Receptor Potential of the Olfactory Organ." In *Handbook of sensory physiology*, edited by Beidler LM, 95-131. Berlin.: Springer.

Ould-Yahoui, A., O. Sbai, K. Baranger, A. Bernard, Y. Gueye, E. Charrat, B. Clement, D. Gigmes, V. Dive, S. D. Girard, F. Feron, M. Khrestchatisky, and S. Rivera. 2013. "Role of matrix metalloproteinases in migration and neurotrophic properties of nasal olfactory stem and ensheathing cells." *Cell Transplant* 22 (6):993-1010. doi: 10.3727/096368912X657468.

Paoli, M., A. Anesi, R. Antolini, G. Guella, G. Vallortigara, and A. Haase. 2016. "Differential Odour Coding of Isotopomers in the Honeybee Brain." *Sci Rep* 6:21893. doi: 10.1038/srep21893.

Paoli, M., D. Munch, A. Haase, E. Skoulakis, L. Turin, and C. G. Galizia. 2017. "Minute Impurities Contribute Significantly to Olfactory Receptor Ligand Studies: Tales from Testing the Vibration Theory." *eNeuro* 4 (3). doi: 10.1523/ENEURO.0070-17.2017.

Patterson, E., J. F. Cryan, G. F. Fitzgerald, R. P. Ross, T. G. Dinan, and C. Stanton. 2014. "Gut microbiota, the pharmabiotics they produce and host health." *Proc Nutr Soc* 73 (4):477-89. doi: 10.1017/S0029665114001426.

Pavlica, S., F. Gaunitz, and R. Gebhardt. 2009. "Comparative in vitro toxicity of seven zinc-salts towards neuronal PC12 cells." *Toxicol In Vitro* 23 (4):653-9. doi: 10.1016/j.tiv.2009.03.003.

Pavlica, S., and R. Gebhardt. 2010. "Comparison of uptake and neuroprotective potential of seven zinc-salts." *Neurochem Int* 56 (1):84-93. doi: 10.1016/j.neuint.2009.09.005.

Pellegrino, R., C. Sinding, R. A. de Wijk, and T. Hummel. 2017. "Habituation and adaptation to odors in humans." *Physiol Behav* 177:13-19. doi: 10.1016/j.physbeh.2017.04.006.

Pelosi, Paolo. 1994. "Odorant-Binding Proteins." *Critical Reviews in Biochemistry and Molecular Biology* 29 (3):199-228.

Perry, Jillian L., Kevin G. Reuter, Marc P. Kai, Kevin P. Herlihy, Stephen W. Jones, J. Chris Luft, Mary Napier, James E. Bear, and Joseph M. DeSimone. 2012. "PEGylated PRINT Nanoparticles: The Impact of PEG Density on Protein Binding, Macrophage Association, Biodistribution, and Pharmacokinetics." *Nano letters* 12 (10):5304-5310. doi: 10.1021/nl302638g.

Persuy, M. A., G. Sanz, A. Tromelin, T. Thomas-Danguin, J. F. Gibrat, and E. Pajot-Augy. 2015. "Mammalian olfactory receptors: molecular mechanisms of odorant detection, 3D-modeling, and structure-activity relationships." *Prog Mol Biol Transl Sci* 130:1-36. doi: 10.1016/bs.pmbts.2014.11.001.

Pevsner, Jonathan. , and Solomon H. Synder. 1990. "Odorant binding protein: odorant transport function in the vertebrate nasal epithelium." *Chemical Senses* 15 (2):217-222.

Pluznick, J. L., R. J. Protzko, H. Gevorgyan, Z. Peterlin, A. Sipos, J. Han, I. Brunet, L. X. Wan, F. Rey, T. Wang, S. J. Firestein, M. Yanagisawa, J. I. Gordon, A. Eichmann, J. Peti-Peterdi, and M. J. Caplan. 2013. "Olfactory receptor responding to gut microbiota-derived signals plays a role in renin secretion and blood pressure regulation." *Proc Natl Acad Sci U S A* 110 (11):4410-5. doi: 10.1073/pnas.1215927110.

Pluznick, J. L., D. J. Zou, X. Zhang, Q. Yan, D. J. Rodriguez-Gil, C. Eisner, E. Wells, C. A. Greer, T. Wang, S. Firestein, J. Schnermann, and M. J. Caplan. 2009. "Functional expression of the olfactory signaling system in the kidney." *Proc Natl Acad Sci U S A* 106 (6):2059-64. doi: 10.1073/pnas.0812859106.

Price, J. L., B. M. Slotnick, and M. F. Revial. 1991. "Olfactory projections to the hypothalamus." *J Comp Neurol* 306 (3):447-61. doi: 10.1002/cne.903060309.

Primeaux, S. D., H. D. Braymer, and G. A. Bray. 2013. "High fat diet differentially regulates the expression of olfactory receptors in the duodenum of obesity-prone and obesity-resistant rats." *Dig Dis Sci* 58 (1):72-6. doi: 10.1007/s10620-012-2421-z.

Pronin, A., K. Levay, D. Velmeshev, M. Faghihi, V. I. Shestopalov, and V. Z. Slepak. 2014. "Expression of olfactory signaling genes in the eye." *PLoS One* 9 (4):e96435. doi: 10.1371/journal.pone.0096435.

Qiu, Limei, Fen Liu, Liangzhong Zhao, Wensheng Yang, and Jiannian Yao. 2006. "Evidence of a Unique Electron Donor−Acceptor Property for Platinum Nanoparticles as Studied by XPS." *Langmuir* 22 (10):4480-4482. doi: 10.1021/la053071q.

Quignon, P., E. Kirkness, E. Cadieu, N. Touleimat, R. Guyon, C. Renier, C. Hitte, C. Andre, C. Fraser, and F. Galibert. 2003. "Comparison of the canine and human

olfactory receptor gene repertoires." *Genome Biol* 4 (12):R80. doi: 10.1186/gb-2003-4-12-r80.

R Singaravelan, S B S Alwar. 2017. "Zinc Nanoparticles: an Investigation of Deleterious Effect on Micro-Organisms." *Glob J Nano.* 1 (4) (555569). doi: DOI: 10.19080/GJN.2017.01.555569.

Raghupathi, K. R., R. T. Koodali, and A. C. Manna. 2011. "Size-dependent bacterial growth inhibition and mechanism of antibacterial activity of zinc oxide nanoparticles." *Langmuir* 27 (7):4020-8. doi: 10.1021/la104825u.

Rai, R., S. C. Shanmuga, and C. Srinivas. 2012. "Update on photoprotection." *Indian J Dermatol* 57 (5):335-42. doi: 10.4103/0019-5154.100472.

Ramon-Cueto, A., and J. Avila. 1998. "Olfactory ensheathing glia: properties and function." *Brain Res Bull* 46 (3):175-87.

Randall, H. W., M. S. Bogdanffy, and K. T. Morgan. 1987. "Enzyme histochemistry of the rat nasal mucosa embedded in cold glycol methacrylate." *Am J Anat* 179 (1):10-7. doi: 10.1002/aja.1001790103.

Rankin, C. H., T. Abrams, R. J. Barry, S. Bhatnagar, D. F. Clayton, J. Colombo, G. Coppola, M. A. Geyer, D. L. Glanzman, S. Marsland, F. K. McSweeney, D. A. Wilson, C. F. Wu, and R. F. Thompson. 2009. "Habituation revisited: an updated and revised description of the behavioral characteristics of habituation." *Neurobiol Learn Mem* 92 (2):135-8. doi: 10.1016/j.nlm.2008.09.012.

Reed, R. R. 2004. "After the holy grail: establishing a molecular basis for Mammalian olfaction." *Cell* 116 (2):329-36.

Reisert, J., and H. R. Matthews. 2000. "Adaptation-induced changes in sensitivity in frog olfactory receptor cells." *Chemical Senses* 25 (4):483-486.

Rink, L., and P. Gabriel. 2000. "Zinc and the immune system." *Proc Nutr Soc* 59 (4):541-52.

Riviere, S., L. Challet, D. Fluegge, M. Spehr, and I. Rodriguez. 2009. "Formyl peptide receptor-like proteins are a novel family of vomeronasal chemosensors." *Nature* 459 (7246):574-577. doi: 10.1038/nature08029.

Rodolfo-Maera, T. 1943. "Su 1'esistenza di un particolare organo olfacttivo nel setto nasale della cavia e di altri roditori." *Arch Ital Anat Embryol*.

Rovati, G. E., V. Capra, and R. R. Neubig. 2007. "The highly conserved DRY motif of class A G protein-coupled receptors: beyond the ground state." *Mol Pharmacol* 71 (4):959-64. doi: 10.1124/mol.106.029470.

Rowe, F. A., and W. E. Smith. 1972. "Effects of peripherally induced anosmia on mating behavior of male mice." *Psychonomic Science* 27 (1):33-34.

Rudd, M. K., R. M. Endicott, C. Friedman, M. Walker, J. M. Young, K. Osoegawa, Nisc Comparative Sequencing Program, P. J. de Jong, E. D. Green, and B. J. Trask. 2009. "Comparative sequence analysis of primate subtelomeres originating from a chromosome fission event." *Genome Res* 19 (1):33-41. doi: 10.1101/gr.083170.108.

Rudd, P. A., R. Cattaneo, and V. von Messling. 2006. "Canine distemper virus uses both the anterograde and the hematogenous pathway for neuroinvasion." *J Virol* 80 (19):9361-70. doi: 10.1128/JVI.01034-06.

Rygg, A. D., A. C. van Duin, and B. A. Craven. 2013. "Molecular dynamics simulations of water/mucus partition coefficients for feeding stimulants in fish and the implications for olfaction." *PLoS One* 8 (9):e72271. doi: 10.1371/journal.pone.0072271.

Samoylov, Alexander M., Tatiana I. Samoylova, Oleg M. Pustovyy, Alexei A. Samoylov, Maria A. Toivio-Kinnucan, Nancy E. Morrison, Ludmila P. Globa, William F. Gale, and Vitaly Vodyanoy. 2005. "Novel Metal Clusters Isolated from Blood Are Lethal to Cancer Cells." *Cells Tissues Organs* 179 (3):115-124.

Sanders, M. E., F. Guarner, R. Guerrant, P. R. Holt, E. M. Quigley, R. B. Sartor, P. M. Sherman, and E. A. Mayer. 2013. "An update on the use and investigation of probiotics in health and disease." *Gut* 62 (5):787-96. doi: 10.1136/gutjnl-2012-302504.

Sannaningannavar, F. M., B. S. Navati, and N. H. Ayachit. 2016. "Activation energy (ΔG*), enthalpy (ΔH*), and entropy (ΔS*) of poly(ethylene glycol) using Higasi method." *Polymer Bulletin* 73 (6):1689-1700. doi: 10.1007/s00289-015-1571-5.

Sanz, Guenhaël, and Edith Pajot-Augy. 2013. "Deciphering Activation of Olfactory Receptors Using Heterologous Expression in Saccharomyces cerevisiae and Bioluminescence Resonance Energy Transfer #." In *T Olfactory Receptors*, 149-160.

Saraiva, L. R., G. Ahuja, I. Ivandic, A. S. Syed, J. C. Marioni, S. I. Korsching, and D. W. Logan. 2015. "Molecular and neuronal homology between the olfactory systems of zebrafish and mouse." *Sci Rep* 5:11487. doi: 10.1038/srep11487.

Sarnat, H. B., and L. Flores-Sarnat. 2017. "Olfactory Development, Part 2: Neuroanatomic Maturation and Dysgeneses." *J Child Neurol* 32 (6):579-593. doi: 10.1177/0883073816685192.

Sarnat, H. B., L. Flores-Sarnat, and X. C. Wei. 2017. "Olfactory Development, Part 1: Function, From Fetal Perception to Adult Wine-Tasting." *J Child Neurol* 32 (6):566-578. doi: 10.1177/0883073817690867.

Sarnat, H. B., and W. Yu. 2016. "Maturation and Dysgenesis of the Human Olfactory Bulb." *Brain Pathol* 26 (3):301-18. doi: 10.1111/bpa.12275.

Sato, K., M. Pellegrino, T. Nakagawa, L. B. Vosshall, and K. Touhara. 2008. "Insect olfactory receptors are heteromeric ligand-gated ion channels." *Nature* 452 (7190):1002-U9. doi: 10.1038/nature06850.

Sato, Y., N. Miyasaka, and Y. Yoshihara. 2007. "Hierarchical regulation of odorant receptor gene choice and subsequent axonal projection of olfactory sensory neurons in zebrafish." *J Neurosci* 27 (7):1606-15. doi: 10.1523/JNEUROSCI.4218-06.2007.

Scott, J. W., and P. E. Scott-Johnson. 2002. "The electroolfactogram: A review of its history and uses." *Microscopy Research and Technique* 58 (3):152-160. doi: 10.1002/jemt.10133.

Segel, I.H. 1976. *Biochemical calculations.* 2d ed. ed. New-York: John Wiley & Sons.

Segel, Irwin. 1975. *Biochemical Calculations*. New York: john Wiley & Sons.

Sensi, S. L., P. Paoletti, A. I. Bush, and I. Sekler. 2009. "Zinc in the physiology and pathology of the CNS." *Nature Reviews Neuroscience* 10 (11):780-U38. doi: 10.1038/nrn2734.

Silbering, A. F., and R. Benton. 2010. "Ionotropic and metabotropic mechanisms in chemoreception: 'chance or design'?" *EMBO Rep* 11 (3):173-9. doi: 10.1038/embor.2010.8.

Simon, M. I., M. P. Strathmann, and N. Gautam. 1991. "DIVERSITY OF G-PROTEINS IN SIGNAL TRANSDUCTION." *Science* 252 (5007):802-808.

Simonson, Thomas, and Charles L. Brooks. 1996. "Charge Screening and the Dielectric Constant of Proteins: Insights from Molecular Dynamics." *Journal of the American Chemical Society* 118 (35):8452-8458. doi: 10.1021/ja960884f.

Singh, P., and S. D. Manning. 2016. "Impact of age and sex on the composition and abundance of the intestinal microbiota in individuals with and without enteric infections." *Ann Epidemiol* 26 (5):380-5. doi: 10.1016/j.annepidem.2016.03.007.

Sinnarajah, S., Carmen W. Dessauer, Deepa Srikumar, Jun Chen, John Yuen, Solomon Yllma, John C. Dennis, Edward E. Morrison, Vitaly Vodyanoy, and John H. Kehrl. 2001. "RGS2 regulates signal transduction in olfactory neurons by attenuating activation of adenylyl cyclase III." *Nature (London, United Kingdom)* 409 (6823):1051-1055.

Sinnarajah, Srikumar, Patrick I. Ezeh, Suram Pathirana, Anthony G. Moss, Edward E. Morrison, and Vitaly Vodyanoy. 1998. "Inhibition and enhancement of odorant-induced cAMP accumulation in rat olfactory cilia by antibodies directed against Gas/olf- and Gai-protein subunits." *FEBS Letters* 426 (3):377-380.

Sirelkhatim, A., S. Mahmud, A. Seeni, N. H. M. Kaus, L. C. Ann, S. K. M. Bakhori, H. Hasan, and D. Mohamad. 2015. "Review on Zinc Oxide Nanoparticles: Antibacterial Activity and Toxicity Mechanism." *Nano-Micro Letters* 7 (3):219-242. doi: 10.1007/s40820-015-0040-x.

Sklar, P. B., R. R. H. Anholt, and S. H. Snyder. 1986. "The Odorant-Sensitive Adenylate-Cyclase of Olfactory Receptor-Cells - Differential Stimulation by Distinct Classes of Odorants." *Journal of Biological Chemistry* 261 (33):5538-5543.

Small, D. M., J. C. Gerber, Y. E. Mak, and T. Hummel. 2005. "Differential neural responses evoked by orthonasal versus retronasal odorant perception in humans." *Neuron* 47 (4):593-605. doi: 10.1016/j.neuron.2005.07.022.

Smith, C. G. 1938. "Changes in the Olfactory Mucosa and the Olfactory Nerves Following Intranasal Treatment with One Per Cent Zinc Sulphate." *Can Med Assoc J* 39 (2):138-40.

Smolne, Sebastian, Stella Weber, and Michael Buback. 2016. "Propagation and Termination Kinetics of Poly(Ethylene Glycol) Methyl Ether Methacrylate in Aqueous Solution." *Macromolecular Chemistry and Physics* 217 (21):2391-2401. doi: 10.1002/macp.201600302.

Solbu, T. T., and T. Holen. 2012. "Aquaporin pathways and mucin secretion of Bowman's glands might protect the olfactory mucosa." *Chem Senses* 37 (1):35-46. doi: 10.1093/chemse/bjr063.

Sommer, F., and F. Backhed. 2013. "The gut microbiota--masters of host development and physiology." *Nat Rev Microbiol* 11 (4):227-38. doi: 10.1038/nrmicro2974.

Speca, D. J., D. M. Lin, P. W. Sorensen, E. Y. Isacoff, J. Ngai, and A. H. Dittman. 1999. "Functional identification of a goldfish odorant receptor." *Neuron* 23 (3):487-98.

Spehr, M., G. Gisselmann, A. Poplawski, J. A. Riffell, C. H. Wetzel, R. K. Zimmer, and H. Hatt. 2003. "Identification of a testicular odorant receptor mediating human sperm chemotaxis." *Science* 299 (5615):2054-8. doi: 10.1126/science.1080376.

Steiger, S. S., V. Y. Kuryshev, M. C. Stensmyr, B. Kempenaers, and J. C. Mueller. 2009. "A comparison of reptilian and avian olfactory receptor gene repertoires: species-specific expansion of group gamma genes in birds." *BMC Genomics* 10:446. doi: 10.1186/1471-2164-10-446.

Stensland, I., J. C. Kim, B. Bowring, A. M. Collins, J. P. Mansfield, and J. R. Pluske. 2015. "A Comparison of Diets Supplemented with a Feed Additive Containing Organic Acids, Cinnamaldehyde and a Permeabilizing Complex, or Zinc Oxide, on Post-Weaning Diarrhoea, Selected Bacterial Populations, Blood Measures and Performance in Weaned Pigs Experimentally Infected with Enterotoxigenic E. coli." *Animals (Basel)* 5 (4):1147-68. doi: 10.3390/ani5040403.

Stephan, A. B., S. Tobochnik, M. Dibattista, C. M. Wall, J. Reisert, and H. Q. Zhao. 2012. "The Na+/Ca2+ exchanger NCKX4 governs termination and adaptation of the mammalian olfactory response." *Nature Neuroscience* 15 (1):131-U164. doi: 10.1038/nn.2943.

Suk, J. S., Q. G. Xu, N. Kim, J. Hanes, and L. M. Ensign. 2016. "PEGylation as a strategy for improving nanoparticle-based drug and gene delivery." *Advanced Drug Delivery Reviews* 99:28-51. doi: 10.1016/j.addr.2015.09.012.

Sullivan, R. M., D. A. Wilson, N. Ravel, and A. M. Mouly. 2015. "Olfactory memory networks: from emotional learning to social behaviors." *Frontiers in Behavioral Neuroscience* 9. doi: ARTN 36 10.3389/fnbeh.2015.00036.

Sun, L. M., H. Y. Wang, J. Hua, J. L. Han, H. Matsunamic, and M. M. Luo. 2009. "Guanylyl cyclase-D in the olfactory CO2 neurons is activated by bicarbonate." *Proceedings of the National Academy of Sciences of the United States of America* 106 (6):2041-2046. doi: 10.1073/pnas.0812220106.

Suzuki, J., K. Yoshizaki, T. Kobayashi, and N. Osumi. 2013. "Neural crest-derived horizontal basal cells as tissue stem cells in the adult olfactory epithelium." *Neuroscience Research* 75 (2):112-120. doi: 10.1016/j.neures.2012.11.005.

Takahashi, L. K., B. R. Nakashima, H. Hong, and K. Watanabe. 2005. "The smell of danger: a behavioral and neural analysis of predator odor-induced fear." *Neurosci Biobehav Rev* 29 (8):1157-67. doi: 10.1016/j.neubiorev.2005.04.008.

Takeda, A. 2000. "Movement of zinc and its functional significance in the brain." *Brain Res Brain Res Rev* 34 (3):137-48.

Takeda, A. 2001. "Zinc homeostasis and functions of zinc in the brain." *Biometals* 14 (3-4):343-351.

Takeda, A., M. Ohnuma, J. Sawashita, and S. Okada. 1997. "Zinc transport in the rat olfactory system." *Neuroscience Letters* 225 (1):69-71.

Tamura, T., R. L. Goldenberg, K. E. Johnston, and M. DuBard. 2000. "Maternal plasma zinc concentrations and pregnancy outcome." *Am J Clin Nutr* 71 (1):109-13.

Thierry, Benjamin, Jane Ng, Tina Krieg, and Hans J. Griesser. 2009. "A robust procedure for the functionalization of gold nanorods and noble metal nanoparticles." *Chemical Communications* (13):1724-1726. doi: 10.1039/B820137D.

Thigpen, M. C., C. G. Whitney, N. E. Messonnier, E. R. Zell, R. Lynfield, J. L. Hadler, L. H. Harrison, M. M. Farley, A. Reingold, N. M. Bennett, A. S. Craig, W. Schaffner, A. Thomas, M. M. Lewis, E. Scallan, and A. Schuchat. 2011. "Bacterial meningitis in the United States, 1998-2007." *N Engl J Med* 364 (21):2016-25. doi: 10.1056/NEJMoa1005384.

Tokushige, M., T. Nishikiori, and Y. Ito. 2010. "Plasma-induced cathodic discharge electrolysis to form various metal/alloy nanoparticles." *Russian Journal of Electrochemistry* 46 (6):619-626. doi: 10.1134/s1023193510060042.

Turin, Luca. 1996. "A spectroscopic mechanism for primary olfactory reception." *Chemical Senses* 21 (6):773-791.

Vallee, B. L., and K. H. Falchuk. 1993. "The biochemical basis of zinc physiology." *Physiol Rev* 73 (1):79-118. doi: 10.1152/physrev.1993.73.1.79.

Viswaprakash, N., J. C. Dennis, A. M. Samoylov, E. M. Josephson, E. E. Morrison, and V. Vodyanoy. 2006. "Enhancement of odorant-induced responses in olfactory receptor neurons by zinc nanoclusters." Society for Neuroscience Annual Meeting, Atlanta, GA, October 16, 2006.

Viswaprakash, N., E. M. Josephson, J. C. Dennis, S. Yilma, E. E. Morrison, and V. J. Vodyanoy. 2010. "Odorant Response Kinetics from Cultured Mouse Olfactory Epithelium at Different Ages in vitro." *Cells Tissues Organs* 192 (6):361-373.

Viswaprakash, Nilmini, John C. Dennis, Ludmila Globa, Oleg Pustovyy, Eleanor M. Josephson, Patrick Kanju, Edward E. Morrison, and Vitaly Vodyanoy. 2009. "Enhancement of Odorant-Induced Response in Olfactory Receptor Neurons by Zinc Nanoparticles." *Chem. Senses* 34:547-557.

Vodyanoy, V. 2010. "Zinc nanoparticles interact with olfactory receptor neurons." *Biometals* 23 (6):1097-1103. doi: 10.1007/s10534-010-9355-8.

Vodyanoy, Vitaly, Yasmine Daniels, Oleg Pustovyy, William A MacCrehan, Shin Muramoto, and Gheorghe Stan. 2016. "Engineered metal nanoparticles in the sub-nanomolar levels kill cancer cells " *Int J Nanomedicine* 11:1-10.

Vosshall, L. B. 2001. "The molecular logic of olfaction in Drosophila." *Chem Senses* 26 (2):207-13.

Wade, F., A. Espagne, M. A. Persuy, J. Vidic, R. Monnerie, F. Merola, E. Pajot-Augy, and G. Sanz. 2011. "Relationship between Homo-oligomerization of a Mammalian Olfactory Receptor and Its Activation State Demonstrated by Bioluminescence Resonance Energy Transfer." *Journal of Biological Chemistry* 286 (17):15252-15259. doi: 10.1074/jbc.M110.184580.

Waldron, K. J., J. C. Rutherford, D. Ford, and N. J. Robinson. 2009. "Metalloproteins and metal sensing." *Nature* 460 (7257):823-30. doi: 10.1038/nature08300.

Wang, J., Z. A. Luthey-Schulten, and K. S. Suslick. 2003. "Is the olfactory receptor a metalloprotein?" *Proc Natl Acad Sci U S A* 100 (6):3035-9. doi: 10.1073/pnas.262792899.

Wang, Ping, Jiajie Fang, Sheng Qin, Yihong Kang, and Da-Ming Zhu. 2009. "Molecular Weight Dependence of Viscosity and Shear Modulus of Polyethylene Glycol (PEG) Solution Boundary Layers." *The Journal of Physical Chemistry C* 113 (31):13793-13800. doi: 10.1021/jp903060q.

Wang, Shige, Kai Li, Yu Chen, Hangrong Chen, Ming Ma, Jingwei Feng, Qinghua Zhao, and Jianlin Shi. 2015. "Biocompatible PEGylated MoS2 nanosheets: Controllable bottom-up synthesis and highly efficient photothermal regression of tumor." *Biomaterials* 39:206-217. doi: http://dx.doi.org/10.1016/j.biomaterials.2014.11.009.

Wang, Xiangyu, Lan Le, Pedro J. J. Alvarez, Fang Li, and Kunqian Liu. 2015. "Synthesis and characterization of green agents coated Pd/Fe bimetallic nanoparticles." *Journal of the Taiwan Institute of Chemical Engineers* 50:297-305. doi: http://dx.doi.org/10.1016/j.jtice.2014.12.030.

Waszak, S. M., Y. Hasin, T. Zichner, T. Olender, I. Keydar, M. Khen, A. M. Stutz, A. Schlattl, D. Lancet, and J. O. Korbel. 2010. "Systematic inference of copy-number genotypes from personal genome sequencing data reveals extensive olfactory receptor gene content diversity." *PLoS Comput Biol* 6 (11):e1000988. doi: 10.1371/journal.pcbi.1000988.

Wiegand, H. F., P. Beed, M. H. Bendels, C. Leibold, D. Schmitz, and F. W. Johenning. 2011. "Complementary sensory and associative microcircuitry in primary

olfactory cortex." *J Neurosci* 31 (34):12149-58. doi: 10.1523/JNEUROSCI.0285-11.2011.

Willander, J., and M. Larsson. 2007. "Olfaction and emotion: the case of autobiographical memory." *Mem Cognit* 35 (7):1659-63.

Wright, R. H. 1954. "Odour and molecular vibration. I. Quantum and thermodynamic considerations." *Journal of Applied Chemistry* 4 (11):611-615. doi: 10.1002/jctb.5010041104.

Xie, J., T. Owen, K. Xia, A. V. Singh, E. Tou, L. Li, B. Arduini, H. Li, L. Q. Wan, B. Callahan, and C. Wang. 2015. "Zinc inhibits Hedgehog autoprocessing: linking zinc deficiency with Hedgehog activation." *J Biol Chem* 290 (18):11591-600. doi: 10.1074/jbc.M114.623264.

Xu, J., and J. I. Gordon. 2003. "Honor thy symbionts." *Proc Natl Acad Sci U S A* 100 (18):10452-9. doi: 10.1073/pnas.1734063100.

Yan, M., S. J. Pamp, J. Fukuyama, P. H. Hwang, D. Y. Cho, S. Holmes, and D. A. Relman. 2013. "Nasal microenvironments and interspecific interactions influence nasal microbiota complexity and S. aureus carriage." *Cell Host Microbe* 14 (6):631-40. doi: 10.1016/j.chom.2013.11.005.

Yang, T., W. A. Hendrickson, and H. M. Colecraft. 2014. "Preassociated apocalmodulin mediates Ca2+-dependent sensitization of activation and inactivation of TMEM16A/16B Ca2+-gated Cl- channels." *Proc Natl Acad Sci U S A* 111 (51):18213-8. doi: 10.1073/pnas.1420984111.

Yoo, M. H., and C. T. Wei. 1967. "Slip Modes of Hexagonal-Close-Packed Metals." *Journal of Applied Physics* 38 (11):4317-4322. doi: doi:http://dx.doi.org/10.1063/1.1709121.

Young, J. M., B. M. Shykind, R. P. Lane, L. Tonnes-Priddy, J. A. Ross, M. Walker, E. M. Williams, and B. J. Trask. 2003. "Odorant receptor expressed sequence tags demonstrate olfactory expression of over 400 genes, extensive alternate splicing and unequal expression levels." *Genome Biol* 4 (11):R71. doi: 10.1186/gb-2003-4-11-r71.

Young, J. M., and B. J. Trask. 2002. "The sense of smell: genomics of vertebrate odorant receptors." *Hum Mol Genet* 11 (10):1153-60.

Zapata, H. J., and V. J. Quagliarello. 2015. "The microbiota and microbiome in aging: potential implications in health and age-related diseases." *J Am Geriatr Soc* 63 (4):776-81. doi: 10.1111/jgs.13310.

Zelano, C., and N. Sobel. 2005. "Humans as an animal model for systems-level organization of olfaction." *Neuron* 48 (3):431-54. doi: 10.1016/j.neuron.2005.10.009.

Zhang, Q., D. Zhang, N. Li, Y. Lu, Y. Yao, S. Li, and Q. Liu. 2016. "Zinc Nanoparticles-equipped Bioelectronic Nose Using a Microelectrode Array for Odorant Detection." *Anal Sci* 32 (4):387-93. doi: 10.2116/analsci.32.387.

Zhao, H., J. M. Otaki, and S. Firestein. 1996. "Adenovirus-mediated gene transfer in olfactory neurons in vivo." *J Neurobiol* 30 (4):521-30. doi: 10.1002/(SICI)1097-4695(199608)30:4<521::AID-NEU7>3.0.CO;2-5.

Zozulya, S., F. Echeverri, and T. Nguyen. 2001. "The human olfactory receptor repertoire." *Genome Biol* 2 (6):RESEARCH0018.

Zufall, F., S. Firestein, and G. M. Shepherd. 1991. "Analysis of Single Cyclic-Nucleotide Gated Channels in Olfactory Receptor-Cells." *Journal of Neuroscience* 11 (11):3573-3580.